Advances in Clinical and Experimental Medicine

MONTHLY ISSN 1899-5276 (PRINT) ISSN 2451-2680 (ONLINE) www.advances.umed.wroc.pl

2018, Vol. 27, No. 8 (August)

Impact Factor (IF) – 1.262
Ministry of Science and Higher Education – 15 pts.
Index Copernicus (ICV) – 155.19 pts.

Wroclaw Medical University

Advances
in Clinical and Experimental Medicine

ISSN 1899-5276 (PRINT) ISSN 2451-2680 (ONLINE) www.advances.umed.wroc.pl

MONTHLY 2018
Vol. 27, No. 8
(August)

Advances in Clinical and Experimental Medicine is a peer-reviewed open access journal published by Wroclaw Medical University. Its abbreviated title is Adv Clin Exp Med. Journal publishes original papers and reviews encompassing all aspects of medicine, including molecular biology, biochemistry, genetics, biotechnology, and other areas. It is published monthly, one volume per year.

Editorial Office
ul. Marcinkowskiego 2–6
50-368 Wrocław, Poland
Tel.: +48 71 784 12 05
E-mail: redakcja@umed.wroc.pl

Publisher
Wroclaw Medical University
Wybrzeże L. Pasteura 1
50-367 Wrocław, Poland

Online edition is the original version of the journal

Editorial Policy

Advances in Clinical and Experimental Medicine (Adv Clin Exp Med) is an independent multidisciplinary forum for exchange of scientific and clinical information, publishing original research and news encompassing all aspects of medicine, including molecular biology, biochemistry, genetics, biotechnology and other areas. During the review process, the Editorial Board conforms to the "Uniform Requirements for Manuscripts Submitted to Biomedical Journals: Writing and Editing for Biomedical Publication" approved by the International Committee of Medical Journal Editors (www.ICMJE.org/). The journal publishes (in English only) original papers and reviews. Short works considered original, novel and significant are given priority. Experimental studies must include a statement that the experimental protocol and informed consent procedure were in compliance with the Helsinki Convention and were approved by an ethics committee.

For all subscription related queries please contact our Editorial Office:

redakcja@umed.wroc.pl

For more information visit the journal's website:

www.advances.umed.wroc.pl

Pursuant to the ordinance no. 134/XV R/2017 of the Rector of Wroclaw Medical University (as of December 28, 2017) from January 1, 2018 authors are required to pay a fee amounting to 700 euros for each manuscript accepted for publication in the journal "Advances in Clinical and Experimental Medicine."

Indexed in: MEDLINE, Science Citation Index Expanded, Journal Citation Reports/Science Edition,

Scopus, EMBASE/Excerpta Medica, Ulrich's™ International Periodicals Directory, Index Copernicus

Typographic design: Monika Kolęda, Piotr Gil
DTP: Wydawnictwo UMW, TYPOGRAF
Cover: Monika Kolęda
Printing and binding: EXDRUK

Advances
in Clinical and Experimental Medicine

MONTHLY 2018, Vol. 27, No. 8 (August)

ISSN 1899-5276 (PRINT)
ISSN 2451-2680 (ONLINE)
www.advances.umed.wroc.pl

Contents

Original papers

Reviews

The increased expression of *Piezo1* and *Piezo2* ion channels in human and mouse bladder carcinoma

Ebru Önalan Etem[1,A,D], Gülay Güleç Ceylan[2,B,C,E,F], Seda Özaydın[1,A–C], Cavit Ceylan[3,A,E], Ibrahim Özercan[4,A,B], Tuncay Kuloğlu[5,A–C]

[1] Department of Medical Biology, Faculty of Medicine, Fırat University, Elazığ, Turkey
[2] Department of Medical Genetics, Faculty of Medicine, Yıldırım Beyazıt University, Ankara, Turkey
[3] Urology Clinics, Yüksek Ihtisas Education and Training Hospital, Ankara, Turkey
[4] Department of Pathology, Faculty of Medicine, Fırat University, Elazığ, Turkey
[5] Department of Histology and Embriology, Faculty of Medicine, Fırat University, Elazığ, Turkey

A – research concept and design; B – collection and/or assembly of data; C – data analysis and interpretation;
D – writing the article; E – critical revision of the article; F – final approval of the article

Advances in Clinical and Experimental Medicine, ISSN 1899-5276 (print), ISSN 2451-2680 (online) *Adv Clin Exp Med*. 2018;27(8):1025–1031

Address for correspondence
Gülay Güleç Ceylan
E-mail: gulayceylan23@gmail.com

Funding sources
None declared

Conflict of interest
None declared

Received on February 18, 2017
Reviewed on April 3, 2017
Accepted on May 7, 2017

Abstract

Background. *Piezo1/2*, a mechanically activated ion channel, is believed to play an important role in bladder carcinogenesis process. *Piezo1/2* expression has not been previously reported in urinary bladder carcinoma, and little is known about its significance in bladder carcinogenesis.

Objectives. In our study, we aimed to evaluate the *Piezo1* and *Piezo2* expression as developmental in mouse bladder tissue and bladder cancer tissue of mice and humans.

Material and methods. The detection of developmental expression was performed on P0–P90 days in bladder tissue of Balb/c strain mice. Mice were divided into bladder cancer (n = 40) and control groups (n = 10). Bladder cancer in mice was created by using *N*-butyl-*N*-(4-hydroxybutyl)nitrosamine (BBN). In the study, 60 human subjects were included, whose normal tissues were used as controls. After the histopathological evaluation, the expression of *Piezo1/2* genes was examined by reverse transcription polymerase chain reaction (RT-PCR) and immunohistochemistry in tumor and normal tissues.

Results. In developmental period of the mice, *Piezo1* expression increased on days 21 and 90, whereas *Piezo2* expression increased on day 7 and decreased on day 90 in mouse bladder tissues. There was a significant increase in the expression of *Piezo1/2* in both cancer groups compared to the control group. *Piezo1* expression was significantly increased at tumor size, stage and grade. *Piezo2* expression was upregulated in high grade tumors in human subjects.

Conclusions. The developmental changes of *Piezo* expression on specific days demonstrate the role of these channels in bladder cancer development. The dysfunction of *Piezo1/2* expression may contribute to the carcinogenesis of bladder cancer by causing proliferative changes and angiogenesis. The expression of *Piezo1/2* can provide new prognostic information for disease progression.

Key words: bladder cancer, messenger RNA expression, *Piezo* channels

DOI
10.17219/acem/71080

Introduction

Bladder cancer is the 4th most common cancer type in men.[1] Nearly 90% of patients with bladder cancer have transitional cell carcinoma of the bladder (TCC). Bladder cancers with a new diagnosis are usually – in 75% of cases – non-muscle invasive.[2] According to several studies, there are many etiological factors that contribute to the disease, such as male gender, tobacco use, chemical agents, diet, exposure to cyclophosphamide, ionizing radiation, phenacetin-containing analgesics, and genetic factors.[3,4]

Some of the channel types localized in the plasma membrane and intracellular organelles are involved in carcinogenesis and contribute to the basic phenotypes, like metabolic reprogramming, migration, unlimited proliferative potential, apoptosis resistance, induction of angiogenesis, and invasion of the cancer cells. The channels that contribute to cancer development and progression have been defined as "oncogenic channels".[5–7]

Mechanotransduction is the conversion of a mechanical stimulus into chemical/biological activity. This is a basic physiological process of mammalian cells and it affects many critical processes, such as pain, embryonic development and vascular tone regulation.[8] Mechanosensitive ion channels (MSCs) are associated with the physiological functions of some biological systems, e.g., the musculoskeletal system, neuromuscular system and/or respiratory system.[9] *Piezo1* and *Piezo2* are a unique class of a conserved family of nonselective cation channels that are activated by physical or mechanical stimuli.[10–12] They have no sequence similarity with any other channel.[13] Both of these *Piezo* channels are cation-selective mechanical channels and they have a selectivity sequence of preference for ions $Ca^{2+} > K^{+} > Na^{+} > Mg^{2+}$.[14,15] *Piezo1* and *Piezo2* are homologous and they were both cloned in 2010.[8,13] *Piezo* proteins form a homotetramer of about 1.2 MDa and have been highlighted as a central pore module.[13,16] Expression profiles of messenger RNA (mRNA) and proteins for *Piezo1* and *Piezo2* have been detected in numerous MSC tissues.[10] The expression of *Piezo1* has been shown in endothelial cells, red blood cells, cochlear hair cells, kidney, skin, lung, and bladder tissue.[11,17,18] *Piezo1* also plays a significant physiological role in the hematopoietic and cardiovascular system.[11,12,19,20] It has been documented for its responsibility for cell volume regulation of red blood cells. Gain-of-function mutations of *Piezo1* have been detected in cases with dehydrated hereditary stomatocytosis (DHS), which is characterized by a decreased volume of intracellular erythrocytes and a mild hemolysis.[21–23]

Homozygous mutant *Piezo1* mice are embryonically lethal.[11,19] However, blood cell-specific *Piezo1* knockout mice display increased erythrocyte size and osmotic fragility.[24] *Piezo2* has been shown to be expressed in the dorsal root and trigeminal ganglia, lung, bladder, and Merkel cells.[17]

The suggestion that *Piezo1* and *Piezo2* channels regulate mammalian development, physiology and carcinogenesis has yet to be clarified. Therefore, in this study, we aimed to evaluate *Piezo1* and *Piezo2* ion channel protein expressions in postnatal period (P0–P90) in mice; we also compared the expressions in human and mouse tumor and non-tumor bladder tissues.

Material and methods

Patients

We conducted a prospective controlled study with patients that were admitted with painless gross hematuria and low urinary tract symptoms (LUTS). The study was approved by the Fırat University (Elazığ, Turkey) Local Ethics Committee and written informed consent was obtained from each participant before the study was initiated. Bladder tissue samples were obtained from 60 patients (14 females and 46 males). Transurethral resection was performed in the presence of bladder tumor and a biopsy was taken if the suspicion was determined. Routine pathological diagnoses were performed according to hematoxylin and eosin (H&E) staining. During the pathological analysis, the samples were categorized according to the WHO/International Society of Urological Pathology (ISUP) 1998 classification.[25] Patients in whom a pathological examination revealed TCC constituted the patient group and those with a benign pathology examination constituted the control. After a histopathological evaluation for urothelial carcinoma, the expression of *Piezo1* and *Piezo2* gene was analyzed by quantitative real-time polymerase chain reaction (qRT-PCR). Immunohistochemistry of the tumor and normal tissues of patients was performed to determine whether there was a difference between the expression of *Piezo1* and *Piezo2* channels in tumor and normal tissues.

Animals

The ethical Animal Research Committee of Fırat University approved the study protocol. Balb/c-type mice were housed in standard plastic cages. Animals were maintained in light rooms for 12 h and in dark rooms for 12 h. All animals were allowed free access to water and food. Bladder tissue samples of 2 mice for each day: P0, P7, P14, P21, P28, P36, and P90 were used in each postnatal period for determining the developmental expression. Mice were arranged as 2 groups: the bladder cancer group (n = 40) and the control group (n = 10). *N*-butyl-*N*-(4-hydroxybutyl) nitrosamine (BBN) (0.05% in the drinking water) was applied to induce bladder cancer in mice for 3 months. Carcinoma formation was expected for 4 months following this process. After the detection of pathologic carcinoma by a pathologist with H&E staining in 2 mice 4 months later, all animals were decapitated after 3% pentobarbital abdominal anesthesia. Bladder tissues were stored in liquid nitrogen at –80°C for qRT-PCR and in 10% neutral buffered formalin for immunohistochemical analysis.

RNA extraction

Total RNA was isolated from human and mouse bladder tissue using Trizol (Life Technologies, San Francisco, USA). Bladder tissue was homogenized using a homogenizer (Next Advance, Inc., Averill Park, USA). Total RNA was dissolved in 100 µL of diethyl pyrocarbonate (DEPC)--treated H_2O, aliquoted and stored at –80°C. A Qubit® 2.0 Fluorometer (Invitrogen by Life Technologies™, Zug, Austria) was used to determine RNA concentration and purity.

Real-time polymerase chain reaction

High Capacity cDNA Reverse Transcription Synthesis Kits (Applied Biosystems, Inc., Foster City, USA) were used for the conversion of total RNA to complementary DNA (cDNA), using 1 µg of total RNA. Complementary DNA isolation was performed in a gradient thermal cycler (Biometra, Göttingen, Germany) with a profile of 25°C for 10 min, 37°C for 120 min, 85°C for 5 min, and 4°C for 60 min. All of the samples were run in batch. As a negative control, samples were run simultaneously with no reverse transcriptase enzyme (RT negative) or RNA (no template controls) to control for RNA and genomic DNA contamination, respectively. ABI Prism 7500 Fast Real Time PCR Instrument (Applied Biosystems) was used for the reverse transcription polymerase chain reaction (RT-PCR) analysis using *Piezo1* (Hs00207230-m1 and Mm01241549-m1) and *Piezo2* (Hs00401026-m1 and Mm01265861-m1). All the results were standardized according to the levels of glyceraldehyde 3-phosphate dehydrogenase (GAPDH) (Hs02758991-g1 and Mm99999915-g1).

Immunohistochemistry staining

Human bladder sections (4–5 µm thick) were prepared from paraffin embedded blocks for immunohistochemical staining. Peptide blocking and immunohistochemical studies were performed with the indirect immunoperoxidase staining technique on paraffin-embedded material.

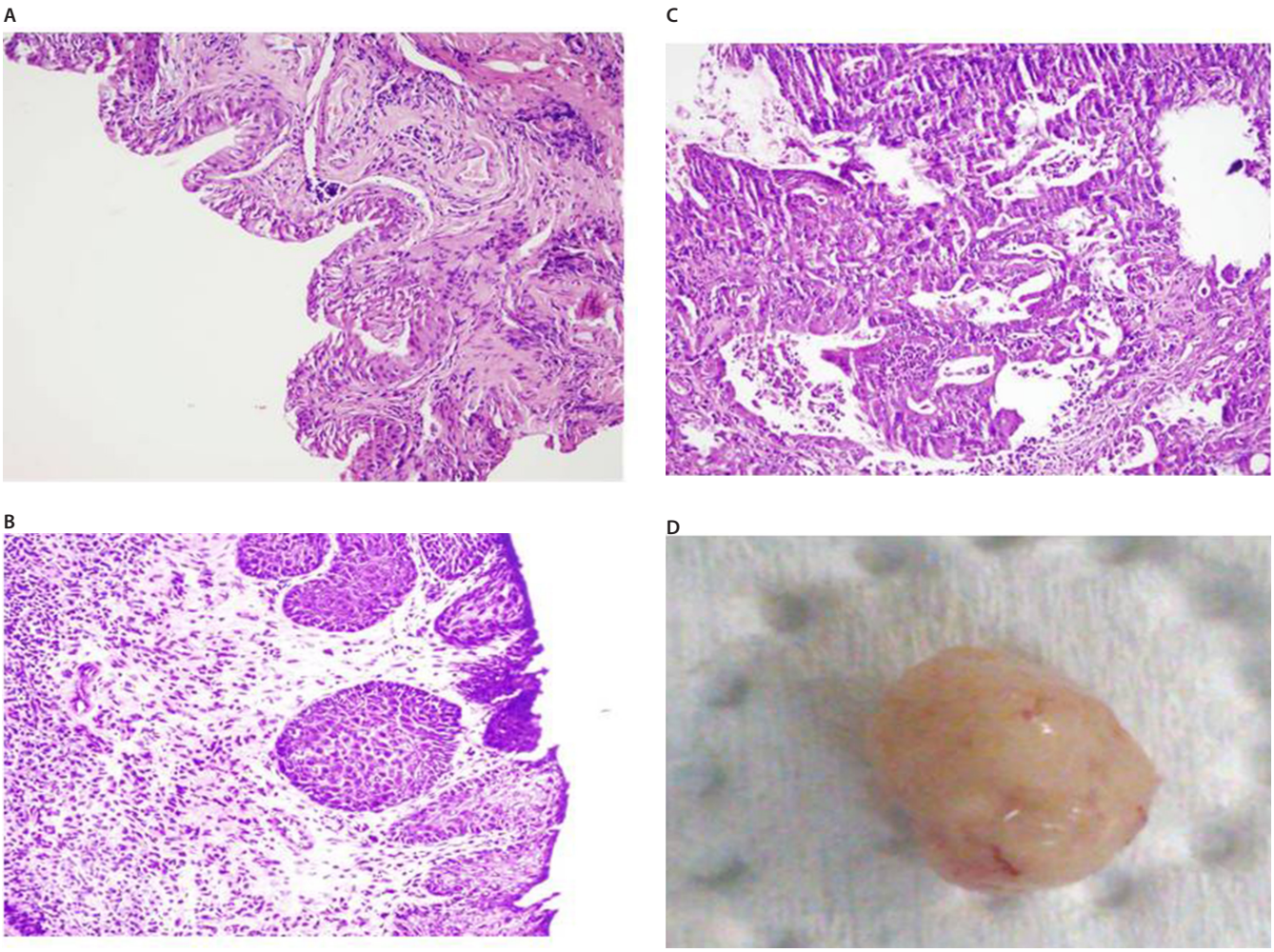

Fig. 1. Representative H&E-stained images of urothelial cross-sections from BBN-induced bladder cancer in mice

Note the urothelial cancers in the BBN-induced mice: A – note the normal-appearing urothelium in the control group of mice; B – note the high-grade carcinoma-in-situ lesion in BBN-treated mice; C – note the high-grade, papillary bladder tumor in BBN-treated mice; magnification: ×400; D – fresh tumor samples with adenocarcinomas in mice.

H&E – hematoxylin and eosin; BBN – *N*-butyl-*N*-(4-hydroxybutyl)nitrosamine.

Non-specific staining was blocked using a 20 min incubation with a serum-blocking solution (Immuno Cruz Staining System; Santa Cruz Biotechnology, Dallas, USA). The sections were incubated with a *Piezo1* (NBP1-78537; Novus Biologicals, Littleton, USA) and *Piezo2* (NBP1-78538; Novus Biologicals) antibody diluted 1:200 for 60 min in a humid chamber at room temperature. The sections were then incubated with streptavidin peroxidase (TS-125-HR; Lab Vision Corp., Fremont, USA) for 30 min after they were washed 3 times with phosphate buffered saline (PBS). Drops of 3-amino-9-ethylcarbazole (AEC) substrate + AEC chromogen (AEC Substrate, TA-015-HAS; AEC Chromogen, TA-002-HAC; Lab Vision Corp.) solution were applied, and the tissues were washed with PBS after labeling was checked by light microscopy. Mayer's hematoxylin was used for the counterstaining of sections, rinsed in PBS and distilled water, and then mounted with a closure solution (Large Volume Vision Mount, TA-125-UG; Lab Vision Corp.). After the slides were analyzed by the BX50 optical microscopy (Olympus Corp., Tokyo, Japan), they were photographed. The evaluation of immunohistochemical staining was performed semi-quantitatively, based on the spreading and levels of the staining. The levels for immunostaining in bladder tissue were detected by subjective visual scoring of the brown stain. Then, they were compared with normal tissue. The scoring levels were as follows: weak staining intensity (nearly equal to normal tissue = 0), moderate staining intensity (1) and strong staining intensity (2).

Statistical analysis

Statistical Package for the Social Sciences (SPSS) software v. 22 for Windows (IBM, Armonk, USA) was used for the analysis of data for each experiment. If the data satisfied the suppositions of normality and homogeneity of parametric analyses (one-way independent measure ANOVA and t-tests), variance was performed along with Tukey's honest significant difference (HSD) post-hoc test, if it was appropriate. A p-value of <0.05 was accepted as statistically significant. All data was presented as mean ± standard deviation (SD) or standard error of the mean (SEM).

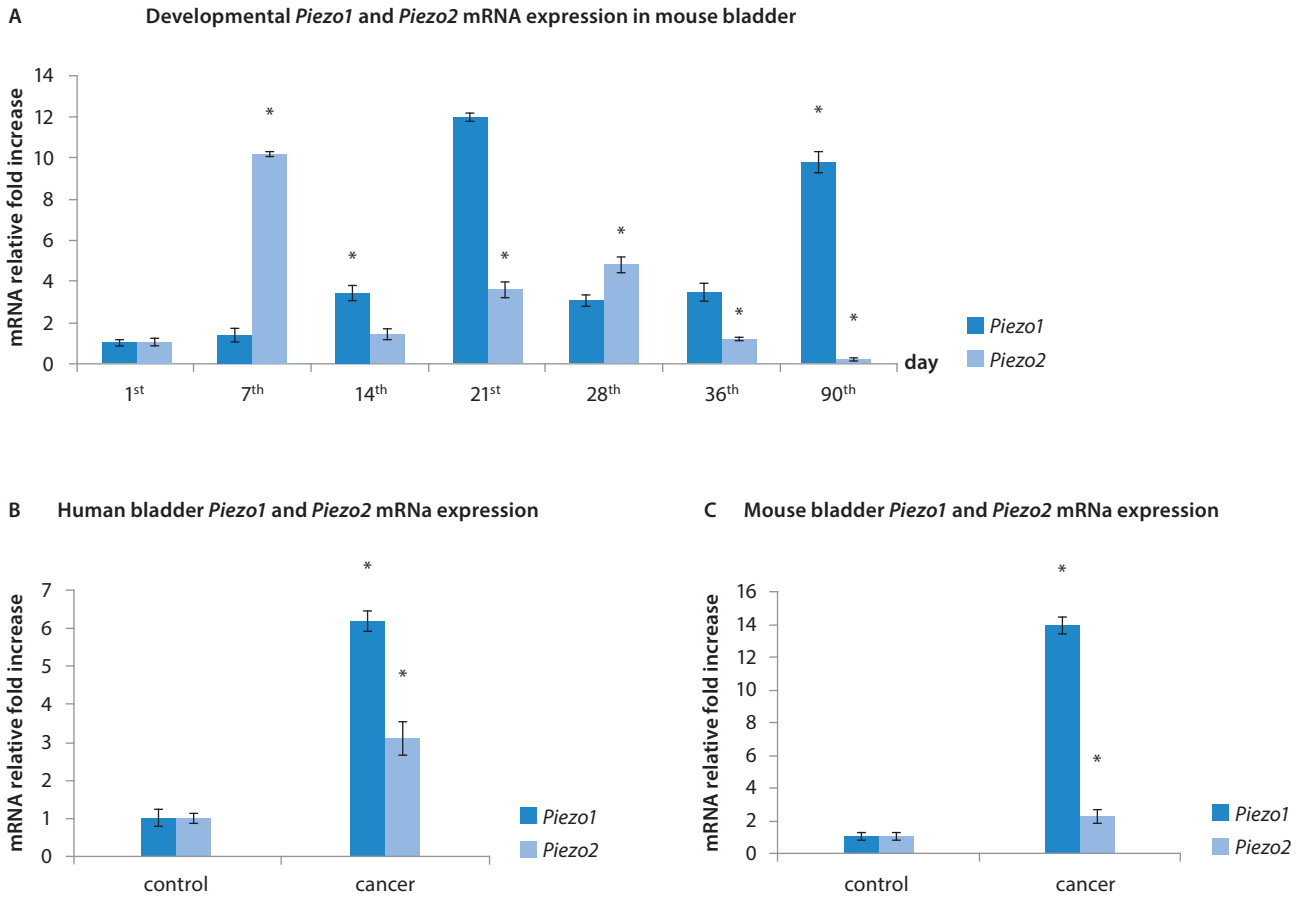

Fig. 2. Quantitative RT-PCR analysis of *Piezo1* and *Piezo2* in bladder tissue in mice and humans

A – results are expressed as mean ±SD for 14 mice (2 mice for each day) on day P0, P7, P14, P21, P28, P36, and P90 for determining the developmental expression; B – results are expressed as mean ±SD for 10 mice from the control group and 31 BBN-treated animals; C – results are expressed as mean ±SD for cancerous and healthy tissue of 60 patients; error bars represent SD significantly different ($p < 0.05$) from control or P0 ; * shows the statistical significance.

RT-PCR – real-time polymerase chain reaction; BBN – *N*-butyl-*N*-(4-hydroxybutyl)nitrosamine.

Results

Molecular findings

A total of 60 patients with urothelial carcinoma were included in the analysis for staging. The majority (63.3%) of the urothelial tumors were in the T1 stage. All patients in the study group were smokers. Patient characteristics are shown in Table 1.

In the BBN-treated group, 9 animals died during the procedure. A histopathologic evaluation of all the bladders was used to determine BBN-induced carcinogenesis and revealed benign proliferative changes in 32.2% (10/31) and urothelial carcinoma in 67.7% (21/31) of the animals treated with BBN (Fig. 1). In situ, carcinoma in 66.6% (14/21) samples and adenocarcinoma in 33.3% (7/21) samples of urothelial carcinomas was also determined. As expected, this contrasted significantly with the control group, in which no evidence of bladder cancer was detected (Fig. 1).

We first performed the gene expression analysis by RT-PCR in tumor samples. *Piezo1* expression significantly increased on day P14, P21, P28, P36, and P90 in comparison with day P1, whereas *Piezo2* expression significantly increased on day P7, P21 and P28, and decreased on day P90 compared to day P1 (Fig. 2A). *Piezo1* was detected to be upregulated in 53.3% (32/60), downregulated in 13.33% (8/60) and not changed in 30.7% (20/60) of the human bladder tissue samples. *Piezo2* was detected to be upregulated in 60% (36/60), downregulated in 20% (12/60) and not changed in 20% (12/60) of the human bladder tissue samples. The expression levels of *Piezo1* and *Piezo2* calculated in all the human bladder cancer group tissues was significantly increased compared to normal tissue (t-test; $p = 0.00$ and $p = 0.00$, respectively) (Fig. 2B). On the other hand, the expression levels of *Piezo1* and *Piezo2* in the BBN-induced bladder cancer group was significantly higher than in the normal control group (t-test; $p < 0.00$ and $p = 0.04$, respectively) (Fig. 2C).

The detection rate of *Piezo1* was 100% in bladder carcinoma specimens. The expression of *Piezo1* in bladder carcinoma was significantly associated with tumor size and stage, but it had no association with other clinicopathological features. The expression of *Piezo1* in bladder carcinoma patients with ≥3 tumor size was

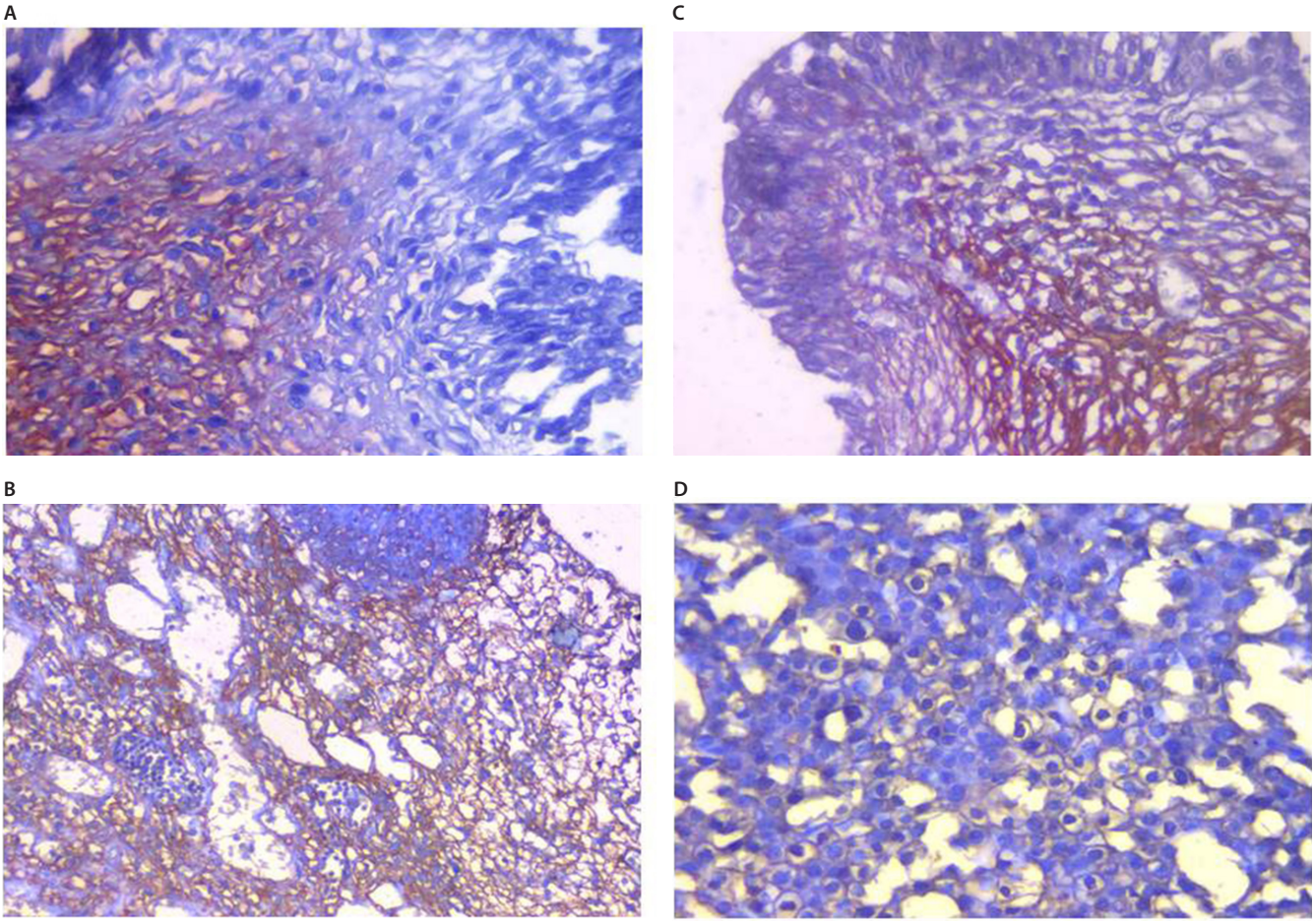

Fig. 3. Immunohistochemical staining for *Piezo1* and *Piezo2* in human bladder tissue

Representative bladder sections stained for *Piezo1* (A – control; B – cancer) and *Piezo2* (C – control; D – cancer) in carcinomas and control tissue in human bladder samples. *Piezo1* and *Piezo2* staining was detected especially in the cytoplasm and membrane urothelial cells. Note the marked upregulation of both *Piezo1* and *Piezo2* in human bladder cancer. Scale bar: 20 µm; magnification ×200.

significantly higher than in bladder carcinoma patients with <3 tumor size (p = 0.00). *Piezo1* expression was significantly upregulated in ≥pT2 (muscle invasive bladder cancer with pathological findings) as compared to pT0 (no evidence of residual carcinoma in the cystectomy specimens after an initial cancer diagnosis in the biopsy or transurethral resection specimens) and pT1 (high-risk non-muscle invasive bladder cancer with pathological findings) patients (pT0 vs ≥pT2, p = 0.006; pT1 vs ≥pT2, p = 0.000, respectively). *Piezo2* expression was increased in ≥pT2 patients as compared to pT0 patients (pT0 vs ≥pT2, p = 0.003). pT0 vs pT1 and pT1 vs ≥pT2 were not significantly different (p > 0.05). A higher expression level of *Piezo2* in high-grade tumors was detected (p = 0.003). The data also demonstrated that the expression level of *Piezo2* had no significant association with tumor grade. *Piezo1* and *Piezo2* expression was not significantly different in bladder cancer specimens with lymph node metastasis as compared to specimens without lymph node metastasis; there were also no differences with regard to age and gender (p > 0.05).

Table 1. Distribution of variables in bladder cancer patients

Characteristics	Values
Age [years], mean ±SD (range)	
male	64.9 ±4.29 (56–76)
female	62.2 ±3.51 (58–70)
Gender, n (%)	
male	46 (76.6%)
female	14 (23.3%)
Tumor size	
<3	34
≥3	26
Lymph node involvement	
no	57
yes	3
Tumor grade	
low	48
high	12
Tumor stage	
pT0	8
pT1	38
≥pT2	14
Total	60

Immunohistochemical findings

To examine the localization of *Piezo1* and *Piezo2* in the human bladder, the immunohistochemical analysis was performed. Immunohistochemistry revealed that *Piezo1* immunoreactivity was mainly observed in the urothelial layer with less immunoreactivity in stromal tissues (Fig. 3A,3B). In contrast, little *Piezo2* expression was detected in urothelial tissues (Fig. 3C,3D). *Piezo1* and *Piezo2* were mainly localized in the plasma membrane and the cytoplasm near the nucleus.

Discussion

In the present study, we investigated pathological changes in *Piezo1* and *Piezo2* in the bladder cancers of humans and mice. We obtained the following novel findings:

- mRNA expressions of *Piezo1* and *Piezo2* genes in cancerous bladder tissues were increased as compared to control bladder tissues;
- *Piezo1* expression was correlated with tumor stage, grade and size;
- *Piezo2* expression increased significantly only in ≥pT2 patients as compared to pT0.

Piezo1 and *Piezo2* proteins take part in mechanosensory processes and they are stretch-activated cation channels. Almost every cell can sense the mechanical signals. In particular, stretch-activated cation channels in cells have a basic role in sensing these mechanical signals.[8,26,27] Coste et al. found that the mRNA expression of *Piezo1* is the highest in the bladder, skin and lungs of adult mice.[10] The loss or absence of *Piezo1* plays an important role in increased cell migration and metastases of lung cancer. A decrease of *Piezo1* in gastric tumors has been related to reduced cell migration.[14,17,28] The authors also described the extrusion of living cells at colon surfaces. This suggests that the loss of *Piezo1* in colon tissue could lead to polyp formation.[17] All of these reports point at *Piezo* proteins as critical for cell migration, elongation and proliferation. In the present study, we observed similar results; mRNA expression was high in bladder cancer tissues, but higher expression levels could lead to cell migration. To support our results, the knockdown of *Piezo1* in gastric epithelium cancer cells was shown to reduce cell migration. The authors suggested that *Piezo1* overexpression promotes the invasion and metastasis of gastric cancer.[17] Increases in the *Piezo* ion channel expression can cause dysfunction and leakage at these ion channels. This process may also result in proliferative changes in bladder cancer tissue.[29]

According to a recent study, haploinsufficiency of *Piezo1* leads to endothelial abnormality, indicating the importance of this gene for vascular structure.[19] Angiogenesis is a finely tuned process, which is the result of the equilibrium between pro- and anti-angiogenic factors. In solid tumor angiogenesis, the balance is highly in favor of the production of new, but poorly functioning blood vessels, which are initially intended to provide growing tumors with nutrients and oxygen.[30] *Piezo1* ion channels may thus affect different hallmarks of cancer, especially tumor angiogenesis.

Yang et al. reported that *Piezo2* knockdown decreased angiogenesis and vascular hyperpermeability, and inhibited endothelial cell proliferation, migration and tube formation. *Piezo2* knockdown in endothelial cells resulted in the suppression of cell proliferation, migration and invasion of glioma tumor cells, which regulate glioma angiogenesis via Ca^{2+}/Wnt11/β-catenin signaling.[26] These studies

provide evidence for *Piezo2* as a critical regulator of tumor angiogenesis and vascular permeability. The present study showed that *Piezo2* expression was increased in bladder tumor samples compared to human and mouse control tissues. Inspired by these findings, we speculated that *Piezo2* may contribute to the carcinogenesis of bladder cancer by regulating tumor angiogenesis. However, the function of *Piezo2* in bladder tumor angiogenesis has not been elucidated.

It is not known whether the changes in *Piezo* channel expression in bladder cancer tissue occur due to the basic steps of cancer progression or secondary to other variations. For this reason, we aimed to investigate postnatal expressions of *Piezo* channels in this study. Expression variation on certain days supports the notion that these channels may play a role in bladder development.

Conclusions

According to our study, *Piezo* proteins are thought to be involved in cancer and they regulate mechanical transmission. Increased expression of *Piezo1* and *Piezo2* in bladder cancer indicates that these channels may be therapeutic targets. The use of blockers for these channels has been determined to inhibit the cell proliferation. Further research will reveal whether *Piezo1* and *Piezo2* are causally involved in the carcinogenesis and progression of bladder cancer, which represents a potential therapeutic target or a prognostic factor.

References

1. Silverman DT, Devesa SS, Moore LE, Rothman N. Bladder cancer. In: Schottenfeld D, Fraumeni J, eds. *Cancer Epidemiology and Prevention*. 3rd ed. New York, NY: Oxford University Press; 2006:156–160.
2. Siegel R, Ma J, Zou Z, Jemal A. Cancer statistics. *CA Cancer J Clin*. 2014;64:9–29.
3. Heney NM, Ahmed S, Flanagan MJ, et al. Superficial bladder cancer: Progression and recurrence. *J Urol*. 1983;130:1083–1086.
4. Vlaovic P, Jewett MA. Cyclophosphamide-induced bladder cancer. *Can J Urol*. 1999;6:745–748.
5. Leanza L, Biasutto L, Managò A, Gulbins E, Zoratti M, Szabò I. Intracellular ion channels and cancer. *Front Physiol*. 2013;4:227.
6. Hoffmann EK, Lambert IH. Ion channels and transporters in the development of drug resistance in cancer cells. *Philos Trans R Soc Lond B Biol Sci*. 2014;369(1638):20130109.
7. Munaron L. Systems biology of ion channels and transporters in tumor angiogenesis: An omics view. *Biochim Biophys Acta*. 2015;1848(10 Pt B):2647–2656.
8. Xiao R, Xu XZ. Mechanosensitive channels: In touch with Piezo. *Curr Biol*. 2010;20:R936–R938.
9. Coste B, Houge G, Murray MF, et al. Gain-of-function mutations in the mechanically activated ion channel *PIEZO2* cause a subtype of distal arthrogryposis. *Proc Natl Acad Sci U S A*. 2013;110:4667–4672.
10. Coste B, Mathur J, Schmidt M, et al. Piezo1 and Piezo2 are essential components of distinct mechanically activated cation channels. *Science*. 2010;330:55–60.
11. Ranade SS, Woo SH, Dubin AE, et al. Piezo2 is the major transducer of mechanical forces for touch sensation in mice. *Nature*. 2014;516:121–125.
12. Woo SH, Ranade S, Weyer AD, et al. Piezo2 is required for Merkel-cell mechanotransduction. *Nature*. 2014;509:622–626.
13. Coste B, Xiao B, Santos JS, et al. Piezo proteins are pore-forming subunits of mechanically activated channels. *Nature*. 2012;483:176–181.
14. Gottlieb PA, Bae C, Sachs F. Gating the mechanical channel Piezo1: A comparison between whole-cell and patch recording. *Channels (Austin)*. 2012;6:282–289.
15. Soattin L, Fiore M, Gavazzo P, et al. The biophysics of Piezo1 and Piezo2 mechanosensitive channels. *Biophys Chem*. 2015;208:26–33.
16. Ge J, Li W, Zhao Q, et al. Architecture of the mammalian mechanosensitive Piezo1 channel. *Nature*. 2015;527:64–69.
17. Yang XN, Lu YP, Liu JJ, et al. Piezo1 is as a novel trefoil factor family 1 binding protein that promotes gastric cancer cell mobility in vitro. *Dig Dis Sci*. 2014;59:1428–1435.
18. Cahalan SM, Lukacs V, Ranade SS, Chien S, Bandell M, Patapoutian A. Piezo1 links mechanical forces to red blood cell volume. *Elife*. 2015;22:4. doi: 10.7554/eLife.07370
19. Bae C, Gnanasambandam R, Nicolai C, Sachs F, Gottlieb PA. Xerocytosis is caused by mutations that alter the kinetics of the mechanosensitive channel PIEZO1. *Proc Natl Acad Sci USA*. 2013;110:E1162–1168.
20. Li J, Hou B, Tumova S, et al. Piezo1 integration of vascular architecture with physiological force. *Nature*. 2014;515:279–282.
21. Faucherre A, Kissa K, Nargeot J, Mangoni ME, Jopling C. Piezo1 plays a role in erythrocyte volume homeostasis. *Haematologica*. 2014;99:70–75.
22. Albuisson J, Murthy SE, Bandell M, et al. Dehydrated hereditary stomatocytosis linked to gain-of-function mutations in mechanically activated PIEZO1 ion channels. *Nat Commun*. 2013;4:1884.
23. Andolfo I, Alper SL, De Franceschi L, et al. Multiple clinical forms of dehydrated hereditary stomatocytosis arise from mutations in PIEZO1. *Blood*. 2013;121:3925–3935.
24. Demolombe S, Duprat F, Honoré E, Patel A. Slower Piezo1 inactivation in dehydrated hereditary stomatocytosis (xerocytosis). *Biophys J*. 2013;105(4):833–834.
25. Epstein JI, Amin MB, Reuter VR, Mostofi FK. The World Health Organization/International Society of Urological Pathology Consensus Classification for urothelial (transitional cell) neoplasms of the urinary bladder. *Am J Surg Pathol*. 1998;22:1435–1438.
26. Yang H, Liu C, Zhou RM, et al. Piezo2 protein: A novel regulator of tumor angiogenesis and hyperpermeability. *Oncotarget*. 2016;7:44630–44643.
27. Zarychanski R, Schulz VP, Houston BL, et al. Mutations in the mechanotransduction protein PIEZO1 are associated with hereditary xerocytosis. *Blood*. 2012;120(9):1908–1915.
28. McHugh BJ, Murdoch A, Haslett C, Sethi T. Loss of the integrin-activating transmembrane protein Fam38A (Piezo1) promotes a switch to a reduced integrin-dependent mode of cell migration. *PLoS ONE*. 2012;7:e40346.
29. Li C, Rezania S, Kammerer S, et al. Piezo1 forms mechanosensitive ion channels in the human MCF-7 breast cancer cell line. *Sci Rep*. 2015;5:8364.
30. Martins JR, Penton D, Peyronnet R, et al. Piezo1-dependent regulation of urinary osmolarity. *Pflugers Arch*. 2016;468:1197–1206.

Structural changes arising from different thawing protocols on cryopreserved human allograft's aortic valve leaflets

Robert Novotný[1–3,A–F], Dáša Slížová[4,C], Jaroslav Hlubocký[1,2,E,F], Otakar Krs[4,B,C], Jaroslav Špatenka[5,6,A,E], Jan Burkert[5,6,B,C], Radovan Fiala[6,7,B], Petr Mitáš[1,2,D,E], Pavel Měricka[8,E,F], Miroslav Špaček[1,2,B], Zuzana Hlubocká[2,8,9,E], Jaroslav Lindner[1,2,A,F]

[1] 2nd Department of Cardiovascular Surgery, General University Hospital, Prague, Czech Republic
[2] 1st Faculty of Medicine, Charles University, Prague, Czech Republic
[3] Transplant Surgery Department, Institute for Clinical and Experimental Medicine, Prague, Czech Republic
[4] Department of Anatomy, Faculty of Medicine, Charles University, Hradec Králové, Czech Republic
[5] Transplant Center, University Hospital Motol, Prague, Czech Republic
[6] Department of Cardiovascular Surgery, Faculty Hospital Motol, Prague, Czech Republic
[7] 2nd Faculty of Medicine, Charles University, Prague, Czech Republic
[8] Tissue Bank, Faculty Hospital Hradec Králové, Faculty of Medicine, Charles University, Czech Republic
[9] 2nd Internal Department of Cardiology and Angiology, General University Hospital, Prague, Czech Republic

A – research concept and design; B – collection and/or assembly of data; C – data analysis and interpretation; D – writing the article; E – critical revision of the article; F – final approval of the article

Advances in Clinical and Experimental Medicine, ISSN 1899-5276 (print), ISSN 2451-2680 (online) *Adv Clin Exp Med.* 2018;27(8):1033–1036

Address for correspondence
Robert Novotný
E-mail: novotny_robert@hotmail.com

Funding sources
None declared

Conflict of interest
None declared

Acknowledgements
The authors would like to thank Prof. Jaroslav Lindner and MUDr. Jaroslav Hlubocký, PhD, from Charles University (Prague, Czech Republic) for providing their opinions and guidance on this research project.

Received on December 8, 2016
Reviewed on March 18, 2017
Accepted on May 12, 2017

DOI
10.17219/acem/73713

Abstract

Background. The aim of our experimental work was to assess the impact and morphological changes that arise during different thawing protocols on human aortic valve (AV) leaflets resected from cryopreserved aortic root allografts (CARAs).

Objectives. Two thawing protocols were tested: 1. CARAs were thawed at a room temperature (23°C); 2. CARAs were placed directly into a water bath at a temperature of 37°C. After all the samples were thawed, non-coronary AV leaflets were sampled from each specimen and fixed in a 4% formaldehyde solution before they were sent for morphological analysis.

Material and methods. All the samples were washed in distilled water for 5 min and dehydrated in a graded ethanol series (70%, 85%, 95%, and 100%) for 5 min at each level. The tissue samples were then immersed in 100% hexamethyldisilazane (HMDS) for 10 min, and then air-dried in an exhaust hood at room temperature. Processed samples were mounted on stainless steel stubs and coated with gold. Histological analysis was performed with the use of an electron microscope on a scanning mode operating at 25 kV – BS 301.

Results. Thawing protocol 1 (room temperature at 23°C): 6 (100%) samples showed loss of the endothelial covering of the basal membrane with no damage to the basal lamina. Thawing protocol 2 (water bath at 37°C): 5 (83%) samples showed loss of the endothelial covering of the basal membrane with no damage to the basal lamina. One (17%) sample showed loss of the endothelial covering the basal membrane with significant damage to the basal membrane.

Conclusions. Based on our experimental work, we can clearly conclude that cryopreserved AV leaflet allografts show identical structural changes at different rates of thawing.

Key words: aortic valve, allograft, thawing, cryopreserved, structural changes

Introduction

The first allograft transplants in cardiac surgery were freshly harvested aortic valves (AVs). The first fresh AV allograft transplant was performed by Murray in 1956.[1] Despite the imperfect hemodynamic outcome of the operation, the allograft performance was outstanding, with perfect leaflet function. Other early experimental and clinical trials, such as Heimbecker, Lam et al. and Kerwin et al., supported the superior properties of fresh AV allografts.[2–4] Nevertheless, the first successful operation with a patient surviving the fresh AV allograft transplant was performed by Ross in 1962, based on Brewin's experimental work.[5,6]

Many cardiac centers started to implement cryopreservation of fresh AV allografts due to the shortage of donors. Cryopreservation of AVs led to a significant decrease of allograft durability, and between the 1960s and the early 1970s this led almost to the abandonment of these types of procedures.[7] This was primarily due to irreversible damage to cell viability and loss of the structural integrity caused by thawing, resulting in the loss of allograft toughness and elastic properties.[8–10] Technical advances in tissue handling led to the reintroduction of allograft transplants back into use in cardiac surgery.[11] To date, there have been no recommended guidelines for cryopreservation and subsequent thawing of cryopreserved allografts that would eliminate damage to the cellular structures.

Material and methods

Allograft harvest and characteristics

All the allografts were harvested in the operation theater from patients that were organ donors and were pronounced "clinically dead" in compliance with the transplant laws of the Czech Republic.

Basic allograft characteristics for thawing protocol 1 (thawing at room temperature of 23°C) are summarized in Table 1. Basic allograft characteristics for thawing protocol 2 (thawing in a water bath at 37°C) are summarized in Table 2.

Allograft processing cryopreservation protocol

All human aortic roots (ARA) underwent an initial decontamination according to the standard protocol of the tissue bank. Afterward, all allografts were stored in an antibiotic cocktail comprised of Cefuroxime 0.2 mg/mL + Piperacillin 0.2 mg/mL + Netilmicin 0.1 mg/mL + Fluconazole 0.1 mg/mL in the tissue culture nutrient medium E 199 for 24 h at 37°C (Altimed Pharmaceutical, Mississauga, Canada). Subsequently, all ARA were moved into a cryoprotectant solution in a sterile laminar flow cabinet; they were packed using a double layer technique (sealed in Gambro Hemofreeze bags; NPBI BV; Gambro, Utrecht, the Netherlands). The cryoprotectant used was 10% dimethyl sulfoxide in the nutritional source for cell culture E 199. All ARA were then cooled at a controlled rate of –1°C/min from 10°C to –60°C, and next rapidly cooled and stored in cryo-containers with a liquid phase of liquid nitrogen at –196°C.

Table 1. Thawing protocol 1 – basic allografts characteristics

Gender	Donor age [years]	Aorta diameter [mm]	ABO, Rh compatibility
Female	55	21	A+
Female	41	21	A+
Male	55	25	AB+
Female	56	24	A+
Male	57	27	B+
Male	59	28	O-

Table 2. Thawing protocol 2 – basic allografts characteristics

Gender	Donor age [years]	Aorta diameter [mm]	ABO, Rh compatibility
Male	34	21	A-
Female	51	24	B+
Male	44	24	B+
Male	44	25	O-
Male	42	27	AB+
Female	37	27	A+

Thawing protocols

Experimental work was based on investigating 12 cryopreserved aortic root allografts (CARAs). They were randomly divided into 2 groups, each group consisting of 6 samples. All allografts were thawed in their original packaging (packed using double layer technique and immersed in 10% dimethyl sulfoxide). Two thawing protocols were tested:

- protocol 1: 6 human CARAs thawed at room temperature of 23°C; thawing times were as follows: min 2 h 49 min, max 4 h 5 min (median: 3 h 19 min);
- protocol 2: 6 human CARAs were placed directly into a water bath at 37°C; thawing times were as follows: min 26 min, max 41 min (median: 32 min).

After all the CARAs were thawed, non-coronary AV leaflets were sampled from each specimen and fixated in a 4% formaldehyde solution before they were sent for morphological analysis. The time variability in both thawing protocols was given by different allografts sizes (Tables 1,2), as well as different amounts of cryoprotectant used for each allograft during the cryopreservation process.

Table 3. Scoring system for electron microscope sample analysis

Score	Morphology
1	morphologically intact endothelium – putative physiological changes are not reflected in the superficial morphology of the endothelial cells
2	confluent endothelium with structural inhomogeneity – irregularities in the form of individual cells and changes of their membranes are detectable
3	disruption of intercellular contacts – continuity of the endothelial covering is lost, endotheliocytes shrink while still adhering to the basal membrane
4	separation of the endothelial cells – endotheliocytes separate from the basal lamina; initially they protrude by their intercellular edges into the lumen
5	complete loss of endothelium – denudation of the endothelial covering with the basal lamina exposed
6	damage of subendothelial layers – the valvular surface is covered only by the remnants of the basal membrane, the fiber structure of the lamina fibrosa and the lamina ventricularis may be dissolved

Microscopic slide preparation

After the thawing protocols were completed, non-coronary AV leaflets were resected and fixed in Baker's solution. Each sample was divided into 5–10 mm subsamples. In order to prevent artificial mechanical damage to the cellular structures, no mechanical stretching of the samples was performed. All samples were washed in distilled water for 5 min, and dehydrated in a graded ethanol series (70%, 85%, 95%, and 100%) for 5 min at each level. The tissue samples were then immersed in 100% hexamethyldisilazane (HMDS) (CAS No. 999-97-3; Fluka Chemie AG, Buchs, Switzerland) for 10 min and air-dried in an exhaust hood at room temperature.

Processed samples were mounted on stainless steel stubs, coated with gold and stored in a desiccator until they were studied and photographed by an electron microscope on scanning mode operating at 25 kV – BS 301. A special scoring system (from 1 to 6) was introduced to analyze the morphological changes of the arterial wall of ARA under the electron microscope (Table 3).[12]

Results

Histological analysis of the ARA arterial wall was as follows:

– thawing protocol 1 (thawing at room temperature of 23°C): 6 (100%) non-coronary AV leaflets showed loss of the endothelial cells covering the basal membrane with no damage to the basal lamina (score 5) (Fig. 1);
– thawing protocol 2 (water bath at 37°C): 5 (83%) non-coronary AV leaflets showed loss of the endothelial cells covering the basal membrane with no damage to the basal lamina (score 5); 1 (17%) non-coronary AV leaflet showed significant damage to the basal membrane (score 6) (Fig. 2).

After further investigation of the samples, it turned out that the severe damage of the non-coronary AV leaflet in thawing protocol 2 was caused by mechanical stresses exerted on the samples during dissection and microscopic sample preparation. The examined sample underwent slight stretching during microscopic slide preparation due to its size. This resulted in more severe structural damage compared to other samples.

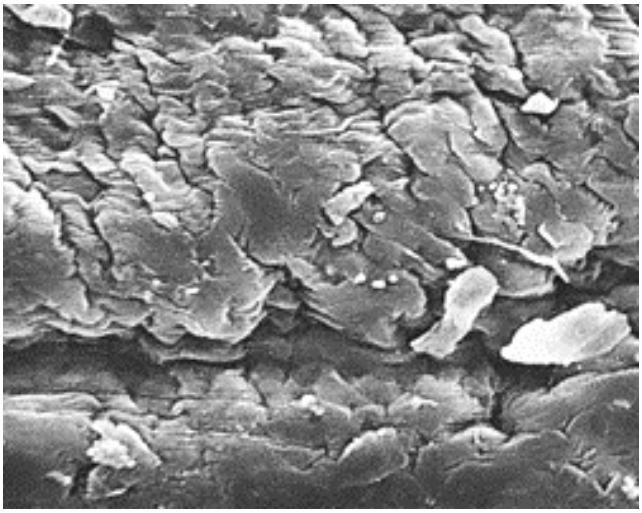

Fig. 1. Non-coronary AV leaflet (magnification: ×520); thawing at a room temperature (23°C)

AV – aortic valve.

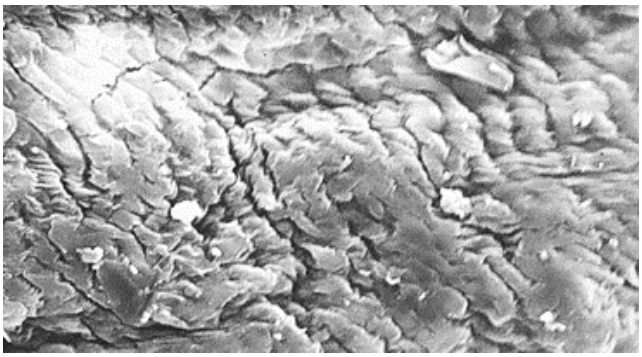

Fig. 2. Non-coronary AV leaflet (magnification: ×520); water bath at 37°C

AV – aortic valve.

Discussion

Since the first successful AV allograft transplant performed by Ross in 1962, over 25000 AV allografts have been implanted to date.[13] Over the time, the procedures of sterilization and storage have evolved immensely; from fresh aseptic harvest with immediate transplantation, through antibiotic sterilization and wet storage at 4°C, up to current antibiotic sterilization and cryopreservation.[14] Even though the durability

of fresh AV allografts is superior to cryopreserved AV allografts, the lack of donors has forced most of the cardiac centers to focus on allograft cryopreservation. Cryopreservation plays a major role in the degeneration of AV allografts, which subsequently leads to progressive calcification and fibrosis, affecting up to 1/4 of all implanted AV allografts.[13] Despite the negative impact of cryopreservation on AV allografts, Fukushima et al. showed that cryopreserved AV allografts were durable for over 15 years.[15] They also showed that allograft durability was closely associated with and affected by obesity and age of the recipient and donor. The most important factor was the surgical technique used during the allograft transplantation.[15] Our experimental results show identical structural changes in both examined thawing protocols; therefore, a faster rate of thawing theoretically does not necessarily mean that AV leaflets will be more structurally damaged or compromised; they would not require more frequent observation after implantation.

Another aspect that is thought to contribute to the cryopreserved AV allografts failure is gender mismatch. However, evidence behind this theory is imprecise, as gender matching is not done routinely before such transplants. Böll et al. demonstrated that gender-mismatched vs gender-matched allografts showed no significant difference in regard to death, need for reoperation and allograft function.[16]

Experimental work by Brockbank et al. showed significantly reduced extracellular matrix damage and well-preserved cellular structures in ice-free leaflets. They also demonstrated that cryopreservation of the transplants of the heart valves at −80°C prevents ice formation, and tissue cracking, and preserves extracellular matrix.[8,17] Improvements in modern antibiotic treatment of AV allografts before cryopreservation have had a significant impact on the infection resistance of AV allografts, as shown in their enhanced bacterial resistance.[18]

The use of cryopreserved allografts has become a gold standard in surgical procedures, such as Ross procedure, or in cases of bacterial endocarditis. However, there is growing evidence that decellularized engineered allografts may be superior to cryopreserved allografts.[19] Decellularized AV allografts have shown outstanding mid-term results after their implantation in terms of their stable structural integrity, low rate of calcification and hemodynamic properties.[20] Despite the promising short and mid-term results, long-term results are still not known.

Even though there have been efforts to minimize the damage inflicted by cryopreservation on AV allografts, there are still many factors that need thorough experimental and clinical examination in order to ensure allografts of highest possible quality and durability.

Conclusions

Our experimental work, based in structural changes occurring during different thawing protocols in cryopreserved AV leaflets, showed that different rates of thawing indicated identical structural changes. Therefore, the rate of thawing does not play a significant role in minimizing structural changes that occur during the thawing of cryopreserved AV leaflets.

References

1. Murray G. Homologous aortic-valve-segment transplants as surgical treatment for aortic and mitral insufficiency. *Angiology*. 1956;7(5):466–471.
2. Heimbecker RO. Durability of fresh homograft. *Ann Thorac Surg*. 1986;42(5):602–603.
3. Lam CR, Aram HH, Munnell ER. An experimental study of aortic valve homografts. *Surg Gynecol Obstet*. 1952;94(2):129–135.
4. Kerwin AG, Lenkei SC, Wilson DR. Aortic valve homograft in the treatment for aortic and mitral insufficiency. *N Eng J Med*. 1962;266:852–857.
5. Ross DN. Homograft replacement of the aortic valve. *Lancet*. 1962;2(7254):487.
6. Brewin EG. The use of tissue transplants in the surgery of cardiac valve disease: An experimental study. *Guys Hosp Rep*. 1956;105(3):328–329.
7. Merin G, McGoon DC. Reoperation after insertion of aortic homograft as a right ventricular outflow tract. *Ann Thorac Surg*. 1973;16(2):122–126.
8. Brockbank KG, Schenke-Layland K, Greene ED, et al. Ice-free cryopreservation of heart valve allografts: Better extracellular matrix preservation in vivo and preclinical results. *Cell Tissue Bank*. 2012;13(4):663–671. doi: 10.1007/s10561-011-9288-7
9. Gerson CJ, Elkins RC, Goldstein S, Heacox AE. Structural integrity of collagen and elastin in SynerGraft® decellularized-cryopreserved human heart valves. *Cryobiology*. 2012;64(1):33–42. doi: 10.1016/j.cryobiol.2011.11.001
10. Moussa M, Dumont F, Perrier-Cornet JM, Gervais P. Cell inactivation and membrane damage after long-term treatments at sub-zero temperature in the supercooled and frozen states. *Biotechnol Bioeng*. 2008;101(6):1245–1255. doi: 10.1002/bit.21981
11. Jashari R, Van Hoeck B, Ngakam R, Goffin Y, Fan Y. Banking of cryopreserved arterial allografts in Europe: 20 years of operation in the European Homograft Bank (EHB) in Brussels. *Cell Tissue Bank*. 2013;14(4):589–599. doi: 10.1007/s10561-012-9359-4
12. Krs O, Burkert J, Slízová D, Kobylka P, Špatenka J. Allograft semilunar cardiac valves processing and cryopreservation – morphology in scanning electron microscope. *Cell Tissue Bank*. 2006;7(3):167–173.
13. Nappi F, Al-Attar N, Spadaccio C, Chello M, Lusini M, Acar C. Aortic valve homograft: 10-year experience. *Surg Technol Int*. 2014;24:265–272.
14. Heng WL, Albrecht H, Chiappini P, Lim YP, Manning L. International heart valve bank survey: A review of processing practices and activity outcomes. *J Transplant*. 2013;2013:163150. doi: 10.1155/2013/163150
15. Fukushima S, Tesar PJ, Pearse B, et al. Long-term clinical outcomes after aortic valve replacement using cryopreserved aortic allograft. *J Thorac Cardiovasc Surg*. 2014;148(1):65–72.e2. doi: 10.1016/j.jtcvs.2013.07.038
16. Böll BM, Vogt F, Boulesteix AL, Schmitz C. Gender mismatch in allograft aortic valve surgery. *Interact Cardiovasc Thorac Surg*. 2015;21(3):329–335. doi: 10.1093/icvts/ivv151
17. Steffen V, Marsch G, Burgwitz K, Kuehn C, Teebken OE. Resistance to infection of long-term cryopreserved human aortic valve allografts. *J Thorac Cardiovasc Surg*. 2016;151(5):1251–1259. doi: 10.1016/j.jtcvs.2015.11.029
18. Neumann A, Cebotari S, Tudorache I, Haverich A, Sarikouch S. Heart valve engineering: Decellularized allograft matrices in clinical practice. *Biomed Tech (Berl)*. 2013;58(5):453–456. doi: 10.1515/bmt-2012-0115.
19. Tudorache I, Theodoridis K, Baraki H, et al. Decellularized aortic allografts versus pulmonary autografts for aortic valve replacement in the growing sheep model: Haemodynamic and morphological results at 20 months after implantation. *Eur J Cardiothorac Surg*. 2016;49(4):1228–1238. doi: 10.1093/ejcts/ezv362
20. da Costa FD, Costa AC, Prestes R, et al. The early and midterm function of decellularized aortic valve allografts. *Ann Thorac Surg*. 2010;90(6):1854–1860. doi: 10.1016/j.athoracsur.2010.08.022

Follow-up monitoring of physical activity after rehabilitation by means of a mobile application: Effectiveness of measurements in different age groups

Tomasz Saran[1,A–F], Agnieszka Pedrycz[2,A–F], Dawid Mucha[3,A–F], Dariusz Mucha[4,A–F]

[1] Department of General and Neurorehabilitation, Witold Chodźko Institute of Rural Health, Lublin, Poland
[2] Department of Histology and Embryology, Medical University of Lublin, Poland
[3] Institute of Humanities, Social Sciences and Tourism, Podhale State College of Applied Sciences in Nowy Targ, Poland
[4] Department of the Biological Renovation and Correction of Defects of Attitudes, Institute of Biomedicine, University School of Physical Education, Kraków, Poland

A – research concept and design; B – collection and/or assembly of data; C – data analysis and interpretation;
D – writing the article; E – critical revision of the article; F – final approval of the article

Advances in Clinical and Experimental Medicine, ISSN 1899-5276 (print), ISSN 2451-2680 (online) *Adv Clin Exp Med*. 2018;27(8):1037–1044

Address for correspondence
Dariusz Mucha
E-mail: nauka.autograf@gmail.com

Funding sources
The study was financed from statutory resources of the Witold Chodźko Institute of Rural Health, Lublin, Poland.

Conflict of interest
None declared

Received on December 3, 2016
Reviewed on January 25, 2017
Accepted on February 23, 2017

Abstract

Background. Active monitoring of the level of daily physical activity seems to be a useful element for secondary prevention in public health. Low physical activity increases the incidence of cardiovascular diseases, obesity, diabetes, musculoskeletal diseases, and causes loss of the previously achieved effects of rehabilitation.

Objectives. The purpose of this study was to assess the level of physical activity in different age groups of adults with the use of the telemedical system based on a mobile application.

Material and methods. The research covered data collected remotely from 927 individuals of both genders, aged 20—80 years (group I: 20—40 years, group II: 41—60 years, group III: 61—80 years). A monitoring system (Activity Measurement Tool) developed in the Department of General Rehabilitation at the Witold Chodźko Institute of Rural Health (Lublin, Poland) was used to measure home physical activity in the examined group. The system uses a dedicated mobile application, cellular data transmission and web data-showing software. Home physical activity was assessed using the International Physical Activity Questionnaire – Short Form (IPAQ-SF) and simultaneous processing of data from a smartphone accelerometer.

Results. The mean level of physical activity in the group of active application users (≥2 days, n = 494), expressed as Metabolic Equivalent of Task (MET)-min/week (IPAQ-SF), was as follows: group I (female participants (F): 5,767.9, n = 73; male participants (M): 4,888.4, n = 251), group II (F: 3,468.7, n = 24; M: 4,053.5, n = 119) and group III (M: 5,769.3, n = 27; no female participants were involved). In 72.3% of users, the registered physical activity was smaller in relation to IPAQ-assessed/7 days physical activity (sign test: n = 494; percentage of negative differences: 72.3%; Z = 9.9; p = 0.00).

Conclusions. The research findings indicate a high level of self-reported physical activity among the users in all age and gender groups, although it is not reflected in the level of registered activity. Although the level of daily physical activity was evaluated, it was mainly among young and middle-aged men who gladly and regularly made use of the measurement possibilities offered by mobile technology.

Key words: motor activity, aging, smartphone, telerehabilitation, patient monitoring

DOI
10.17219/acem/69131

Introduction

Contemporary medicine, making use of the rapid development of cellular telephony and mobile technologies with the use of a network of wireless broadband Internet (Long-Term Evolution – LTE), enables the opening of new opportunities in relations between the elderly or disabled people and the healthcare service.

Technologies which provide a means for continuous physiological monitoring of patients at home are especially useful in cardiac rehabilitation.[1,2] The innovation of telemedicine enables the supplementation of conventional medical care for hemiparetic patients in the patient's home.[3]

The problem of an ageing society is a tremendous challenge for contemporary medicine. Regular physical activity in this group of patients is an extremely important factor in not only primary, but even more so, in secondary prevention.[4] The findings from extensive research emphasize a strong correlation between regular physical activity and the prevention of many diseases, which is reflected in the improved quality of life in this population group.[5,6] Physical activity, not only in the group of elderly people, constitutes an important factor affecting a person's health condition. The development of civilization largely contributes to the progress of hypokinesis in society, which affects, to a large extent, the acceleration of the aging process and the development of many civilization-related diseases.[7–9] Research findings indicate that physical activity with a total energy expenditure higher than 4,200 kJ/week reduces the risk of developing ischemic heart disease by 30–50%, and reduces mortality even by 30%. Regular physical effort is used in the prevention of cancerous diseases, osteoporosis, type 2 diabetes and, as a result of increased energy expenditure, also overweight and obesity.[10,11]

The beneficial impact of physical activity is commonly known and is reflected in everyday life. Another problem is the development of reliable measurement tools. A particularly recommended research tool in the assessment of the level of physical activity in research environments, such as the European Physical Activity Surveillance System (EUPASS) or the European Health Interview Survey (EUROHIS), is the International Physical Activity Questionnaire (IPAQ), which enables the compilation of a comprehensive image of the physical activity of a given individual.[12]

The purpose of this paper was to assess the level of physical activity in different age groups of adults with the use of the telemedical system, using the IPAQ-short form and smartphone accelerometer data.

Material and methods

Study group

The research covered the analysis of data from 927 individuals of both genders (female participants (F): 24%; male participants (M): 76%); age range: 20–80 years. All individuals used the mobile application when performing different types of daily physical activity for 1–7 days (days with a short night break 10.00 pm–7.00 am), as well as 8 days and more. People using the application for 1 day, 8 h or shorter (n = 433) were excluded from the physical activity analysis (incorrect interpretation).

The examined group was divided by age into 3 subgroups: group I: 20–40 years (F: 29.9 ±5.4 years; M: 32.2 ±4.8 years) (69%); group II: 41–60 years (F: 48.8 ±6.1 years; M: 48.2 ±5.9 years) (27%), group III: 61–80 years (M: 65.9 ±4.2 years) (4%) (Fig. 1).

Diseases in the analyzed group of users were studied on the basis of a remote anonymous interview via a mobile application. In a great majority of subjects, no coexistence of diseases which could potentially have an impact on the degree of physical activity was confirmed. In group I, pulmonary and heart diseases were present only in 4% of the surveyed and bone diseases in 8%; in addition, the prevailing part of the group showed professional activity (76%) (Fig. 2). The situation was slightly different in group II, where heart diseases were present in 20% of the examined participants, pulmonary diseases only in 5% and bone diseases in 18%. As many as 75% of the examined people in this age group (41–60 years) were professionally active (Fig. 3). The frequency of the diseases increased with age, which is depicted in the distribution in group III. Cardiovascular system diseases were present in 37% of cases, pulmonary diseases were similar for groups I and II – present in 5% of cases, and skeletal system diseases were detected in as many as 39% of cases. Compared to other age groups, only 51% of the examined indicated professional activity (Fig. 4).

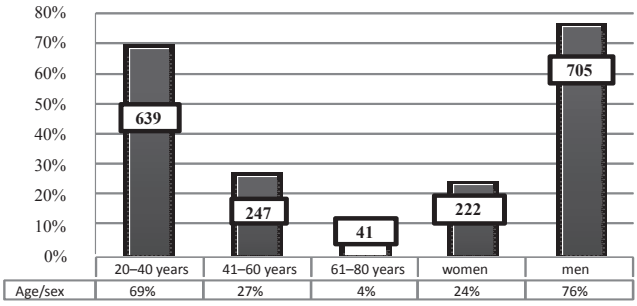

Fig. 1. Characteristics of the examined groups

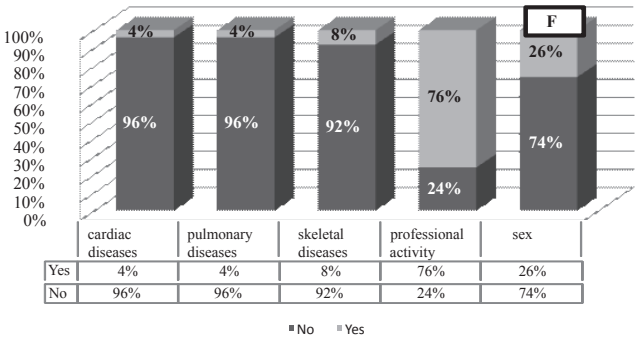

Fig. 2. Characteristics of the examined group in terms of coexisting diseases (20–40 years)

F – female participants.

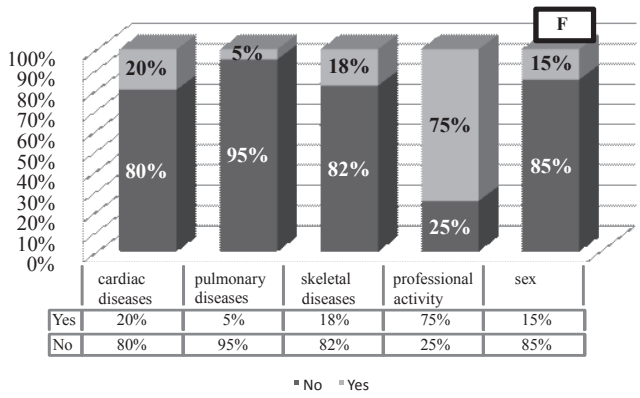

Fig. 3. Characteristics of the examined group in terms of coexisting diseases (41–60 years)

F – female participants.

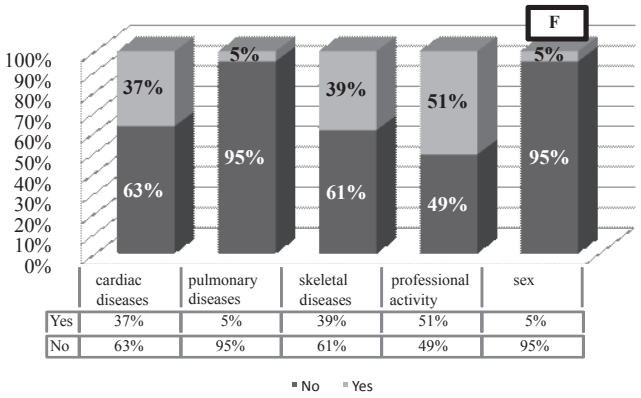

Fig. 4. Characteristics of the examined group in terms of coexisting diseases (61–80 years)

F – female participants.

Body mass index (BMI) was within normal limits only in the 20–40 age group – among females (24.4 ±4.7 kg/m^2) and in male participants (26.8 ±4.5 kg/m^2), and increased with age, indicating overweight. In the following groups BMI was higher then healthy range: II F – 27 ±3.9 kg/m^2; M – 28.3 ±4.6 kg/m^2, III M – 27.5 ±3.3 kg/m^2.

Procedures

An innovative telemedical system developed in the Department of General Rehabilitation at the Witold Chodźko Institute of Rural Health (Activity Measurement Tool) was applied to assess the measurement of physical activity in the examined groups.[13] The system makes use of cellular data transmission and the potential of smartphones.

Table 1. Parameters assessing the level of physical activity in the examined groups

Parameter	20–40 years		41–60 years		61–80 years	
Sex	F (n = 73)	M (n = 251)	F (n = 24)	M (n = 119)	F (n = 0)	M (n = 27)
Age [years]	29.9 ±5.4 20–39	32.2 ±4.8 21–40	48.8 ±6.1 41–59	48.2 ±5.9 41–60	NONE The group aged 61–80 years included 2 women – both used the application for 1 day	65.9 ±4.2 61–77
BMI [kg/m^2]	24.4 ±4.7 16.9–39.3	26.8 ±4.5 16.3–45.6	27 ±3.9 21.3–36.8	28.3 ±4.6 21.1–44.6		27.5 ±3.3 21–36.2
Days of intensive physical activity	1.9 ±1.7 0–7	1.6 ±1.7 0–7	1.4 ±1.3 0–5	1.5 ±1.7 0–7		2.6 ±1.8 0–6
Time of intensive physical activity [min]	93.3 ±90.6 0–360	71.9 ±96.4 0–600	76.9 ±71.3 0–280	62 ±84.2 0–480		92.9 ±91.3 0–360
Days of moderate physical activity	2.8 ±2.1 0–7	2.8 ±2.2 0–7	2.6 ±2.4 0–7	2.8 ±2.1 0–7		4.3 ±2.4 0–7
Time of moderate physical activity [min]	114 ±105.4 0–480	104.4 ±126.9 0–780	97.8 ±108.8 0–420	100.3 ±109.1 0–720		85.5 ±71.4 0–300
Days of walking	5.5 ±2.1 0–7	5.1 ±2.4 0–7	4.2 ±2.6 0–7	5.1 ±2.3 0–7		6.1 ±1.5 2–7
Time of walking [min]	106.8 ±113.9 0–600	77.2 ±108 0–840	50.7 ±37.5 0–120	71.2 ±72 0–360		83.1 ±67.7 0–240
MET-min/week ±SD (intensive efforts)	1,826 ±2,853.3 0–16,240	1,669.4 ±3,849.6 0–28,800	1,172 ±1,264.5 0–4,480	1,397.3 ±3,268.9 0–26,880		2,568.6 ±3,928.1 0–17,280
MET-min/week ±SD (moderate efforts)	1,729.1 ±2,281.2 0–10,080	1,710.7 ±2,859.1 0–21,840	1,446.8 ±2,534.3 0–11,760	1,302.5 ±1,551.9 0–7,800		1,424.7 ±1,304.8 0–4,800
MET-min/week ±SD (walking)	2,212.8 ±2,637.5 0–13,860	1,508.3 ±2,476.1 0–19,404	849.9 ±953.3 0–2,772.2	1,353.7 ±1,582.4 0–7,623		1,775.9 ±1,602.7 0–5,544
Total score IPAQ-SF MET-min/week ±SD	5,767.9 ±5,254.4 149–23,650	4,888.4 ±6,774.0 0–53,004	3,468.7 ±3,126.2 33–13,146	4,053.5 ±4,890.8 0–37,392		5,769.3 ±5,510.6 450–23,544
Registered activity (mean accelerometer data per one day) MET-min/day ±SD	639.4 ±1,726.7 22.2–14,062.5	364.7 ±1,609.8 5–18,124.4	364 ±635.9 5.2–2,508.1	362.5 ±1,008.8 6.1–10,201		516.6 ±524.7 10.2–1,997.2

BMI – body mass index; F – female participants; M – male participants; MET – Metabolic Equivalent of Task; IPAQ-SF – International Physical Activity Questionnaire – Short Form; SD – standard deviation.

The purpose of the developed application was to maintain rehabilitation effects by motivating the users to lead an active lifestyle after the end of individual rehabilitation programs for low-back pain and other musculosceletal disturbances.

The application uses the telemedical potential of contemporary smartphones and is available free of charge. Registered individuals may use "reverse communication" and, at the same time, remain under the supervision of a specialized team of physicians and physiotherapists. People seeing a physiotherapist have the opportunity to receive explanations and answers to questions about the telemonitoring system.

Physiotherapists have an opportunity to individually follow their patients at home by means of web software.

Consent for medical monitoring and scientific evaluation of anonymous data was expressed during the installation of the application.

The assessment of the intensity and frequency of physical activity was obtained by processing data from the accelerometer of the application and using International Physical Activity Questionnaire – Short Form, average week (IPAQ-SF). As a result, information was collected regarding time spent in the sitting position, time dedicated to walks, and moderate and intensive physical activity. Additional questions included in the application made it possible to gather information about comorbidities (heart, pulmonary, musculoskeletal) or calculate body mass index (BMI).

The particular types of physical activity may be expressed by the unit Metabolic Equivalent of Task (MET)-min/week, by multiplying the coefficient assigned to a given physical activity (walking – 3.3; moderate activity – 4.0; intensive activity – 8.0) by the number of days (a week) and the amount of time (min) when a given patient engages in physical activity. Summing-up the findings of every kind of physical activity, a 1-week measurement was obtained for a given individual, on the basis of which patients were assigned to particular groups, depending on the level of the intensity of physical activity:

– high – 3 or more days of intensive physical effort (min 1,500 MET-min/week); 7 or more days of any combination of efforts (walking, moderate/intensive efforts exceeding 3,000 MET-min/week);

– sufficient – 3 or more days of intensive physical efforts (min 20 MET-min/day); 5 or more days of moderate efforts or walking (min 30 min/day); 5 or more days of any combination of efforts (walking, moderate/intensive efforts exceeding 600 MET-min/week);

– insufficient (level of physical activity insufficient to fulfill the conditions of high/sufficient level, or lack of physical activity).

The criteria used to assess the level of physical activity take account of the present health recommendations, the basis of which is regular physical activity.[14]

In the research, the measurement of physical activity was obtained by processing data from the accelerometer in the user's smartphone thanks to empirically prepared algorithms, eliminating the impact of the sensitivity of the accelerometer and separate factors, such as the location of the user's smartphone. Two kinds of calibration were used: static and dynamic. The value of gravitational acceleration was measured on an accelerometer (static calibration) by placing the mobile phone flat and pressing the measuring button for 3 s ($g = \mathrm{sqrt}(x^2 + y^2 + z^2)$), and then calculating the average of measurements for 3 s (x, y, z → temporary components of acceleration from the accelerometer). To eliminate the differences of sensitivity of accelerometers related to different types of smartphones, but also to the different places smartphones are in during the day (trousers, shirt), dynamic calibration was used. The smartphone user was asked to push the button that activates the application and walk on flat ground for 1 min until he/she received the calibration completion signal (dynamic correction = 3.3/MET-min for 1 min of walking) (Fig. 5). Calibrating parameters were obtained by multiple adjustments of calculation coefficients on the basis of tests carried out in the Activities Test Laboratory of the Institute of the Witold Chodźko Institute of Rural Health in Lublin. The measurement algorithm, application and network software were developed in cooperation with mobilesqerbox (Grzegorz Golec).

The system made it possible to adjust daily motor activity based on the interviews and anthropometric data of the user. The application monitors daily physical activity from 7 am to 11 pm and – through a diagram of a filling heart and text messages – motivates the user to intensify physical activity (Fig. 6). The most important element of the application is sending a data package to the server of the Institute once a day – the data is presented on collective charts, and in this way secure access to any measurement data is enabled. Data from the survey and measurements is collected by web software in the form of anonymous records available for researchers, however, without the

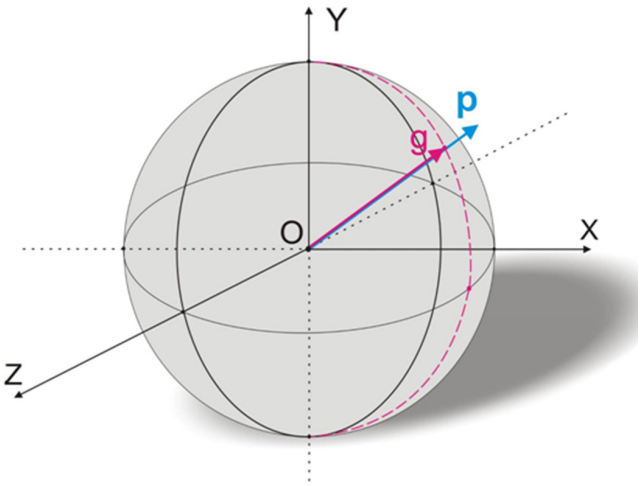

Fig. 5. Method of processing data from an accelerometer

Measurement of activity from an accelerometer MET-min = $\sum(|p - g|)$; the sum of activity for each minute estimated as the absolute value of differences in accelerations p and g.

Fig. 6. Measuring application (application interface) and a sample reading of physical activity of 1 user (web data-showing interface)

possibility of personal identification of the user without their consent.

Statistical analysis

Statistical data was prepared using STATISTICA v. 12.0 software (StatSoft Polska Sp. z o.o., Kraków, Poland) and basic descriptive statistics, sign tests and Spearman's R correlation.

Ethical approval

The study was performed in compliance with the World Medical Association Declaration of Helsinki on ethical principles for medical research involving human subjects. The authors requested the opinion of the Ethics Committee at the Institute of Rural Health and obtained consent for the study. Participants of the study were informed about the goal of the study and approach to be used. Consent was signed by all the participants prior to the study.

Results

In the assessment of the level of physical activity, the most important element was time and the number of days of physical activity above the average 7 days and according to IPAQ. Efforts at the intensive level were taken, on average (MET-min/week ±SD), in group I: F – 1,826 ±2,853.3; M – 1,669.4 ±3,849.6; in group II: F – 1,172 ±1,264.5; M – 1,397.3 ±3,268.9; and

in group III: F – n = 0; M – 2,568.6 ±3,928.1. Efforts at the moderate level were taken, on average, in group I: F – 1,729.1 ±2,281.2; M – 1,710.7 ±2,859.1; in group II: F – 1,446.8 ±2,534.3; M – 1,302.5 ±1,551.9; and in group III: F – n = 0; M – 1,424.7 ±1,304.8. The effort connected with walking was as follows: group I: F – 2,212.8 ±2,637.5; M – 1,508.3 ±2,476.1; group II: F – 849.9 ±953.3; M – 1,353.7 ±1,582.4; group III: F – n = 0; M – 1,775.9 ±1,602.7. The total level of physical activity expressed as MET-min/week ±SD amounted to: in group I: F – 5,767.9 ±5,254.4; M – 4,888.4 ±6,774.0); in group II: F – 3,468.7 ±3,126.2; M – 4,053.5 ±4,890.8; and in group III: F – n = 0; M – 5,769.3 ±5,510.6. The research results indicate that, according to a subjective assessment of the users, the whole group can be qualified into physical activity at a high level (1,500–3,000 MET-min/week). However, taking into account the average number of days of performing various physical activities, the group exceeded standards for this level of activity. Characteristic of the high level was activity on at least 3/7 days, and for the sufficient level – 3/5 days. The average value of days of intensive physical effort occurred in group I: F – 1.9 ±1.7; M – 1.6 ±1.7; group II: F – 1.4 ±1.3; M – 1.5 ±1.7; group III: F – n = 0; M – 2.6 ±1.8. The average value of days of moderate physical effort occurred in group I: F – 2.8 ±2.1; M – 2.8 ±2.2; group II: F – 2.6 ±2.4; M – 2.8 ±2.1; group III: F – n = 0; 4.3 ±2.4. The criterion was fulfilled by walking activity in group I: F – 5.5 ±2.1; M – 5.1 ±2.4; group II: F – 4.2 ±2.6; M – 5.1 ±2.3; group III: F – n = 0; M – 6.1 ±1.5, which made it possible to qualify the group into the level of sufficient activity. This level is characterized by effort in various combinations of activity; therefore, objectively, the group should be qualified to the level of insufficient physical activity (Table 1).

Table 2. Assessment of the level of real physical activity in the examined group

Sign test				
variables	n	percentage of negative differences	Z	p-value
Real activity and declared activity	494	72.3%	9.9	0

Registered 1-day mean activity of the analyzed individuals: group I: F – 639.4 ±1,726.7; M – 364.7 ±1,609.8; group II: F – 364 ±635.9; M – 362.5 ±1,008.8; group III: F – n = 0; M – 516.6 ±524.7. In 72.3% of users in the examined group, registered 1-day activity was smaller in relation to IPAQ-assessed activity per 1 day (sign test: n = 494; percentage of negative differences: 72.3%; Z = 9.9; p = 0.00) (Table 2).

The research findings indicate the existence of a positive correlation between age and BMI in the examined group (F = 0.246, M = 0.235; p < 0.05000) (Table 3). Body mass index was the highest in group II (41–60 years); the lowest level of physical activity was also observed in this group (MET-min/week). The group of the oldest people, in spite of a high BMI (overweight), showed the highest level of self-reported physical activity in relation to other groups (Table 1; Fig. 7,8).

Table 3. Correlations of parameters: BMI, MET and age in the examined group

Variable	Spearman's rank-order correlation p < 0.05000			
	sex	age	BMI [kg/m^2]	MET
Age	M	1.000	0.235*	–0.019
BMI [kg/m^2]	M	0.235*	1.000	–0.048
MET-min/week	M	–0.019	–0.048	1.000
Age	F	1.000	0.246*	–0.174
BMI [kg/m^2]	F	0.246*	1.000	–0.030
MET-min/week	F	–0.174	–0.030	1.000

* significant correlation; BMI – body mass index; MET – Metabolic Equivalent of Task; F – female; M – male.

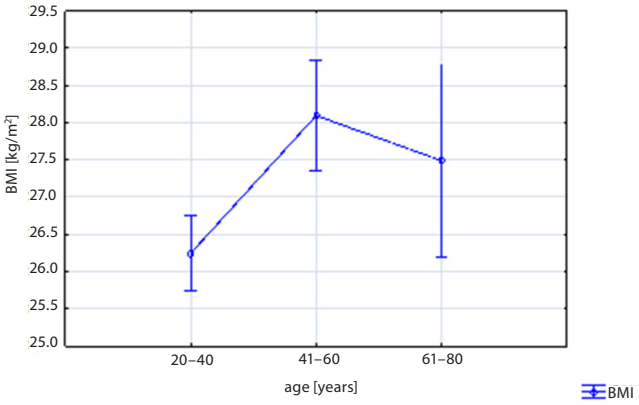

Fig. 7. Assessment of BMI in the examined age groups. Average chart, confidence interval 95%

BMI – body mass index.

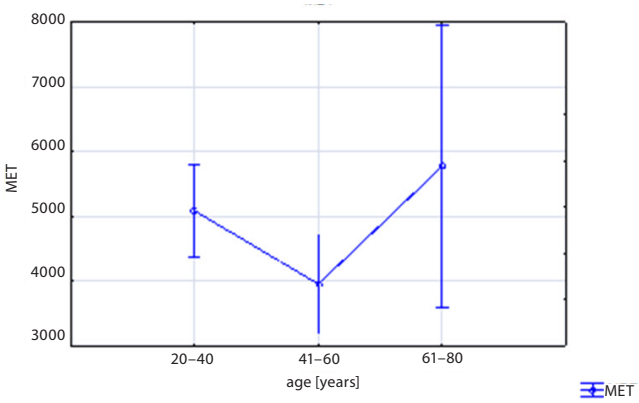

Fig. 8. Assessment of MET-min/week total IPAQ-SF in the examined age groups. Average chart, confidence interval 95%

MET – Metabolic Equivalent of Task.

Discussion

Effective monitoring of the level of physical activity of the population is an essential element for primary and secondary prevention in public health.[15] The implementation

of prevention programs requires the assessment of the level of physical activity in different subpopulations. Research findings indicate that as much as 31.1% of the population worldwide are inactive adults, ranging from 17% in south-eastern Asia to about 43% in America and the eastern part of the Mediterranean Sea. In addition, lack of movement increases with age, especially in highly-developed countries, with a higher trend in the population of women.[16]

According to the guidelines of the World Health Organization (WHO), to counteract the development of civilization-related diseases and sustain health in adults (18–64 years), it is advisable to undertake physical activity at a moderate level (≥150 min/week) or intensive level (≥75 min/week), or an equivalent combination of both physical efforts.[17] The findings of the presented study indicate that only in the group of women – group I: 93.3 ±90.6 and group II: 76.9 ±71.3, and in the group of men – group III: 92.9 ±91.3, the conditions for making intensive efforts were fulfilled. In groups I and II (M), the average time of intensive activity was too low – group I: 71.9 ±96.4; group II: 62 ±84.2. On the other hand, no group fulfilled the criteria for moderate effort – group I: F – 114 ±105.4; M – 104.4 ±126.9; group II: F – 97.8 ±108.8; M – 100.3 ±109.1; group III: M – 85.5 ±71.4.

Regular physical activity plays an important role in the reduction of body mass.[18,19] Recent research findings made it possible to prepare detailed criteria for the activity of people with overweight or obesity. Moderate activity (60–90 min/day) is necessary to reduce BMI and maintain weight at the appropriate level. In the current study, average values in terms of time of activity relate to the whole week, which indicates an insufficient level of physical effort. Scott et al. emphasize that the effectiveness of physical activity takes place during efforts lasting ≥10 min, and an increase in its level affects reduction in body mass.[20] In this paper, the existence of a positive correlation between age and BMI in the examined group was observed: (F – 0.246, M – 0.235; $p < 0.05000$). Body mass index was the highest in group II (41–60 years); the lowest level of physical activity (MET-min/week) was also recorded in this group. In spite of high BMI (overweight), the oldest age group showed the highest level of physical activity in relation to other groups. In addition, the findings of multi-center research emphasize that an unsuitable level of physical activity, or its lack, is strictly associated with the development of civilization-related diseases, which, in consequence, cause 1.9 million deaths worldwide.[21,22]

Research conducted in 8 countries of the European Union assessed the level of physical activity among a large group of the population. The statistical data for particular countries were as follows: Belgium – 67 MET-h/week, Finland – 70.2 MET-h/week, France – 63.8 MET-h/week, Germany – 84.5 MET-h/week, Italy – 19.6 MET-h/week, the Netherlands – 56.4 MET-h/week, Spain – 39.3 MET-h/week, and the UK – 27.6 MET-h/week.[23] The findings of the presented study, after conversion of MET-min/week into MET-h/week, were as follows: group I: F – 96.1; M – 81.4; group II: F – 57.9; M – 67.5; group III: F – n = 0; M – 96.1. The level of physical activity in the examined groups was relatively high, which enables the qualification of the users into the level of high activity. However, taking into account the average number of days of performing various physical activities, the group exceeded the standards for this level of activity. A characteristic of the high level of activity was at least 3/7 days, and the sufficient level at 3/5 days. The average number of days of intensive physical effort in group I: F – 1.9 ±1.7; M – 1.6 ±1.7; group II: F – 1.4 ±1.3; M – 1.5 ±1.7; group III: F – n = 0; M – 2.6 ±1.8. The average number of days of moderate physical effort in group I: F – 2.8 ±2.1; M – 2.8 ±2.2; group II: F – 2.6 ±2.4; M – 2.8 ±2.1; group III: F – n = 0; M – 4.3 ±2.4. The only fulfilled criterion by activity was in walking in group I: F – 5.5 ±2.1; M – 5.1 ±2.4; group II: F – 4.2 ±2.6; M– 5.1 ±2.3; group III: F – n = 0; M – 6.1 ±1.5, which enables qualifying the group into the level of sufficient activity. This level is characterized by various combinations of activity; therefore, objectively, the group should be qualified to the level of insufficient physical activity. Shephard emphasizes that in subjective assessment, individuals most often significantly raise the real level of activity, which is confirmed by the present research, which shows that in as many as 72.3% of subjects, the real activity was lower than the declared activity (self-reported) (Table 2).[24]

One of the fundamental problems in measuring the level of physical activity in everyday life of an individual is the development of a precise way of assessment. Many methods have been developed for the promotion of strategies for physical activity, including, among others, IPAQ, which is used worldwide.[25] Many studies indicate the high reliability of this method, not only in the measurement of time and intensity of physical effort, but, above all, the assessment of total energy expenditure within the whole week.[26,27] The IPAQ has been developed for the age range 15–69 years, although it is increasingly more often used in the group of elderly people.[28] In this study, the examined group was divided into 3 age subgroups: I – 20–40 years, II – 41–60 years, III – 61–80 years, in order to check the intensity and degree of physical activity in these age groups, including elderly people. Apart from IPAQ, the telemedical potential of contemporary smartphones was used, thanks to which it was possible to assess the actual level of daily physical activity, and the results were compared with the declared values in a given application user. The research showed the level of registered physical activity as being lower, although through using the application the result can be monitored, and if it is too low, it is possible to change it by motivating and, even more so, by educating the user.

Limitations of the study

The objective of the study was achieved; nevertheless, attention should be paid to the limitations which occur

mainly in the area of measurements of physical activity, and result from the natural characteristics of telemedical measurements. The first limitation is a varied duration and continuity of independently performed measurements of physical activity after rehabilitation. Another limitation is the way of completing IPAQ-SF. In the present study, a survey was performed via a mobile application. The application contains detailed hints and guidelines to individual questions; however, IPAQ, according to its authors, was designed to be completed in a written form or on telephone. The abovementioned shortcomings result in a considerable variability of the results of measurements in individual groups, which limits the possibilities of drawing conclusions.

Conclusions

As a result of using the mobile application and the telemedical system developed at the Witold Chodźko Institute of Rural Health, it is possible to assess the level of physical activity at home, although mainly among younger people (<60), who gladly make use of the measurement possibilities of the smartphone, which indicates the usefulness of this low cost method in the active maintenance of the effects of general rehabilitation.

References

1. Frederix I, Vanhees L, Dendale P, Goetschalckx K. A review of telerehabilitation for cardiac patients. *J Telemed Telecare*. 2015;21:45–53.
2. Whittaker F, Wade V. The costs and benefits of technology-enabled, home-based cardiac rehabilitation measured in a randomised controlled trial. *J Telemed Telecare*. 2014;20:419–422.
3. Seiter J, Derungs A, Schuster-Amft C, Amft O, Tröster G. Daily life activity routine discovery in hemiparetic rehabilitation patients using topic models. *Methods Inf Med*. 2015;54(3):248–255.
4. Buchner DM. Physical activity and prevention of cardiovascular disease in older adults. *Clin Geriatr Med*. 2009;25(4):661–675.
5. Spirduso WW, Cronin DL. Exercise dose-response effects on quality of life and independent living in older adults. *Med Sci Sports Exerc*. 2001;33(6):598–608.
6. Taylor AH, Cable NT, Faulkner G, et al. Physical activity and older adults: A review of health benefits and the effectiveness of interventions. *J Sports Sci*. 2004;22(8):703–725.
7. Parkkari J, Natri A, Kannus P, et al. A controlled trial of the health benefits of regular walking on a golf course. *Am J Med*. 2000;109(2):102–108.
8. Wannamethee GS, Shaper GA, Walker M. Physical activity and risk of cancer in middle-aged men. *Br J Cancer*. 2001;85(9):1311–1316.
9. Waxman A. WHO's global strategy on diet, physical activity and health response to a worldwide epidemic of non-communicable diseases. *Scand J Nutrition*. 2004;48:58–60.
10. Abu-Omar K, Rutten A, Lahtinen V. Mental health and physical activity in the European Union. *Soz Praventivmed*. 2004;49:301–309.
11. Raglin J, Wilson GS, Galper D. Exercise and its effects on mental health. In: Bouchard C, Blair SN, Haskell WL, eds. *Physical Activity and Health*. Champaign, IL: Human Kinetics; 2007.
12. International Physical Activity Questionnaire: Ki. http://www.ipaq.ki.se. Accessed June 8, 2016.
13. Saran T, Horoch A. Telemedyczne podtrzymywanie aktywności ruchowej za pomocą smartfonów – system telemonitorujący w Instytucie Medycyny Wsi [in Polish]. *MONZ*. 2013;19(4):500–503.
14. Pate RR, Prat M, Blair SN, et al. Physical activity and public health. A recommendation from the Centers for Disease Control and Prevention and the American College of Sports Medicine. *J Am Med Assoc*. 1995;273(5):402–407.
15. Brown WJ, Trost SG, Bauman A, Mummery K, Owen N. Test-retest reliability of four physical activity measures used in population surveys. *J Sci Med Sport*. 2007;7(2):205–215.
16. Hallal PC, Andersen LB, Bull FC, Guthold R, Haskell W, Ekelund U. Global physical activity levels: Surveillance progress, pitfalls, and prospects. *Lancet*. 2012;380(9838):247–257.
17. *Global Recommendations on Physical Activity for Health*. Geneva: World Health Organisation; 2010.
18. Hemmingsson E, Ekelund U. Is the association between physical activity and body mass index obesity dependent? *Int J Obes (Lond)*. 2007;31(4):663–668.
19. Haskell WL, Lee IM, Pate RR, et al. Physical activity and public health: Updated recommendations for adults from the American College of Sports Medicine and the American Heart Association. *Med Sci Sport Exer*. 2007;39(8):1423–1434.
20. Scott JS, Holleman RG, Richardson CR, Ronis DL, Swartz AM. Objective physical activity accumulation in bouts and nonbouts and relation to markers of obesity in US Adults. *Prev Chronic Dis*. 2008;5(4):A131.
21. Singh RB, Pella D, Mechirova V, et al.; The Five City Study Group. Prevalence of obesity, physical inactivity and undernutrition, a triple burden of diseases during transition in a developing economy. *Acta Cardiol*. 2007;62:119–27.
22. *The World Health Report 2002: Reducing Risk, Promoting Health Life*. Geneva: World Health Organization; 2002:61.
23. Rutten A, Ziemainz H, Schena F, et al. Using different physical activity measurements in eight European countries. Results of the European Physical Activity Surveillance System (EUPASS) time series survey. *Public Health Nutr*. 2003;6:371–376.
24. Shephard RJ. Limits to the measurement of habitual physical activity by questionnaires. *Br J Sports Med*. 2003;37:197–206.
25. Meisinger C, Lowel H, Thorand B, Doring A. Leisure time physical activity and the risk of type 2 diabetes in men and women from the general population. The MONICA/KORA Augsburg Cohort Study. *Diabetologia*. 2005;48:27–34.
26. Deng HB, Macfarlane DJ, Thomas GN, et al. Reliability and validity of the IPAQ-Chinese: The Guangzhou Biobank Cohort study. *Med Sci Sports Exerc*. 2008;40:303–307.
27. Kwak L, Proper KI, Hagströmer M, Sjöström M. The repeatability and validity of questionnaires assessing occupational physical activity – a systematic review. *Scand J Work Environ Health*. 2011;37(1):6–29.
28. Grimm EK, Swartz AM, Hart T, et al. Comparison of the IPAQ-Short Form and accelerometry predictions of physical activity in older adults. *J Aging Phys Act*. 2012;20:64–79.

Performance evaluation of HBsAg by Lumipulse HBsAg-HQ: The agreement with HBsAg by Architect HBsAg-QT and the effectiveness in predicting liver tissue pathological states of chronic hepatitis B patients

Zhanqing Zhang[1,A,C,D,F], Rongrong Ding[1,B,D], Wei Lu[1,B,E], Zhiqiang Yang[2,E], Yanbing Wang[1,B], Xinlan Zhou[1,B], Dan Huang[1,B], Xiufen Li[1,B], Yanling Feng[1,B]

[1] Shanghai Public Health Clinical Center, Fudan University, China
[2] Fujirebio Shanghai Representative Office, China

A – research concept and design; B – collection and/or assembly of data; C – data analysis and interpretation; D – writing the article; E – critical revision of the article; F – final approval of the article

Advances in Clinical and Experimental Medicine, ISSN 1899-5276 (print), ISSN 2451-2680 (online) *Adv Clin Exp Med*. 2018;27(8):1045–1054

Address for correspondence
Zhanqing Zhang
E-mail: doctorzzqsphc@163.com

Funding sources
This work was supported by the "The Twelfth Five-Year" National Science and Technology Key Projects of China (No. 2013ZX10002005), and the key scientific research project of Shanghai Municipal Health and Family Planning Commission of China (No. 20134032).

Conflict of interest
None declared

Acknowledgements
The Lumipulse HBsAg kits were kindly provided by Fujirebio Shanghai Representative Office.

Received on October 28, 2016
Reviewed on January 29, 2017
Accepted on March 1, 2017

Abstract

Background. A novel high-sensitivity HBsAg quantification assay, Lumipulse HBsAg-HQ, was developed. However, its performance in practical application has not yet been adequately investigated.

Objectives. The aim of the study was to evaluate the agreement of serum HBsAg by Lumipulse HBsAg-HQ (HBsAg-HQ) with HBsAg by Architect HBsAg-QT (HBsAg-QT) and comparatively investigate the efficacy of serum HBsAg-HQ and HBsAg-QT in predicting the liver tissue pathological states of chronic hepatitis B (CHB) patients.

Material and methods. A total of 147 HBeAg-positive and 128 HBeAg-negative patients were enrolled. HBsAg-HQ and HBsAg-QT were measured using CLEIA Lumipulse G1200 and CMIA Abbott Architect I2000 automatic analyzer, respectively. The Scheuer standard was used for the pathological diagnosis of liver tissue samples.

Results. In both HBeAg-positive and HBeAg-negative patients, HBsAg-HQ was significantly positively correlated with HBsAg-QT ($r = 0.913$ and $r = 0.959$, respectively), the overall disagreement rates between HBsAg-HQ and HBsAg-QT were 2.72% (4/147) and 4.69% (6/128), respectively. In HBeAg-positive patients, the area under the ROC curve (AUC) of HBsAg-HQ and HBsAg-QT for predicting the grade ≥G3 (0.686 and 0.684, respectively) and stage ≥S4 (0.739 and 0.745, respectively) were the greatest compared with other pathological states; the optimal cutoffs of HBsAg-HQ and HBsAg-QT for predicting the grade ≥G3 were $<2.244 \times 10^7$ mIU/mL and $<3.589 \times 10^7$ mIU/mL, and those for predicting the stage ≥S4 were 7.328×10^6 mIU/mL and $<6.194 \times 10^6$ mIU/mL, respectively.

Conclusions. HBsAg-HQ is highly correlated and in agreement with HBsAg-QT in both HBeAg-positive and HBeAg-negative patients; HBsAg-HQ and HBsAg-QT are very valuable in predicting the grade ≥G3 and stage ≥S4 in HBeAg-positive patients.

Key words: hepatitis B surface antigen, performance evaluation, Lumipulse HBsAg-HQ, pathology, non-invasive diagnosis

DOI
10.17219/acem/69247

Introduction

The detection of serum hepatitis B surface antigen (HBsAg) is the leading hallmark for screening and diagnosing hepatitis B virus (HBV) infection. In the past 10 years, serum HBsAg quantification assays have been developing rapidly. Among them, Architect HBsAg-QT (Abbott Laboratories, Chicago, USA) and Elecsys HBsAg II (Roche Diagnostics GmbH, Mannheim, Germany) have been widely studied and preliminary applied.[1–4] Several studies have demonstrated that the levels of serum HBsAg are different during the various phases of natural history and are associated with the liver tissue pathological states of chronic HBV infection.[5–8] Furthermore, some evidence has reinforced its value in predicting drug efficacy and evaluating the prognosis in patients with chronic hepatitis B (CHB).[9,10]

Recently, a novel high-sensitivity linearized HBsAg quantification assay, Lumipulse HBsAg-HQ (Fujirebio Inc., Tokyo, Japan), was developed.[11] The original studies on this assay indicated that the detection of serum HBsAg by Lumipulse HBsAg-HQ (HBsAg-HQ) could potentially assist in diagnosing occult hepatitis B infection[12–15] and showed consistent results with the qualitative and quantitative detection of serum HBsAg by Architect HBsAg-QT (HBsAg-QT) and HBsAg by Elecsys HBsAg II (HBsAg-E II).[16,17] However, the correlation between the serum HBsAg-HQ levels and the natural history and the liver tissue pathological states of chronic HBV infection have not yet been adequately investigated.[18]

Objectives

The objective of this study is to further evaluate the agreement of serum HBsAg-HQ with HBsAg-QT and comparatively investigate the effectiveness of serum HBsAg-HQ and HBsAg-QT in predicting the liver tissue pathological states of CHB patients.

Material and methods

Patients

A total of 275 Chinese patients with chronic HBV infection who were hospitalized in the Shanghai Public Health Clinical Center of Fudan University (Shanghai, China) between August 2012 and July 2015 were prospectively enrolled, among whom 147 and 128 patients were hepatitis B e antigen (HBeAg)-positive and HBeAg-negative, respectively. The diagnoses of all the patients were in accordance with the standards set forth in the Asian-Pacific clinical practice guidelines for the management of hepatitis B (2015 update).[19] Patients with other forms of viral hepatitis, drug-induced liver injuries, hereditary liver diseases, schistosomiasis japonica infection, autoimmune diseases, endocrine and metabolic diseases, and blood system diseases were excluded. Patients who had been treated with interferon alpha, nucleosi(t)des, steroids, or licorices were also excluded.

All patients provided written consent prior to a liver biopsy, and all clinical investigations were conducted according to the principles expressed in the 1995 Declaration of Helsinki.

Histological assessment

Ultrasound-assisted liver biopsies were performed using a 1-second liver biopsy needle (16G). The biopsies were collected immediately after the procedure and transferred into plastic tubes for freezing. One pathologist, who was blinded to all biochemical, serologic and virological parameters, was assigned to review all biopsy specimens. A biopsy length of at least 10 mm was required for inclusion in this study. The pathological diagnosis of liver tissues was performed independently by 1 experienced pathologist. The pathological diagnosis referred to the Scheuer standard,[20] in which a grade is used to describe the intensity of the necro-inflammatory activity, and a stage is used as a measure of fibrosis and architectural alteration. The grades include 5 levels, G0–G4, and the stages include 5 levels, S0–S4.

Laboratory assays

Serum samples used for measurements were taken within 1 week before and 1 week after liver biopsy and stored at –40°C. Serum HBsAg-HQ and HBsAg-QT were quantified using chemiluminescence enzyme immunoassay (CLEIA) in a Lumipulse G1200 automated analyzer (Fujirebio Inc., Tokyo, Japan) and chemiluminescence microparticle immunoassay (CMIA) in an Abbott Architect I2000 automated analyzer (Abbott Laboratories, Chicago, USA), respectively. The HBsAg-HQ reagents were provided by Fujirebio Inc., and the HBsAg-QT reagents were purchased from Abbott Laboratories. The linear detection range of the HBsAg-HQ was from 5 to 150 000 mIU/mL. If the serum exceeded the upper detection limit, it was diluted 1,000 times and remeasured. Similarly, the linear detection range of the HBsAg-QT was 50 to 250 000 mIU/mL, and if the serum exceeded the upper detection limit, it was diluted 500 times and remeasured.

The serum HBeAg was measured using CMIA Abbott Architect I2000 automated analyzer, with a lower detection limit of 1 S/CO. The serum HBV DNA was measured using Bio-Rad Icycler PCR System (Bio-Rad Laboratories, Inc., USA), and the polymerase chain reaction (PCR) kits were obtained from Qiagen Shenzhen Co. Ltd. (Shenzhen, China). The linear detection range of HBV DNA was 5×10^2 IU/mL to 5×10^7 IU/mL.

Statistical analysis

Statistical analyses were performed using MedCalc v. 15.1 (MedCalc Software, Broekstraat, Mariakerke, Belgium). A paired-samples t-test was used to compare the differences between the serum HBsAg-HQ and HBsAg-QT. Pearson correlation, linear regression analysis and Bland-Altman plots were used to evaluate the agreement between the HBsAg-HQ and HBsAg-QT quantitation. Spearman's correlation analysis was used to analyze the correlation of the serum HBsAg-HQ and HBsAg-QT levels with the liver tissue pathological grade and stage. The receiver operating characteristic (ROC) curve was used to assess the effectiveness of serum HBsAg-HQ and HBsAg-QT for predicting the different liver tissue pathological states. The paired-samples DeLong non-parametric test was used to compare the differences in the area under the ROC curve (AUC) between the serum HBsAg-HQ and HBsAg-QT for predicting the same liver tissue pathological states. A 2-sided p-value of less than 0.05 was considered to be significant.

Results

Clinical characteristics of the patients

There was no significant difference in the male-to-female ratio (p = 0.490) between the HBeAg-positive and HBeAg-negative patients; however, there was a significant difference in the average age (p = 0.000) between the HBeAg-positive and HBeAg-negative patients. The difference in alanine transaminase (ALT) (p = 0.947) between the HBeAg-positive and HBeAg-negative patients was not statistically significant. The differences in the serum HBsAg-HQ, HBsAg-QT and HBV DNA (all p = 0.000) between the HBeAg-positive and HBeAg-negative patients were all statistically significant. There was a significant difference (p = 0.046) in the frequency of the different pathological grades, but there was no significant difference (p = 0.469) in the frequency of the different pathological stages between the HBeAg-positive and HBeAg-negative patients (Table 1).

In the HBeAg-positive patients, the serum HBsAg-HQ and HBsAg-QT had a significant negative correlation with the serum ALT (r = −0.258; p = 0.002 and r = −0.254; p = 0.002). In the HBeAg-negative patients, the serum HBsAg-HQ and HBsAg-QT did not have a significant correlation with the serum ALT (r = −0.094; p = 0.291 and r = −0.067; p = 0.454) (Fig. 1A–D). In both the HBeAg-positive and HBeAg-negative patients, the serum HBsAg-HQ and HBsAg-QT levels were significantly positively correlated with the serum HBV DNA (r = 0.524; p = 0.000 and r = 0.501; p = 0.000 in the HBeAg-positive patients, and r = 0.350; p = 0.000 and r = 0.390; p = 0.000 in the HBeAg-negative patients) (Fig. 2A–D).

Comparison between HBsAg-HQ and HBsAg-QT levels

Regardless of serum HBeAg state and HBsAg levels, there was no significant difference between the serum HBsAg-HQ and HBsAg-QT (p = 0.691). Grouping the patients according to serum HBeAg state and HBsAg levels showed that there were no significant differences between serum HBsAg-HQ and HBsAg-QT in patients with both HBeAg-positive (p = 0.853) and HBeAg-negative (p = 0.647) and in patients with both higher HBsAg levels (HBsAg-QT ≥100 000 mIU/mL) (p = 0.942) and lower HBsAg levels (HBsAg-QT <100 000 mIU/mL) (p = 0.089) (Table 2).

Correlation and agreement between HBsAg-HQ and HBsAg-QT

Independent of the serum HBeAg state and the HBsAg levels, the serum HBsAg-HQ had a significantly positive correlation with HBsAg-QT (r = 0.955; p = 0.000) (Fig. 3A, Table 3). The linear regression analysis showed that HBsAg-HQ = 0.892 + 0.866 × HBsAg-QT (t = 53.087; p = 0.000). The Bland-Altman analysis showed that, compared to the serum HBsAg-QT levels, the serum HBsAg-HQ levels had an upward bias of 0.04 $\log_{10}$mIU/mL with a 95% limit of agreement (LOA) of −0.61 to 0.69 mIU/mL. The disagreement rates of ≤95% LOA and ≥95% LOA were 0.73% (2/275) and 2.91% (8/275), respectively, and that the

Table 1. Clinical characteristics of the patients according to their serum HBeAg state

Characteristics	HBeAg-positive (n = 147)	HBeAg-negative (n = 128)	χ^{2a}/t^{b}	p-value*
Gender (male:female)	93:54	87:41	0.478	0.490[a]
Age [mean ±SD (range)], [years]	35.48 ±11.29 (15–72)	43.88 ±12.51 (19–78)	5.851	0.000[b]
Serum ALT [mean ±SD (range)], × ULN[#]	3.22 ±6.34 (0.25–37.85)	3.18 ±5.31 (0.18–30.45)	0.067	0.947[b]
Serum HBsAg-HQ [mean ±SD (range)], [$\log_{10}$ mIU/mL]	6.932 ±0.764 (4.724–8.176)	5.830 ±0.930 (1.906–7.101)	10.647	0.000[b]
Serum HBsAg-QT [mean ±SD (range)], [$\log_{10}$ mIU/mL]	6.915 ±0.856 (4.375–8.097)	5.773 ±1.053 (1.778–7.226)	9.777	0.000[b]
Serum HBV DNA [median (range)], [$\log_{10}$ IU/mL]	6.498 ±1.554 (UD ->7.699)	3.901 ±1.380 (UD ->7.644)	14.557	0.000[b]
Pathological grade (G1:G2:G3)	75:33:39	84:22:22	6.164	0.046[a]
Pathological grade (S1:S2:S3:S4)	56:38:21:32	58:28:21:21	2.533	0.469[a]

[#] ULN – upper limit of normal = 40 IU/L; * HBeAg-positive vs HBeAg-negative; [a] χ^2 test; [b] independent samples t-test.

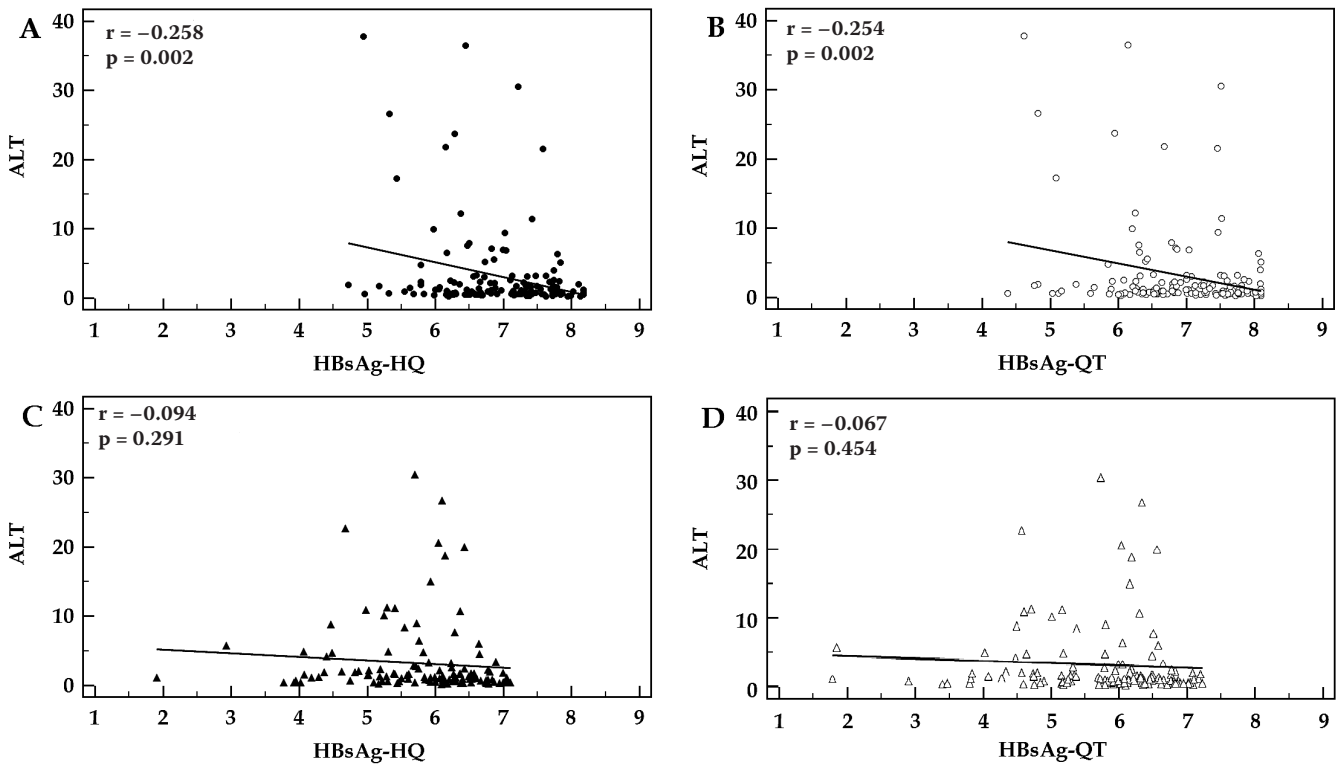

Fig. 1. Correlations of the serum HBsAg-HQ and HBsAg-QT with serum ALT in HBeAg-positive (A, B) and HBeAg-negative (C, D) patients

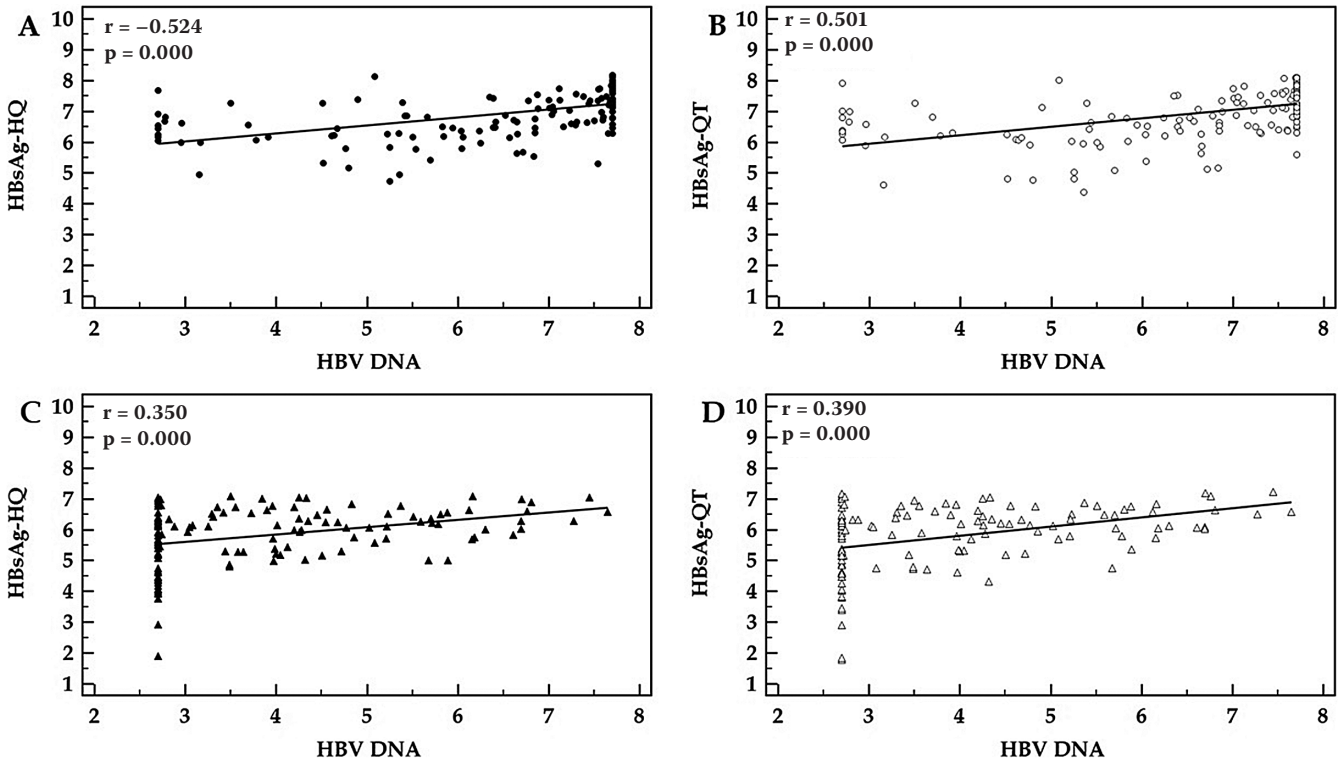

Fig. 2. Correlations of the serum HBsAg-HQ and HBsAg-QT with serum HBV DNA in HBeAg-positive (A, B) and HBeAg-negative (C, D) patients

overall disagreement rate was 3.64% (10/275) between the serum HBsAg-HQ and HBsAg-QT (Fig. 3B, Table 3).

In the HBeAg-positive patients, the serum HBsAg-HQ had a significantly positive correlation with HBsAg-QT (r = 0.913; p = 0.000) (Fig. 1C, Table 3), and HBsAg-HQ = 1.296 + 0.815 × HBsAg-QT (t = 26.929; p = 0.000). The overall disagreement rate was 2.72% (4/147) between the serum HBsAg-HQ and HBsAg-QT (Fig. 1D, Table 3).

Table 2. Comparison between the serum HBsAg-HQ and HBsAg-QT levels

Study population	N	HBsAg-HQ (±SD)	HBsAg-QT (±SD)	t-test	p-value
Overall	275	6.419 ±1.007	6.383 ±1.109	0.397	0.691
HBeAg-positive	147	6.932 ±0.764	6.915 ±0.856	0.185	0.853
HBeAg-negative	128	5.830 ±0.930	5.773 ±1.053	0.459	0.647
HBsAg-QT ≥5.000 $\log_{10}$ mIU/mL	244	6.655 ±0.752	6.660 ±0.790	0.072	0.942
HBsAg-QT <5.000 $\log_{10}$ mIU/mL	31	4.564 ±0.823	4.206 ±0.806	1.732	0.089

The measurement units for HBsAg-HQ and HBsAg-QT were both $\log_{10}$ mIU/mL.

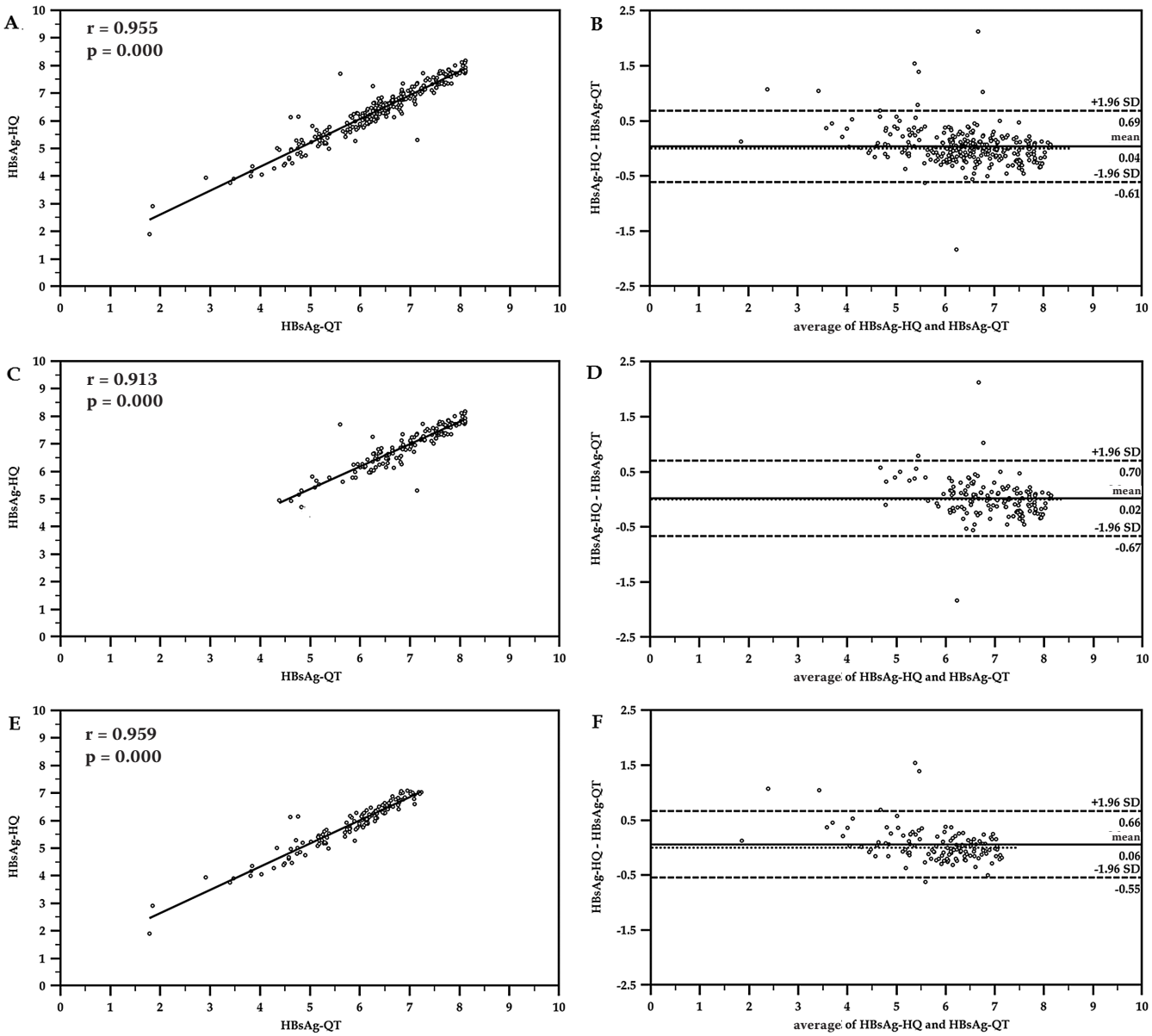

Fig. 3. Correlation and agreement between the serum HBsAg-HQ and HBsAg-QT

The measurement units of HBsAg-HQ and HBsAg-QT were both $\log_{10}$ mIU/mL. A, C and E show the scatter diagrams of the correlation between serum HBsAg-HQ and HBsAg-QT in the overall, HBeAg-positive and HBeAg-negative patients; B, D and F show the Bland–Altman plots of the agreement between the serum HBsAg-HQ and HBsAg-QT in the overall, HBeAg-positive and HBeAg-negative patients, in which the upper and lower horizontal solid lines represent the upper and lower limits of the 95% LOA, respectively, and the middle horizontal solid lines represent the average of the serum HBsAg-HQ and HBsAg-QT difference. The horizontal dotted lines represent an average value of 0 for the serum HBsAg-HQ and HBsAg-QT differences.

In HBeAg-negative patients, the serum HBsAg-HQ had a significantly positive correlation with HBsAg-QT (r = 0.959; p = 0.000) (Fig. 1E, Table 3); HBsAg-HQ = 0.963 + 0.843 × HBsAg-QT (t = 37.740; p = 0.000). The overall disagreement rate was 4.69% (6/128) between serum HBsAg-HQ and HBsAg-QT (Fig. 1F, Table 3).

Table 3. Pearson correlation and agreement between the serum HBsAg-HQ and HBsAg-QT

Study population	N	r	p-value	Bias	95% LOA	Inconsistency rate (%)		
						≤95% LOA	≥95% LOA	Sum
Overall	275	0.955	0.000	0.04	−0.61–0.69	2/275(0.73)	8/275(2.91)	10/275(3.64)
HBeAg-positive	147	0.913	0.000	0.02	−0.67–0.70	2/147(0.68)	3/147(2.04)	4/147(2.72)
HBeAg-negative	128	0.959	0.000	0.06	−0.55–0.66	1/128(0.78)	5/128(3.91)	6/128(4.69)
HBsAg-QT ≥5.000	244	0.929	0.000	−0.01	−0.58–0.57	2/244(0.82)	4/244(0.16)	6/244(0.25)
HBsAg-QT <5.000	31	0.861	0.000	0.36	−0.49–1.20	0/31(0.00)	2/31(6.45)	2/31(6.45)

The measurement units forHBsAg-HQ and HBsAg-QT were both $\log_{10}$ mIU/mL; bias – the average of serum HBsAg-HQ and HBsAg-QT differences; LOA – limit of agreement.

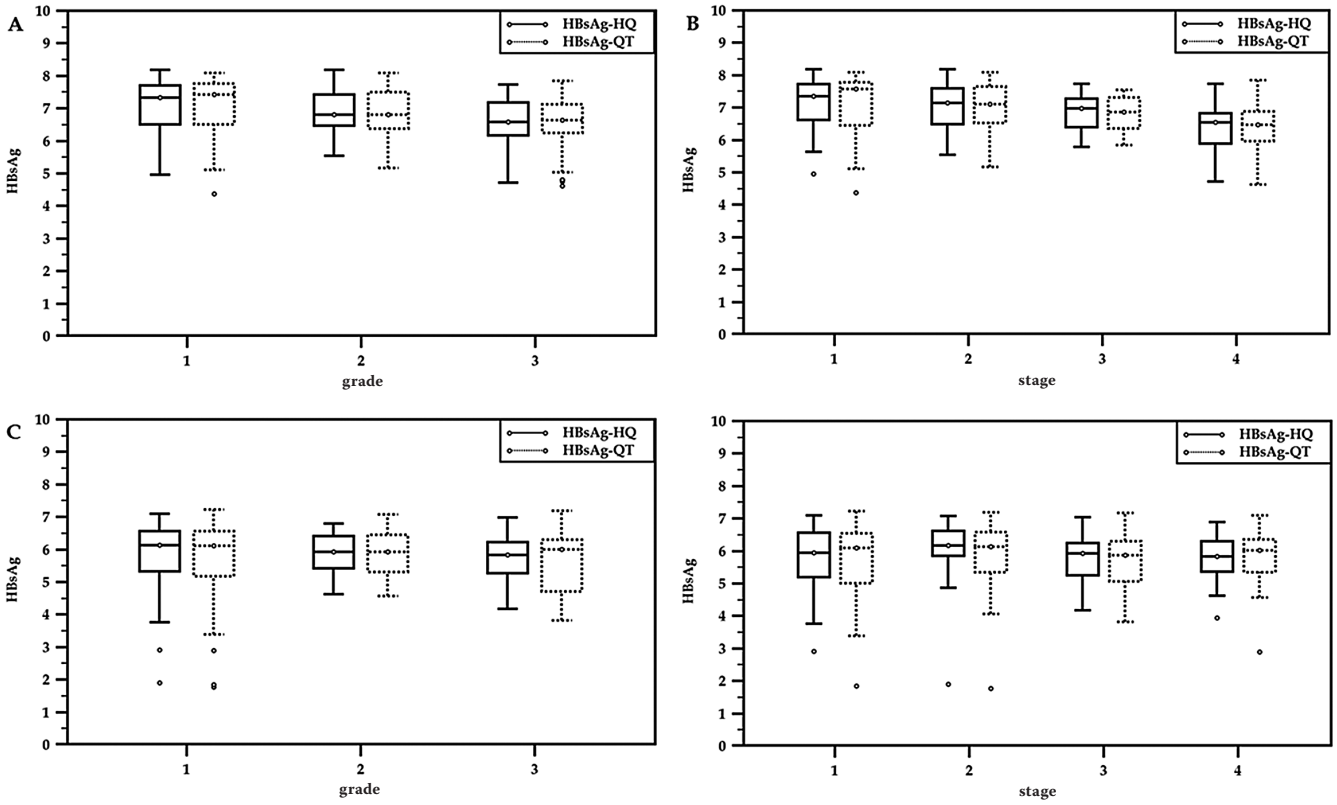

Fig. 4. Correlation of the serum HBsAg-HQ and HBsAg-QT levels with the liver tissue pathological grade and stage

The measurement units of HBsAg-HQ and HBsAg-QT were both $\log_{10}$ mIU/mL. The box-plots represent the serum distributions of HBsAg-HQ and HBsAg-QT in different pathological grades and stages in the HBeAg-positive (A, B) and HBeAg-negative patients (C, D), in which the top and bottom of the box indicates the upper and lower quartile, and the horizontal line in the box indicates the median. The upper and lower horizontal lines outside the box indicate the 95% quintile, and the circle indicates the extreme value.

In patients with higher HBsAg levels (HBsAg-QT ≥100 000 mIU/mL), the serum HBsAg-HQ had a significantly positive correlation with HBsAg-QT (r = 0.929; p = 0.000) (Table 3), such that HBsAg-HQ = 0.762 + 0.885 × HBsAg-QT (t = 39.150; p = 0.000). The overall disagreement rate was 0.25% (6/244) between the serum HBsAg-HQ and HBsAg-QT levels (Table 3). In patients with lower HBsAg levels (HBsAg-QT <100 000 mIU/mL), the serum HBsAg-HQ had a significantly positive correlation with HBsAg-QT (r = 0.861; p = 0.000) (Table 3), with HBsAg-HQ = 0.869 + 0.879 × HBsAg-QT (t = 9.098; p = 0.000). The overall disagreement rate was 6.45% (2/31) between the serum HBsAg-HQ and HBsAg-QT (Table 3).

Correlation of HBsAg-HQ and HBsAg-QT with pathological grade and stage

In HBeAg-positive patients, the serum HBsAg-HQ and HBsAg-QT were significantly negatively correlated with the pathological grade (r_s = −0.298; p = 0.000 and r_s = −0.320; p = 0.000, respectively) and stage (r_s = −0.366; p = 0.000 and r_s = −0.373; p = 0.000, respectively) (Fig. 4A,B). In HBeAg-negative patients, the serum HBsAg-HQ and HBsAg-QT levels were not significantly correlated with the pathological grade (r_s = −0.127; p = 0.155 and r_s = −0.073; p = 0.411, respectively) and stage (r_s = −0.045; p = 0.615 and r_s = −0.011; p = 0.903, respectively) (Fig. 4 C,D).

Performance of HBsAg-HQ and HBsAg-QT in predicting pathological states

In HBeAg-positive patients, all AUCs of the serum HBsAg-HQ and HBsAg-QT for predicting the pathological grades ≥G2 and ≥G3, and stages ≥S2, ≥S3 and ≥S4 were significantly greater than the area under the diagonal reference line (all $p < 0.01$). Of these, only the AUCs of serum HBsAg-HQ and HBsAg-QT for predicting pathological stage ≥S3 and ≥S4 were >0.70 (Table 4, Fig. 5). In the HBeAg-negative patients, all the AUCs of serum HBsAg-HQ and HBsAg-QT for predicting pathological grades ≥G2 and ≥G3, and stages ≥S2, ≥S3 and ≥S4 were not significantly greater than the area under diagonal reference line (all $p > 0.05$) (Table 4).

In HBeAg-positive patients there were no significant differences for predicting all the same pathological states (all $p > 0.05$) between the AUCs of the serum HBsAg-HQ and HBsAg-QT (Table 4). In the HBeAg-negative patients, there were no significant differences for predicting the same pathological states except for predicting the pathological stage ≥S4 between the AUCs of serum HBsAg-HQ and HBsAg-QT ($p = 0.046$ for predicting the pathological stage ≥S4, $p > 0.05$ for predicting the other pathological states) (Table 4).

The optimal cut-offs of serum HBsAg-HQ and HBsAg-QT for predicting a pathological grade ≥G3 were $< 2.244 \times 10^7$ mIU/mL and $< 3.589 \times 10^7$ mIU/mL, respectively, and the corresponding sensitivity, specificity were 87.18% and 97.44%, and 43.52% and 38.89%, respectively. The optimal cut-offs of serum HBsAg-HQ and HBsAg-QT for predicting the pathological stage ≥S4 were $< 7.328 \times 10^6$ mIU/mL and $< 6.194 \times 10^6$ mIU/mL, respectively, and the corresponding sensitivity, specificity were 81.25% and 75%, and 64.35% and 67.83%, respectively (Table 5).

Table 4. AUCs of serum HBsAg-HQ and HBsAg-QT for predicting the different liver tissue pathological states

Pathological states	HBsAg	HBeAg-positive					HBeAg-negative				
		AUC*	SE#	Z^	p-value	95% CI	AUC*	SE#	Z^	p-value	95% CI
≥G2	HBsAg-HQ	0.651[a]	0.046	3.290	0.001	0.568~0.727	0.573[f]	0.051	1.425	0.154	0.482~0.660
	HBsAg-QT	0.670[a]	0.045	3.755	0.000	0.588~0.745	0.547[f]	0.052	0.781	0.435	0.451~0.629
≥G3	HBsAg-HQ	0.686[b]	0.047	3.957	0.000	0.604~0.760	0.584[g]	0.064	1.317	0.188	0.493~0.671
	HBsAg-QT	0.684[b]	0.046	4.038	0.000	0.602~0.758	0.558[g]	0.068	0.778	0.437	0.463~0.641
≥S2	HBsAg-HQ	0.659[c]	0.049	3.266	0.001	0.576~0.735	0.492[h]	0.054	0.145	0.885	0.402~0.582
	HBsAg-QT	0.660[c]	0.050	3.213	0.001	0.577~0.736	0.514[h]	0.053	0.156	0.876	0.418~0.598
≥S3	HBsAg-HQ	0.712[d]	0.042	5.045	0.000	0.632~0.784	0.572[i]	0.052	1.391	0.164	0.481~0.659
	HBsAg-QT	0.720[d]	0.041	5.327	0.000	0.640~0.791	0.540[i]	0.053	0.645	0.519	0.444~0.623
≥S4	HBsAg-HQ	0.739[e]	0.046	5.159	0.000	0.660~ 0.808	0.552[j]	0.064	0.810	0.418	0.461~0.640
	HBsAg-QT	0.745[e]	0.045	5.476	0.000	0.666~0.813	0.508[j]	0.065	0.058	0.954	0.414~0.593

95% CI – 95% confidence interval; * AUC – area under the ROC curve; # SE – standard error; Z^ – independent samples DeLong non-parametric test; [a-j] paired-samples DeLong non-parametric test; [a] Z = 1.005, p = 0.315; [b] Z = 0.071, p = 0.943; [c] Z = 0.034, p = 0.973; [d] Z = 0.391, p = 0.696; [e] Z = 0.238, p = 0.812; [f] Z = 1.511, p = 0.131; [g] Z = 1.131, p = 0.258; [h] Z = 0.211, p = 0.833; [i] Z = 1.826, p = 0.068; [j] Z = 1.992, p = 0.046.

Table 5. Optimal cut-offs of serum HBsAg-HQ and HBsAg-QT for predicting different pathological states and the corresponding diagnostic parameters in HBeAg-positive patients

Pathological states	HBsAg	Cut-off	SEN (%)	SPE (%)	YI	PPV (%)	NPV (%)	ACC
≥G2	HBsAg-HQ	<7.216	73.61	58.67	0.323	63.1	69.8	0.329
	HBsAg-QT	<7.555	88.89	46.67	0.356	61.5	81.4	0.429
≥G3	HBsAg-HQ	<7.351	87.18	43.52	0.307	35.8	90.4	0.262
	HBsAg-QT	<7.555	97.44	38.89	0.363	36.5	97.7	0.342
≥S2	HBsAg-HQ	<7.622	89.01	42.86	0.319	71.7	70.6	0.423
	HBsAg-QT	<7.555	84.62	51.79	0.364	74.0	67.4	0.414
≥S3	HBsAg-HQ	<7.315	86.79	53.19	0.400	51.1	87.7	0.388
	HBsAg-QT	<7.555	98.11	44.68	0.428	50.0	97.7	0.477
≥S4	HBsAg-HQ	<6.865	81.25	64.35	0.456	38.8	92.5	0.313
	HBsAg-QT	<6.792	75.00	67.83	0.428	39.3	90.7	0.300

The measurement units of HBsAg-HQ and HBsAg-QT were both $\log_{10}$ mIU/mL; SEN – sensitivity; SPE – specificity; YI – Youden index; PPV – positive predictive value; NPV – negative predictive value; ACC – accuracy.

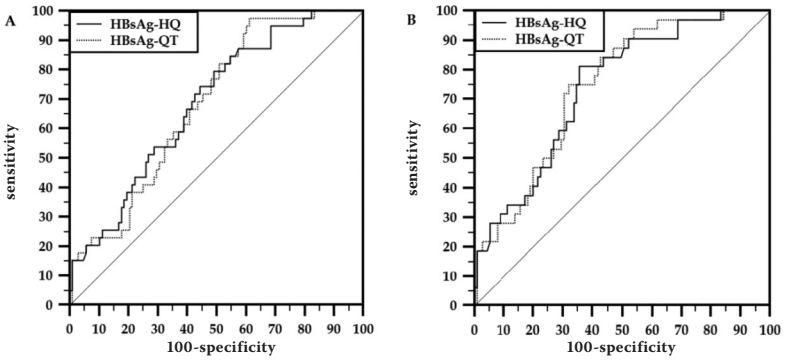

Fig. 5. ROC curves of serum HBsAg-HQ and HBsAg-QT for predicting a pathological grade ≥G3 and stage ≥S4 in HBeAg-positive patients

Discussion

Choi et al. confirmed that the qualitative results of serum HBsAg-HQ highly agreed with those of the serum HBsAg-QT, with a concordance rate of 99.8% (k = 1.00; 95% CI, 0.99–1.00). Of the 315 HBsAg-QT-positive samples, 314 were HBsAg-HQ-positive. Of the 685 HBsAg-QT-negative samples, 684 were HBsAg-HQ-negative.[16] Recently, Yang et al. evaluated and compared the agreement of the qualitative and quantitative results of serum HBsAg-HQ with HBsAg-QT and HBsAg-EII.[17] The results showed that of the 2,043 samples tested, 1,844 samples gave negative results for both HBsAg-HQ and HBsAg-QT, and 172 samples yielded positive results for both HBsAg-HQ and HBsAg-QT. Of the remaining 27 samples that had inconsistent HBsAg results, 3 were HBsAg-QT-positive and 24 were HBsAg--HQ-positive. Among these, none of the 3 HBsAg-QT--positive samples were subsequently confirmed to be positive. Twenty of the 24 HBsAg-HQ-positive samples were confirmed to be positive, 3 were confirmed to be negative and 1 gave an indeterminate result and therefore was excluded from the specificity calculation for HBsAg-HQ. The specificity was 99.84% for HBsAg-HQ and 99.84% for HBsAg-QT. Yang et al. also found that, of the 112 tested samples, HBsAg-HQ displayed an excellent correlation with both HBsAg-QT and HBsAg-EII (r = 0.985 and r = 0.990); the Bland-Altman analyses demonstrated that, compared to HBsAg-QT and HBsAg-EII, HBsAg-HQ had an upward bias of 0.19 $\log_{10}$ IU/mL with a 95% LOA of −0.01 to 0.39 $\log_{10}$ mIU/mL and 0.07 $\log_{10}$ IU/mL with a 95% LOA of −0.12 to 0.25 $\log_{10}$ mIU/mL, respectively.[17]

In this study, the serum HBsAg-HQ was significantly correlated with HBsAg-QT. The Bland-Altman analyses showed that, compared to the serum HBsAg-QT, the HBsAg-HQ had a slight bias of 0.04 $\log_{10}$ mIU/mL with a 95% LOA of −0.61 to 0.69 $\log_{10}$ mIU/mL; the overall disagreement rate was 3.64%. Further analyses of the grouping according to the HBeAg state (HBeAg-positive and HBeAg-negative) and the HBsAg levels (higher HBsAg levels (HBsAg-QT ≥100 000 mIU/mL) and lower HBsAg levels (HBsAg-QT < 100 000 mIU/mL)) also showed similar results. This further demonstrated that the serum HBsAg-HQ levels were highly correlated and highly agreed with HBsAg-QT.

Seto et al. comparatively investigated the changes in the serum HBsAg-HQ and HBsAg-EII in different phases in the natural history of chronic HBV infection.[18] The changes in the serum HBsAg-HQ in different phases were consistent with previous research based on the same criterion for the division of the natural history of chronic HBV infection.[5,6,21–23] Unexpectedly, the serum HBsAg-HQ levels were significantly higher than the HBsAg-EII levels in either the immune tolerance or the activation phase of the HBeAg-positive patients. However, the serum HBsAg-HQ levels were similar to the HBsAg-EII levels in either the immune escape or control phase of the HBeAg-negative patients. However, the reason why the serum HBsAg-HQ levels in HBeAg-positive patients were significantly higher than HBsAg-E levels is not clear. The investigators speculated that this could possibly be due to the enhanced detection of minor viral populations with "a" determinant mutations in patients with higher viral loads. However, Yang et al. reported that the S gene mutations within the "a" determinant, such as T126A, T126S, Q129H, Q129R, T140S, and G145E, did not affect the correlation and agreement observed between the serum HBsAg-HQ and HBsAg-QT and HBsAg-EII.[17]

In this study, regardless of the serum HBeAg state and HBsAg levels, the difference between the serum HBsAg-HQ and HBsAg-QT levels was not significant. Further analyses of the grouping according to the HBeAg state and HBsAg levels also showed similar results. Our results agreed with the study by Yang et al. but failed to find a serum HBsAg-HQ level that was not significantly higher than HBsAg-QT.[17] This result was not consistent with the findings of a previous study conducted by Seto et al.[18]

For the cause-specific indexes, several studies have shown that serum HBsAg and HBV DNA in HBeAg-positive patients and HBV DNA but HBsAg in HBeAg-negative patients are valuable in predicting liver tissue pathological states.[7,24–29] However, the predicable optimal pathological state of serum HBsAg and HBVDNA in the HBeAg-positive patients was not consistent between the different studies,[7,24–27] although for the HBV DNA in the HBeAg-negative patients, there was an agreement in the pathological grade ≥G2 and stage ≥S2.[28,29] The results of this study were consistent with the findings by Cheng et al. and Jia

et al., but not those of Martinot-Peignoux et al., Xun et al. and Seto et al.[7,24–27] Furthermore, we did not observe significant differences in the AUCs for predicting the same liver tissue pathological states between the serum HBsAg-HQ and HBsAg-QT in the HBeAg-positive patients. This study further demonstrated that, in the HBeAg-positive patients, serum HBsAs for predicting the liver tissue pathological states was valuable. Importantly, the efficacies of serum HBsAg-HQ for predicting the liver tissue pathological states were highly consistent with those of HBsAg-QT.

The results of this study showed that, in HBeAg-positive patients, the optimal cut-off of serum HBsAg-HQ for predicting a pathological grade ≥G3 was < 7.351 $\log_{10}$ mIU/mL (2.244×10^7 mIU/mL), with a difference of −0.204 $\log_{10}$ mIU/mL (−0.625 mIU/mL) from HBsAg-QT. The corresponding sensitivity, specificity, and positive and negative predictive values were 87.18%, 43.52%, 35.8%, and 90.4%, respectively. The optimal cut-off of serum HBsAg-HQ for predicting a pathological stage ≥S4 was < 6.865 $\log_{10}$ mIU/mL (7.328×10^6 mIU/mL), with a difference of 0.073 $\log_{10}$ mIU/mL (1.183 mIU/mL) from HBsAg-QT. The corresponding sensitivity, specificity, and positive and negative predictive values were 81.25%, 64.35%, 38.8%, and 92.5%, respectively. This suggests that, in HBeAg-positive patients, the optimal cut-offs of serum HBsAg-HQ for predicting pathological grade ≥G3 and stage ≥S4 should be highly consistent with those of HBsAg-QT, and serum HBsAg-HQ and HBsAg-QT should be very valuable for predicting pathological grade ≥G3 and stage ≥S4.

In conclusion, this study further evaluated the agreement between the serum HBsAg-HQ and HBsAg-QT levels and comparatively investigated the effectiveness of serum HBsAg-HQ and HBsAg-QT in predicting the liver tissue pathological states of CHB. The results showed that the serum HBsAg-HQ was highly correlated and agreed with the HBsAg-QT in both the HBeAg-positive and HBeAg-negative patients, regardless of whether they presented with higher or lower HBsAg levels. Furthermore, serum HBsAg-HQ and HBsAg-QT had good predictive efficacy on the pathological grade ≥G3 and stage ≥S4 in HBeAg-positive patients, but did not have predictive efficacy on the pathological states in HBeAg-negative patients.

References

1. Deguchi M, Yamashita N, Kagita M, et al. Quantitation of hepatitis B surface antigen by an automated chemiluminescent microparticle immunoassay. *J Virol Methods*. 2004;115:217–222. doi:10.1016/j.jviromet.2003.10.002
2. Wong GLH, Chan HLY. Use of quantitative hepatitis B surface antigen with hepatitis B virus DNA in clinical practice. *Clin Liver Dis*. 2013;2:8–10. doi:10.1002/cld.165
3. Zhou B, Liu M, Lv G, et al. Quantification of hepatitis B surface antigen and e antigen: Correlation between Elecsys and Architect assays. *J Viral Hepat*. 2013;20:422–429. doi:10.1111/jvh.12044
4. Park Y, Hong DJ, Shin S, et al. Performance evaluation of new automated hepatitis B viral markers in the clinical laboratory: Two quantitative hepatitis B surface antigen assays and an HBV core-related antigen assay. *Am J Clin Pathol*. 2012;137:770–777. doi:10.1309/AJCP8QDN7NAUXJFJ
5. Tan Z, Li M, Kuang X, et al. Clinical implications of hepatitis B surface antigen quantitation in the natural history of chronic hepatitis B virus infection. *J Clin Virol*. 2014;59:228–234. doi:10.1016/j.jcv.2014.01.013
6. Wang L, Zou ZQ, Wang K, et al. Role of serum hepatitis B virus marker quantitation to differentiate natural history phases of HBV infection. *Hepatol Int*. 2016;10:133–138. doi:10.1007/s12072-015-9657-6
7. Martinot-Peignoux M, Carvalho-Filho R, Lapalus M, et al. Hepatitis B surface antigen serum level is associated with fibrosis severity in treatment-naïve, e antigen-positive patients. *J Hepatol*. 2013;58:1089–1095. doi:10.1016/j.jhep.2013.01.028
8. Goyal SK, Jain AK, Dixit VK, et al. HBsAg level as predictor of liver fibrosis in HBeAg positive patients with chronic hepatitis B virus infection. *J Clin Exp Hepatol*. 2015;5:213–220. doi:10.1016/j.jceh.2015.04.008
9. Moucari R, Marcellin P. Quantification of hepatitis B surface antigen: A new concept for the management of chronic hepatitis B. *Liver Int*. 2011;31(Suppl 1):122–128. doi:10.1111/j.1478-3231.2010.02390.x
10. Tseng TC, Liu CJ, Yang HC, et al. Serum hepatitis surface antigen levels help predict disease progression in patients with low hepatitis B virus loads. *Hepatology*. 2013;57:441–450. doi:10.1002/hep.26041
11. Matsubara N, Kusano O, Sugamata Y, et al. A novel hepatitis B virus surface antigen immunoassay as sensitive ashepatitis B virus nucleic acid testing in detecting early infection. *Transfusion*. 2009;49:585–595. doi:10.1111/j.1537-2995.2008.02026.x
12. Seto WK, Tanaka Y, Wong DK, et al. Evidence of serologic activity in chronic hepatitis B after surface antigen (HBsAg) seroclearance documented by conventional HBsAg assay. *Hepatol Int*. 2013;7:98–105. doi:10.1007/s12072-012-9354-7
13. Seto WK, Tanaka Y, Wong DK, et al. Longitudinal profiles of highly sensitive hepatitis B surface antigen levels: Re-evaluation of HBsAg seroclearance. *Liver Int*. 2016;36:642–650. doi:10.1111/liv.12980
14. Shinkai N, Matsuura K, Sugauchi F, et al. Application of a newly developed high-sensitivity HBsAg chemiluminescent enzyme immunoassay for hepatitis B patients with HBsAg seroclearance. *J Clin Microbiol*. 2013;51:3484–3491. doi:10.1128/JCM.00726-13
15. Duong LT, Coignard C. Evaluation of a new high sensitive, qualitative and quantitative Hepatitis B surface antigen assay. *J Clin Virol*. 2015;70(Suppl 1):S95.
16. Choi SJ, Park Y, Lee EY, et al. Performance evaluation of Lumipulse G1200 autoimmunoanalyzer for the detection of serum hepatitis B virus markers. *J Clin Lab Anal*. 2013;27:204–206. doi:10.1002/jcla.21584
17. Yang R, Song G, Guan W, et al. The Lumipulse G HBsAg-Quant assay for screening and quantification of the hepatitis B surface antigen. *J Virol Methods*. 2016;228:39–47. doi:10.1016/j.jviromet.2015.11.016
18. Seto WK, Wong DK, Fung J, et al. Linearized hepatitis B surface antigen and hepatitis B core-related antigen in the natural history of chronic hepatitis B. *Clin Microbiol Infect*. 2014;20:1173–1180. doi:10.1111/1469-0691.12739
19. Sarin SK, Kumar M, Lau GK, et al. Asian-Pacific clinical practice guidelines on the management of hepatitis B: A 2015 update. *Hepatol Int*. 2016;10:1–98. doi:10.1007/s12072-015-9675-4
20. Brunt EM. Grading and staging the histopathological lesions of chronic hepatitis: The Knodell histology activity index and beyond. *Hepatology*. 2000;31:241–246. doi:10.1002/hep.510310136
21. Cheng XD, Song LW, Fang LL, et al. Comparison of three luminescent immunoassays for hepatitis B virus surface antigen quantification during the natural history of chronic hepatitis B virus infection. *Clin Vaccine Immunol*. 2014;21:1521–1527. doi:10.1128/CVI.00529-14
22. Suh SJ, Bae SI, Kim JH, et al. Clinical implications of the titer of serum hepatitis B surface antigen during the natural history of hepatitis B virus infection. *J Med Virol*. 2014;86:117–123. doi:10.1002/jmv.23767
23. Zeng LY, Lian JS, Chen JY, et al. Hepatitis B surface antigen levels during natural history of chronic hepatitis B: A Chinese perspective study. *World J Gastroenterol*. 2014;20:9178–9184. doi:10.3748/wjg.v20.i27.9178
24. Cheng PN, Tsai HW, Chiu YC, et al. Clinical significance of serum HBsAg levels and association with liver histology in HBeAg positive chronic hepatitis B. *J Clin Virol*. 2013;57:323–330. doi:10.1016/j.jcv.2013.04.012
25. Jia W, Qi X, Ji YY, et al. Low serum hepatitis B surface antigen level predicts compensated cirrhosis caused by chronic hepatitis B in HBeAg positive patients in east China. *Hepat Mon*. 2015;15:e29183. doi:10.5812/hepatmon.29183

26. Xun YH, Zang GQ, Guo JC, et al. Serum hepatitis B surface antigen quantification as a useful assessment for significant fibrosis in hepatitis B e antigen-positive hepatitis B virus carriers. *J Gastroenterol Hepatol.* 2013;28:1746–1755. doi:10.1111/jgh.12304
27. Seto WK, Wong DK, Fung J, et al. High hepatitis B surface antigen levels predict insignificant fibrosis in hepatitis B e antigen positive chronic hepatitis B. *PLoS One.* 2012;7:e43087. doi:10.1371/journal.pone.0043087
28. Alam S, Ahmad N, Mustafa G, et al. Evaluation of normal or minimally elevated alanine transaminase, age and DNA level in predicting liver histological changes in chronic hepatitis B. *Liver Int.* 2011;31:824–830. doi:10.1111/j.1478-3231.2011.02491.x
29. Croagh CMN, Bell SJ, Slavin J, et al. Increasing hepatitis B viral load is associated with risk of significant liver fibrosis in HBeAg-negative but not HBeAg-positive chronic hepatitis B. *Liver Int.* 2010;30:1115–1122. doi:10.1111/j.1478-3231.2010.02267.x

Hydroxyapatite coating on titanium endosseous implants for improved osseointegration: Physical and chemical considerations

Magdalena Łukaszewska-Kuska[1,A–F], Piotr Krawczyk[2,A,B,D–F], Agnieszka Martyla[3,B–F], Wiesław Hędzelek[1,A,E,F], Barbara Dorocka-Bobkowska[4,C,E,F]

[1] Department of Prosthodontics, Poznan University of Medical Sciences, Poland
[2] Institute of Chemistry and Technical Electrochemistry, Poznan University of Technology, Poland
[3] Institute of Non-Ferrous Metals, Central Laboratory of Batteries and Cells, Poznań, Poland
[4] Department of Oral Pathology, Poznan University of Medical Sciences, Poland

A – research concept and design; B – collection and/or assembly of data; C – data analysis and interpretation; D – writing the article; E – critical revision of the article; F – final approval of the article

Advances in Clinical and Experimental Medicine, ISSN 1899-5276 (print), ISSN 2451-2680 (online) *Adv Clin Exp Med*. 2018;27(8):1055–1059

Address for correspondence
Barbara Dorocka-Bobkowska
E-mail: b.dorocka@gmail.com

Funding sources
Ministry of Science and Higher Education research project No. N403 010 32/0480.

Conflict of interest
None declared

Received on August 10, 2016
Reviewed on September 13, 2016
Accepted on February 21, 2017

Abstract

Background. For many years, hydroxyapatite (HA) has been used as a bioactive endosseous dental implant coating to improve osseointegration. As such, the coating needs to be of high purity, adequate thickness, crystalline, and of a certain roughness in order to stimulate rapid fixation and form a strong bond between the host bone and the implant. There are a number of ways of preparing the HA coating, resulting in various coating properties. Herein, we report the preparation of the HA coating using a direct electrochemical method without the need for subsequent heat treatment.

Objectives. The aim of this study was to investigate the physicochemical properties of the HP coating, deposited on titanium implants by a modified electrochemical method.

Material and methods. The coating was characterized in terms of surface chemical composition, structure, morphology, coating thickness and roughness.

Results. The coating was found to be composed of homogenous HA with Ca/P and Ca/O ratios of 1.62 and 0.35, respectively. No other forms of calcium phosphate were detected. The degree of crystallinity of HA was 92.4%. The surface roughness was moderate (Sa = 1.04 μm) with the coating thickness of 2–3 μm. The scanning electron microscopy (SEM) analysis revealed a uniform, integrated layer of rod-like HA crystals with the longitudinal axes parallel to the implant surface.

Conclusions. The coating reported herein was found to have potentially favorable chemical and physical characteristics fostering osseointegration.

Key words: surface properties, hydroxyapatite, electrochemical techniques, endosseous implants

DOI
10.17219/acem/69084

Introduction

In recent years, the number of endosseous dental implants fitted to patients has risen worldwide. The clinical success of implantation is largely dependent on implant osseointegration. In addition, the integration process is affected by a wide range of factors, such as the patient's age, gender, habits, systemic diseases, anatomical location of the implant, implant size and design, surgical procedure, implant load, and, in particular, the implant surface characteristics.[1,2] Hence, the implant surface morphology and composition has been progressively modified over the years in order to optimize the bone-to-implant contact and improve osseointegration.

Hydroxyapatite ($Ca_{10}(PO_4)_6(OH)_2$, HA) has been used for many years as a bioactive implant coating to improve osseointegration.[3,4] It has a large capacity for adsorbing proteins, it improves osteoblast proliferation, enhances bone formation and reduces bone loss.[5–9] These properties induce a more rapid fixation and stronger bonding between the host bone and the implant, and are conducive to uniform bone ingrowth at the bone-implant interface.[3,9] The HA coating is able to limit the formation of any fibrous membrane and convert a motion-induced fibrous membrane into a bony anchorage.[9,10]

The most common method of applying the HA coating onto endosseous implants is the plasma spraying technique. This method, used since the mid 1980s, requires high temperatures for the application of the HA coating.[3] Despite the widespread use of this technique, there are significant concerns about the integrity of the bonding between the HA layer and the implant surface. High temperatures lead to the formation of the amorphous HA phase, which results in a higher bio-dissolution rate compared to a highly crystalline coating.[4,5] The amorphous phase also causes resorption, re-absorption and degradation of the HA coating in a biological environment, which can lead to the disintegration of the coating, resulting in the reduction of both the coating–substrate bond strength and implant fixation. There is also a risk of coating delamination and disintegration with the formation of debris particles.[10] Therefore, alternative HA coating processes have been extensively researched in order to avoid these undesirable effects of plasma application. One of the most promising methods is electrochemical deposition. It has many advantages: coating composition and structure can be controlled, the temperature of the process is relatively low, coating composition is homogeneous, and the coating layer is relatively thin. The formation of an irregular surface (roughness) is also an advantage. All these factors impart favorable biomedical properties to the coating.

The aim of the present work was to characterize the HA coating obtained by a modified process involving the electrochemical formation of HA on Ti screw dental implants. The physiochemical roperties of the HA coatings were characterized in terms of structural (X-ray diffraction – XRD) and morphological (scanning electron microscopy – SEM) properties, as well as surface chemical composition (X-ray photoelectron spectroscopy – XPS), coating thickness and surface roughness.

Material and methods

Electrochemical deposition

Commercially pure Titanium class IV screw implants, 4 mm in diameter and 7 mm in length, were used (Osteoplant, Poznań, Poland). Prior to electrodeposition, the implants were sandblasted with corundum grit (Al_2O_3) of a diameter of 53–75 μm and etched with 0.5 M H_2SO_4. The process of HA electrodeposition was carried out using an AUTOLAB potentiostat-galvanostat (PGSTAT 302N; Metrohm Autolab, Utrecht, the Netherlands) with a 2-electrode system in a galvanostatic mode, with a current of 5 mA. The implant was used as the working electrode and a platinum mesh served as a counter electrode. The electrolyte consisted of 2.08×10^{-4} M $CaCl_2$, 1.25×10^{-4} M NaH_2PO_4 and 0.1 M NaCl in distilled water. The pH was adjusted to 6.3 with NaOH solution. The process was carried out for 105 min at a temperature of 100°C. A 100 mL 3-neck flask was used as an electrochemical reactor and immersed in a thermostated oil bath.

Physiochemical characteristics of the HA layer

The chemical composition of the deposited coating surface was evaluated using XPS. The measurements were made using a VG Scientific photoelectron spectrometer ESCALAB-210 (VG Scientific, East Grinstead, UK) with Al Ka radiation (1486.6 eV) from an X-ray source, operating at 15 kV and 20 mA. Survey spectra were recorded in the energy range of 0–1350 eV, with a 0.4 eV step. High-resolution spectra were recorded with a 0.1 eV step, 100 ms dwell time and 20 eV pass energy. The 90-degree take-off angle was used in all measurements. Curve fitting was performed using the AVANTAGE software (Thermo Electron, Beverly, USA), which describes each component of the complex envelope as a Gaussian-Lorentzian sum function. A constant 0.3 (±0.05) G/L ratio was used and the background was fitted using a nonlinear Shirley model. Scofield sensitivity factors and a measured transmission function were used for quantification. Aromatic carbon C 1 s peak at 285 eV was used as a reference for binding energy.[11]

The chemical composition, as well as the structural properties of the coating, were evaluated using XRD. The identification of the HA phase on Ti was performed using an XRD powder diffractometer (PW 1050; Philips, Amsterdam, the Netherlands), with CuKα lamp radiation and a Ni filter. X-ray spectra were recorded in the angular range of 20–60° (2Θ) with a step size of 0.020° and a normalized count time of 1 s/step.[12]

The degree of crystallinity (Xc), corresponding to the fraction of the crystalline phase present in the examined volume, was evaluated by applying the equation:

$$X_c = \left[1 - \left(\frac{V_{112/300}}{I_{300}}\right)\right]$$

where I_{300} is the intensity of the (300) reflection and $V_{112/300}$ is the intensity of the hollow between (112) and (300) reflections, which completely disappears in non-crystalline samples.[13]

The surface morphology of the coating was examined with a scanning electron microscope (Tescan Vega, Pleasanton, USA).

Coating roughness was measured with an optical Wyko NT1100 profilometer (Veeco Instruments, Plainview, USA) in VSI Mode, the measured area was 0.9 × 1.2 mm, under ×20 magnification. The Wyko Vision software v. 3.0 for NT1100 was used. The Plane Fit function was used to remove linear tilt from surface measurements. After that, the S-parameters analysis was used to assess the value of parameters. The surface roughness of the examined implants was measured at 5 random locations in the area planned to be in contact with bone.

To assess the coating thickness, the coated implants were potted in Poly/Bed 812 epoxy resin (Polysciences, Warrington, USA). The disks were then sectioned through the middle with a band saw, then ground and polished, and prepared for the SEM analysis. The coating thickness was measured at 5 locations (twice on the thread tops, twice in the thread valleys and once on the flank) using the distance measurement facility in the scanning electron microscope.

Results

The XPS analysis revealed HA to be the principal component of the electrodeposited coating. The Ca/P and Ca/O ratios were found to be 1.62 and 0.35, respectively, which is in agreement with the theoretical ratio for HA (1.67 and 0.38).[14,15] In addition, small amounts (up to 1%) of F, Si, N, Na were detected as surface impurities (Fig. 1).

The XRD pattern of the HA coatings at Ti surface is shown in Fig. 2. The peaks indicated a hexagonal crystalline structure for HA.[16] No other forms of calcium phosphate, such as $Ca(HPO_4)_2 \times 2\ H_2O$ $Ca_3(PO_4)_2$, $Ca_4H(PO_4)_3$, were detected, indicating that the HA coating was of high purity.[17]

Intense reflexes from the titanium base were detected in the XRD spectrum, which overlapped with the HA peaks and may be attributed to a thin HA layer. Metallic titanium produces low-intensity HA reflexes, but does not interfere with the HA crystallinity determination.

Mineral crystallinity is the mass ratio of the measured HA crystal fraction compared to the whole mineral in the

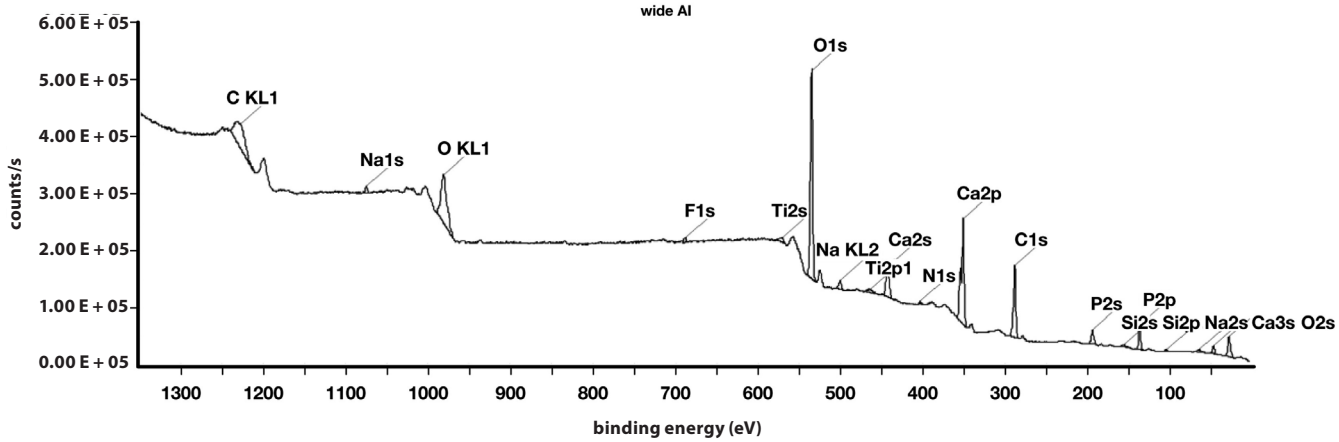

Fig. 1. XPS survey spectrum of the electrochemically deposited HA coating on a titanium implant

XPS – X-ray photoelectron spectroscopy; HA – hydroxyapatite.

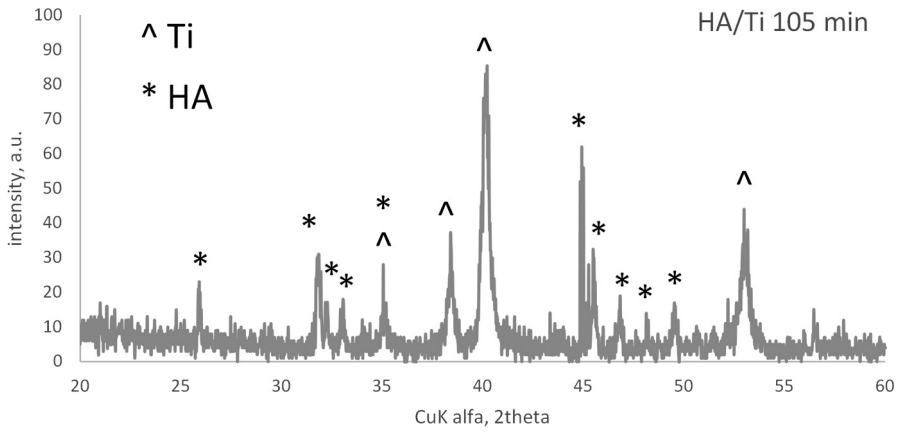

Fig. 2. XRD pattern of the HA coatings electrochemically deposited on a titanium implant

XRD – X-ray diffraction; HA – hydroxyapatite.

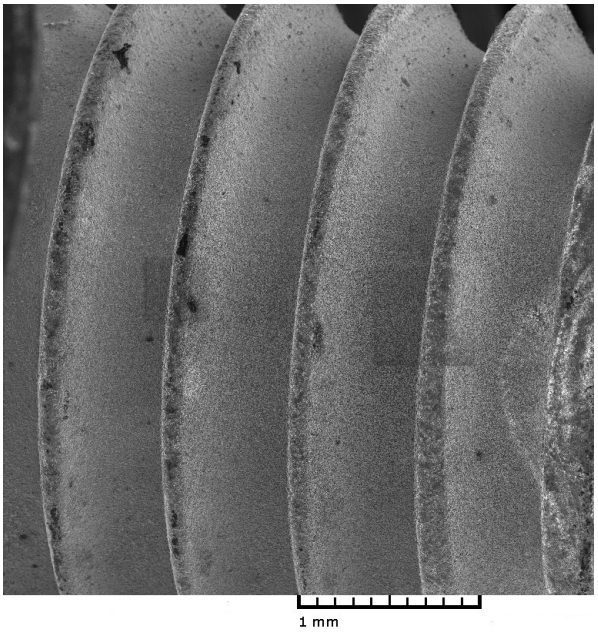

Fig. 3. SEM micrograph of the HA coating electrochemically deposited on a titanium implant thread (×66 magnification)

SEM – scanning electron microscopy; HA – hydroxyapatite.

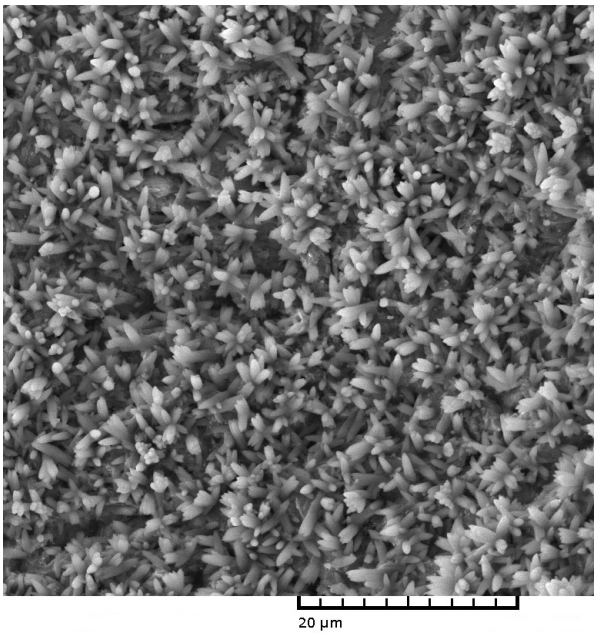

Fig. 4. SEM micrograph of the HA coating electrochemically deposited on a titanium implant (×4000 magnification)

SEM – scanning electron microscopy; HA – hydroxyapatite.

examined sample. The higher the crystallinity, the better the mechanical properties of a material.[18] The HA/Ti degree of crystallinity was found to be 92.4%, which is not the highest possible value; however, the results were obtained for the HA coating on a titanium surface, as opposed to a pure powder.[19]

The SEM analysis revealed a uniform, integrated layer of rod-like HA crystals on the titanium surface with the longitudinal axes parallel to the implant surface (Fig. 3, 4).

Optical profilometry showed moderate surface roughness with Sa = 1.04 ±0.12 µm.

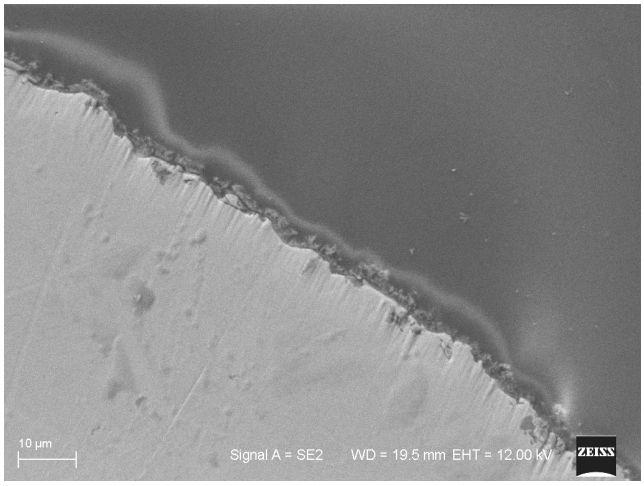

Fig. 5. Thickness of the HA coating layer observed by SEM

HA – hydroxyapatite; SEM – scanning electron microscopy.

The thickness of the HA coating layer, as observed by SEM, was within the range of 2–3 µm, indicating a thin and evenly formed HA layer on the corundum-blasted surface (Fig. 5).

Discussion

In this study, we presented a method of homogeneous HA coating deposition on a titanium implant surface. Like other researchers, we were able to deposit the HA coating without the presence of any other forms of Ca and P with an almost ideal Ca:P ratio.[14,15,20–22] The coating was relatively thin and it was possible to detect reflexes from the titanium base in the XRD spectrum.

The preparation of the coating was a 1-stage procedure. The synthesis and deposition of HA was performed simultaneously in situ compared with other techniques, thus shortening and simplifying the process.[20,22]

In contrast to other techniques, the sintering process was not implemented after electrochemical deposition.[21,22] Sintering increases the density of the coating and eliminates the pores, but it can also bring about mechanical degradation of the titanium and decomposition, delamination and microcracking of the HA coating.[20–22] Although sintering was not undertaken in our study, the coating was uniform and pore-free. High-temperature HA decomposition may also affect the biocompatibility of coatings, compromising the osseointegration of implants in bone.[20]

The HA/Ti crystallinity was found to be high, while the amorphous phase, which is susceptible to rapid dissolution and degradation in a biological environment, was limited to 7.6%.[23,24] Thus, the potential for a reduction of both the coating–substrate bond strength and implant fixation, due to the disintegration of the coating, was significantly mitigated.[3,5,18] A high coating crystallinity is also critical for the attachment of bone forming cells in the initial healing phase; it also stimulates the proliferation and differentiation of osteoblast cells.[25,26]

The SEM micrographs of the HA coating were similar in appearance to the electrodeposited and electrostatic sprayed coatings reported by other authors.[21,22,27] The advantage of such a dentate morphology on the Ti surface is that it can reduce the surface area which bears shearing strength while increasing the surface area bearing compressive strength.[21]

It has been reported that establishing a uniform micron-thick HA layer can prevent the exfoliation of the coating layer more effectively than a thicker coating layer.[25,26,28,29] The SEM measurements in the present study confirmed that the specimens had a uniform HA coating thicknesses (2–3 μm). Thus, it can be assumed that the HA coating technique employed in the present study provides resistance to delamination. However, future studies should include tensile strength testing in order to test the bond strength between the coating layer and the titanium implant surface. A uniform, micron-thick coating layer could also maintain the original microtexture of the sandblasted implant surface, which has a proven potential for osseointegration.[30]

To improve the bonding strength between HA and titanium implants, the surface of a Ti screw was etched with H_2SO_4 before electrodeposition. Etching produces small pits on the titanium surface, which act as a thin scaffold between the HA coating and Ti substrate. Thus, the HA coating is able to endure greater compressive loads compared to tensile and shear loads.[21]

According to Wennerberg et al., optimal surfaces for intense bone reaction require a moderate surface roughness (Sa = 1–2 μm).[30] A review of over 100 publications showed that such surfaces facilitate better bone reaction than smooth (Sa < 0.5 μm) or minimally rough (Sa 0.5–1 μm) surface implants, or some implants with rough surfaces (Sa > 2 μm).

Conclusions

Using a modified electrochemical deposition method, the HA coating was deposited on pure titanium implant surfaces during a 105-minute electrodeposition process. The obtained coating was found to be highly pure, homogenous HA, which was uniform, crack-free and thin. Moreover, its moderate surface roughness and coating crystallinity was potentially conducive to tissue reaction.

References

1. Jokstad A, Braegger U, Brunski JB, Carr AB, Naert I, Wennerberg A. Quality of dental implants. *Int Dent J.* 2003:53,409–443.
2. Albrektsson T, Branemark PI, Hansson HA, Lindstrom J. Osseointegrated titanium implants: Requirements for ensuring a longlasting, direct bone-to-implant anchorage in man. *Acta Orthop Scand.* 1981;52:155–170.
3. Narayanan R, Seshadri SK, Kwon TY, Kim KH. Calcium phosphate-based coatings on titanium and its alloys. *J Biomed Mater Res Part B: Appl Biomater.* 2008;85B:279–299.
4. Yang Y, Dennison D, Ong JL. Protein adsorption and osteoblast precursor cell attachment to hydroxyapatite of different crystallinities. *Int J Oral Maxillofac Implants*. 2005;20:187–192.
5. O'Hare P, Meenan BJ, Burke GA, Byrne G, Dowling D, Hunt JA. Biological responses to hydroxyapatite surfaces deposited via a co-incident microblasting technique. *Biomaterials.* 2010;3:515–522.
6. Wang C, Karlis GA, Anderson GI, et al. Bone growth is enhanced by novel bioceramic coatings on Ti alloy implants. *J Biomed Mater Res A.* 2009;90:419–428.
7. Le Guéhennec L, Soueidan A, Layrolle P, Amouriq Y. Surface treatments of titanium dental implants for rapid osseointegration. *Dent Mater.* 2007;23:844–854.
8. Shen JW, Wu T, Wang Q, Pan HH. Molecular simulation of protein adsorption and desorption on hydroxyapatite surfaces. *Biomaterials.* 2008;29:513–532.
9. Kilpadi KL, Chang PL, Bellis SL. Hydroxylapatite binds more serum proteins, purified integrins and osteoblast precursor cells than titanium or steel. *J Biomed Mater Res.* 2001;57:258–267.
10. Sun L, Berndt CC, Gross KA, Kucuk A. Material fundamentals and clinical performance of plasma-sprayed hydroxyapatite coatings: A review. *J Biomed Mater Res B Appl Biomater.* 2001;58:570–592.
11. Beamson G, Briggs D. *High Resolution XPS of Organic Polymers. The Scienta ESCA300 Database.* Chichester: John Wiley & Sons; 1992.
12. Jenkins R, Snyder RL. *Introduction to X-Ray Powder Diffractomerty.* New York , NY: John Wiley & Sons; 1996.
13. Stötzel C, Müller FA, Reinert F, Niederdraenk F, Barralet JE, Gbureck U. Ion adsorption behaviour of hydroxyapatite with different crystallinities. *Colloids Surf B Biointerfaces.* 2009;74:91–95.
14. Milella E, Cosentino F, Licciulli A, Massaro C. Preparation and characterisation of titania/hydroxyapatite composite coatings obtained by sol-gel process. *Biomaterials.* 2001;22:1425–1431.
15. Zhu X, Eibl O, Scheideler L, Geis-Gerstorfer J. Characterization of nano hydroxyapatite/collagen surfaces and cellular behaviors. *J Biomed Mater Res A.* 2006;79:114–127.
16. Hanawalt JD, Rinn HW, Frevel LK. Chemical analysis by X-ray diffraction. *Anal Chem.* 1938;10:457–512.
17. Saremi M, Mottaghi Golshan B. Electrodeposition of nano size hydroxyapatite coating on Ti alloy. *IJMSE.* 2006;3:1–5.
18. Ostrowski K, Dziedzic-Gocławska A, Stachowicz W, Michalik J. Radiation-induced paramagnetic centres in research on bone physiology. *Clin Orthop Relat Res.* 1991;272:21–29.
19. Landi W, Tampieri A, Celotti G, Sprio S. Densification behaviour and mechanisms of synthetic hydroxyapatites. *J Eur Ceram Soc.* 2000;20:2377–2387.
20. Hu R, Lin CJ, Shi HY. A novel ordered nano hydroxyapatite coating electrochemically deposited on titanium substrate. *J Biomed Mater Res A.* 2007;80:687–692.
21. Chen F, Lam WM, Lin CJ, et al. Biocompatibility of electrophoretical deposition of nanostructured hydroxyapatite coating on roughen titanium surface: In vitro evaluation using mesenchymal stem cells. *J Biomed Mater Res B Appl Biomater.* 2007;82:183–191.
22. Lin C, Han H, Zhang F, Li A. Electrophoretic deposition of HA/MWNTs composite coating for biomaterial applications. *J Mater Sci Mater Med.* 2008;19:2569–2574.
23. Burke EM, Lucas LC. Dissolution kinetics of calcium phosphate coatings. *Implant Dent.* 1998;7:323–330.
24. Eanes ED. Amorphous calcium phosphate. *Oral Sci.* 2001;18:130–147.
25. Yang Y, Bumgardner JD, Cavin R, Carnes DL, Ong JL. Osteoblast precursor cell attachment on heat-treated calcium phosphate coatings. *J Dent Res.* 2003;82:449–453.
26. Jung UW, Hwang JW, Choi DY, et al. Surface characteristics of a novel hydroxyapatite-coated dental implant. *J Periodontal Implant Sci.* 2012; 42:59–63.
27. Huang J, Jayasinghe SN, Best SM, et al. Novel deposition of nanosized silicone substituted hydroxyapatite by electrostatic spraying. *J Mater Sci Mater Med.* 2005;16:1137–1142.
28. Katto M, Ishibashi K, Kurosawa K, et al. Crystallized hydroxyapatite coatings deposited by PLD with targets of different densities. *J Phys Conf Ser.* 2007;59:75–78.
29. Cleries L, Fernandez-Pradas JM, Sardin G, Morenza JL. Dissolution behaviour of calcium phosphate coatings obtained by laser ablation. *Biomaterials*. 1998;19:1483–1487.
30. Wennerberg A, Albrektson T. Effects of titanium surface topography on bone integration: A systematic review. *Clin Oral Implants Res*. 2009;20:172–184.

Use of *MTHFR C677T* polymorphism and plasma pharmacokinetics to predict methotrexate toxicity in patients with acute lymphoblastic leukemia

Lobna Ben Mahmoud[1,A–F], Moez Mdhaffar[2,A–D,F], Rim Frikha[3,A,B], Hanen Ghozzi[1,A–C], Ahmed Hakim[1,A], Zouheir Sahnoun[1,A], Moez Elloumi[2,A,E], Khaled Zeghal[1,A,B,E,F]

[1] Department of Pharmacology, Faculty of Medicine, University of Sfax, Tunisia
[2] Department of Hematology, Hedi Chaker University Hospital, Sfax, Tunisia
[3] Department of Histology, Faculty of Medicine, University of Sfax, Tunisia

A – research concept and design; B – collection and/or assembly of data; C – data analysis and interpretation; D – writing the article; E – critical revision of the article; F – final approval of the article

Advances in Clinical and Experimental Medicine, ISSN 1899-5276 (print), ISSN 2451-2680 (online) *Adv Clin Exp Med*. 2018;27(8):1061–1068

Address for correspondence
Lobna Ben Mahmoud
E-mail: benmahmoud_lobna@medecinesfax.org

Funding sources
None declared

Conflict of interest
None declared

Received on November 13, 2016
Reviewed on February 19, 2017
Accepted on March 27, 2017

Abstract

Background. Methotrexate (MTX) is a key component of acute lymphoblastic leukemia (ALL) therapy, but it is associated with serious toxicities in a considerable number of patients.

Objectives. The aim of the current study was to determine which variables were associated with MTX toxicity in children, adolescents and young adults with ALL.

Material and methods. In this prospective study, 35 patients with newly diagnosed ALL, treated according to the 58951 European Organization for Research and Treatment of Cancer – Children's Leukemia Group (EORTC-CLG) protocol, were prospectively enrolled. Toxicity data was collected objectively after each high-dose methotrexate (HD-MTX) course. The risk factors of MTX toxicity were determined using multiple linear regression analysis, with age, gender, immunophenotype, risk group, plasma MTX levels, plasma homocysteine (HCY) levels, and *MTHFR C677T* included as independent variables.

Results. Twenty-five (71.4%) patients experienced toxicity on at least 1 course of HD-MTX. In the univariate linear regression, the global toxicity score was associated with a significant rise in plasma HCY concentrations within 48 h after MTX administration ($\beta = 0.4$; $R^2 = 0.12$; $p = 0.02$). In the multiple regression model, the global toxicity score was significantly associated with a higher MTX plasma levels at 48 h ($\beta = 0.5$; $R^2 = 0.38$; $p = 0.001$) and CT 677 *MTHFR* genotype ($\beta = 0.3$; $R^2 = 0.38$; $p = 0.01$).

Conclusions. Routine monitoring of plasma MTX concentrations is essential to detect patients at a high risk of MTX toxicity. *MTHFR C677T* genotyping may be useful for predicting MTX toxicity.

Key words: methotrexate, acute lymphoblastic leukemia, *MTHFR C677T* polymorphism, toxicity

DOI
10.17219/acem/69802

Introduction

Acute lymphoblastic leukemia (ALL) is the most common pediatric cancer; its survival rate has improved, with 5-year event-free survival (EFS) rates of 70–80% and overall cure rates of 80%.[1,2] Such an improvement in the treatment outcome is largely due to the advances in chemotherapy. Methotrexate (MTX), an antifolate chemotherapeutic agent, plays an important role in the chemotherapy regimen for ALL and has significantly reduced the recurrence rate of ALL in children.[3]

Methotrexate is predominantly taken up into cells via the reduced folate carrier (RFC).[4] Inside the cell, MTX is converted to its active polyglutamate forms (methotrexate polyglutamates – MTXPGs).[5] Both MTX and MTXPGs inhibit dihydrofolate reductase, an enzyme that catalyzes the conversion of dihydrofolate to its active form tetrahydrofolate (THF), a substrate of thymidylate synthase (TS), to convert deoxyuridine monophosphate to deoxythymidine-5'-monophosphate, resulting in DNA synthesis.[6] Tetrahydrofolate deficiency leads to the depletion of intracellular folates, and thereby to decreased synthesis of both purines and pyrimidines, contributing to the inhibition of nucleic acid synthesis and favoring cell death.[7] Methotrexate polyglutamates can also interfere with methylenetetrahydrofolate reductase (*MTHFR*), which converts 5,10-methylene-THF to 10-methyl-THF, the major circulating form of folate that provides a methyl group for homocysteine (HCY) methylation to methionine, and channels the methyl group into DNA and protein methylation reactions.[6]

A high-dose methotrexate (HD-MTX) refers to infused MTX in doses of more than 1 g/m^2.[8] The use of HD-MTX has shown great benefit in the treatment of childhood ALL and the prevention of extramedullary leukemia, i.e., central nervous system (CNS) leukemia and testicular leukemia.[2] However, MTX is associated with various toxicities, including severe mucositis, myelosuppression, gastrointestinal toxicity, hepatic toxicity, neurotoxicity, and hematological toxicity, requiring a dose reduction and the interruption of chemotherapy, and subsequently an increased risk of relapse.[9] Methotrexate-related toxicity remains a common and often unpredictable clinical problem, because of a wide interindividual variation in pharmacokinetics and pharmacodynamics of this drug.[8]

The aim of the current study was, therefore, to determine factors associated with the high risk of MTX toxicity that could help to develop personalized therapies in children, adolescents and young adults with ALL.

Material and methods

Patients and study design

From January 2013 to December 2014, 35 patients with newly diagnosed ALL were prospectively enrolled from the Hematology Department of Hedi Chaker University Hospital (Sfax, Tunisia). The diagnosis of ALL was based on morphologic, cytochemical and immunophenotypical criteria.

Patients were selected according to the following inclusion criteria: availability of clinical data, treatment according to the European Organization for Research and Treatment of Cancer – Children's Leukemia Group (EORTC-CLG) 58951 protocol, administration of at least 1 course of intravenous MTX chemotherapy, and no history of other active malignancies requiring a modification of chemotherapy regimen.[10]

Patients were stratified into 4 risk groups (low-risk – LR; average risk 1 – AR1; average risk 2 – AR2, and high-risk – HR) on the basis of their presenting clinical features, the biologic features of their leukemic cells, and their early response to remission-induction treatment.[10,11]

This study was conducted in accordance with the Helsinki Declaration and informed consent was given by all the persons participating in this study.

Treatment

All patients were treated according to the 58951 EORTC-CLG protocol, a Berlin–Frankfurt–Munster-like trial, with treatment phases including induction (IA), consolidation (IB/IB9), CNS prophylaxis without cranial irradiation, late intensification II, and maintenance.[11,12]

According to this protocol, the infusion of HD-MTX was given intravenously in each course at 5 g/m^2 body surface area (BSA) over a 4-hour period. Intravenous hydration and urinary alkalinization were performed 1 day before HD-MTX administration, and continued during and after MTX infusion. Leucovorin rescue (25 mg/m^2) was administered every 6 h, starting at 24 h after the initiation of HD-MTX infusion.

High-dose methotrexate infusions were administered during the interval therapy to all patients, in the induction phase to AR2/HR-ALL, in the consolidation phase to HR-ALL and in the R1-R2 Bloc to HR-ALL.

Plasma methotrexate and homocysteine levels determination

In each course of HD-MTX, blood samples were collected in ethylenediaminetetraacetic acid (EDTA)-containing tubes at the following times: at 24, 48 and 72 h from the start of intravenous MTX infusion. Plasma was recuperated by centrifugation at 3000 rpm for 10 min and was stored at –20°C for the determination of MTX and HCY levels.

Plasma levels of MTX and HCY were determined by a fluorescence polarization immunoassay. Plasma MTX levels were considered high if the concentration was above 10 µmol/L at 24 h, 1 µmol/L at 48 h or 0.1 µmol/L at 72 h.[13,14]

MTHFR C677T genotyping

The *MTHFR C677T* polymorphism was determined in 28 patients with ALL and 70 healthy subjects taken from the general population (35 males and 35 females, age range: 18–29 years). DNA was extracted from peripheral blood samples and polymerase chain reaction-restriction fragment length polymorphism (PCR-RFLP) was performed for the molecular diagnosis of the *C677T MTHFR* polymorphism. The primers, lengths and restriction enzymes have been described previously.[15] The 677C → T base pair substitution creates a *Hinf1* restriction site. Then, CC genotype would be reflected by a single band of 265 bp, CT genotype by 3 bands of 265, 171, and 94 bp, and TT genotype by 2 bands of 171 and 94 bp.

Toxicity

Toxicity data obtained from questionnaires and case records were prospectively collected objectively after each HD-MTX course, in the period from the end of HD-MTX infusion to the next HD-MTX course or until 14 days after HD-MTX infusion.

The toxicity was graded according to the Common Terminology Criteria for Adverse Events (CTCAE, v. 5.0).[16]

According to the modified method of Radtke et al., the global toxicity score for each patient was calculated in our study by adding up the grading of all adverse events that occurred during courses of MTX.[17] This score integrates both frequency and severity of MTX toxicity. In the study, the higher grade of toxicity in each HD-MTX course was considered.

Statistical analysis

All statistical analyses were performed using the IBM SPSS Statistics v. 20 software (Chicago, USA). Quantitative variables were expressed as means and standard error of the mean (SEM); they were compared using the t-test or the Wilcoxon-Mann-Whitney test according to the characteristics of the distribution. Qualitative variables were presented as a total number and proportion, and were compared using the χ^2 test or Fisher's exact test according to sample sizes.

To identify the risk factors of MTX toxicity, a multivariate linear regression model was constructed, using variables identified from the univariate analysis, which included age, gender, immunophenotype, risk group, MTX plasma levels, HCY plasma levels, and *MTHFR C677T*. A stepwise selection was used with probability value of $p < 0.2$ for entry and $p < 0.05$ for removal. For all comparisons, differences were considered statistically significant at $p < 0.05$.

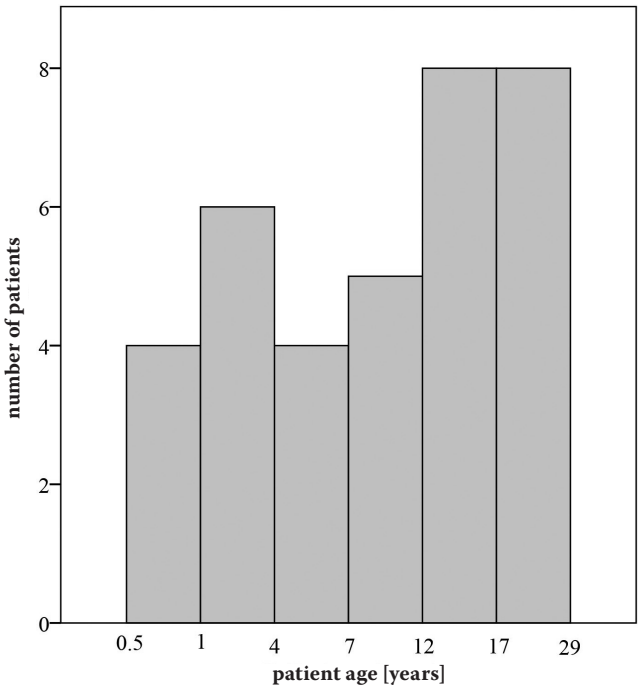

Fig. 1. Age distribution of patients

Results

Patient characteristics and plasma levels of methotrexate and homocysteine

A total of 35 patients (21 males and 14 females) with newly diagnosed ALL treated with the 58951 EORTC-CLG protocol were enrolled in this study. The mean patient age at diagnosis was 11.7 ±9 years (median: 10.1 years; range: 0.5–29 years) (Fig. 1). Patients' characteristics were shown in Table 1.

According to risk stratification, 12 patients were from AR1 group, 13 from AR2 group and 10 from HR group. A total of 173 courses of HD-MTX at 5 g/m^2 were administered.

In the study, 168 plasma MTX levels and 125 plasma HCY levels were analyzed. The results of these analyses are presented in Table 1.

Methotrexate levels ranged from 0.9 to 13 µmol/L at 24 h, from 0.02 to 6.7 µmol/L at 48 h and from 0.01 to 0.9 µmol/L at 72 h. Homocysteine levels ranged from 8 to 19 µmol/L at 24 h, from 5 to 15.5 µmol/L at 48 h and from 0.13 to 17 µmol/L at 72 h.

High-dose methotrexate-related toxicity

Of 35 patients, 25 (71.4%) experienced toxicity on at least 1 course of HD-MTX. The mean of global toxicity score for these patients was 5.1 ±2.1 (range: 1–12). A total of 59 cases of MTX-related toxicity were observed among 173 courses of HD-MTX (on average, 2 cases of toxicity per patient; range: 1–9) (Table 1).

Table 1. Characteristics of patients, their clinical condition and toxicity experienced

Characteristics of patients	Total number of patients (n = 35)	
Age at diagnosis [years], mean ±SEM (min–max) <10 years, n (%) ≥10 years, n (%)	11.7 ±1.6 (0.5–29) 17 (48.6) 18 (51.4)	
Gender male, n (%) female, n (%)	 21 (60) 14 (40)	
Immunophenotype B-ALL, n (%) T-ALL, n (%)	 23 (65.7) 12 (34.3)	
Weight [kg], mean ±SEM (min–max)	41.5 ±4 (11–60)	
Height [cm], mean ±SEM (min–max)	138 ±5.5 (80–183)	
BSA [m^2], mean ±SEM (min–max)	1.2 ±0.1 (0.5–2)	
Risk group AR1, n (%) AR2, n (%) HR, n (%)	 12 (34.3) 13 (37.1) 10 (28.6)	
MTX-related toxicity	Total number of patients (n = 35)*	Total number of HD-MTX courses (n = 173)
Hepatotoxicity, n (%) grade 2 grade 3 grade 4	13 (37.1) 7 4 2	17 (9.8) 9 6 2
Gastrointestinal toxicity, n (%) grade 1 grade 2 grade 3	10 (28.6) 1 3 7	17 (9.8) 1 9 7
Mucositis, n (%) grade 3 grade 4	6 (17.1) 3 4	8 (4.6) 3 5
Neurotoxicity, n (%) grade 1 grade 3 grade 4	3 (8.6) 1 2 2	5 (2.9) 1 2 2
Skin toxicity, n (%) grade 1 grade 2 grade 3	6 (17.1) 1 1 4	6 (3.4) 1 1 4
Hematotoxicity, n (%) grade 1 grade 4	2 (2.7) 1 1	2 (1.1) 1 1
Renal toxicity, n (%) grade 2	1 (2.8) 1	1 (0.6) 1
Phlebitis, n (%)	2 (2.7)	3 (1.7)
Plasma MTX levels [µM]	Total number (n = 168)	
24 h (n = 66), mean ±SEM, 48 h (n = 54), mean ±SEM 72 h (n = 48), mean ±SEM	5.6 ±0.6 1.3 ±0.3 0.1 ±0.02	
Plasma HCY levels [µM]	Total number (n = 125)	
24 h (n = 49), mean ±SEM 48 h (n = 48), mean ±SEM 72 h (n = 28), mean ±SEM	12.2 ±30.6 10 ±0.5 8 ±0.8	

BSA – body surface area; AR – average risk; HR – high risk; MTX – methotrexate; HCY – homocysteine; HD-MTX – high-dose methotrexate; SEM – standard error of the mean; * the upper grade of toxicity in each HD-MTX course was considered.

Hepatic and gastrointestinal toxicities were the most frequently observed toxicities, accounting for 57.6% of the total number of observed toxicities. Methotrexate-induced hepatotoxicity was expressed by elevated aspartate aminotransferase/alanine aminotransferase (ASAT/ALAT). There were 55 cases of toxicity (93.2%) with grade 2 or greater, and only 4 cases of toxicity with grade 1 (6.8%) (Table 1).

Plasma methotrexate levels and methotrexate-related toxicity

The univariate linear regression revealed that the global toxicity score was significantly associated with plasma levels of MTX at 24 h ($\beta = 0.64$; $R^2 = 0.41$; $p = 0.001$), 48 h ($\beta = 0.43$; $R^2 = 0.19$; $p = 0.01$) and 72 h ($\beta = 0.37$; $R^2 = 0.14$; $p = 0.03$) (Table 2).

Methotrexate plasma levels ≥10 µmol/L at 24 h were significantly associated with higher HCY plasma levels at 24 and 48 h after the initiation of MTX infusion (Table 3).

Table 2. Risk factors for MTX toxicity (univariate linear regression)

Patients	p-value (Fisher's exact test, global)	β	β0	R^2 (%)
Age at diagnosis [years]	0.45	0.13	3.1	1.7
Gender (M vs F)	0.78	0.04	3.1	0.2
Immunophenotype (T vs B)	0.67	–0.07	4.5	0.6
Weight	0.37	0.15	2.7	2.4
Height	0.4	0.1	1.5	2.1
BSA	0.35	0.16	2.3	2.6
Risk group (AR1, AR2, HR)	0.14	0.2	0.5	0.6
Plasma levels of MTX 24 h 48 h 72 h	 10^{-3} 0.01 0.03	 0.64 0.43 0.37	 0.9 2.4 2.5	 41.1 19.1 14.3
Plasma levels of HCY 24 h 48 h 72 h	 0.14 0.02 0.18	 0.28 0.4 –0.31	 2.4 2.1 1.3	 4.5 12.8 4.8
MTHFR C677T (*CT* vs *CC*)	0.02	0.4	1.8	19

BSA – body surface area; MTX – methotrexate; HCY – homocysteine; M – males; F – females; AR – average risk; HR – high risk; β – regression coefficient; β0 – intercept coefficient.

As shown in Table 3, the global toxicity score was significantly correlated with MTX levels >10 µmol/L at 24 h, 1 µmol/L at 48 h and 0.1 µmol/L at 72 h. Gastrointestinal and skin toxicity were significantly associated with high MTX plasma levels 48 and 72 h after MTX infusion (Table 3).

Plasma homocysteine levels and methotrexate-related toxicity

The univariate linear regression revealed a positive correlation between global toxicity score and plasma HCY

Table 3. Correlation between folate pathway and MTX toxicity

Plasma HCY and MTX toxicity	Plasma MTX						*MTHFR*	
	at 24 h (n = 31)		at 48 h (n = 32)		at 72 h (n = 30)			
	<10 μM (n = 25)	≥10 μM (n = 6)	<1 μM (n = 18)	≥1 μM (n = 14)	<0.1 μM (n = 19)	≥0.1 μM (n = 11)	CC (n = 22)	CT (n = 6)
Plasma HCY at 24 h [μM], mean ±SEM	11.6 ±0.6	15 ±1.8*	12.2 ±0.8	12.3 ±1.3	12 ±0.7	13 ±1.3	12 ±0.7	13.3±2
Plasma HCY at 48 h [μM], mean ±SEM	8.8 ±0.5	11.6 ±0.9*	9.2 ±0.6	10 ±0.7	9.1 ±0.6	10 ±0.8	8.2 ±0.5	10 ±0.9
Plasma HCY at 72 h [μM], mean ±SEM	8.5 ±0.8	6.3 ±4	9.6 ±1	7 ±1.1	8.7 ±1	8.2 ±1.7	8.1 ±0.9	5.9 ±3
Global toxicity, mean ±SEM	2.5 ±0.5	7.5 ±1.6*	1.6 ±0.5	6.3 ±0.7*	1.5 ±0.4	6.7 ±0.8*	2.5 ±0.6	6.1 ±1.7*
Gastrointestinal toxicity (n)	8	3	4	9†	4	7†	8	3
Mucositis (n)	2	2	1	4	1	5†	2	1
Nausea/vomiting/diarrhea (n)	4	3	2	7†	3	4	4	3
Abdominal pain (n)	3	1	2	3	1	3	4	1
Liver toxicity (n)	6	5	6	6	6	6	5	4
Renal toxicity (n)	0	1	0	1	0	1	0	1
Neurotoxicity (n)	2	2	1	3	1	1	1	2
Seizure (n)	1	0	0	1	0	0	1	0
Somnolence (n)	1	0	1	0	1	0	0	1
Paralysis (n)	0	1	0	1	0	1	–	–
Agitation (n)	1	0	0	1	0	0	1	0
Anxiety/mood disorder (n)	0	1	0	1	0	0	0	1
Skin toxicity (n)	4	3	1	6†	2	5†	3	2
Hematotoxicity (n)	2	0	2	0	1	1	2	0
Thrombocytopenia (n)	1	0	1	0	1	0	1	0
Hemorrhage (n)	1	0	1	0	0	1	1	0
Phlebitis (n)	1	1	1	1	1	1	1	1

MTX – methotrexate; HCY – homocysteine; SEM – standard error of the mean; * statistically significant differences between groups estimated using Mann-Whitney U test; † statistically significant differences between groups estimated using Fisher's exact test.

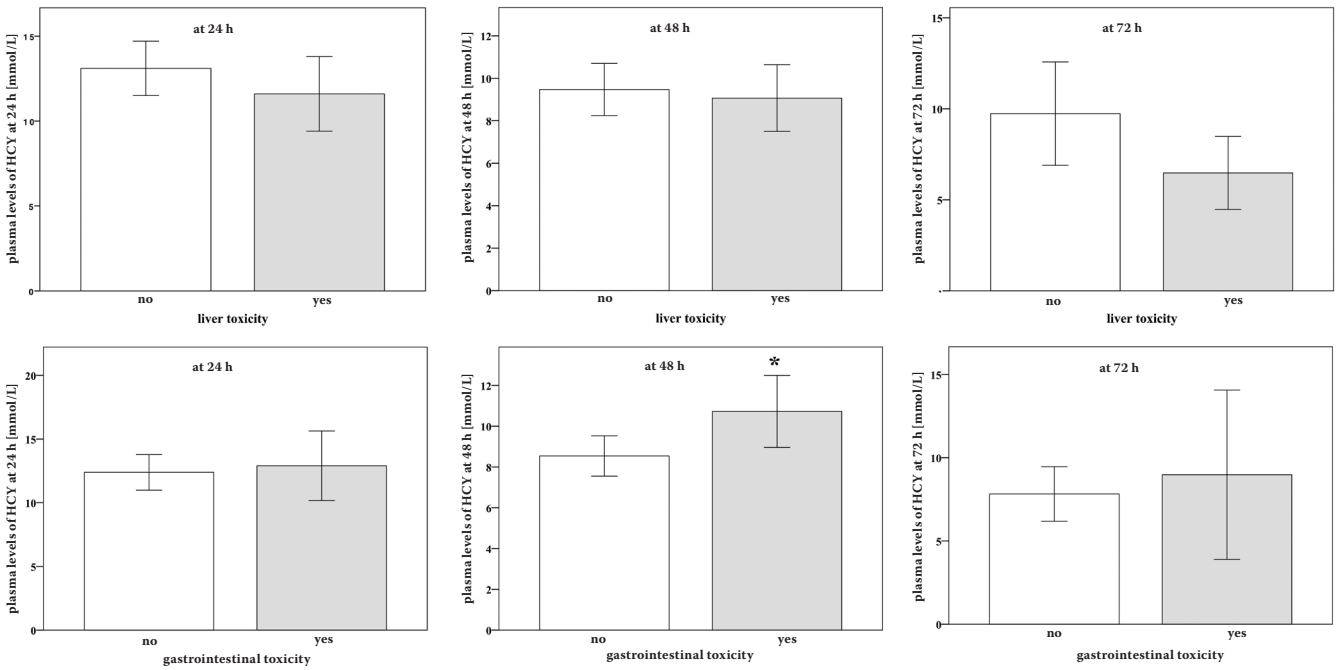

Fig. 2. Association of liver toxicity and gastrointestinal toxicity with plasma homocysteine levels

Each column represents mean with standard deviation (±SD); HCY – homocysteine; * p = 0.02.

levels within 48 h after MTX administration (β = 0.4; R^2 = 0.12; p = 0.02) (Table 2). Figure 2 shows that HCY plasma levels at 48 h were significantly higher in patients with gastrointestinal toxicity (p = 0.02).

Gene polymorphisms and methotrexate-related toxicity

The *MTHFR C677T* polymorphism was in Hardy-Weinberg equilibrium. *MTHFR 677C>T* was of the wild type (CC) in 22 patients (78.6%) and 70 controls (100%), and heterozygous (CT) in 6 (21.4%).

The influence of this polymorphism on MTX toxicity was analyzed in 28 patients with ALL included in this study. The mean global toxicity score was significantly higher in *MTHFR 677 CT* genotype than in wild genotype (p = 0.02) (Tables 2,3).

There was no significant association between *MTHFR 677 C>T* polymorphism and plasma MTX levels.

Risk factors for methotrexate toxicity

In a multiple regression model, the global toxicity score was significantly associated with 2 variables: higher MTX plasma levels at 48 h (≥1µmol/L) (β = 0.5; R^2 = 0.38; p = 0.001) and CT 677 *MTHFR* genotype (β = 0.3; R^2 = 0.38; p = 0.01).

Discussion

Intravenous HD-MTX is a key component in the therapy of ALL.[3] However, despite leucovorin rescue with hydration and urinary alkalinization, MTX is associated with serious toxicities in a considerable number of patients.[15] This could lead to the interruption of treatment, which may increase relapse risk.

This study identified several clinical variables that influence MTX toxicity in patients with ALL treated according to the EORTC-CLG 58951 protocol. We used the global toxicity score that integrates both severity and frequency of MTX toxicity during 173 HD-MTX courses.

One of the major limitations of the current study was the small sample size; studies with a greater number of patients would be necessary to confirm our results. However, a homogenous diagnosis, a standardized treatment protocol followed by all patients, objective and well-recorded toxicity data make the results credible.

High-dose methotrexate was associated with toxicities in the majority of patients included in this study (71.1%). Consistent with previous studies, we found that the most common side effects following HD-MTX therapy were hepato-, skin and gastrointestinal toxicity, particularly the oral mucositis.[18]

This toxicity is unpredictable because of large inter-patient variability in the pharmacokinetics and pharmacodynamics of this drug, even with the same treatment protocol.[5,7,18] The mechanism of MTX-induced toxicity could be mainly explained by an inhibition of normal cells and tissue adjacent to the target abnormal cells.[8]

In this study, acute MTX-induced hepatotoxicity was expressed by elevated ASAT/ALAT and was observed in 37.1% of patients. The pathophysiology of this side effect remains unclear. Holmboe et al. suggested that 7-OH-MTX, a main metabolite of MTX, was involved in the development of HD-MTX hepatic toxicity in patients with osteosarcoma treated with HD-MTX.[19]

Oral mucositis was the most severe MTX-related toxicity observed in this study. Considerable effort has been expended to identify the etiopathophysiology of this side effect.[20,21] Pico et al. reported that MTX may be secreted in the saliva, leading to increased direct mucotoxicity.[22]

In the present study, we analyzed the relation between MTX pharmacokinetics and MTX-related toxicities during HD-MTX courses. In multiple linear regression analysis, we found that plasma MTX levels at 48 h were significantly correlated with the global toxicity score. Currently, few studies among patients with ALL have reported that the plasma levels of MTX may influence the risk of MTX toxicity.[23–25]

In the current study, acute MTX-induced hepatotoxicity, which was the most common side effect, was not associated with plasma MTX levels. This can be explained by the fact that the small number of children in this study could influence its power to detect a significant association.

We found that the risk of oral mucositis was significantly associated with high MTX plasma levels 72 h after drug infusion (Table 3). This finding is consistent with those of Cheng, who revealed that 64% of children with oral mucositis had plasma MTX levels above the defined upper limit of the expected profile at 66 h.[25] It is rather remarkable to find a higher frequency of nausea/vomiting episodes in patients with high MTX plasma levels at 48 h. Although the exact mechanism is unclear, it was reported that nausea/vomiting can lead to dehydration, causing decreased glomerular filtration rates, and thus limited renal clearance of MTX.[24]

It was also reported that MTX-related toxicity might be explained through the disruption of folate homeostasis.[26] In this study, we determined the plasma HCY levels, since it was considered a sensitive marker of deficient folate homeostasis.[27]

We found that elevated levels of HCY were associated with higher MTX plasma levels at 24 h, which is consistent with the previous study.[28] This can be explained by the interference of MTX with the metabolism of HCY by reducing the level of 5-methyl-THF, which serves as the donor of the methyl group for the methylation of HCY to methionine. As a result, the levels of HCY increase, whereas the levels of methionine decrease.[29]

Moreover, we found that global toxicity score, particularly gastrointestinal toxicity, was associated with

a significant rise in plasma HCY levels within 48 h after MTX administration. Although a strong association between blood levels of HCY and the risk of the development of CNS disorders has been shown, there are few studies reporting such an association with gastrointestinal toxicity.[30–32] Hyperhomocysteinemia may induce cell damage through a number of complex mechanisms, including interference with the methylation process and disturbance of oxidative stress balance.[33–35]

Therefore, an increased level of HCY might be considered a sensitive marker of MTX toxicity.

The *MTHFR* gene is located at the end of the short arm of chromosome 1 (1p36.3), and the encoded protein, *MTHFR*, is a key enzyme in folate metabolism.[36,37] The C677T single nucleotide polymorphism (SNP) is the most studied polymorphism in the *MTHFR* gene and results in an alanine-to-valine substitution at codon 222. Its variant alleles cause a substantial reduction of the *MTHFR* enzyme activity in vitro compared with the wild type allele.[38] People with a heterozygous *MTHFR 677 CT* genotype have 60% enzyme activity compared with those with the wild-type allele.[39] In the present study, we investigated whether there exists an influence of *MTHFR C677T* polymorphism on MTX-related toxicity. We found a significantly increased risk of MTX-related toxicity in patients with 677CT genotype compared with the wild genotype 677CC. This result was consistent with previous studies.[40,41] A meta-analysis of studies concerning the toxicity of low-dose MTX (10–15 mg/week) in rheumatoid arthritis suggested that C677T polymorphism was significantly associated with increased toxicity.[40] Another meta-analysis in ALL patients, including 21 articles published before September 2010, supported this association and suggested that the 677T allele serves as a toxicity predictor during treatment with MTX.[41]

In conclusion, the results of our study suggest that routine monitoring of plasma MTX levels during 48–72 h is essential to detect patients at a high risk of developing toxicity and to adjust leucovorin rescue and hydration. Moreover, we suggest that *MTHFR C677T* genotyping may be useful for predicting MTX toxicity. Future studies with large sample sizes should be undertaken to verify current findings, which may provide further biomarkers of treatment efficacy and toxicity in patients with ALL.

References

1. Pui CH, Evans WE. Treatment of acute lymphoblastic leukemia. *N Engl J Med*. 2006;354:166–178.
2. Pui CH, Relling MV, Downing JR. Acute lymphoblastic leukemia. *N Engl J Med*. 2004;350:1535–1548.
3. de Beaumais TA, Jacqz-Aigrain E. Intracellular disposition of methotrexate in acute lymphoblastic leukemia in children. *Curr Drug Metab*. 2012;13:822–834.
4. Assaraf YG. Molecular basis of antifolate resistance. *Cancer Metastasis Rev*. 2007;26:153–181.
5. Mikkelsen TS, Thorn CF, Yang JJ, et al. PharmGKB summary: Methotrexate pathway. *Pharmacogenet Genomics*. 2011;21:679–686.
6. Bagley PJ, Selhub J. A common mutation in the methylenetetrahydrofolate reductase gene is associated with an accumulation of formylated tetrahydrofolates in red blood cells. *Proc Natl Acad Sci USA*. 1998;95:13217–13220.
7. Ongaro A, De Mattei M, Della Porta MG, et al. Gene polymorphisms in folate metabolizing enzymes in adult acute lymphoblastic leukemia: Effects on methotrexate-related toxicity and survival. *Haematologica*. 2009;94:1391–1398.
8. Treon SP, Chabner BA. Concepts in use of high-dose methotrexate therapy. *Clin Chem*. 1996;42:1322–1329.
9. Tantawy AA, El-Bostany EA, Adly AA, et al. Methylene tetrahydrofolate reductase gene polymorphism in Egyptian children with acute lymphoblastic leukemia. *Blood Coagul Fibrinolysis*. 2010;21:28–34.
10. Vilmer E, Suciu S, Ferster A, et al.; Children Leukemia Cooperative Group. Long-term results of three randomized trials (58831, 58832, 58881) in childhood acute lymphoblastic leukemia: A CLCG-EORTC report. *Leukemia*. 2000;14:2257–2266.
11. De Moerloose B, Suciu S, Bertrand Y, et al. Improved outcome with pulses of vincristine and corticosteroids in continuation therapy of children with average risk acute lymphoblastic leukemia (ALL) and lymphoblastic non-Hodgkin lymphoma (NHL): Report of the EORTC randomized phase 3 trial 58951. *Blood*. 2010;116:36–44.
12. Domenech C, Suciu S, De Moerloose B, et al. Dexamethasone (6 mg/m^2/day) and prednisolone (60 mg/m^2/day) were equally effective as induction therapy for childhood acute lymphoblastic leukemia in the EORTC CLG 58951 randomized trial. *Haematologica*. 2014;99:1220–1227.
13. Nirenberg A, Mosende C, Mehta BM, Gisolfi AL, Rosen G. High-dose methotrexate with citrovorum factor rescue: Predictive value of serum methotrexate concentrations and corrective measures to avert toxicity. *Cancer Treat Rep*. 1977;61:779–783.
14. Paci A, Veal G, Bardin C, et al. Review of therapeutic drug monitoring of anticancer drugs. Part 1: Cytotoxics. *Eur J Cancer*. 2014;50:2010–2019.
15. Ayad MW, El Naggar AA, El Naggar M. *MTHFR C677T* polymorphism: Association with lymphoid neoplasm and effect on methotrexate therapy. *Eur J Haematol*. 2014;93:63–69.
16. National Institutes of Health. National Cancer Institute CTEP CTCAE v. 5.0. 2016. http://ctep.cancer.gov/. Accessed November 27, 2017.
17. Radtke S, Zolk O, Renner B, et al. Germline genetic variations in methotrexate candidate genes are associated with pharmacokinetics, toxicity, and outcome in childhood acute lymphoblastic leukemia. *Blood*. 2013;121:5145–5153.
18. Schmiegelow K. Advances in individual prediction of methotrexate toxicity: A review. *Br J Haematol*. 2009;146:489–503.
19. Holmboe L, Andersen AM, Mørkrid L, Slørdal L, Hall KS. High dose methotrexate chemotherapy: Pharmacokinetics, folate and toxicity in osteosarcoma patients. *Br J Clin Pharmacol*. 2012;73:106–114.
20. Sonis ST. Mucositis as a biological process: A new hypothesis for the development of chemotherapy-induced stomatotoxicity. *Oral Oncol*. 1998;34:39–43.
21. Sonis ST, Elting LS, Keefe D, et al.; Mucositis Study Section of the Multinational Association for Supportive Care in Cancer, International Society for Oral Oncology. Perspectives on cancer therapy-induced mucosal injury: Pathogenesis, measurement, epidemiology, and consequences for patients. *Cancer*. 2004;100:1995–2025.
22. Pico JL, Avila-Garavito A, Naccache P. Mucositis: Its occurrence, consequences, and treatment in the oncology setting. *Oncologist*. 1998;3:446–451.
23. Rask C, Albertioni F, Bentzen SM, Schroeder H, Peterson C. Clinical and pharmacokinetic risk factors for high-dose methotrexate-induced toxicity in children with acute lymphoblastic leukemia – a logistic regression analysis. *Acta Oncol*. 1998;37:277–284.
24. Relling MV, Fairclough D, Ayers D, et al. Patient characteristics associated with high-risk methotrexate concentrations and toxicity. *J Clin Oncol*. 1994;12:1667–1672.
25. Cheng KK. Association of plasma methotrexate, neutropenia, hepatic dysfunction, nausea/vomiting and oral mucositis in children with cancer. *Eur J Cancer Care* (*Engl*). 2008;17:306–311.
26. Cole PD, Beckwith KA, Vijayanathan V, Roychowdhury S, Smith AK, Kamen BA. Folate homeostasis in cerebrospinal fluid during therapy for acute lymphoblastic leukemia. *Pediatr Neurol*. 2009;40:34–41.
27. Valik D, Radina M, Sterba J, Vojtesek B. Homocysteine: Exploring its potential as a pharmacodynamic biomarker of antifolate chemotherapy. *Pharmacogenomics*. 2004;5:1151–1162.

28. Kubota M, Nakata R, Adachi S, et al. Plasma homocysteine, methionine and S-adenosylhomocysteine levels following high-dose methotrexate treatment in pediatric patients with acute lymphoblastic leukemia or Burkitt lymphoma: Association with hepatotoxicity. *Leuk Lymphoma*. 2014;55:1591–1595.
29. Tufekci O, Yilmaz S, Karapinar TH, et al. A rare complication of intrathecal methotrexate in a child with acute lymphoblastic leukemia. *Pediatr Hematol Oncol*. 2011;28:517–522.
30. Seshadri S, Wolf PA, Beiser AS, et al. Association of plasma total homocysteine levels with subclinical brain injury: Cerebral volumes, white matter hyperintensity, and silent brain infarcts at volumetric magnetic resonance imaging in the Framingham Offspring Study. *Arch Neurol*. 2008;65:642–649.
31. Bottiglieri T. Homocysteine and folate metabolism in depression. *Prog Neuropsychopharmacol Biol Psychiatry*. 2005;29:1103–1112.
32. Haagsma CJ, Blom HJ, van Riel PL, et al. Influence of sulphasalazine, methotrexate, and the combination of both on plasma homocysteine concentrations in patients with rheumatoid arthritis. *Ann Rheum Dis*. 1999;58:79–84.
33. Crider KS, Yang TP, Berry RJ, Bailey LB. Folate and DNA methylation: A review of molecular mechanisms and the evidence for folate's role. *Adv Nutr*. 2012;3:21–38.
34. Ientile R, Curro' M, Ferlazzo N, Condello S, Caccamo D, Pisani F. Homocysteine, vitamin determinants and neurological diseases. *Front Biosci* (*Schol Ed*). 2010;2:359–372.
35. Papatheodorou L, Weiss N. Vascular oxidant stress and inflammation in hyperhomocysteinemia. *Antioxid Redox Signal*. 2007;9:1941–1958.
36. Goyette P, Sumner JS, Milos R, et al. Human methylenetetrahydrofolate reductase: Isolation of cDNA, mapping and mutation identification. *Nat Genet*. 1994;7:195–200.
37. Kim YI. Folate and carcinogenesis: Evidence, mechanisms, and implications. *J Nutr Biochem*. 1999;10:66–88.
38. Yamada K, Chen Z, Rozen R, Matthews RG. Effects of common polymorphisms on the properties of recombinant human methylenetetrahydrofolate reductase. *Proc Natl Acad Sci USA*. 2001;98:14853–14858.
39. Robien K, Ulrich CM. 5,10-methylenetetrahydrofolate reductase polymorphisms and leukemia risk: A HuGE minireview. *Am J Epidemiol*. 2003;157:571–582.
40. Fisher MC, Cronstein BN. Metaanalysis of methylenetetrahydrofolate reductase (*MTHFR*) polymorphisms affecting methotrexate toxicity. *J Rheumatol*. 2009;36:539–545.
41. Yang L, Hu X, Xu L. Impact of methylenetetrahydrofolate reductase (*MTHFR*) polymorphisms on methotrexate-induced toxicities in acute lymphoblastic leukemia: A meta-analysis. *Tumour Biol*. 2012; 33:1445–1454.

Opioidergic conditioning of the human heart muscle in nitric oxide-dependent mechanism

Marcin Kunecki[1,A–D], Tomasz Roleder[2,A–C], Jolanta Biernat[3,C,E,F], Paweł Kukla[4,D,E], Lidia Tomkiewicz-Pająk[1,C,E,F], Marek A. Deja[5,A,E,F], Piotr Podolec[1,E,F], Krzysztof S. Gołba[3,A,E,F], Wojciech Płazak[1,D–F]

[1] Department of Cardiac and Vascular Diseases, John Paul II Hospital, Jagiellonian University Medical College, Kraków, Poland
[2] Department of Cardiology, Medical University of Silesia in Katowice, Poland
[3] Department of Electrocardiology and Heart Failure, Medical University of Silesia in Katowice, Poland
[4] Faculty of Health Sciences, Jagiellonian University Medical College, Kraków, Poland
[5] Department of Cardiac Surgery, Medical University of Silesia in Katowice, Poland

A – research concept and design; B – collection and/or assembly of data; C – data analysis and interpretation;
D – writing the article; E – critical revision of the article; F – final approval of the article

Advances in Clinical and Experimental Medicine, ISSN 1899-5276 (print), ISSN 2451-2680 (online) *Adv Clin Exp Med*. 2018;27(8):1069–1073

Address for correspondence
Marcin Kunecki
E-mail: mkunecki@op.pl

Funding sources
None declared

Conflict of interest
None declared

Received on February 18, 2016
Reviewed on November 28, 2016
Accepted on April 4, 2017

Abstract

Background. Opioidergic conditioning is well documented to trigger cardioprotection against ischemia/reperfusion (I/R) injury. Previous studies on animal models have suggested that nitric oxide (NO) mediates the beneficial effect of opioids, but the role of NO in humans seems to be controversial.

Objectives. The aim of the study was to assess the influence of NO modulators on opioid-induced cardioprotection in the human myocardium.

Material and methods. Trabeculae of the human right atria were electrically driven in an organ bath and subjected to simulated I/R injury. The non-selective inhibitor of nitric oxide synthase (NOS) – *N*-methyl-L-arginine (LNMMA), the donor of NO – *S*-Nitroso-*N*-acetylpenicillamine (SNAP) or morphine (in the amount of 10^{-4} M) were used at the time of re-oxygenation. The additional trabecula was subjected to the hypoxia protocol only (control). The contractility of the myocardium was assessed as the maximal force of a contraction (Amax), the rate of rise of the force of a contraction (Slope L) and the cardiac muscle relaxation – as the rate of decay of the force of a contraction (Slope T).

Results. The application of 100 μM LNMMA resulted in the decrease of Amax, Slope L and Slope T during the re-oxygenation period as compared to control. The application of 10^{-4} M morphine and/or 100 μM SNAP resulted in a partial reversal of the detrimental influence of LNMMA.

Conclusions. At the re-oxygenation period, the blockade of NO synthesis has a deleterious effect on the systolic and diastolic function of the human myocardium as well as attenuates the beneficial effect of morphine conditioning.

Key words: ischemia, nitric oxide, reperfusion, morphine

DOI
10.17219/acem/70192

Introduction

Ischemic heart disease is known as the leading cause of morbidity and mortality in adults. Early reperfusion is necessary to restore perfusion of the ischemic heart muscle. However, reperfusion may induce a cascade of pathophysiological reactions, increasing the infarct area of the myocardium by up to 50% of the final size.[1] Sequences of brief episodes of non-lethal ischemia and reperfusion applied before (ischemic preconditioning – IPC) or after (ischemic postconditioning – POC) the coronary occlusion are well documented to reduce ischemia/reperfusion (I/R) injury. Regarding the fact that applying these techniques in humans is impractical, as well as that the results from human trials have been controversial,extensive research efforts have been made to find pharmacological agents which can mimic these cardioprotective strategies.[2–4] The mechanisms underlying IPC or POC are still not clarified, but strong experimental evidence suggests that opioids may be a part of the endogenous cardioprotective response to I/R injury and trigger intracellular enzyme cascades, leading ultimately to the closure of the mitochondrial permeability transition pores (mPTP), responsible for the induction of cell damage.[5] Previous studies on animal models have suggested the nitric oxide (NO)/cyclic guanosine monophosphate (cGMP) signaling as the main pathway involved in the beneficial effect of opioids, but our understanding of the role of nitric oxide synthases (NOS) in modulating I/R injury in humans remains limited. We hypothesize that the opioid receptor activation provides cardioprotection in the human heart muscle through a NO-dependent pathway, which may give insight into explaining the protective mechanisms against I/R injury.

Material and methods

Material

The experiments were performed on muscular trabeculae obtained from the right heart atrial appendages of 58 consecutive patients (35 males and 23 females) subjected to the coronary artery bypass surgery. Patients diagnosed with significant valvular heart disease or with severe heart failure were excluded from the study. The patients' demographic data is presented in Table 1.

Methods

Fragments of the human right heart atria were transported from the cardiac surgery room to the laboratory in the ice-cold Krebs-Henseleit solution ([M]: 118.0 NaCl, 4.70 KCl, 1.52 $CaCl_2$, 1.64 $MgSO_4$, 24.88 $NaHCO_3$, 1.18 KH_2PO_4, 11.0 glucose, and 2.0 sodium pyruvate; pH 7.4). Two muscular trabeculae were dissected from the right heart atria and incubated in 2 separate organ baths (Schuler Organ Bath, Hugo Sachs Elektronik – HSE, March-Hugstetten, Germany), both filled with the Krebs-Henseleit solution warmed up to 37°C. To avoid core hypoxia, the trabeculae included in the study had a cross-sectional area <1 mm in diameter. Two trabeculae from each patient were always studied simultaneously and exposed to the hypoxia protocol including 60 min of hypoxia (incubation in the Krebs-Henseleit buffer deprivated of glucose and pyruvate saturated with 95% argon and 5% carbon dioxide) with subsequent 60 min of re-oxygenation (incubation in the Krebs-Henseleit buffer saturated with the 95% oxygen and 5% carbon dioxide). The buffer was replaced every 15 min, except the time of hypoxia. Every trabecula was stretched to 90% of its optimal tension strength according to the Frank-Starling relationship, and all trabeculae were driven throughout the experiments with 1 Hz 50 ms square stimuli, using platinum field electrodes and a stimulator (Type 215, HSE). The contractive function of every trabecula was recorded with the use of a transducer (Type 372, HSE). The signal was enhanced with a bridge amplifier (Type 336, HSE), and recorded by a PowerLab/4SP system and analyzed off-line using Chart software (ADInstruments, Chalgrove, UK). Each experimental protocol was completed with the application of 10 μM of norepinephrine (NE) to assess the viability of the trabeculae.

Table 1. The patients' demographic data, preoperative drug treatment and preoperative left ventricular ejection fraction

1	men/women, n	35/23
2	age [years]	62.8 ±5.7
3	ejection fraction, mean ±SD	52.3 ±2.39%
4a	diabetes, n (%)	12 (20)
4b	diabetes with insulin treatment, n (%)	7 (12)
5	Drugs, n (%)	
5a	beta-blockers	43 (75)
5b	calcium channel blockers	10 (18)
5c	angiotensin II converting enzyme inhibitors	30 (52)
5d	angiotensin II receptor blockers	2 (3)
5e	statins	40 (69)

SD – standard deviation.

Protocols

To determine the effects of modulation of the NO pathway, the non-selective inhibitor of NOS – *N*-methyl-L-arginine (LNMMA), the donor of NO – *S*-nitroso-*N*-acetylpenicillamine (SNAP) or morphine (in the amount of 10^{-4} M) were used at the time of re-oxygenation. The other trabecula was subjected only to the hypoxia protocol (control). The experimental protocols are depicted in Fig. 1.

The contractility of the myocardium assessed as the maximal force of a contraction (maximal amplitude of the peak – Amax), the rate of rise of the force of a contraction (the slope of the leading edge of the peak

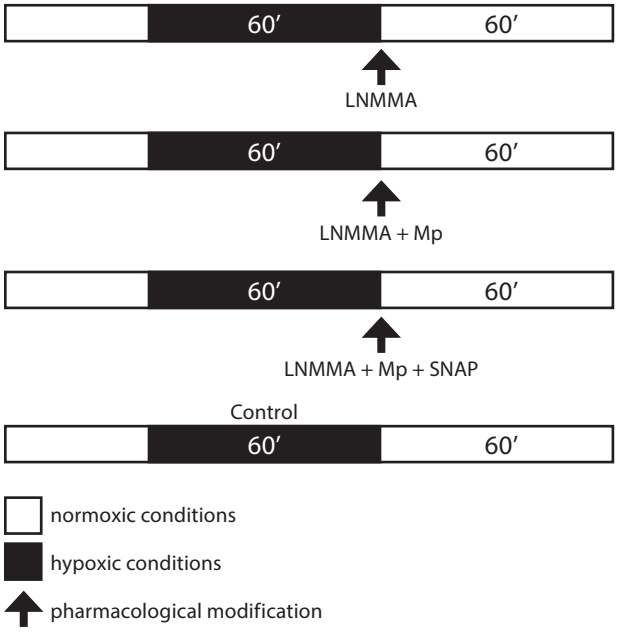

Fig. 1. Protocols for the experimental groups

Mp – morphine.

– Slope L) and the cardiac muscle relaxation – as the rate of decay of the force of a contraction (the slope of trailing edge of the peak – Slope T) were obtained in the 5th, 10th, 15th, 30th, 45th, and 60th min of re-oxygenation and after the NE application.

Data analysis

The results are presented as the percentages of the values obtained before the experimental protocol application. All continuous data is presented as a mean ± standard error of the mean (SEM). Two-way analysis of variance (ANOVA) with Holm-Sidack test was used to compare the values from the 5th to the 60th min of re-oxygenation. The p-values <0.05 were considered statistically significant. Statistical analysis was performed using SigmaPlot software v. 10.0.1.2. (Systat Software Inc., San Jose, USA).

The approval of the local bioethics committee for the use of human tissue was obtained and individual patient consent was waived. All experiments were performed according to the principles stated in the Declaration of Helsinki.

Results

There were no significant differences in age, sex and pharmacotherapy between the patients from whom the trabeculae were taken and subjected to each experimental protocol.

The application of the NOS blocker – LNMMA at a concentration of 10^{-4} M resulted in the decrease of Amax, Slope L and Slope T as compared to control. The co-application of 10^{-4} M morphine with LNMMA, or the application of LNMMA, morphine and SNAP at a concentration of 10^{-4} M partially reversed the detrimental effect of LNMMA. All detailed results are depicted in Fig. 2.

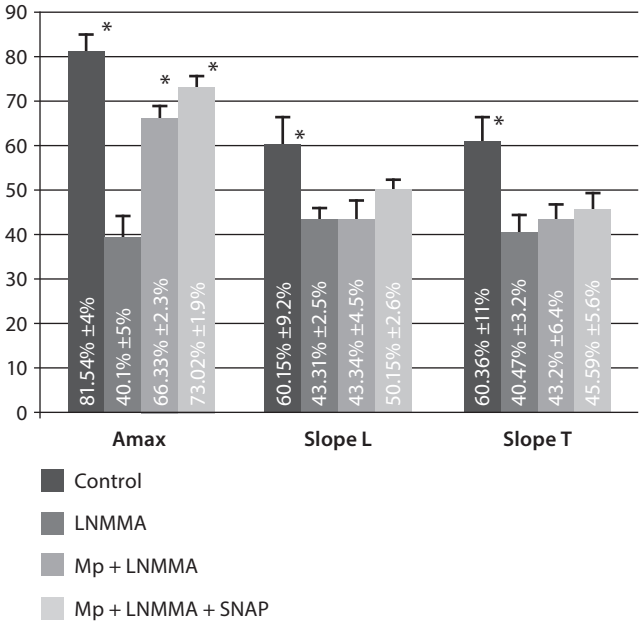

Fig. 2. The effect of *N*-methyl-L-arginine (LNMMA), morphine (Mp) and/or *S*-nitroso-*N*-acethylpenicillamine (SNAP) on the function of the human myocardium during the re-oxygenation period

Control – the protocol with hypoxic conditions only.

Discussion

Due to the role of NO in cardioprotection, the use of NO donors has been proposed for the prevention of I/R injury and the treatment of chronic cardiovascular diseases.

Accordingly to the earlier obtained data,we reported the cardioprotective effect of morphine on the function of the human heart muscle.[6,7] In this study, we showed that NO plays an important role in intermediating the beneficial influence of opioids. The NOS blockade completely abrogated the effect of morphine. Moreover, the NOS blockade constituted a deleterious factor on the myocardium that is strong enough to outweigh the protective influence of morphine and of the NO donor. To our knowledge, this is the first presentation of the fact that the NO signaling pathway is crucial in the mechanism of protection in relation to the function of the human heart muscle.

Previous studies on the influence of opioids and the NO pathway on I/R injury utilized mainly animal models. We assessed the effect of the co-operation of opioids with NO on the systolic and diastolic function of the hypoxic human myocardium in vitro. Our study was performed on isolated fragments of the human right

atria. For functional studies, due to atrial tissue sampling, it is possible to avoid the influence of confounding factors, like the effect of drugs or the presence of collateral circulation. In this model we did not assess the infarct size, but the differences of contractility as functional consequences of cardiac ischemia.

Morphine is commonly used as an analgetic drug in acute myocardial infarction. This was the first opioid drug shown to be cardioprotective against I/R injury. Opioids also appear to mediate cardioprotective strategies – IPC and POC, brief non-lethal episodes of acute lethal I/R injury – applied respectively before the onset of the re-oxygenation period.[8,9] The beneficial effect of opioids, IPC or POC has been shown in many studies using animal models and clinical trials,although the intracellular mechanism responsible for this phenomena remains not fully understood.[10–12]

It is well-known that NO acts as a modulator of the analgetic effect of morphine and the inhibitors of the NO/cGMP pathway attenuate this effect.[13] Several studies reported that the NO inhalation effectively reduced the infarct size of the heart muscle and improved the cardiac function in porcine and rodent models of I/R injury.[14,15] Recently, it has been shown that remote intrathecal fentanyl preconditioning induces cardioprotective effects in rats via the activation of NOS, and that the NOS inhibitor – N omega--nitro-L-arginine methyl ester (L-NAME) abolished this effect.[16,17] Further studies highlight the role of the increased expression and activity of NOS in delayed protective effects of IPC.[18] POC also increases NOS activity; likewise, the NOS blockade with L-NAME abrogates the beneficial effect of POC.[19]

In our study, the use of the NO-donor, SNAP, improved the systolic and diastolic function of human myocardium in the re-oxygenation period. In a rat model, the administration of SNAP reduced the size of necrosis.[20] Moreover, the use of a substrate for the synthesis of NO, L-arginine, resulted in a reduction in infarct size and improved the cardiac systolic function.[19] Apart from the fact that SNAP releases NO, providing a mediator of intracellular pathways, it has also the ability to inhibit the inducible NOS (iNOS) expression, responsible for the synthesis of the highly reactive peroxynitrite ($ONOO^-$), preventing damage generated by oxidative stress.[21] Although higher SNAP concentrations did not confer protection, which results from twofold nature of NO.[20] The cardioprotective effect depends on the balance between NO and reactive oxygen species (ROS). ROS released during re-oxygenation lead to the opening of mPTP, which triggers the depolarization of the mitochondrial inner membrane, resulting in the adenosine triphosphate (ATP) depletion, the respiratory chain inhibition and the rupture of the mitochondrial outer membrane. The activation of protein kinases, such as Akt, glycogen synthase kinase 3β (GSK-3β), which consists of the element downstream of NO/cGMP in the intracellular pathway of opioids, prevents the opening of mPTP.[22] Physiological NO concentration inhibits the mPTP opening, whereas a high concentration of NO favors the creation of $ONOO^-$ and triggers the mPTP opening related to the formation of disulfide bonds.[23] Furthermore, the transient activation of NOS during reperfusion involves the rapid consumption of L-arginine and tetrahydrobiopterin, causing the production of the superoxide anion instead of NO.[24]

It is feasible that the cooperation of opioids with NO in the cardioprotective effect arises from the common signaling pathway. On the contrary, the double-edge sword effect of NO donors explains the diverging results, which is reflected in the exogenous nitrate tolerance.[24]

Limitations

The results must be interpreted within the limitations of the methodology. The construction of our experiment assumes a control group derived from the same patient, and the same factors potentially affecting the test. We must note, however, that the simulated ischemic model differs from in vivo conditions. In our experiment, we utilized the buffer, so there were no elements transporting or binding opioids, like peptides. However, the pathophysiological and functional changes that took place in our model of I/R injury are comparable to the change that takes place in in vivo conditions. The instantaneous NO concentration is crucial in many processes, but its evaluation is hard to obtain, which constitutes the limitation of the method.

Conclusions

In the re-oxygenation period, the blockade of NO synthesis has a deleterious effect on the systolic and diastolic function of the human myocardium.

All protocols were preceded by a stabilization period of 45–60 min. This was followed by 60 min of simulated ischemia (superfusion with the hypoxic, substrate-free Krebs-Henseleit solution and a pacing at 1 Hz) and 60 min of superfusion with the re-oxygenated Krebs-Henseleit solution. In protocols with a pharmacological modification, *N*-methyl-L-arginine at a concentration of 10^{-4} M, *S*-nitroso-*N*-acetylpenicillamine at a concentration of 10^{-4} M and/or morphine at a concentration of 10^{-4} M were used. Control – the protocol with hypoxia conditions only.

Figures present parameters of the contraction as maximal force of a contraction (Amax), the rate of rise of the force of a contraction (Slope L) and the relaxation parameter – the rate of decay of the force of a contraction (Slope T); * indicates significantly higher values ($p < 0.05$) vs LNMMA.

References

1. Hausenloy DJ, Yellon DM. Preconditioning and postconditioning: New strategies for cardioprotection. *Diabetes Obes Metab*. 2008;10(6):451–459.
2. Meybohm P; RIPHeart Study Collaborators. A multicenter trial of remote ischemic preconditioning for heart surgery. *NEJM*. 2015;373(15):1397–1407. doi:10.1056/ NEJMoa1413579
3. Hausenloy DJ, Yellon DM; ERICCA Trial Investigators. Remote ischemic preconditioning and outcomes of cardiac surgery. *NEJM*. 2015;373(15):1408–1417. doi:10.1056/NEJMoa1413534
4. Hahn JY, Yu CW, Park HS, et al. Long-term effects of ischemic postconditioning on clinical outcomes: 1-year follow-up of the POST randomized trial. *Am Heart J*. 2015;169(5):639–646. doi:10.1016/j.ahj.2015.01.015
5. Lu XH, Ran K, Xiao YY, et al. Protective effects of morphine preconditioning in delayed phase on myocardial ischemia – reperfusion injury in rabbits. *Gen Mol Res*. 2015;14(3):8947–8954. doi:10.4238/2015
6. Roleder T, Gołba KS, Kunecki M, et al. The co-application of hypoxic preconditioning and postconditioning abolishes their own protective effect on systolic function in human myocardium. *Cardiol J*. 2013;20:472–477. doi:10.5603/CJ.2013.0131
7. Kunecki M, Roleder T, Biernat J, et al. Ochronne działanie układu opioidowego na czynność niedotlenionego ludzkiego mięśnia sercowego w warunkach in vitro. *Folia Med Cracov*. 2015;55(Suppl 1):48–49.
8. Valtchanova-Matchouganska A, Ojewole JA. Mechanisms of opioid delta and kappa receptors' cardioprotection in ischaemic preconditioning in a rat model of myocardial infarction. *Cardiovasc J S Afr*. 2003;14:73–80.
9. Chen Z, Li T, Zhang B. Morphine postconditioning protects against reperfusion injury in the isolated rat hearts. *J Surg Res*. 2008;145:287–294.
10. Headrick JP, See Hoe LE, Du Toit EF, Peart JN. Opioid receptors and cardioprotection: 'Opioidergic conditioning' of the heart. *Brit J Pharm*. 2015;172:2026–2050. doi:10.1111/bph.13042
11. Wong GT, Huang Z, Ji S, Irwin MG. Remifentanil reduces the release of biochemical markers of myocardial damage after coronary artery bypass surgery: A randomized trial. *J Cardiothorac Vasc Anesth*. 2010;24(5):790–796.
12. Araszkiewicz A, Grygier M, Pyda M, Rajewska J, Lesiak M, Grajek S. Postconditioning attenuates early ventricular arrhythmias in patients with high-risk ST-segment elevation myocardial infarction. *J Cardiol*. 2015;65(6):459–465. doi:10.1016/j.jjcc.2015.02.010
13. Hayashida K, Takeuchi T, Shimizu H, Ando K, Harada E. Lactoferrin enhances opioid-mediated analgesia via nitric oxide in the rat spinal cord. *Am J Physiol*. 2003;285:R302.
14. Nagasaka Y, Fernandez BO, Garcia-Saura MF, et al. Brief periods of nitric oxide inhalation protect against myocardial ischemia – reperfusion injury. *Anesthesiology*. 2008;109:675–682.
15. Neye N, Enigk F, Shiva S, et al. Inhalation of NO during myocardial ischemia reduces infarct size and improves cardiac function. *Intensive Care Med*. 2012;38:1381–1391.
16. Lu Y, Hu J, Zhang Y, Dong C. Spinal neuronal NOS activation mediates intrathecal fentanyl preconditioning induced remote cardioprotection in rats. *Int Immunopharmacol*. 2014;19:127. doi:10.1016/j.intimp.2014.01.013
17. Correa F, Buelna-Chontal M, Chagoya V, et al. Inhibition of the nitric oxide/cyclic guanosine monophosphate pathway limited the cardioprotective effect of post-conditioning in hearts with apical myocardial infarction. *Eur J Pharmacol*. 2015;765:472–481. doi:10.1016/j.ejphar.2015.09.018
18. Takano H, Manchikalapudi S, Tang XL, et al. Nitric oxide synthase is the mediator of late preconditioning against myocardial infarction in conscious rabbits. *Circulation*. 1998;98:441–449.
19. Liang F, Gao E, Tao L, et al. Critical timing of L-arginine treatment in post-ischemic myocardial apoptosis-role of NOS isoforms. *Cardiovasc Res*. 2004;62(3):568–577.
20. Yellon DM, Hausenloy DJ. Myocardial reperfusion injury. *NEJM*. 2007;357:1121–1135.
21. Hattori Y, Kasai K, Gross SS. NO suppresses while peroxynitrite sustains NF-kappaB: A paradigm to rationalize cytoprotective and cytotoxic actions attributed to NO. *Cardiovasc Res*. 2004;63(1):31–40.
22. Beręsewicz A, Maczewski M, Duda M. Effect of classic preconditioning and diazoxide on endothelial function and O_2^- and NO generation in the post-ischemic guinea-pig heart. *Cardiovasc Res*. 2004;63(1):118–129.
23. Ohtani H, Katoh H, Tanaka T, et al. Effects of nitric oxide on mitochondrial permeability transition pore and thiol-mediated responses in cardiac myocytes. *Nitric Oxide*. 2012;26(2):95–101. doi:10.1016/j.niox.2011.12.007
24. Folino A, Losano G, Rastaldo. Balance of nitric oxide and reactive oxygen species in myocardial reperfusion injury and protection. *J Cardiovasc Pharmacol*. 2013;62:567–575.

Pathophysiological implications of actin-free Gc-globulin concentration changes in blood plasma and cerebrospinal fluid collected from patients with Alzheimer's disease and other neurological disorders

Alina Kułakowska[1,D], Joanna Tarasiuk[1,D], Katarzyna Kapica-Topczewska[1,D], Monika Chorąży[1,D], Robert Pogorzelski[1,D], Agnieszka Kulczyńska-Przybik[2,A], Barbara Mroczko[2,A], Robert Bucki[3,D]

[1] Department of Neurology, Medical University of Bialystok, Poland
[2] Department of Neurodegeneration Diagnostics, Medical University of Bialystok, Poland
[3] Department of Microbiological and Nanobiomedical Engineering, Medical University of Bialystok, Poland

A – research concept and design; B – collection and/or assembly of data; C – data analysis and interpretation; D – writing the article; E – critical revision of the article; F – final approval of the article

Advances in Clinical and Experimental Medicine, ISSN 1899-5276 (print), ISSN 2451-2680 (online) *Adv Clin Exp Med*. 2018;27(8):1075–1080

Address for correspondence
Joanna Tarasiuk
E-mail: amirtarasiuk@wp.pl

Funding sources
This work was supported by the National Science Center (Poland) with grant No. UMO-2015/17/B/NZ6/03473 (to RB) and Medical University of Bialystok grant No. N/ST/2B/16/002/1144 (to AK).

Conflict of interest
None declared

Received on December 10, 2016
Reviewed on April 7, 2017
Accepted on April 12, 2017

Abstract

Background. The extracellular actin scavenging system (EASS) is composed of plasma Gc-globulin and gelsolin, and is responsible for the elimination of toxic actin from the bloodstream.

Objectives. In this study, we assessed the actin-free Gc-globulin concentrations in blood plasma and cerebrospinal fluid (CSF) obtained from subjects with neurodegenerative and inflammatory diseases of the central nervous system (CNS) as well as in a control group.

Material and methods. Using an enzyme-linked immunosorbent assay (ELISA), we measured the actin-free Gc-globulin concentrations in blood plasma and CSF obtained from subjects diagnosed with Alzheimer's disease (AD) (n = 20), amyotrophic lateral sclerosis (ALS) (n = 12), multiple sclerosis (MS) (n = 42), tick-borne encephalitis (TBE) (n = 12), and from a control group (n = 20).

Results. The concentrations of free Gc-globulin in plasma collected from patients diagnosed with AD (509.6 ±87.6 mg/L) and ALS (455.5 ±99.8 mg/L) did not differ significantly between each other, but were significantly higher compared to the reference group (311.7 ±87.5 mg/L) ($p < 0.001$ and $p < 0.006$, respectively) as well as to MS (310.8 ±66.6 mg/L) ($p < 0.001$ and $p < 0.001$, respectively) and TBE (256.7 ±76 mg/L) ($p < 0.001$ and $p < 0.003$, respectively). In CSF collected from patients diagnosed with AD and ALS, the concentrations of free Gc-globulin were 2.6 ±1.1 mg/L and 2.7 ±1.9 mg/L, respectively. They did not differ significantly between each other and were significantly higher compared to the reference group (1.5 ±0.9 mg/L) ($p < 0.005$ and $p < 0.041$, respectively). Interestingly, in patients with AD, significantly higher values of Gc-globulin were detected compared to MS patients (1.7 ±0.9 mg/L) ($p < 0.013$).

Conclusions. Higher concentrations of free Gc-globulin in blood plasma and CSF collected from patients suffering from neurodegenerative diseases may indicate a potential role of this protein in their pathogenesis, and represent a potential tool for the diagnosis of CNS diseases.

Key words: Alzheimer's disease, amyotrophic lateral sclerosis, multiple sclerosis, tick-borne encephalitis, Gc-globulin

DOI
10.17219/acem/70441

Introduction

Gc-globulin (vitamin D binding protein) is a multifunctional, monomeric glycoprotein belonging to the α2-globulin fraction. This peptide is composed of 458 amino acids with 3 domains and has a molecular weight of 51–58 kDa. Gc-globulin is mainly produced by the liver, but it is also found in the kidneys, lungs, heart, spleen, and brain, as well as in several body fluids, including blood plasma, saliva, semen, breast milk, and cerebrospinal fluid (CSF).[1] The serum concentration of free Gc-globulin (actin-free Gc-globulin) ranges between 92 and 332 mg/L.[2] The laboratory standard for the Gc-globulin concentration in CSF has not been established.

The primary function of Gc-globulin is the removal of actin. Circulating G-actin, released from injured tissues, polymerizes and forms F-actin filaments promoting certain disorders, including disseminated intravascular coagulation (DIC).[1,2] F-actin filaments are depolymerized by gelsolin releasing G-actin monomers, which are subsequently bound to Gc-globulin. The G-actin-gelsolin and G-actin-Gc-globulin complexes are primarily removed from the circulation by mononuclear phagocytes.[3,4] Low concentrations of Gc-globulin correspond to a poor prognostic outlook in acute liver failure, multiple organ dysfunction syndrome and sepsis.[5,6] Gc-globulin is also involved in the transport of vitamin D with its metabolites, fatty acids and endotoxins, functions in the activation of osteoclasts and macrophages, and serves as a chemotactic cue for leukocytes.[1,2,7]

Cerebrospinal fluid provides valuable information about biochemical changes in the central nervous system (CNS); the examination of CSF is an important tool in the diagnosis of CNS diseases.[8] Pathological CNS processes are reflected in the protein composition of CSF. Information on the concentration of free Gc-globulin in the blood and CSF of patients with neurodegenerative diseases is limited.

The aim of the current study was to measure and compare the concentration of free Gc-globulin in the serum and CSF of patients with: 1. neurodegenerative diseases, including Alzheimer's disease (AD) and amyotrophic lateral sclerosis (ALS); 2. diseases associated with inflammatory and neurodegenerative etiopathogenesis, such as multiple sclerosis (MS); 3. infectious inflammatory disease, e.g., tick born encephalitis (TBE); 4. and in a control group consisting of patients suffering from conditions which do not alter the standard parameters of CSF, such as idiopathic headache and idiopathic facial nerve palsy.

Material and methods

Patients and the preparation of samples

Blood and CSF samples were obtained from patients admitted to the Department of Neurology and the Department of Infectious Diseases and Neuroinfections of The Medical University of Białystok Clinical Hospital, Poland. The study was approved by the Medical University of Bialystok Ethics Committee for Research on Humans and Animals (R-I-002/382/2012) and written consent was obtained from all subjects. All individuals underwent lumbar puncture for diagnostic purposes. The clinical characteristics of patients are shown in Table 1.

The diagnosis of AD was based on the criteria of the National Institute of Neurologic, Communicative Disorders and Stroke/Alzheimer's Disease and Related Disorders Association (NINCDS-ADRDA).[9,10] All patients had memory loss and impaired cognitive function lasting more than 6 months validated using psychological tests and biochemical assessment (Table 2).

The relapsing-remitting MS diagnosis was based on the McDonald criteria.[11] The degree of disability of MS patients was assessed using the Expanded Disability Status Scale (EDSS), with a mean score of 1.5 ±0.6 indicating the early stage of disease.[12] All patients underwent head magnetic resonance imaging (MRI) examination, which demonstrated multiple disseminated demyelinating

Table 1. Patient clinical characteristics

Clinical characteristics of patients					CSF	
diagnosis	number of patients (women)	age [years]	EDSS	Q Alb	total protein [μg/mL]	lymphocytes (0–5 cells/μL)
AD	20 (13)	69.9 ±10.4	–	5.7 ±1.3	38.3 ±17.2	1.25 ±1.0
ALS	12 (9)	57.5 ±10.3	–	6.1 ±2.3	39.7 ±15.3	2.2 ±2.3
MS*	42 (25)	35.5 ±10.5	1.5 ±0.5	6.3 ±1.5	375 ±125	3.8 ±2.1
TBE	12 (3)	53.1 ±24.3	–	12.4 ±1.2**	882 ±157**	110 ±15.6**
Reference group (n = 20)						
Idiopathic headache	13 (11)	40.2 ±20.4	–	6.5 ±1.3	409 ±155	3.0 ±2.1
Idiopathic facial nerve palsy	7 (5)	48.4 ±15.3	–	7.5 ±0.6	357 ±179	5.1 ±2.1

CFS – cerebrospinal fluid; AD – Alzheimer's disease; ALS – amyotrophic lateral sclerosis; MS – multiple sclerosis; TBE – tick-borne encephalitis; Q Alb – coefficient of albumin; EDSS – Expanded Disability Status Scale; * all patients with MS in CSF presented oligoclonal bands of IgG (type 2 or 3); ** incorrect values.

plaques. None of the patients were treated with corticosteroids or immunomodulating drugs (beta-interferon, glatiramer acetate, natalizumab).

The clinically definite ALS was diagnosed using the Airlie House/El Escorial Revisited World Federation of Neurology criteria.[13,14] All patients with ALS showed features of damage to upper and lower motor neurons as confirmed by electromyography (EMG) examination. None of the patients were treated with riluzol.

The diagnosis of TBE was confirmed by the detection of antibodies against the TBE virus in serum and CSF by enzyme-linked immunosorbent assay (ELISA) tests (Virion-Serion Kit; SERION® Immunologics, Würzburg, Germany). All patients with TBE received symptomatic treatment with no corticosteroids.

The reference group consisted of patients with idiopathic headache and idiopathic facial nerve palsy (Bell's palsy), with no active inflammatory process. None of the patients with idiopathic facial nerve palsy were immunocompromised or had herpes simplex virus 1 antibodies in blood as measured by ELISA (ELISA kit; Genzyme Virotech GmbH, Rüsselsheim, Germany).

The samples of anticoagulated blood were centrifuged and the collected plasma was frozen at –80°C. After collection, CSF underwent a standard examination. The CSF samples were then centrifuged (2000 × g, 20 min) and the supernatants were subjected to total protein analysis and frozen at –80°C. CSF analysis included physical properties, cytosis, the total protein concentration and Q Alb ratio (Q Alb = albumin in CSF [mg] / serum albumin [g] × 1000) indicating the efficiency of the blood-CSF barrier. In patients with clinically probable AD, we assessed the average concentration of Aβ1-42, Aβ1-40, the Aβ1-42/Aβ1-40 ratio and the average concentration of Tau and phosphorylated Tau (pTau) protein using the ELISA INNOTEST® kits (Innogenetics GmbH, Hannover, Germany) and ELISA Kits (IBL International GmbH, Hamburg, Germany). The average values of Aβ1-42, Aβ1-40, the Aβ1-42/Aβ1-40 ratio, Tau, and pTau were typical for patients with AD (Table 2).

The Gc-globulin actin-free ELISA Kit from BioPorto Diagnostics (Hellerup, Denmark) was used to assess free Gc-globulin.

Statistical analysis

The results were analyzed statistically using the Kruskal-Wallis test followed by post hoc analysis with the Dwass-Steel-Critchlow-Fligner test. A p-value <0.05 was considered statistically significant.

Results

Our results show significantly higher concentrations of free Gc-globulin in the serum and CSF of patients with neurodegenerative diseases compared to either the reference group or patients with inflammatory disease. The concentration of free Gc-globulin in the serum of patients with AD (509.6 ±87.6 mg/L) or ALS (455.5 ±99.8 mg/L) did not differ significantly; however, in both groups, these concentrations were significantly higher than in the reference group (311.7 ±87.5 mg/L) ($p < 0.001$ and $p < 0.006$, respectively). This is in agreement with previous studies demonstrating that the concentrations of free Gc-globulin in the serum of patients suffering from neurodegenerative diseases were greater than the values reported for healthy subjects.[2] Furthermore, the concentration of free Gc-globulin in the serum of patients with AD or ALS was also higher than in subjects with inflammatory diseases, such as TBE (256.7 ±76 mg/L) ($p < 0.001$ and $p < 0.003$, respectively) and MS (310.8 ±66.6 mg/L) ($p < 0.001$ and $p < 0.001$, respectively) (Fig. 1).

The standard parameters for CSF evaluation were representative of the studied diseases (AD, ALS) and are presented in Table 1. The concentration of free Gc-globulin in CSF displayed trends similar to those observed

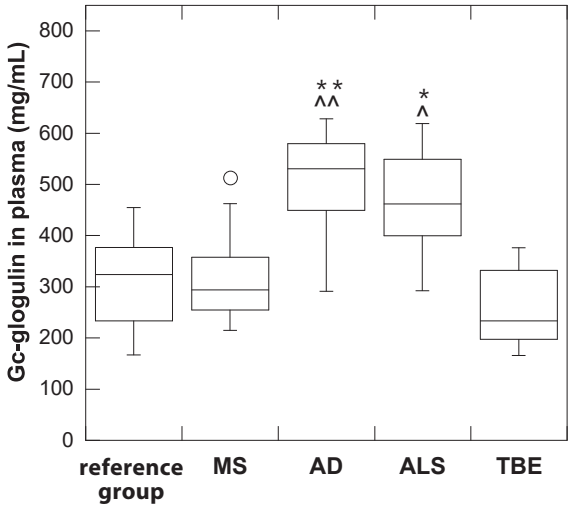

Fig. 1. Comparison of the free Gc-globulin concentration in blood plasma

* $p < 0.006$; ** $p < 0.001$ compared to the reference group; ^ $p < 0.003$; ^^ $p < 0.001$ compared to patients with tick-borne encephalitis; ° $p < 0.001$ compared to patients with multiple sclerosis; AD – Alzheimer's disease; ALS – amyotrophic lateral sclerosis; MS – multiple sclerosis; TBE – tick-borne encephalitis; the Kruskal-Wallis test with post hoc Dwass-Steele-Critchlow-Fligner test.

Table 2. Biomarkers of neurodegeneration in patients with Alzheimer's disease

Aβ1-42 (cut-off = 590 pg/mL)	Tau (cut-off = 300 pg/mL)	pTau (cut-off = 50 pg/mL)	Ratio Aβ1-42/Aβ1-40 (cut-off = 0.030)
466.45 ±296.65	353.35 ±176.13	55.2 ±21.67	0.0251 ±0.014

Aβ1-40 – β-amyloid containing 40 amino acids; Aβ1-42 – β-amyloid containing 42 amino acids; Tau – Tau protein; pTau – excessively phosphorylated Tau protein.

for serum. The concentration of free Gc-globulin in patients with AD (2.6 ±1.1 mg/L) and ALS (2.7 ±1.9 mg/L) did not differ significantly between each other, but were significantly higher compared to the reference group (1.5 ±0.9 mg/L) ($p < 0.005$ and $p < 0.041$, respectively). The average concentrations of free Gc-globulin in the CSF of MS (1.7 ±0.9 mg/L) and TBE (1.8 ±1.2 mg/L) patients were not significantly different than in the case of the reference group. However, there was observed a significant difference between the concentrations of free Gc-globulin in the CSF of patients with AD and MS ($p < 0.013$) (Fig. 2).

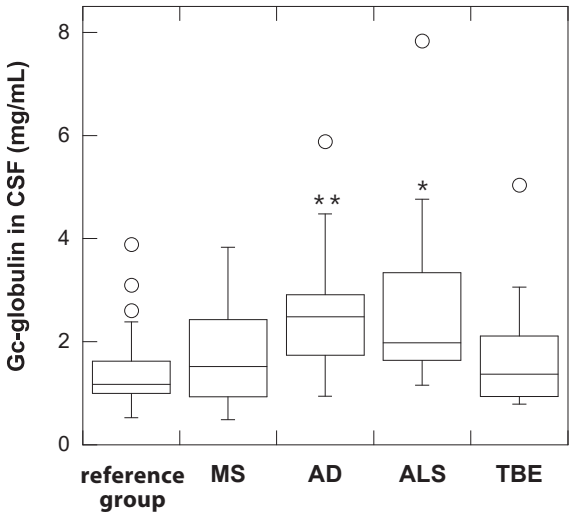

Fig. 2. Comparison of the free Gc-globulin in cerebrospinal fluid (CSF)

* $p < 0.041$; ** $p < 0.005$ compared to the reference group; ° $p < 0.013$ compared to patients with multiple sclerosis; AD – Alzheimer's disease; ALS – amyotrophic lateral sclerosis; MS – multiple sclerosis; TBE – tick-borne encephalitis; the Kruskal-Wallis test with post hoc Dwass-Steele-Critchlow-Fligner test.

Discussion

There are few reports concerning the concentration and function of free Gc-globulin in the pathogenesis of neurodegenerative diseases. Our earlier studies indicate that there are no significant differences between the Gc-globulin concentrations in the plasma and CSF of MS patients compared to control subjects.[4] In a previous study on patients with dementive diseases, including AD, Parkinson's disease and Pick's disease, the Gc-globulin concentration was higher compared to patients with head trauma, autoimmune or cerebrovascular disorders.[15] Furthermore, Zhang et al., using a multiplex analysis of CSF proteins, demonstrated a statistically significant increase in the concentration of free Gc-globulin in the CSF of patients with AD and Parkinson's disease compared to a group of healthy controls.[16]

Increased levels of Gc-globulin in the serum and CSF of patients with AD and ALS may be associated with neurodegeneration in the CNS. The breakdown of neurons has been described for both AD and ALS. In AD, this process primarily occurs in the cerebral cortex/hippocampus and for ALS – in the upper and lower motor neurons. Actin released from damaged tissue is removed from blood and purportedly from CSF through the extracellular actin scavenging system (EASS).[17–20] It is likely that the chronic nature of neurodegenerative disease initiates a compensatory increase in the hepatic and intrathecal synthesis of Gc-globulin as a response to elevated levels of actin. In our patients with AD and ALS, the high concentration of free Gc-globulin in CSF may be due to the increased neuronal synthesis, because the patients were at an early stage of the disease and there was no disruption of the blood-CSF barrier, as indicated by Q Alb (Table 1).

Alternatively, the increased concentration of free Gc-globulin observed in both the serum and CSF of patients suffering from neurodegenerative diseases may indicate impaired G-actin binding. G-actin is released from F-actin filaments through the severing activity of gelsolin. Previous studies report reduced gelsolin expression in both the choroid plexus and CSF from AD patients.[21] Effectively, the dysfunction of the EASS may switch on compensatory mechanisms, including increased Gc-globulin expression. Moreover, gelsolin is a Ca^{2+}/phosphatidylinositol 4,5-bisphosphate (PIP_2)-regulated protein. Its PIP_2 binding domain interacts with several acidic lipid signaling molecules, including PIP_2, lysophosphatidic acid (LPA), lipoteichoic acid (LTA), lipopolysaccharide (LPS), sphingosine 1-phosphate (S1P), and its synthetic structural analogue fingolimod (FTY720P).[22–25] When complexed with bioactive lipids, gelsolin loses the ability to bind and sever actin filaments as well as alters the ability of the lipids to function as cell agonists. In AD, inflammatory processes such as activation of microglia and astrocytes as well as the production of inflammatory cytokines occur within and around amyloid plaques.[26] Alterations to the sphingolipids profile are linked to the pathogenesis of AD, and fingolimod seems to be a promising therapeutic agent reducing the accumulation of amyloid β.[27–30] Taken together, this data suggests that, during the course of the neurodegenenerative process, the association of gelsolin with bioactive sphingolipids leads to a reduction in its ability to depolymerize F-actin and to prevent the release of G-actin monomers. As a consequence, elevated levels of unbound, free Gc-globulin may be observed.

Neurodegeneration also plays an important role in the pathogenesis of MS, but inflammatory processes dominate the early stages of disease.[31–35] All the patients included in this study were in the early stage of the disease (EDSS of 1.5 ±0.5); diagnostic lumbar puncture confirmed this diagnosis. Therefore, the results obtained from these patients and from patients with TBE, a representative disease of infectious inflammatory etiology, are very similar. In inflammatory processes, lower concentrations of free Gc-globulin in serum and CSF may result from the fact that inflammation proceeds more rapidly compared to neurodegeneration.[36] It is possible that the rapid

inflammatory process causes excessive cell destruction, causing high Gc-globulin consumption and insufficient activation of compensatory pathways.

In addition to actin scavenging, Gc-globulin plays a crucial role in vitamin D metabolism.[1,2] In recent years, vitamin D has attracted much attention, and there is growing evidence that beyond its physiologic effects on calcium/phosphorus homeostasis, low vitamin D status is associated with several diseases, including cancer, diabetes mellitus, rheumatoid arthritis, and other autoimmune conditions.[37,38] Recently, vitamin D deficiency has been shown to be a risk factor for dementia and AD.[39] However, it seems rather unlikely that altered levels of vitamin D affect the concentrations of Gc-globulin. In physiological conditions, only 5% of total plasma Gc-globulin is occupied by vitamin D and the plasma clearance of Gc-globulin does not appear to be altered by vitamin D binding.[1,2]

In conclusion, the results of our preliminary studies suggest that significantly higher concentrations of free Gc-globulin in serum and CSF in neurodegenerative diseases may result from their pathogenesis. Since neurodegeneration begins much earlier than the appearance of clinical signs, determining the concentration of certain proteins involved in its pathogenesis, such as Gc-globulin, may be important in the early diagnosis of CNS disease.

References

1. White P, Cooke N. The multifunctional properties and characteristics of vitamin D-binding protein. *Trends Endocrinol Metab*. 2000;11:320–327.
2. Meier U, Gressner O, Lammert F, Gressner AM. Gc-globulin: Roles in response to injury. *Clin Chem*. 2006;52:1247–1253.
3. Kułakowska A, Zajkowska JM, Ciccarelli NJ, Mroczko B, Drozdowski W, Bucki R. Depletion of plasma gelsolin in patients with tick-borne encephalitis and Lyme neuroborreliosis. *Neurodegener Dis*. 2011;8:375–380.
4. Kułakowska A, Ciccarelli NJ, Wen Q, et al. Hypogelsolinemia, a disorder of the extracellular actin scavenger system, in patients with multiple sclerosis. *BMC Neurol*. 2010;10:107.
5. Schiødt FV, Bangert K, Shakil AO, et al. Predictive value of actin-free Gc-globulin in acute liver failure. *Liver Transpl*. 2007;13:1324–1329.
6. Bagchi A, Kumar S, Ray PC, Das BC, Gumma PK, Kar P. Predictive value of serum actin-free Gc-globulin for complications and outcome in acute liver failure. *J Viral Hepat*. 2015;22:192–200.
7. Łukaszewicz-Zajac M, Mroczko B, Kułakowska A, Szmitkowski M. The significance of Gc-globulin in clinical practice [in Polish]. *Postepy Hig Med Dosw*. 2008;62:625–631.
8. Bredesen DE, Rao RV, Mehlen P. Cell death in the nervous system. *Nature*. 2006;443:796–802.
9. Dubois B, Feldman HH, Jacova C, et al. Research criteria for the diagnosis of Alzheimer's disease: Revising the NINCDS-ADRDA criteria. *Lancet Neurol*. 2007;6:734–746.
10. Croisile B, Auriacombe S, Etcharry-Bouyx F, Vercelletto M; NIoA & Alzheimer's Association. The new 2011 recommendations of the National Institute on Aging and the Alzheimer's Association on diagnostic guidelines for Alzheimer's disease: Preclinical stages, mild cognitive impairment, and dementia [in French]. *Rev Neurol (Paris)*. 2012;168:471–482.
11. Polman CH, Reingold SC, Banwell B, et al. Diagnostic criteria for multiple sclerosis: 2010 revisions to the McDonald criteria. *Ann Neurol*. 2011;69:292–302.
12. Kurtzke JF. Rating neurologic impairment in multiple sclerosis: An expanded disability status scale (EDSS). *Neurology*. 1983;3:1444–1452.
13. Brooks BR, Miller RG, Swash M, Munsat TL; World Federation of Neurology Research Group on Motor Neuron Disease. El Escorial revisited: Revised criteria for the diagnosis of amyotrophic lateral sclerosis. *Amyotroph Lateral Scler Other Motor Neuron Disord*. 2000;1:293–299.
14. Chieia MA, Oliveira AS, Silva HC, Gabbai AA. Amyotrophic lateral sclerosis: Considerations on diagnostic criteria. *Arq Neuropsiquiatr*. 2010;68:837–842.
15. Gressner OA, Schifflers MC, Kim P, Heuts L, Lahme B, Gressner AM. Questioning the role of actinfree Gc-Globulin as actin scavenger in neurodegenerative central nervous system disease: Relationship to S-100B levels and blood-brain barrier function. *Clin Chim Acta*. 2009;400:86–90.
16. Zhang J, Sokal I, Peskind ER, et al. CSF multianalyte profile distinguishes Alzheimer and Parkinson diseases. *Am J Clin Pathol*. 2008;129:526–529.
17. Agdeppa ED, Kepe V, Liu J, et al. Binding characteristics of radiofluorinated 6-dialkylamino-2-naphthylethylidene derivatives as positron emission tomography imaging probes for beta-amyloid plaques in Alzheimer's disease. *J Neurosci*. 2001;21:RC189.
18. Ashford JW, Shih WJ, Coupal J, et al. Single SPECT measures of cerebral cortical perfusion reflect time-index estimation of dementia severity in Alzheimer's disease. *J Nucl Med*. 2000;41:57–64.
19. Gomme PT, Bertolini J. Therapeutic potential of vitamin D-binding protein. *Trends Biotechnol*. 2004;22:340–345.
20. Dahl B, Schiødt FV, Ott P, et al. Plasma concentration of Gc-globulin is associated with organ dysfunction and sepsis after injury. *Crit Care Med*. 2003;31:152–156.
21. Antequera D, Vargas T, Ugalde C, et al. Cytoplasmic gelsolin increases mitochondrial activity and reduces Abeta burden in a mouse model of Alzheimer's disease. *Neurobiol Dis*. 2009;36:42–50.
22. Bucki R, Kulakowska A, Byfield FJ, et al. Plasma gelsolin modulates cellular response to sphingosine 1-phosphate. *Am J Physiol Cell Physiol*. 2010;299:C1516–1523.
23. Bucki R, Byfield FJ, Kulakowska A, et al. Extracellular gelsolin binds lipoteichoic acid and modulates cellular response to proinflammatory bacterial wall components. *J Immunol*. 2008;181:4936–4944.
24. Bucki R, Georges PC, Espinassous Q, et al. Inactivation of endotoxin by human plasma gelsolin. *Biochemistry*. 2005;44:9590–9597.
25. Bucki R, Janmey PA. Interaction of the gelsolin-derived antibacterial PBP 10 peptide with lipid bilayers and cell membranes. *Antimicrob Agents Chemother*. 2006;50:2932–2940.
26. Lukiw WJ, Bazan NG. Survival signalling in Alzheimer's disease. *Biochem Soc Trans*. 2006;34:1277–1282.
27. Takasugi N, Sasaki T, Ebinuma I, et al. FTY720/fingolimod, a sphingosine analogue, reduces amyloid-β production in neurons. *PLoS One*. 2013;8:e64050.
28. Takasugi N, Sasaki T, Suzuki K, et al. BACE1 activity is modulated by cell-associated sphingosine-1-phosphate. *J Neurosci*. 2011;31:6850–6857.
29. Fukumoto K, Mizoguchi H, Takeuchi H, et al. Fingolimod increases brain-derived neurotrophic factor levels and ameliorates amyloid β-induced memory impairment. *Behav Brain Res*. 2014;268:88–93.
30. Brunkhorst R, Vutukuri R, Pfeilschifter W. Fingolimod for the treatment of neurological diseases-state of play and future perspectives. *Front Cell Neurosci*. 2014;8:283.
31. Dutta R, Trapp BD. Mechanisms of neuronal dysfunction and degeneration in multiple sclerosis. *Prog Neurobiol*. 2011;93:1–12.
32. Trapp BD, Nave KA. Multiple sclerosis: An immune or neurodegenerative disorder? *Annu Rev Neurosci*. 2008;31:247–269.
33. Nave KA, Trapp BD. Axon-glial signaling and the glial support of axon function. *Annu Rev Neurosci*. 2008;31:535–561.
34. Micu I, Jiang Q, Coderre E, et al. NMDA receptors mediate calcium accumulation in myelin during chemical ischaemia. *Nature*. 2006;439:988–992.
35. Bennett JL, Stüve O. Update on inflammation, neurodegeneration, and immunoregulation in multiple sclerosis: Therapeutic implications. *Clin Neuropharmacol*. 2009;32:121–132.
36. Gelpi E, Preusser M, Laggner U, et al. Inflammatory response in human tick-borne encephalitis: Analysis of postmortem brain tissue. *J Neurovirol*. 2006;12:322–327.
37. Holick MF. Vitamin D status: Measurement, interpretation, and clinical application. *Ann Epidemiol*. 2009;19:73–78.

38. Binkley N, Ramamurthy R, Krueger D. Low vitamin D status: Definition, prevalence, consequences, and correction. *Endocrinol Metab Clin North Am*. 2010;39:287–301.
39. Littlejohns TJ, Henley WE, Lang IA, et al. Vitamin D and the risk of dementia and Alzheimer disease. *Neurology*. 2014;83:920–928.

Risk factors of the *Clostridium difficile* infection in patients with chronic kidney disease

Łukasz Lis[A–F], Patryk Jerzak[A,B,E,F], Andrzej Konieczny[C–F], Michał Sroka[A,B], Barbara Noceń-Rychlewska[E,F], Paweł Podgórski[E,F], Wojciech Witkiewicz[E,F], Zbigniew Hruby[A,C–F]

Research and Development Center, Provincial Specialist Hospital in Wrocław, Poland

A – research concept and design; B – collection and/or assembly of data; C – data analysis and interpretation; D – writing the article; E – critical revision of the article; F – final approval of the article

Advances in Clinical and Experimental Medicine, ISSN 1899-5276 (print), ISSN 2451-2680 (online) *Adv Clin Exp Med*. 2018;27(8):1081–1084

Address for correspondence
Andrzej Konieczny
E-mail: andrzej_konieczny@yahoo.com

Funding sources
None declared

Conflict of interest
None declared

Received on February 10, 2017
Reviewed on April 15, 2017
Accepted on April 27, 2017

Abstract

Background. *Clostridium difficile* (*C. difficile*) is a Gram-positive bacillus responsible for diarrhea and colitis, mainly among hospitalized patients. It is a leading cause of nosocomial infections.

Objectives. The main goal of the study was to assess the risk factors of the *C. difficile* infection in patients with chronic kidney disease (CKD).

Material and methods. We evaluated the medical records of all patients treated at the Department of Nephrology and Renal Transplantation of the Research and Development Center in the Provincial Specialist Hospital in Wrocław, Poland, between February 2009 and May 2012, who developed diarrhea, abdominal pain and/or fever within 72 h after admission. In patients with these symptoms, an enzyme cassette immunoassay was performed to detect antigens of *C. difficile* toxins A and B in stool.

Results. There were 207 patients enrolled in the study, presented with the symptoms of the *C. difficile* infection. Out of these patients, 69 (33%) persons were positive for *C. difficile* toxins. Longer hospitalization time and lower initial serum albumin concentration significantly increased the risk of infection ($p < 0.05$). Apart from the *C. difficile* infection, age, the number of used antibiotics, longer hospitalization time, and lower initial serum albumin concentration significantly augmented the risk of death ($p < 0.05$).

Conclusions. In patients with CKD, longer hospitalization time and lower serum albumin concentration significantly increased the risk of the *C. difficile* infection. The *C. difficile* infection, age, the number of used antibiotics, longer hospitalization time, and lower initial serum albumin concentration notably augmented the risk of death. Although the incidence of the *C. difficile* infection did not correlate with the estimated glomerular filtration rate (eGFR), 67% of patients who tested positive were class 5 of CKD, whereas only 5.7% were class 1.

Key words: malnutrition, *Clostridium difficile*, chronic renal insufficiency, pseudomembranous enterocolitis

DOI
10.17219/acem/70809

Introduction

The *Clostridium difficile* (*C. difficile*, CD) infection is the most frequent cause of diarrhea in patients treated with antibiotics who were admitted to hospital.[1] Whereas the course of the disease is mild in most cases, in some instances it may lead to severe dehydration, septic shock or even death.[2] Damage to the intestinal mucosa, initiating colorectal inflammation is caused by toxins A, B and newly diagnosed, highly virulent, toxin C.[3] Well-established risk factors of the CD infection include prolonged treatment with antibiotics, proton pump inhibitors (PPIs), antidepressants, advanced age, chemotherapy, immunosuppression, and long hospitalization time.[4–6] In recent years, a number of reports have appeared, indicating an increased incidence and morbidity of CD-associated infections in patients with chronic kidney disease (CKD).[7,8] These observations corroborated current clinical experience in our Department, which is why we sought to assess the incidence, morbidity and risk factors of the CD infection in our CKD patients.

Material and methods

We evaluated the medical records of the patients hospitalized in the Department of Nephrology and Renal Transplantation of the Research and Development Center in the Provincial Specialist Hospital in Wrocław, Poland, between February 2009 and May 2012, who during their hospital stay developed symptoms indicating CD-associated enterocolitis. Qualifying symptoms were as follows: diarrhea, abdominal pain and/or fever within at least 72 h after admission to hospital. In all patients meeting these criteria, a rapid enzyme cassette immunoassay was performed, detecting antigens of toxins A and B of *C. difficile* in stool (TOX A/B QUIK CHEK®; Techlab, Blackburg, USA). The sample material was taken with a spatula to the test tube, transferred to the test cassette and read after 15 min of incubation at room temperature.

Detailed data was accrued, pertaining to the patients' age, gender, concomitant diseases, and pharmacotherapy with the emphasis on antibiotics, PPIs and antidepressants. Laboratory tests were done in the hospital lab, using standard methods, including the measurement of serum creatinine and albumin concentrations. The shortened Modification of Diet in Renal Disease (MDRD) equation was used to calculate the glomerular filtration rate (eGFR).

Numerical data was expressed as means and standard deviations (SD). Statistical analysis was performed utilizing the STATISTICA v. 12 software (StatSoft Inc., Tulsa, USA). Normal distribution verified with the Kolmogorov-Smirnov test enabled the assessment of the differences between the 2 groups with Student's t test, the homogeneity of variations being checked with Fisher's test. In the case of nonparametric distribution, statistical importance of the differences was evaluated with the use of the Mann-Whitney U test. For quantitative data, the χ^2 analysis was done. Statistical significance cut-off level was set at $p = 0.05$.

Results

A total of 207 patients were enrolled in the study (104 males and 103 females), aged 20–91 years (64.5 years ±15.79), hospitalized at the Department of Nephrology

Table 1. Clinical features of patients tested positive and negative for CD (mean values)

Parameter	Positive result of the test for CD toxins (1)	Negative result of the test for CD toxins (2)	p-value (1) vs (2)
Number of patients	69	138	–
Age [years]	65.7	63.2	0.29
Gender, M/F	35/34	69/69	–
Body mass [kg]	73.8	77.5	0.29
Number of patients treated with antibiotics, n (%)	61 (88)	114 (82)	–
Number of antibiotics used	2.1	2.0	0.66
Duration of antibiotic therapy [days]	12.8	11.2	0.19
Number of patients with diabetes, n (%)	18 (26)	47 (34)	0.24
Number of patients treated with PPIs, n (%)	46 (66)	87 (63)	0.6
Number of patients treated with H2 blockers, n (%)	8 (11)	9 (6)	0.2
Number of patients treated with statins, n (%)	22 (31)	48 (34)	0.67
Number of patients treated with immunosuppressant drugs, n (%)	23 (33)	47 (34)	0.8
eGFR [mL/min/1.73 m^2]	30.2	39.9	0.24
Serum albumin concentration at admission [g/dL]	2.95	3.43	0.000079*
Duration of hospitalization [days]	33.2	24.3	0.004319*
Number of deaths, n (%)	20 (28)	12 (8.7)	0.0001*

M – male; F – female; PPIs – proton pump inhibitors; eGFR – glomerular filtration rate; * statistically significant.

and Renal Transplantation from February 2009 to May 2012. Patients were found to have CKD of various etiology: primary and secondary glomerulonephritis (23 cases – 11.1%); secondary nephropathies – ischemic, diabetic, obstructive (53 cases – 25.6%); acute kidney injury evolved to chronic kidney failure (24 cases – 11.6%). Of these patients, 77 (37.2%) were subjected to renal replacement therapy (RRT) (75 hemodialyses and 2 peritoneal dialyses) and 27 (13.0%) persons were kidney allograft recipients. The common feature of all these cases was impaired renal function (eGFR: 35.05 mL/min/1.73 m^2 ±12.3).

Among 207 patients demonstrating the symptoms of acute enterocolitis, in 69 (33%) persons, positive results of the cassette immunoassay for toxins A and B of CD were found.

In our study, longer hospitalization time and lower initial serum albumin concentration significantly increased the risk of infection (Table 1).

Moreover, it was demonstrated that the patients who died during the hospital stay not only more frequently tested positive for CD toxins (Table 1), but also had lower serum albumin concentration at admission, were older, were given more antibiotics during hospitalization, and their hospital stay lasted longer (Table 2). The mean morbidity coefficient for the CD infection was 12.5 per 1,000 hospitalizations.

It was not observed in the study group that lower eGFR, body weight, treatment with PPIs, H2-receptor blockers, immunosuppression, or statins, and the presence of diabetes increased significantly the risk of the CD infection. Furthermore, the length of antibiotic therapy and the number of used antibiotics did not increase considerably the risk of infection.

The stratification of CKD patients with symptoms of acute enterocolitis referring to the classes of CKD is presented in Table 3.

Table 2. Clinical characteristics of patients deceased during hospitalization (mean values)

Parameter	Patients who died during hospitalization	Patients discharged from hospital	p-value
Number of patients	32	175	–
Age [years]	76.7	61.8	0.000001
Number of antibiotics	2.84	1.88	0.000575
Hospitalization [days]	40.4	24.7	0.000101
Serum albumin concentration at admission [g/dL]	2.56	3.07	0.039297
eGFR at admission [mL/min/1.73 m^2]	17.5	34.5	0.11

eGFR – glomerular filtration rate.

Table 3. Classes of CKD in patients demonstrating the symptoms of acute enterocolitis

Class of CKD	Number of patients	%
1	12	5.7
2	11	5.3
3	27	13
4	21	10.1
5	136	65.7

CKD – chronic kidney disease.

Discussion

The prevalence of the CD infection in the results presented herein: 12.5/1000 hospitalizations is strikingly high when compared to the American (9/1000) and European (4.1/1000)populations, respectively.[9,10] Similarly, in one of the few Polish publications related to the CD infection in nephrology wards, the prevalence of 9.9/1000 hospitalizations was reported.[8] High prevalence of the CD infection in CKD patients of our Department confirms our observations, indicating a higher prevalence of the infection in nephrological patients when compared both to the general population and to patients hospitalized in other wards.[6,11] It also indicates that CKD, especially class 5, is an independent risk factor of the CD infection. The duration of hospitalization and lower serum albumin concentration at admission are significantly related to a higher frequency of the CD infection, as demonstrated in our study. Moreover, we documented an increased risk of death in CD-infected patients. In our study, age, prolonged hospitalization time and lower serum albumin concentration were proven as risk factors of death. Some authors underline the importance of malnutrition, especially among older patients as one of the main agents of mortality. Thus, it is important to focus on proper nutritional therapy in patients with the CD infection.[12] On the other hand, the study under discussion failed to confirm the importance of many established risk factors of the CD infection, such as prolonged use of antibiotics, PPIs and immunosuppressant drugs.[4,5,10,11] This may be attributable to the fact that the control group in our study consisted of CD-negative patients with diarrhea, instead of all persons hospitalized in the analyzed period (the available data on the treatment of these patients was incomplete).

Recent reports concerning the impact of CKD on the prevalence of the CD infection are inconsistent. A higher risk of infection has been observed in chronically dialyzed patients,[7] whereas this relation has not been confirmed in CKD subjects not requiring RRT.[13] At least 1 report showed a higher risk of the CD infection in patients with both acute and chronic renal injury.[14] In the present report, it was not documented that reduced eGFR augmented the risk of the CD infection; however, the patients tested positive for CD toxins had on average eGFR lower by 9.7 mL/min/1.73 m^2. Moreover, the investigated group of patients was dominated by persons with class 5 CKD: 137 of 207 (65.7%) with 77 (37.2%) of them chronically dialyzed.

Compliance with ethical standards

All procedures applied in the studies involving human participants were in accordance with the ethical standards of the institutional and/or national research committee, and with the 1964 Helsinki Declaration and its later amendments or comparable ethical standards. For this type of study, formal consent was not required.

References

1. Barbut F, Corthier G, Charpak Y, et al. Prevalence and pathogenicity of clostridium difficile in hospitalized patients: A French multicenter study. *Arch Intern Med*. 1996;156:1449–1454.
2. Kyne L, Merry C, O'Connell B, Kelly A, Keane C, O'Neill D. Factors associated with prolonged symptoms and severe disease due to *Clostridium difficile*. *Age Ageing*. 1999;28:107–113.
3. Loo VG, Poirier L, Miller MA, et al. A predominantly clonal multi-institutional outbreak of *Clostridium difficile*-associated diarrhea with high morbidity and mortality. *N Engl J Med*. 2005;353:2442–2449.
4. Bignardi GE. Risk factors for *Clostridium difficile* infection. *J Hosp Infect*. 1998;40:1–15.
5. Howell MD, Novack V, Grgurich P, et al. Iatrogenic gastric acid suppression and the risk of nosocomial clostridium difficile infection. *Arch Intern Med*. 2010;170:784–790.
6. Keller JM, Surawicz CM. *Clostridium difficile* infection in the elderly. *Clin Geriatr Med*. 2014;30:79–93.
7. Eui Oh S, Lee SM, Lee YK, et al. *Clostridium difficile*-associated diarrhea in dialysis patients. *Kidney Res Clin Pract*. 2013;32:27–31.
8. Kujawa-Szewieczek A, Adamczak M, Kwiecien K, Dudzicz S, Prazak Z, Wiecek A. Analysis of *Clostridium difficile* infections in patients hospitalized at the nephrological ward in Poland. *Postepy Hig Med Dosw* (*online*). 2016;70:505–513.
9. Lucado J, Gould C, Elixhauser A. *Clostridium difficile* Infections (CDI) in hospital stays, 2009. HCUP Statistical Brief #124. January, 2012. Agency for Healthcare Research and Quality, Rockville, USA. http://www.hcup-us.ahrq. Accessed February 10, 2017.
10. Alcala L, Martin A, Marin M, et al. The undiagnosed cases of *Clostridium difficile* infection in a whole nation: Where is the problem? *Clin Microbiol Infect*. 2012;18:E204–213.
11. Leekha S, Aronhalt KC, Sloan LM, Patel R, Orenstein R. Asymptomatic *Clostridium difficile* colonization in a tertiary care hospital: Admission prevalence and risk factors. *Am J Infect Control*. 2013;41:390–393.
12. Zarroug N, Lewthwaite P, Beeching N, Beadsworth M. A novel algorithm for the management of clostridum difficile associated diarrhoea. *J Infect*. 2011;63:e94–e95.
13. Eddi R, Malik MN, Shakov R, Baddoura WJ, Chandran C, Debari VA. Chronic kidney disease as a risk factor for *Clostridium difficile* infection. *Nephrology* (*Carlton*). 2010;15:471–475.
14. Cunney RJ, Magee C, McNamara E, Smyth EG, Walshe J. *Clostridium difficile* colitis associated with chronic renal failure. *Nephrol Dial Transplant*. 1998;13:2842–2846.

Safety of adipose-derived cell (stromal vascular fraction – SVF) augmentation for surgical breast reconstruction in cancer patients

Sławomir Mazur[1,A–C,F], Aleksandra Zołocińska[2,C,D], Katarzyna Siennicka[2,C,D], Karolina Janik-Kosacka[2,C,D], Anna Chrapusta[3,C,E], Zygmunt Pojda[2,A,D,F]

[1] Department of Breast Cancer and Reconstructive Surgery, Maria Skłodowska-Curie Memorial Cancer Center and Institute of Oncology, Warszawa, Poland
[2] Department of Regenerative Medicine, Maria Skłodowska-Curie Memorial Cancer Center and Institute of Oncology, Warszawa, Poland
[3] Department of Plastic and Reconstructive Surgery, Ludwik Rydygier Memorial Specialized Hospital in Kraków, Poland

A – research concept and design; B – collection and/or assembly of data; C – data analysis and interpretation;
D – writing the article; E – critical revision of the article; F – final approval of the article

Advances in Clinical and Experimental Medicine, ISSN 1899-5276 (print), ISSN 2451-2680 (online) *Adv Clin Exp Med*. 2018;27(8):1085–1090

Address for correspondence
Zygmunt Pojda
E-mail: zpojda@coi.waw.pl

Funding sources
The project was supported by a research grant from the National Centre for Research and Development, Poland (STRATEGMED 1/233224/10/NCBR/2014).

Conflict of interest
None declared

Received on October 27, 2016
Reviewed on March 12, 2017
Accepted on April 27, 2017

DOI
10.17219/acem/70798

Abstract

Background. Progress in breast cancer surgery results in a decreased frequency of mastectomy, in the early phases of cancer replaced by breast conserving therapy (lumpectomy). Increased popularity of breast reconstruction by fat or adipose stem cells (ASC)-enriched fat transfer raised uncertainty about the possible risk of increased cancer recurrence. In vitro studies suggest that locally secreted cytokines and reconstructed local blood vessels may stimulate cancer expansion or cancer de novo induction from glandular tissue remaining after lumpectomy.

Objectives. The purpose of the study was to evaluate the risk of cancer recurrence in breast cancer patients related to the stromal vascular fraction (SVF) augmentation during autologous fat grafting for breast reconstruction.

Material and methods. The tumor recurrence ratio in 56 patients having the breast reconstructed with autologous ASC (transplanted as the subpopulation present in SVF) was compared with the frequency of tumor recurrence in 252 matched patients treated in clinics without subsequent breast reconstruction. Adipose tissue was collected by the Coleman technique and split into 2 portions: one was used for breast reconstruction, the other was enzymatically digested, and isolated cells were used for the augmentation of fat implanted into the breast area. Cancer recurrence in the experimental and matched control group was evaluated following 3-year-long observation time, and the statistical significance of difference in cancer recurrence between the experimental and control group was evaluated.

Results. Cancer recurrence in the group of patients treated with ASC-enriched fat for breast reconstruction was 3.7% and did not differ significantly from the control group data (4.13%). No adverse effects of therapy were observed.

Conclusions. Our study does not produce any data suggesting increased cancer risk following breast reconstruction after a mastectomy or a lumpectomy combined with local radiotherapy. It may be concluded that an autologous transplantation of fat augmented with ASC is a safe and efficient procedure. Longer observation time and the observation of larger numbers of patients would be useful for strengthening the conclusion.

Key words: mesenchymal stem cells, adipose tissue, treatment-associated cancer

Introduction

The purpose of the study was to evaluate the risk of cancer recurrence in breast cancer patients related to the stromal vascular fraction (SVF) augmentation during autologous fat grafting for breast reconstruction.

Breast cancer treatment results in permanent tissue injuries in the region of cancer localization. The problem is not restricted only to esthetic aspects; surgery and local radiotherapy produce injuries of connective tissue, blood and lymphatic vessels, or nerves, resulting in pain, lymphedema and deformations. The method of autologous fat grafting is growing in popularity, as it is more physiological than the implantation of artificial substances like silicone implants or injectable fillers. The disadvantage of the lipofilling technique is fat resorption ranging from 25% to 80%.

Adipose stem cells (ASC), when added to transplanted fat, may differentiate into new adipocytes, thus preserving more permanently the volume of fat used for breast reconstruction. When adding the mixed cell population (stromal vascular fraction – SVF) obtained as a result of enzymatic fat digestion, such cells as endothelial progenitor cells (EPC) may strengthen the effect of ASC on neoangiogenesis, increasing the survival of transplanted adipocytes. Immune system cells, also present in SVF, prevent infections immediately after fat grafting, before new blood vessels colonize transplanted adipose tissue. The antiapoptotic role of ASC, their role in tissue repair and adipogenesis as well as the angiogenetic role of EPC and infection prevention by immune cells are strong arguments supporting the use of SVF for breast conserving therapy.[1,2] There is, however, a not fully clarified problem concerning the possible risk of cancer recurrence induced by ASC. Adipose tissue, even when not supplemented with ASC, contains approx. 3×10^5/mL mesenchymal stem cells (MSC), which in in vitro and in animal experiments may stimulate cancer cells.[3]

The problem of the supportive activity of MSC for cancer recurrence, expansion or metastases has been widely researched. All supportive evidence suggesting the stimulatory role of MSC in cancerogenesis originates from in vitro studies and, less numerous, animal experiments.[4] To our knowledge, no clinical evidence of oncostimulatory activity has been reported from clinical trials, and the evidence from clinical observations suggests no increase of cancer recurrence. The relatively low number of clinical observations of the MSC – cancer interrelations and the low number of patients included in the studies – make it necessary to collect new data before formulating a final conclusion regarding the safety of MSC therapies in patients cured from cancers.

Table 1. Characteristics of patients in respect to the histological type of disease

Histological type	Number of patients	Age [years]	Transplanted fat volume [mL]	Number of transplanted cells [×10⁶]
Cdis	4/56 (7.1%)	46 ±10.2	65.2 ±17.5	68.9 ±56.2
Cdis, Nst	1/56 (1.8%)	55	N/A	41.0
Fibrosa	1/56 (1.8%)	73	20.0	50.8
Lobular	5/56 (8.9%)	49.4 ±7.6	75.3 ±19.3	51.4 ±22.9
Nst	40/56 (71.4%)	49.2 ±10.1	88.9 ±31.9	85.4 ±73.0
Tubular	5/56 (8.9%)	52.6 ±11.5	69.6 ±32.5	91.5 ±68.8
Average	–	49.8 ±10.2	82.9 ±31.7	80.3 ±67.3

Cdis – carcinoma ductale in situ; Nst – invasive carcinoma of no special type; N/A – not available.

Material and methods

The Bioethics Committee of the Polish Ministry of Health approved the clinical experiment based on the transplantation of autologous fat augmented with ASC into patients cured from breast cancer (approval No. OKB-4/12).

Patients

A total number of 56 patients who had undergone breast cancer treatment were enrolled in the study. The control group was matched among patients treated for breast cancer in the years 2012–2015 in Maria Skłodowska-Curie Memorial Cancer Center and Institute of Oncology in Warszawa, Poland.

The inclusion criteria were: the age of 18–75 years, completely cured breast cancer, min 12 months after the completion of treatment, no syndrome of cancer recurrence, and min 2 mm of fat tissue between the breast skin and the chest wall. The exclusion criteria were: cancer recurrence during the last 12 months, the coexistence of different cancer types, autoimmunological diseases, keloid, connective tissue diseases, chronic anticoagulants treatment (<15 days before the therapy), body mass index (BMI) >30, contraindications for magnetic resonance imaging (MRI), expected survival time <12 months, and family predispositions for breast cancer, including *BRCA1* and *BRCA2* gene carriers. The summary of the enrolled patients' characteristics is shown in Tables 1–3. Data on breast reconstruction using autologous fat augmented with autologous ASC of 56 patients was compared with the results of 252 control group patients. The control group included patients of matched age, year of admission to the clinic, histological type of cancer, and treatment protocol – the only difference was the lack of breast reconstruction treatment.

SVF isolation

All procedures were performed under general anesthesia according to Coleman method.[5] Prior to liposuction, 20–30 mL of sterile saline solution supplemented with epinephrine and lignocaine was evenly distributed

into the collection site by needle injection. Subsequently, 200 mL of fat tissue was aspirated into 20 mL syringes. The collected lipoaspirate was divided into 2 portions: one was used for breast reconstruction, the other was enzymatically digested as we described before to isolate SVF cells.[6] Briefly, phosphate-buffered solution (PBS) (Life Technologies, Waltham, USA)-diluted fat tissue was incubated with 0.025% collagenase from *Clostridium histolyticum* (Sigma-Aldrich; St Louis, USA) at 37°C for 1.5 h. The resulting mixture was diluted in PBS + 2% human albumin (Kedrion Biophrama, Barga, Italy) and centrifuged (400 g, 10 min). Following phase separation, the cell pellet was resuspended in physiological salt solution for patient injections + 5% human albumin.

Cells analysis

The number (Burker's chamber and the Sysmex analysis) and viability (acridine orange + ethidium bromide staining, fluorescence microscopy) of cells were determined and sterility control was carried out for every sample (BACTEC, Bact/Alert; Becton Dickinson, Franklin Lakes, USA; blood agar and BHI agar). The cytometric analysis of the SVF cells and adherent fraction cells (ASC) phenotype was performed for the presence of surface markers (CD29, CD31, CD34, CD45, CD73, CD90, CD105, Lin1, CXCR4, and HLA-DR). In vitro proliferation potential (doubling time), clonality (the colony-forming unit (CFU) test) and capability to differentiate into osteogenic, chondrogenic and adipogenic lineage were analyzed in order to confirm the MSC character of the cells (Fig. 1).

SVF application

The SVF cells were resuspended in physiological salt solution and were used for the augmentation of fat implanted into the breast area in an average amount of 8.4×10^5 cells for every 1 mL of fat tissue transplanted earlier. The time between fat and cell injections did not exceed 4 h.

Statistical analysis

Cancer recurrence in experimental vs control group was evaluated using the Fisher's exact test; $p < 0.05$ was considered statistically significant. The data was presented as the average values and standard deviations (SD).

Results

In patients treated with ASC-augmented adipose tissue, the histological classification of cancer type (Table 1) revealed the prevalence of invasive carcinoma of no special type (40 patients), 5 cases of tubular carcinoma, 5 cases of lobular carcinoma,, 4 cases of carcinoma ductale in situ, and single cases of ductale/no special type and fibrosa. Both cases of cancer recurrence were of invasive no special type, similarly as 10 recurrences in the control group. The number of patients in respect to molecular subtype of cancer, tumor size and the number of lymph nodes involved is presented in Table 2. As reflected in Table 3, most patients were treated by surgical mastectomy combined with radiotherapy (21), mastectomy alone (6), mastectomy combined with implant (9), lumpectomy (7), and transverse rectus abdominis myocutaneous (TRAM) (9). Total reconstruction was performed in 1 patient, rarely ulceration (1) and lymphatic edema (1) were observed. The average volume of transplanted fat varied

Table 2. Characteristics of patients in respect to histological/molecular subtype, tumor size and the number of lymph nodes involved

Histological type/ molecular subtype	Number of patients	Tumor size [mm]	Number of involved lymph nodes
Cdis	4/56 (7.1%)	34.5 ±25.8	0
Cdis, Nst/Luminal A	1/56 (1.8%)	60	0
Fibrosa/ –	1/56 (1.8%)	40.0	0
Lobular/Lum B (Her2–)	2/56 (3.6%)	28.0 ±4.2	1.0 ±1.4
Lobular/Luminal A	2/56 (3.6%)	33.5 ±9.2	0
Lobular NoLum/Her2+	1/56 (1.8%)	31.0	4
Nst/Lum B (Her2–)	7/56 (12.5%)	32.0 ±2.7	1.1 ±0.9
Nst/Lum B (Her2+)	4/56 (7.1%)	33.5 ±2.7	3.5 ±0.6
Nst/Luminal A	22/56 (39.3%)	34.8 ±3.9	0.5 ±0.5
Nst/Non Luminal	3/56 (5.4%)	35.3 ±0.6	5.3 ±1.5
Nst/Triple neg	4/56 (7.1%)	28.5 ±5.1	3.0 ±1.8
Tubular/Luminal A	5/56 (8.9%)	13.0 ±3.4	0

Cdis – carcinoma ductale in situ; Nst – invasive carcinoma of no special type; Lum – luminal; NoLum – non luminal; neg – negative.

Table 3. Characteristics of patients in respect to the treatment protocol

Treatment protocol	Number of patients	Age [years]	Transplanted fat volume [mL]	Number of transplanted cells [×10^6]
BCT	7/56 (12.5%)	50.7 ±7.2	78.5 ±37.4	102.8 ±74.3
Implant	9/56 (16.1%)	52.0 ±10.3	80.1 ±24.6	67.9 ±41.0
M	6/56 (10.7%)	40.3 ±11.1	79.8 ±26.6	97.3 ±37.9
M+RT	21/56 (37.5%)	50.1 ±10.2	82.4 ±32.0	76.5 ±87.2
Lymphatic edema	1/56 (1.8%)	61.0	108.0	36.0
Ulceration	2/56 (3.6%)	67.5 ±7.7	23.5 ±4.9	59.4 ±12.1
Total reconstruction	1/56 (1.8%)	43.0	141.0	49.7
TRAM	9/56 (16%)	48.2 ±7.3	96.2 ±23.7	85.7 ±48.8
Average	–	49.8 ±10.2	82.9 ±31.6	80.3 ±67.3

BCT – breast conserving therapy; M – mastectomy; M+RT – mastectomy and radiotherapy; TRAM – transverse rectus abdominis myocutaneous.

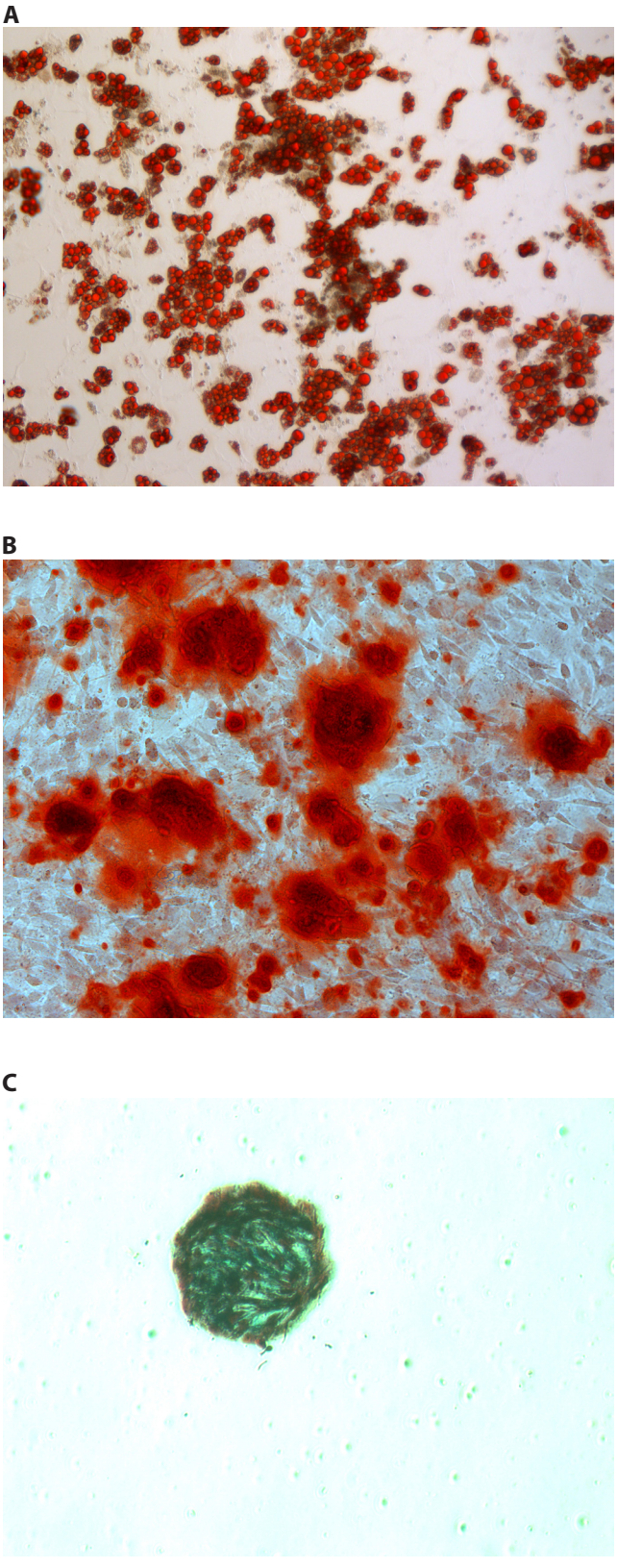

Fig. 1. Differentiation of adipose stem cells (ASC) into adipogenic (a), osteogenic (b) and chondrogenic (c) lineages

The cells were treated by differentiation media (all from Lonza, Allendale, USA) according to the manufacturer's protocol, and stained by Oil Red O for adipogenic differentiation, Alizarin Red for osteogenic differentiation and Messon's Trichrome for chondrogenic differentiation (Sigma-Aldrich, St. Louis, USA).

from 23.5 mL (ulceration treatment) up to 141 mL (total reconstruction). The average number of the SVF cells transplanted varied between 36 × 10^6 (lymphatic edema) and 102.8 × 10^6 (breast conserving therapy) (Table 3). Locoregional cancer recurrence in the experimental group in patients with invasive no special type carcinoma was 2/54 and in the matched control group it was 10/242, which constituted 3.70% and 4.13%, respectively. The difference between cancer recurrence in the experimental vs control group was statistically insignificant (the Fisher's exact test, p = 1.0).

Discussion

Mesenchymal stem cells are present in all the tissues of the human body as the cellular component of connective tissue. Their capacities, like a regulatory role in tissue repair, an immunomodulatory role in suppressing immune reactions against own and transplanted allogeneic tissues, and differentiation into several tissues make them prime candidates for regeneration medicine treatments. Their medical applications are, however, at the stage of in vivo tests or clinical trials, none of them being utilized in regular clinical procedures. They are most frequently tested in orthopedics and plastic surgery, and also in neurology, cardiology or transplantology.

Mesenchymal stem cells may be collected from adult donors, which makes it possible to use them for autologous purposes. The source containing the highest number of MSC, which may be easily collected, is adipose tissue (adipose stem cells – ASC). These cells fulfill the morphologic and functional criteria listed by the International Society for Cellular Therapy Committee as mandatory for mesenchymal stem (stromal) cells.[7,8] One of these criteria is differentiation into adipose tissue, which is the main reason for the application of ASC for the supplementation of fat used for breast reconstruction in oncological patients. The other ASC capability when transplanted into fat-reconstructed breast

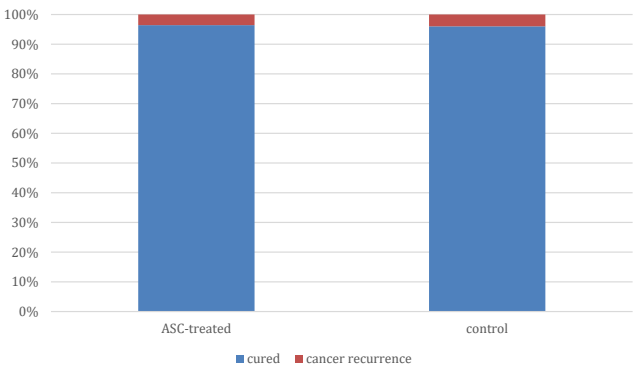

Fig. 2. Comparison of the cancer recurrence rate in the experimental (SVF-enriched fat lipofilling) and control group of patients

ASC – adipose stem cells; SVF – stromal vascular fraction.

is its angiogenic potential resulting in the production of blood vessels, and preventing the apoptosis or necrosis of transplanted adipocytes. The beneficial effects of the ASC enrichment of fat used for breast reconstruction have been experimentally confirmed. Matsumoto et al. observed that ASC are transplanted with vascular endothelial cells and contribute to neoangiogenesis in the acute phase of transplantation.[9] The unanswered question was how important the transplanted ASC are in the compensation of fat resorption by the production of new adipocytes. The question was solved by the elegant experiment done by Kolle et al., who implanted fat deposits into the upper arms of healthy volunteers.[10] After 121 days, the fat deposits were removed, their content was histologically analyzed and the volumes of fat deposits, enriched by the ASC addition, were compared with the volumes of fat implanted without the addition of ASC. The volumes of ASC-enriched fat deposits were 80.9% of the initial volume, whereas fat-only deposits were 16.3%.

A still unsolved dispute concerns the risk of cancer induction by MSC. There is no data available on the possible cancer transformation of the transplanted MSC (up to several months of in vitro culture prior to transplantation).[11] Animal studies confirmed that even very high numbers (up to 450×10^6 cells per animal) of allogeneic MSC were transplanted without any negative effects.[12] There is, however, some data from in vitro and, to a lesser extent, animal in vivo experiments (immunocompromised mice with heterotopic cancer) documenting the possibility of cancer stimulation by MSC co-cultured in vitro or injected into animals.[13–19] In vitro, ASC in co-culture with breast cancer cell lines promote the proliferation, induction of epithelial-to-mesenchymal transition (EMT) (through P13K/AKT signaling in breast cancer cells), enhancement of migration, invasion of breast cancer cells by cell-cell contact, and the secretion of IL-6 and IL-8.[13] When adding MSC to 3D-cultured hepatocarcinoma cells, they upregulate the matrix metaloproteinase (MMP), EMT-related genes and increase the migration ability, thus enhancing the tumor metastasis ability.[14]

Bone marrow MSC, mixed with weakly metastatic human breast carcinoma cells, increased their metastatic potency, secreting de novo CCL5 chemokine (RANTES).[15] Adipose stem cells of phenotype ($CD45^+$, $CD34^+$, $CD31^+$, $CD13^+$, $CD140b^+$) generated pericytes and were efficient in promoting local tumor growth, inducing EMT gene expression in luminal breast cancer cells.[16] In in vivo experiments in immunocompromised mice, the co-injection of human ASC from lipotransfer contributed to tumor vascularization and significantly increased tumor growth and metastases in orthotopic models of human breast cancer.[17,18] Eterno et al. reported that ASC are not tumorigenic per se and are not able to induce the metastatic transformation of normal mammary cells, and that breast cancer recurrence and the enhancement of tumor cell migration and tumor cell renewal resulted from the HGF/c-Met crosstalk between ASC and breast cancer cells.[19]

Surprisingly, this data is not reflected by the observations collected from clinical trials involving patients cured from cancer, treated with autologous or allogeneic MSC. The results of the implantation of ASC-containing grafts into patients treated for osteosarcoma, chondrosarcoma or Ewing sarcoma did not produce any side effects, including cancer recurrence.[20] A multicenter study on breast reconstruction with ASC-enriched fat also did not produce breast cancer induction by ASC added to lipofilling material.[21] The authors of a recently published study based on the analysis of extensive literature data conclude that "recent reports concerning SVF/ASC enrichment of fat graft did not describe any significant worsening of prognosis for patients; however, further studies and longer follow-ups are needed to confirm the safety of procedures using SVF/ASC enrichment during post-surgical breast reconstruction".[22] Likewise, the authors of a similar analysis of published data conclude: "If the family history is negative for breast cancer and no additional risk factors for breast cancer are evident, fat grafting can be considered a surgical option."[23] The difference between the in vitro and in vivo (mice) studies and clinical data may be explained by the fact that both in vitro research and animal studies are very simplified when compared to the clinical situation. Such an experimental design does not allow for the immune system involvement, and tests ASC in an artificial environment, which may change their secretome production. In contrast, enriching adipose tissue with ASC makes only a quantitative, but not qualitative, difference, since non-enriched fat also contains a relatively high number of ASC and the ASC additionally admixed into fat are placed in their "native" environment. There are also scant reports on the anticancer activity of ASC. Human MSC in a hepatoma model inhibit the malignant phenotypes of human liver cancer lines, which includes the proliferation, colony-forming ability and oncogene expression, both in vitro and in vivo.[24] Otsu et al. observed that in an in vivo tumor model, direct MSC inoculation at high numbers into subcutaneous melanomas induced apoptosis and abrogated tumor growth due to their antiangiogenic mechanism.[25] Similarly, the anticancer activity of marrow MSC was observed in an experimental model of Kaposi sarcoma, and in an in vitro or in vivo model when ASC induced pancreatic cancer death.[26,27]

The clinical benefits of breast reconstruction were not analyzed due to the relatively low number of patients and a high heterogeneity of cancer types, disease stages and cancer therapy protocols. The clinical outcome (residual pain, lymphatic edemas) and their satisfaction levels were better in the breast reconstruction group. Our study was concentrated on the evaluation of the safety of the SVF treatment in patients cured from cancer. Our observation time was relatively short, hence the conclusions must be considered with caution. However, in other papers, the follow-up period was 12 months, 14–48 months vs our 24–36-month follow-up time.[21,28]

It may be concluded that breast reconstruction using fat augmented with autologous adipose-derived stem cells does not increase the risk of cancer recurrence. The relatively short observation time (3 years) and the heterogeneity of both cancer types and cancer treatment protocols suggest a cautious interpretation of our results.

References

1. Rigotti G, Marchi A, Galie M, et al. Clinical treatment of radiotherapy tissue damage by lipoaspirate transplant: A healing process mediated by adipose-derived adult stem cells. *Plast Reconstr Surg*. 2007;119:1409–1422.
2. Ryden M, Dicker A, Gotherstrom C, et al. Functional characterization of human mesenchymal stem cell-derived adipocytes. *Biochem Biophys Res Commun*. 2003;311:391–397.
3. Muehlberg FL, Song YH, Krohn A, et al. Tissue-resident stem cells promote breast cancer growth and metastasis. *Carcinogenesis*. 2009;30:589–597.
4. Zimmerlin L, Donnenberg AD, Rubin JP, Basse P, Landreneau RJ, Donnenberg VS. Regenerative therapy and cancer: In vitro and in vivo studies of the interaction between adipose-derived stem cells and breast cancer cells from clinical isolates. *Tissue Eng Part A*. 2011;17:93–106.
5. Coleman SR. Facial recontouring with lipostructure. *Cain Plast Surg*. 1997;24(2):347–367.
6. Siennicka K, Zołoćińska A, Stępień K, et al. Adipose-derived cells (stromal vascular fraction) transplanted for orthopedical or neurological purposes: Are they safe enough? *Stem Cells Int*. 2016; 2016. doi.10.1155/2016/5762916
7. Dominici M, Le Blanc K, Mueller I, et al. Minimal criteria for defining multipotent mesenchymal stromal cells: The International Society for Cellular Therapy position statement. *Cytotherapy*. 2006;8:315–317.
8. Horwitz EM, Le Blanc K, Dominici M, et al.; International Society for Cellular Therapy. Clarification of the nomenclature for MSC: The International Society for Cellular Therapy position statement. *Cytotherapy*. 2005;7:393–395.
9. Matsumoto D, Sato K, Gonda K, et al. Cell-assisted lipotransfer: Supportive use of human adipose-derived cells for soft tissue augmentation with lipoinjection. *Tissue Eng*. 2006;12:3375–3382.
10. Kolle S-FT, Fischer-Nielsen A, Mathiasen AB, et al. Enrichment of autologous fat grafts with ex-vivo expanded adipose tissue-derived stem cells for graft survival: A randomised placebo-controlled trial. *Lancet*. 2013;382:1113–1120.
11. Rubio D, Garcia-Castro J, Martin MC, et al. Spontaneous human adult stem cell transformation. *Cancer Res*. 2005;65:3035–3039.
12. McDonald CA, Oehme D, Pham Y, et al. Evaluation of the safety and tolerability of a high-dose intravenous infusion of allogeneic mesenchymal precursor cells. *Cytotherapy*. 2015;17:1178–1187.
13. Ritter A, Friemel A, Fornoff F, et al. Characterization of adipose-derived stem cells from subcutaneous and visceral adipose tissues and their function in breast cancer cells. *Oncotarget*. 2015;6:34475–34493.
14. Liu C, Liu Y, Xu XX, Guo X, Sun GW, Ma XJ. Mesenchymal stem cells enhance the metastasis of 3D-cultured hepatocellular carcinoma cells. *BMC Cancer*. 2016;16:566. doi:10.1186/s12885-016-2595-4
15. Karnoub AE, Dash AB, Vo AP, et al. Mesenchymal stem cells within tumor stroma promote breast cancer metastasis. *Nature*. 2007;449:557–563.
16. Orecchioni S, Gregato G, Martin-Padura I, et al. Complementary populations of human adipose CD34+ progenitor cells promote growth, angiogenesis, and metastasis of breast cancer. *Cancer Res*. 2013;73:5880–5891.
17. Manzotti M, Lohsiriwat V, Rietjens M, Petit JY, Bertolini F. The white adipose tissue used in lipotransfer procedures is a rich reservoir of CD34+ progenitors able to promote cancer progression. *Cancer Res*. 2012;72:325–334.
18. Kamat P, Schweizer R, Kaenel P, et al. Human adipose-derived mesenchymal stromal cells may promote breast cancer progression and metastatic spread. *Plast Reconstr Surg*. 2015;136:76–84.
19. Eterno V, Zambelli A, Pavesi L, et al. Adipose-derived mesenchymal stem cells (ASCs) may favour breast cancer recurrence via HGF/c-Met signaling. *Oncotarget*. 2013;5:613–633.
20. Veriter S, Andre W, Auassar N, et al. Human adipose-derived mesenchymal stem cells in cell therapy: Safety and feasibility in different "hospital exemption" clinical applications. *PLoS One*. 2015. doi:10.1371/journal.pone.0139566
21. Perez-Cano R, Vrancks JJ, Lasso JM, et al. Prospective trial of adipose-derived regenerative cell (ADRC)-enriched fat grafting for partial mastectomy defects: The RESTORE-2 trial. *Eur J Surg Oncol*. 2012;38:382–389.
22. Bielli A, Scioli MG, Gentile P, Cervelli V, Orlandi A. Adipose tissue-derived stem cell therapy for post-surgical breast reconstruction: More light than shadows. *Adv Clin Exp Med*. 2015;24(3):545–548.
23. Krumboeck A, Giovanoli P, Plock JA. Fat grafting and stem cell enhanced fat grafting to the breast under oncological aspects: Recommendations for patient selection. *The Breast*. 2013;22:579–584.
24. Qiao L, Xu Z, Zhao T, et al. Suppression of tumorigenesis by human mesenchymal stem cells in a hepatoma model. *Cell Res*. 2008;18:500–507.
25. Otsu K, Das S, Houser SD, Quadri SK, Bhattacharta S, Bhattacharya J. Concentration-dependent inhibition of angiogenesis by mesenchymal stem cells. *Blood*. 2009;113:4197–4205.
26. Zhu W, Xu W, Jiang R, et al. Mesenchymal stem cells derived from bone marrow favor tumor cell growth in vivo. *Exp Mol Pathol*. 2006;80:267–274.
27. Cousin B, Ravet E, Poglio S, et al. Adult stromal cells derived from human adipose tissue provoke pancreatic cancer cell death both in vitro and in vivo. *PLoS One*. 2009;4:e6278.
28. Mestak O, Hromadkova V, Fajfrova M, et al. Evaluation of oncological safety of fat grafting after breast-conserving therapy: A prospective study. *Ann Surg Oncol*. 2016;23:776–781.

Electrocardiographic abnormalities in amateur male marathon runners

Anna M. Kaleta[1,A–D,F], Ewa Lewicka[1,A–C,E,F], Alicja Dąbrowska-Kugacka[1,A–C,E,F], Zuzanna Lewicka-Potocka[1,A–C], Elżbieta Wabich[1,A–C], Anna Szerszyńska[2,B,C], Julia Dyda[2,B,C], Jakub Sobolewski[2,B,C], Jakub Koenner[2,B,C], Grzegorz Raczak[1,A,E,F]

[1] Department of Cardiology and Electrotherapy, Medical University of Gdańsk, Poland
[2] Students' Cardiology Scientific Association, Department of Cardiology, Medical University of Gdańsk, Poland

A – research concept and design; B – collection and/or assembly of data; C – data analysis and interpretation;
D – writing the article; E – critical revision of the article; F – final approval of the article

Advances in Clinical and Experimental Medicine, ISSN 1899-5276 (print), ISSN 2451-2680 (online) *Adv Clin Exp Med*. 2018;27(8):1091–1098

Address for correspondence
Anna M. Kaleta
E-mail: ania.m.kaleta@gmail.com

Funding sources
None declared

Conflict of interest
None declared

Received on November 21, 2016
Reviewed on April 19, 2017
Accepted on May 11, 2017

Abstract

Background. Sports activity has become extremely popular among amateurs. Electrocardiography is a useful tool in screening for cardiac pathologies in athletes; however, there is little data on electrocardiographic abnormalities in the group of amateur athletes.

Objectives. The aim of this study was to analyze the abnormalities in resting and exercise electrocardiograms (ECGs) in a group of amateur athletes, and try to determine whether the criteria applied for the general population or for athletes' ECGs should be implemented in this group.

Material and methods. In 40 amateur male marathon runners, 3 consecutive 12-lead ECGs were performed: 2–3 weeks before (stage 1), just after the run (stage 2) and 2–3 weeks after the marathon (stage 3). Resting (stage 1) and exercise (stage 2) ECGs were analyzed following the refined criteria for the assessment of athlete's ECG (changes classified as training-related, borderline or training-unrelated).

Results. In resting ECGs, at least 1 abnormality was found in 92.5% of the subjects and the most common was sinus bradycardia (62.5%). In post-exercise ECGs, at least 1 abnormality was present in 77.5% of the subjects and the most common was right atrium enlargement (RAE) (42.5%). Training-related ECG variants were more frequent at rest (82.5% vs 42.5%; $p = 0.0008$), while borderline variants – after the run (22.5% vs 57.5%; $p = 0.0004$). Training-unrelated abnormalities were found in 15% and 10% of the subjects, respectively (p-value – nonsignificant), and the most common was T-wave inversion.

Conclusions. Even if the refined criteria rather than the criteria used for normal sedentary population were applied, the vast majority of amateur runners showed at least 1 abnormality in resting ECGs, which were mainly training-related variants. However, at rest, in 15% of the subjects, pathologic training-unrelated abnormalities were found. The most frequent post-exercise abnormality was right atrial enlargement. General electrocardiographic screening in amateur athletes should be taken into consideration.

Key words: electrocardiography, athlete's heart, sports cardiology, refined criteria, amateur runners

DOI
10.17219/acem/73700

Introduction

Electrocardiography is a generally accepted and effective tool in athletes' screening for cardiac pathologies.[1,2] Electrocardiographic abnormalities are common among athletes and they most often reflect physiological structural adaptive changes, a phenomenon known as 'athlete's heart'. Thus, in the assessment of athlete's resting electrocardiogram (ECG), specific criteria have to be used. Moreover, the so called 'refined criteria' appear to be the most specific and sensitive in screening for cardiac pathologies (most often hypertrophic cardiomyopathy) in both white and black elite athlete populations.[3] Nowadays, apart from professional athletes, there is an increasingly growing number of amateurs who participate in numerous competitive sports events, even as strenuous as a marathon run. That is why we found it interesting to examine the impact of intensive exercise such as a marathon run on the electrocardiographic findings in this population. As participating in a marathon requires regular physical preparation from people who are amateurs, we decided to apply the same criteria for their electrocardiographic findings assessment which are used in elite athletes.[3]

On this ground, a question arises whether electrocardiographic screening would be reasonable also among amateur athletes.

Material and methods

Data collection

This was a prospective and observational study performed in a group of amateur runners who participated in the 2nd PZU Gdańsk Marathon. The study was divided into 3 stages: the 1st measurement was carried out 2–3 weeks before the marathon; the 2nd – on the day of the marathon on the finish line; and the 3rd stage – 2-3 weeks after the marathon. The 1st and 3rd examination took place in the Department of Cardiology and Electrotherapy of the Medical University of Gdańsk, Poland. At each stage, a standard 12-lead ECG was recorded in the supine position, using a digital electrocardiograph (Mortara, ELI 250c with baseline filter, AC interference filter 50/60 Hz and low-pass 40 Hz filter; Mortara Instrument, Milwaukee, USA) at a paper speed of 25 mm/s. At stage 1 and 3 it was recorded after 3 min of rest, during quiet respiration, and at stage 2 – just after finishing the marathon, on the finish line. The interpretation of the ECGs followed the criteria as listed below.

The study protocol was approved by the Bioethics Committee of the Medical University of Gdańsk, Poland (No. NKBBN 104/2016) and a written consent was obtained from each participant.

Study group

The study group consisted of 40 male amateur marathon runners with no history of diagnosed chronic illnesses. Information about personal health and the intensity of training defined in hours per week was obtained by anamnesis.

ECG measurements

The following criteria for the evaluation of ECG abnormalities were used. Sinus bradycardia was defined as a sinus rhythm below 60 bpm. The P-waves were analyzed in the context of left atrium enlargement (LAE) and right atrium enlargement (RAE). LAE was defined as the P-wave duration >120 ms in lead I or II, or a negative portion of the P-wave of ≥0.1 mV in depth and ≥40 ms in duration in lead V_1. RAE was defined as the P-wave amplitude ≥0.25 mV in lead II, III or aVF. Figure 1 illustrates the measurement of P-waves in the context of LAE/RAE. Left ventricular hypertrophy (LVH) was defined when at least 1 of the following criteria was fulfilled: Sokolow-Lyon criteria or Cornell criteria, R-wave in lead aVL >1.1 mV, or R-wave in lead I and S-wave in lead III >2.5 mV, given there were no intraventricular conduction delays. Right ventricular hypertrophy (RVH) was defined when at least 1 of the following criteria was fulfilled: R-wave in lead aVR ≥0.5 mV, or R-wave in lead V_1 ≥0.7 mV, or R-wave in lead V_1 and S-wave in lead V_5 or V_6 >1.05 mV. T-wave inversion (TWI) was defined as negative T-waves >1 mm in depth in ≥2 leads: V_2–V_6, II and aVF, or I and aVL (excludes leads III, aVR and V_1). QT intervals were measured manually. QT dispersion was calculated as the difference between

Table 1. Classification of variants of electrocardiographic abnormalities

Training-related	Borderline	Training-unrelated
		ST segment depression
		Pathological Q-waves
		Ventricular preexcitation
		TWI beyond V_1
Sinus bradycardia	LAE	LBBB
1st degree AVB (PR > 200 ms)	RAE	RBBB
nRBBB	Left QRS axis deviation	QTc ≥ 470 ms
ER	Right QRS axis deviation	QTc < 320 ms
Isolated QRS voltage criteria for LVH	RVH	Brugada-like ER
		Atrial arrhythmias
		Ventricular arrhythmias
		≥2 PVCs/10s tracing
		≥2 borderline variants

AVB – atrioventricular block; nRBBB – non-complete right bundle branch block; ER – early repolarization; LVH – left ventricular hypertrophy; LAE – left atrial enlargement; RAE – right atrial enlargement; RVH – right ventricular hypertrophy; TWI – T-wave inversion; LBBB – left bundle branch block; RBBB – right bundle branch block; PVCs – premature ventricular contractions.

the longest (QT_{max}) and the shortest (QT_{min}) QT interval in the 12-lead ECG. QTc values for heart rates between 60 bpm and 110 bpm were calculated using Bazett's formula. Framingham formula was used for heart rates lower than 60 bpm and higher than 110 bpm. Prolonged QT was defined as QTc ≥ 470 ms in males, following the refined criteria.[3] Short QT interval was defined as QTc < 320 ms, following the Seattle criteria.[4] Brugada-like early repolarization (ER) pattern was defined as 'upsloping' ST-segment elevation with ST_J/ST_{80} ratio < 1 (ST_J = elevation of ST-segment measured at J point; ST_{80} = elevation of ST-segment measured 80 ms from J point).[5]

The ECG findings were divided into 3 groups, following the refined criteria for the interpretation of athlete's ECG, namely: training-related, borderline and training-unrelated (pathological) (Table 1).[3] We used the refined criteria, which are the latest recommendations on this topic. If at least 2 borderline variants were found on the ECG, it was categorized as 'training-unrelated variant', but it did not apply if the left and right atrial enlargement came together.

All ECGs were interpreted independently by 2 investigators. Disagreements were resolved by the 3rd investigator.

Each participant presenting with any training-unrelated variant underwent further detailed investigations (however, their results are not the subject of this particular study).

Statistical analysis

Data is presented as mean values with standard deviation (SD), participant numbers and percentages. Normally distributed variables were compared using the Student's t test, and the Mann-Whitney U test was used to compare independent non-normally distributed variables. Differences between categorical variables were assessed using the χ^2 test. Statistical analysis was performed using the Stata software v. 12.1 (StataCorp LLC, College Station, USA). A p-value <0.05 was considered statistically significant.

Results

Study group

A total of 40 Caucasian male amateur runners aged between 22 and 55 years were enrolled in the study. The intensity of training was expressed as a number of hours of running a week and by the number of kilometers run a week. Table 2 shows demographic data and the intensity of training in the studied group.

There were no significant differences in the ECG findings between stages 1 and 3, and for comparison with exercise ECG (stage 2) we used the data collected at stage 1. Results of the measurements of electrocardiographic parameters are shown in Table 3.

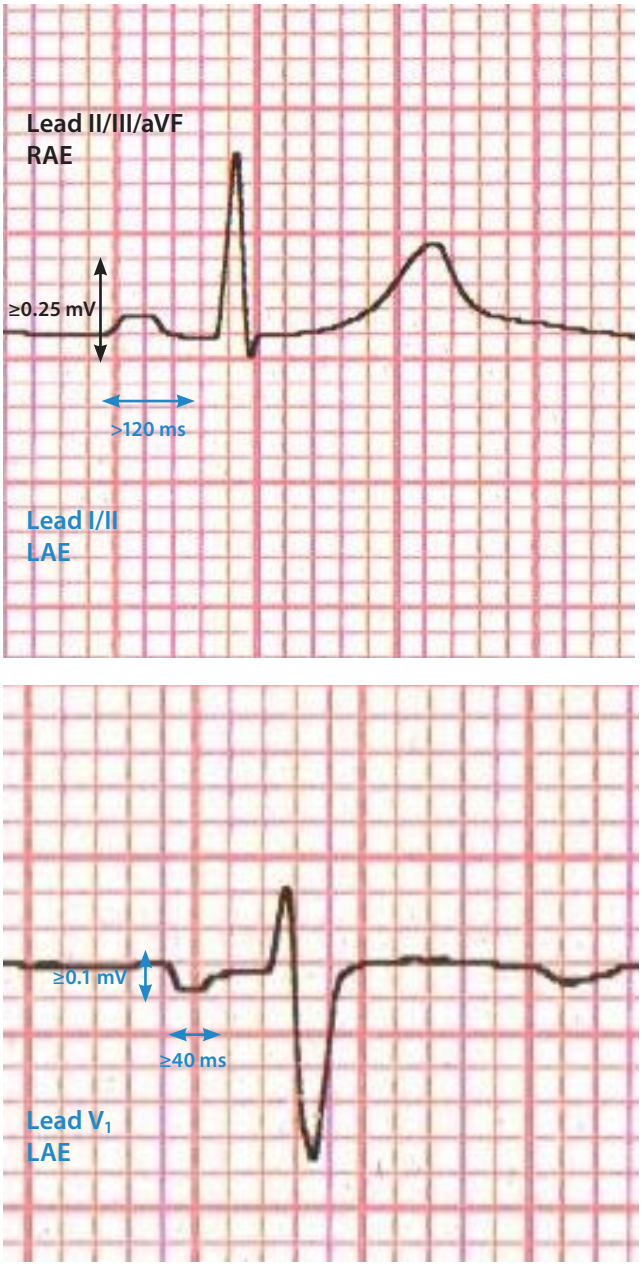

Fig. 1. Principles of measurement of P-waves in the context of LAE/RAE (voltage: 10 mm = 1 mV; paper speed: 25 mm/s)

LAE – left atrial enlargement; RAE – right atrial enlargement.

Table 2. Demographic data and intensity of training in the studied group of amateur marathon runners

Demographics and intensity of training	Amateur runners (n = 40)
Age [years]	39 ±8
Gender	40 males (100%)
BMI [kg/m^2]	25 ±2
Ethnicity	40 Caucasian (100%)
Training intensity: hours of running/week kilometers run/week	 6.2 ±2.3 54.5 ±18.6

BMI – body mass index.

Table 3. Electrocardiographic measurements at rest (stage 1) and after the marathon run (stage 2) in the studied group

Parameter	Stage 1	Stage 2	p-value
Heart rate [bpm]	57 ±11	94 ±10	<0.0001
QRS [ms]	96 ±12	95 ±10	0.6
PQ interval [ms]	166 ±23	160 ±19	0.2
P-wave duration [ms]	103 ±14	105 ±13	0.4
P-wave amplitude [mV]	0.1 ±0.04	0.2 ±0.1	<0.0001
QT interval [ms]	417 ±31	346 ±23	<0.0001
QTc [ms]	430 ±23	407 ±24	<0.0001
QT_{min} [ms]	398 ±31	331 ±24	<0.0001
QT_{max} [ms]	435 ±31	369 ±25	<0.0001
QT dispersion [ms]	37 ±16	37 ±14	0.9

stage 1 – examination performed 2–3 weeks before the marathon run; stage 2 – examination on the day of the marathon on the finish line.

ECG measurements

The mean heart rate at rest (57 ±11 bpm) was significantly lower than the mean heart rate after the marathon run (94 ±10 bpm). There were no significant differences between the QRS and PQ interval duration. The duration of the P-wave showed no significant differences, but its amplitude was significantly higher after the run (0.1 ±0.04 mV vs 0.2 ±0.1 mV; $p < 0.0001$).

We observed significant differences regarding the duration of QT interval. After the marathon run, the QT and QTc interval, as well as QT_{min} and QT_{max}, were significantly shorter compared to resting ECGs. However, there was no significant difference between QT dispersion at stage 1 and stage 2 (37 ±16 ms and 37 ±14 ms, respectively).

Classification of ECG variants

At least 1 electrocardiographic abnormality was found in 37 subjects at rest (92.5%), and in 31 – after the marathon run (77.5%). Table 4 shows the results of the ECG findings classified as training-related, borderline or training-unrelated (pathological).

In ECGs performed at rest, 25 participants (62.5%) presented sinus bradycardia and the lowest basic heart rate was 41 bpm, seen in 2 subjects. Sinus bradycardia was the most common training-related finding, followed by LVH by voltage criteria in 12 (30%) subjects and early repolarisation in 11 (20.4%). First degree atrioventricular block (AVB) was found in 4 (10%) participants, and non-complete right bundle branch block (nRBBB) in 2 (5%).

After the marathon run, neither sinus bradycardia nor 1st degree AVB were observed. There were no significant differences regarding the occurrence of nRBBB, LVH or ER compared to resting ECGs.

The total number of training-related variants was significantly higher at stage 1 compared to stage 2 (54 vs 23;

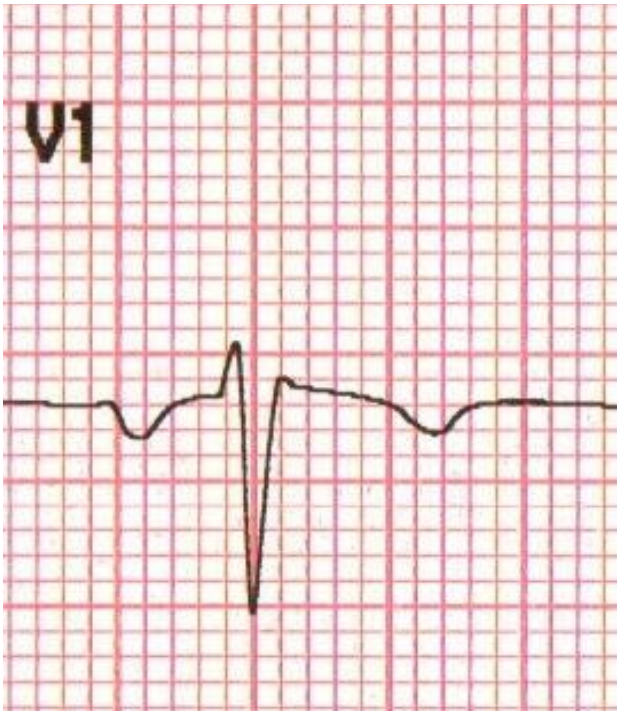

Fig. 2. Stage 1. LAE. Negative portion of P-wave of 0.12 mV in depth and 70 ms in duration in lead V_1 (voltage: 10 mm = 1 mV; paper speed: 25 mm/s)

LAE – left atrial enlargement.

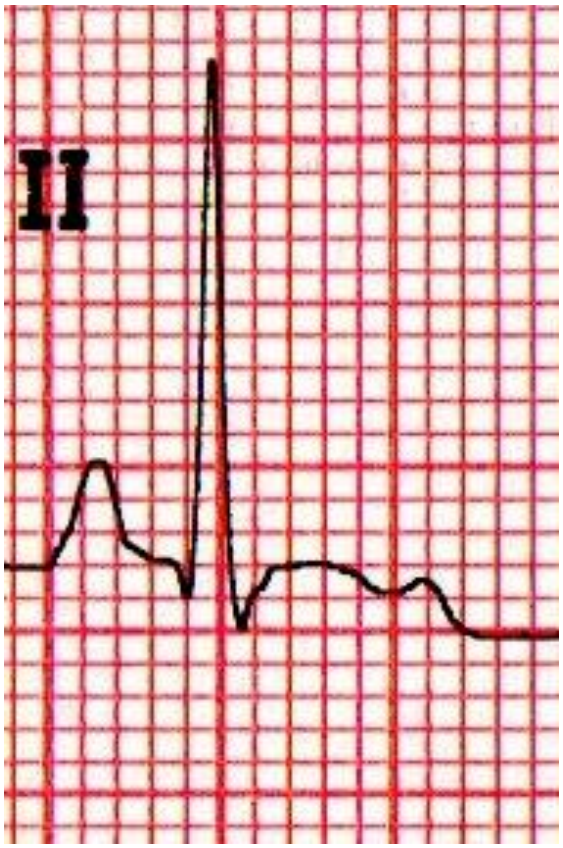

Fig. 3. Stage 2. RAE. P-wave amplitude of 0.3 mV in lead II (voltage: 10 mm = 1 mV; paper speed: 25 mm/s)

RAE – right atrial enlargement.

p = 0.0004), mainly due to frequent sinus bradycardia, which was a common finding in resting ECGs.

When analyzing borderline ECG variants, all of them were isolated and none of the participants had more than 1 borderline ECG variant. The most common finding was LAE. The example of LAE in 1 of the participants at stage 1 is shown in Fig. 2.

The number of ECGs meeting the criteria for LAE was higher after the marathon run, which was borderline significant (15 vs 8 at rest; p = 0.05). What is more, we found that the incidence of right atrium enlargement was significantly higher at stage 2 (0 vs 17; p < 0.0001). Figure 3 shows the example of RAE in one of the participants at stage 2.

The total number of borderline variants was significantly higher at stage 2 (35 vs 9; p < 0.0001), due to common RAE and LAE findings after the marathon run.

Training-unrelated ECG variants were the least common findings in the studied group and TWI dominated (Table 4). In resting ECGs, 5 participants presented abnormal TWI compared to 2 participants after the run, who also showed TWI at rest. Figure 4 shows TWI in one of the participants at stage 1. Changes in inferior leads occurred slightly more often than in lateral leads. There were no TWI in anterior leads. In 1 case, TWI in both lateral and inferior leads was observed after the run (Table 5, Fig. 5). QTc interval prolongation was present in 1 case at stage 1 and in 2 cases at stage 2 (Table 4), and the longest QTc in our group was 470 ms.

Training-related variants were more common at rest (p = 0.0008); borderline variants were more frequently observed after exercise (p = 0.0004), while there was no difference in the rate of training-unrelated changes between stage 1 and 2 (Table 6). In some cases, participants presented abnormalities belonging to more than 1 variant. At stage 1, 4 subjects had both training-related and borderline variants, 3 had both training-related and unrelated variants, while 2 had training-related, borderline and training-unrelated variants. At stage 2, 2 subjects had training-related, borderline and training-unrelated variants and 8 subjects had both training-related and borderline variants.

Discussion

This pilot study is the first one performed among Polish amateur marathon runners that assesses and compares the ECG changes in such a study population. We noticed that even in a relatively small study group of healthy male amateur runners, various ECG abnormalities can be found. If the criteria used for the general population had been applied, then the abnormalities in resting ECGs would have been observed in 92.5% of subjects. If classified as training-related, according to the refined criteria for elite athletes, these findings would also have been found in the vast

Table 4. Variants of electrocardiographic abnormalities at rest (stage 1) and after the marathon run (stage 2) in the studied group of amateur marathon runners

Parameter	Stage 1 (n = 40)	Stage 2 (n = 40)	p-value
Training-related variants			
Sinus bradycardia	25 (62.5%)	0 (0%)	<0.0001
1st degree AVB	4 (10%)	0 (0%)	0.05
nRBBB	2 (5%)	2 (5%)	0.9
LVH (isolated voltage criteria)	12 (30%)	14 (35%)	0.5
ER	11 (20.4%)	7 (17.5%)	0.4
Total	54 (78.3%)*	23 (37.1%)#	0.0004
Borderline variants			
Left QRS axis deviation	0 (0%)	0 (0%)	na
Right QRS axis deviation	0 (0%)	1 (2.5%)	0.3
LAE	8 (20%)	15 (37.5%)	0.05
RAE	0 (0%)	17 (42.5%)	<0.0001
RVH	1 (2.5%)	2 (5%)	0.5
Total	9 (13%)*	35 (56.5%)#	<0.0001
Training-unrelated variants			
ST segment depression	0 (0%)	0 (0%)	na
Pathological Q-waves	0 (0%)	0 (0%)	na
Ventricular preexcitation	0 (0%)	0 (0%)	na
TWI beyond V_1	5 (12.5%)	2 (5%)	0.3
Brugada-like ER	0 (0%)	0 (0%)	na
Atrial arrhythmias	0 (0%)	0 (0%)	na
Ventricular arrhythmias	0 (0%)	0 (0%)	na
≥2 PVCs/10s tracing	0 (0%)	0 (0%)	na
QTc ≥ 470 ms	1 (2.5%)	2 (5%)	0.5
QTc <320 ms	0 (0%)	0 (0%)	na
LBBB	0 (0%)	0 (0%)	na
RBBB	0 (0%)	0 (0%)	na
Total	6 (8.7%)*	4 (6.5%)#	0.6

ECG – electrocardiography; AVB – atrioventricular block; nRBBB – non-complete right bundle branch block; LVH – left ventricular hypertrophy; ER – early repolarization; LAE – left atrial enlargement; RAE – right atrial enlargement; RVH – right ventricular hypertrophy; TWI – T-wave inversion; PVCs – premature ventricular contractions; LBBB – left bundle branch block; RBBB – right bundle branch block; na – not applicable; * percentage of all electrocardiographic abnormalities at stage 1 (n = 69); # percentage of all electrocardiographic abnormalities found at stage 2 (n = 62).

Table 5. T-wave inversion and its localisation in the ECGs at rest (stage 1) and after the marathon run (stage 2) in the studied group

Leads	Stage 1	Stage 2	p-value
Normal isolated anterior (V_1)	24 (60%)	3 (7.5%)	<0.0001
Normal isolated inferior (III)	18 (45%)	16 (40%)	0.9
Abnormal anterior (V_2–V_4)	0 (0%)	0 (0%)	na
Lateral (I, aVL, V_5, V_6)	2 (5%)	1* (2.5%)	0.6
Inferior (II, aVF)	3 (7.5%)	2* (5%)	0.7

ECGs – electrocardiographs; na – not applicable; * 1 participant at stage 2 had findings in more than 1 location.

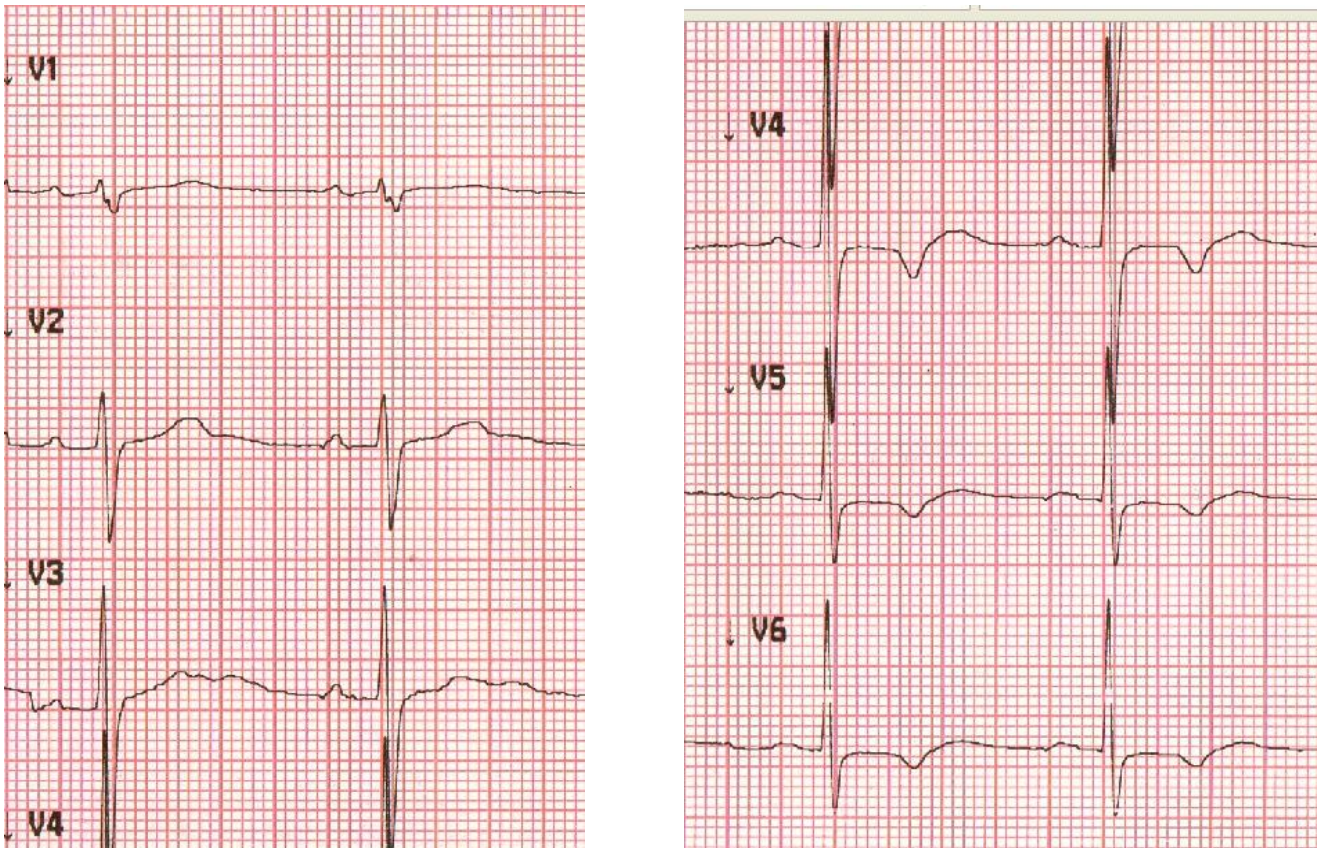

Fig. 4. Stage 1. T-wave inversions in leads V4, V5, V6 (voltage: 10 mm = 1 mV; paper speed: 25 mm/s)

majority of the studied group: 82.5%.[3] Moreover, 15% of the subjects presented pathological, training-unrelated variants in their resting ECGs. This data shows that amateur athletes should undergo ECG screening, especially if they plan to participate in competitions.

In our group, sinus bradycardia was the most commonly observed ECG finding (62.5% of the participants). A heart rate below 60 bpm is frequently reported among athletes. A commonly believed reason for resting bradycardia in athletes is an increased vagal tone, but recent studies focus also on another mechanism, namely the ion channel remodeling of the sinus node.[6–8] There are studies that show the relationship between the autonomic tone variations and atrial fibrillation. Bettomi and Zimmermann indicated that an increased vagal tone may contribute to the development of atrial fibrillation in athletes by shortening and increasing the dispersion of atrial refractory period, and thus creating a re-entry pathway.[9]

Among borderline variants, the most common finding in resting ECGs was LAE (20% of the participants). The data regarding the relationship of LAE and the occurrence of supraventricular arrhythmias in athletes is conflicting and requires further research. Pelliccia et al. stated that, although LAE and remodeling are common in athletes and subjects undertaking long-time regular physical training, their clinical significance and long-term arrhythmic consequences remain unresolved, based on the average 7-year follow-up period.[10] On the other hand, it has been shown that accumulated lifetime physical activity and left atrial size are risk factors for lone atrial fibrillation.[11] Gabrielli et al. investigated the contractile performance, size and deformation of both atria in athletes, and showed that higher contractile performance of the left and right atrium was compensated by working at higher wall stress and changed the wall geometry, which may predispose to the development of atrial arrhythmias.[12]

Left atrium enlargement found in our group may suggest that even in amateur athletes, left atrium undergoes changes that may predispose to the development of atrial fibrillation. Although LAE occurred in a significant percentage of the participants of our study, none of them presented with any supraventricular arrhythmias in their history. Nevertheless, conclusions can be drawn only after a longer follow-up period.

After the marathon, the most frequent finding was RAE, and the most likely reason for this could be an increase in adrenergic tone. As investigated by Bayés de Luna et al., both sympathetic overdrive and hypoxia (in this case exercise-induced hypoxia) can result in the so-called electrocardiographic 'false-positive' RAE.[13] Nevertheless, right ventricular overload might be taken into consideration as well. A recent study has shown that after a running race, acute exercise dose-dependent impairment in atrial function, but especially of the right atrium, can occur.[14]

In our group, 15% of the subjects presented with pathological training-unrelated variants in their resting ECGs. We found this percentage significant, because every single training-unrelated variant needs to be further investigated, as it may indicate the presence of cardiac pathologies. Pathological TWI was the most prevalent group. Inferior leads TWI came out in 3 subjects (7.5%), whereas TWI in lateral leads – in 2 subjects (5%).

Interestingly, in the case of training-related TWI (leads V_1, III), the normalization of T-waves was observed after the marathon run. In lead V_1, the difference between the frequency of TWI at stage 1 and stage 2 was statistically significant ($p < 0.0001$). The explanation for this finding may be a high adrenergic tone after strenuous exercise. It was shown in patients with hypertrophic cardiomyopathy who presented negative T-waves on the resting ECG that T-waves became less deeper after the treadmill exercise test in all cases. Moreover, the higher the exercise level, the less deeper T-waves were.[15] Zeppilli et al. investigated the effect of maximal exercise on TWI in top athletes.[16] In some cases, the exercise-induced normalization of TWI was observed, and the authors considered the neurogenic mechanism of the phenomenon.

Our results show that in the assessment of amateur athletes' ECGs, the criteria for athletes' ECGs, rather than those for the general population, should be used. Many changes that could suggest pathologies in the general population are benign findings in the ECGs of active people practicing sport. In this particular study, we used the refined criteria that are the latest recommendations on this topic. However, a significant percentage of training-related variants suggests that even amateur athletes should undergo ECG screening before participating in competitions.

Table 6. Number of subjects presenting ECG variants at rest (stage 1) and after the marathon run (stage 2)

ECG variant	Number of participants, n (%)		p-value
	stage 1	stage 2	
Training-related	33 (82.5%)	17 (42.5%)	0.0008
Borderline	9 (22.5%)	23 (57.5%)	0.0004
Training-unrelated	6 (15%)	4 (10%)	0.6

ECG – electrocardiograph.

In the ECGs recorded after the marathon run, statistically significant differences in QT interval duration and frequency of RAE were observed, and we link these findings with the adrenergic activation of the heart after the run. It has to be emphasized that refined criteria (as well as the Seattle criteria) have been used so far only in the interpretation of resting ECGs. Our study is the first one that applies these criteria to ECGs performed soon after exercise. Although in some cases 2 borderline variants came together, i.e., LAE and RAE, we did not categorize them as training-unrelated because of the abovementioned adrenergic activation. The results of our study show that the refined criteria can be used for the interpretation of athletes' ECGs both at rest and after exercise.

Limitations

The study group was relatively small and involved only white men living in the Pomeranian Voivodeship, Poland. That is why our findings may not be applicable for larger cohorts and for cohorts with ethnic variability. Moreover,

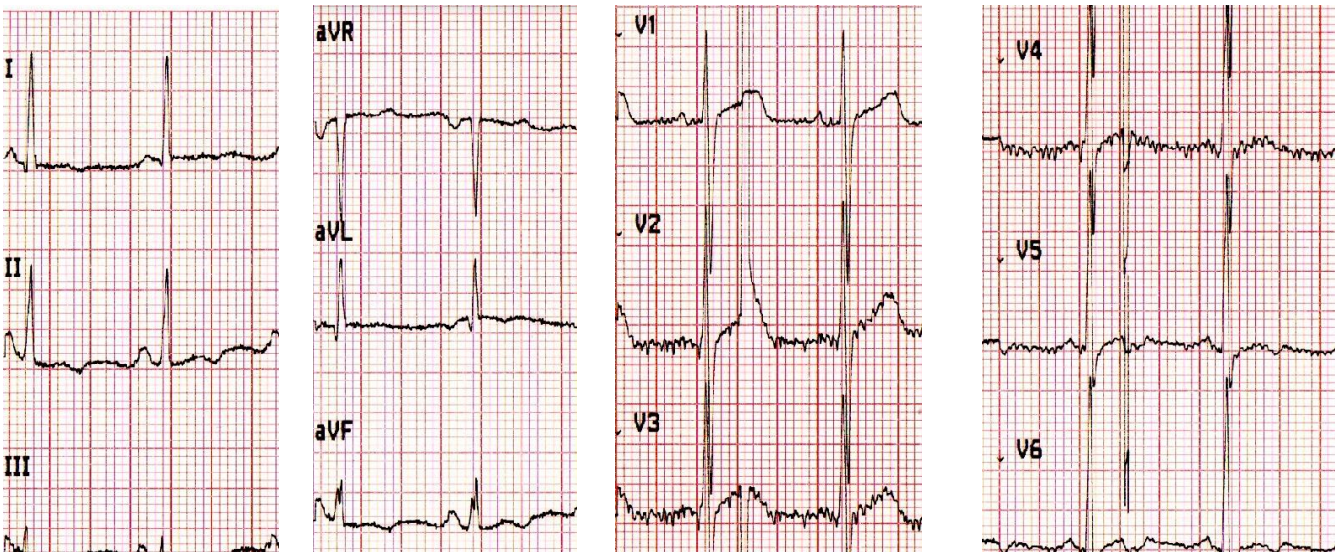

Fig. 5. Stage 2. T-wave inversions in both lateral and inferior leads (ECG performed just after the run on the finish line; voltage: 10 mm = 1 mV; paper speed: 25 mm/s)

ECG – electrocardiograph.

no women were included in the study; therefore, we cannot draw any conclusions regarding this group of amateur runners. Additionally, there can be doubts whether our subjects could be regarded as 'amateurs'. A single strict definition of an athlete does not actually exist. An athlete is defined as a person who is trained in or good at sports, games or exercises that require physical skill and strength, whereas, according to Italian criteria, an athlete is a person who participates in an organized sports program that requires regular training and competition.[17,18] Both definitions could be applied also to our study population. However, at this point another question arises, namely where the border between amateur and professional running can actually be set.

Conclusions

Electrocardiograms of amateur runners include many variants that could be misinterpreted as pathological if general criteria were used for their assessment. That is why criteria applied for athletes' ECGs should be implemented in this group. The most commonly observed abnormalities in both resting and exercise ECGs in our study were training-related changes, which were proved to be benign and require no further examinations. Nevertheless, at rest, in 15% of the subjects, pathologic training-unrelated abnormalities were found. A high prevalence of abnormalities in our relatively small study group suggests the need of common ECG screening not only among elite athletes, but also in the population of amateurs.

References

1. Corrado D, Pelliccia A, Heidbuchel H, et al.; Section of Sports Cardiology, European Association of Cardiovascular Prevention and Rehabilitation. Recommendations for interpretation of 12-lead electrocardiogram in the athlete. *Eur Heart J*. 2010;31:243–259.
2. Drezner JA, Fischbach P, Froelicher V, et al. Normal electrocardiographic findings: Recognizing physiological adaptations in athletes. *Br J Sports Med*. 2013;47:125–136.
3. Sheikh N, Papadakis M, Ghani S, et al. Comparison of electrocardiographic criteria for the detection of cardiac abnormalities in elite black and white athletes. *Circulation*. 2014;129:1637–1649.
4. Drezner JA, Ackerman MJ, Anderson J, et al. Electrocardiographic interpretation in athletes: the Seattle criteria. *Br J Sports Med*. 2013;47:122–124.
5. Corrado D, Pelliccia A, Antzelevitch C, et al. *ST Segment Elevation and Sudden Death in the Athlete. The Brugada Syndrome: From Bench to Bedside*. Oxford: Blackwell Futura; 2005.
6. Boyett MR, D'Souza A, Zhang H, Morris GM, Dobrzynski H. Monfredi O. Viewpoint: Is the resting bradycardia in athletes the result of remodeling of the sinoatrial node rather than high vagal tone? *J Appl Physiol*. 2013;114:1351–1355.
7. Baldesberger S, Bauersfeld U, Candinas R, et al. Sinus node disease and arrhythmias in the long-term follow-up of former professional cyclists. *Eur Heart J*. 2008;29:71–78.
8. D'Souza A, Bucchi A, Johnsen AB, et al. Exercise training reduces resting heart rate via downregulation of the funny channel HCN4. *Nat Commun*. 2014;5:3775.
9. Bettomi M, Zimmermann M. Autonomic tone variations before the onset of paroxysmal atrial fibrillation. *Circulation*. 2002;105:2753–2759.
10. Pelliccia A, Maron BJ, Di Paolo FM, et al. Prevalence and clinical significance of left atrial remodeling in competitive athletes. *J Am Coll Cardiol*. 2005;46:690–696.
11. Mont L, Tamborero D, Elosua R, et al.; GIRAFA (Grup Integrat de Recerca en Fibrillació Auricular) Investigators. Physical activity, height, and left size are independent risk factors for lone atrial fibrillation in middle-aged healthy individuals. *Europace*. 2008;10:15–20.
12. Gabrielli L, Bijnens BH, Butakoff C, et al. Atrial functional and geometrical remodeling in highly trained male athletes: For better or worse? *Eur J Appl Physiol*. 2014;114(6):1143–1152.
13. Bayés de Luna A, Boada FX, Casellas A et al. Concealed atrial electrical activity. *J Electrocardiol*. 1978;11:301–305.
14. Sanz-de la Garza M, Grazioli G, Bijnens BH, et al. Acute, exercise dose-dependent impairment in atrial performance during an endurance race: 2D ultrasound speckle-tracking strain analysis. *JACC Cardiovasc Imaging*. August 11, 2016 [ahead of print]. doi:10.1016/j.jcmg.2016.03.016
15. Sugishita Y, Yamaguchi T, Ogawa T, et al. Variability of negative T wave in hypertrophic cardiomyopathy: Possible role of beta-adrenergic function. *Acta Cardiol*. 1987;42(2):115–133.
16. Zeppilli P, Pirrami MM, Sassara M, Fenici R. T wave abnormalities in top-ranking athletes: effects of isoproterenol, atropine, and physical exercise. *Am Heart J*. 1980;100(2):213–222.
17. http://www.merriam-webster.com/dictionary/athlete. Accessed March 20, 2017.
18. Corrado D, Basso C, Rizzoli G, et al. Does sports activity enhance the risk of sudden death in adolescents and young adults? *J Am Coll Cardiol*. 2003;42:1959–1963.

Diffusion and perfusion MR patterns of central nervous system lymphomas

Małgorzata Neska-Matuszewska[A–E], Anna Zimny[A–C,E,F], Joanna Bladowska[A,E], Marek Sąsiadek[E,F]

Department of General and Interventional Radiology and Neuroradiology, Wroclaw Medical University, Poland

A – research concept and design; B – collection and/or assembly of data; C – data analysis and interpretation;
D – writing the article; E – critical revision of the article; F – final approval of the article

Advances in Clinical and Experimental Medicine, ISSN 1899-5276 (print), ISSN 2451-2680 (online) *Adv Clin Exp Med*. 2018;27(8):1099–1108

Address for correspondence
Małgorzata Neska-Matuszewska
E-mail: neskamatuszewska@gmail.com

Funding sources
None declared

Conflict of interest
None declared

Received on December 29, 2016
Reviewed on April 20, 2017
Accepted on May 19, 2017

Abstract

Background. Central nervous system lymphomas (CNSLs) are rare tumors which may show variable appearance in standard magnetic resonance imaging (MRI) depending on their origin (primary or secondary) or patients' immunological status.

Objectives. The aim of the study was to analyze imaging patterns of different CNSLs, using diffusion-weighted imaging (DWI) and perfusion-weighted imaging (PWI).

Material and methods. Our material consisted of 16 CNSLs (14 primary, 2 secondary, 13 immunocompetent, 3 immunodeficient) which underwent magnetic resonance (MR) examinations including DWI and T2* dynamic susceptibility contrast (DSC) perfusion (without a preload in 13 cases, with a preload in 3 subjects). In DWI, apparent diffusion coefficient (ADC), and in PWI, parameters of relative cerebral blood volume (rCBV), relative peak height (rPH) and relative percentage of signal recovery (rPSR) were analyzed within the entire tumor (mean values) and in regions with minimal diffusion (ADC_{min}) and maximal perfusion values ($rCBV_{max}$, rPH_{max}, $rPSR_{max}$).

Results. All CNSLs showed low values of ADC_{mean} ($0.70 \times 10–3$), ADC_{min} ($0.54 \times 10–3$), $rCBV_{mean}$ (0.80), $rCBV_{max}$ (1.27), rPH_{mean} (1.05), rPH_{max} (1.59), as well as high values of $rPSR_{mean}$ (1.99) and $rPSR_{max}$ (2.41). There were no significant differences in $rCBV_{max}$, as well as in all ADC, rPH and rPSR values between primary and secondary CNSLs or between tumors in immunocompetent and immunodeficient patients. Dynamic susceptibility contrast PWI with a preload resulted in significantly higher rCBV, rPH and lower rPSR values.

Conclusions. Despite various MR appearances, both primary and secondary CNSLs in immunocompetent and immunodeficient patients show very typical patterns of restricted diffusion and hypoperfusion with signal intensity curves returning above the baseline. Dynamic susceptibility contrast perfusion without a preload is recommended.

Key words: central nervous system lymphomas, diffusion-weighted imaging, perfusion-weighted imaging, magnetic resonance imaging

DOI
10.17219/acem/73894

Introduction

Central nervous system lymphomas (CNSLs) are an inhomogeneous group of rare brain tumors consisting of 2 main subtypes: primary and secondary CNSLs. Primary CNSLs account for approx. 7% of newly diagnosed CNS tumors.[1–3] Recently, their incidence has increased in immunocompetent patients, though their prevalence is still higher in immunocompromised subjects, such as those with acquired immune deficiency syndrome (AIDS), after organ or bone marrow transplantations, or with inherited immunodeficiency, often due to Epstein-Barr virus (EBV) activation.[1–6] The majority of primary CNSL tumors are of the highly aggressive diffuse large cell subtypes, usually of B-cell phenotypic origin.[4,7,8] They are mostly intra-axial lesions located within brain parenchyma, either periventricularly within deep structures, or peripherally along leptomeningeal surfaces.[1–3,5] They may present as solitary or multiple lesions with usually strong homogeneous enhancement. Lesions found in immunocompromised patients have more commonly multiple locations and tend to enhance less strongly, very often show ring enhancement, as well as features of bleeding and necrosis.[3,5,6] Secondary CNSLs are metastases to the central nervous system (CNS) from systemic lymphomas, in majority of nodular type; however, metastases to the CNS from extranodal location, including very rare orbital lymphoma, are also possible.[1–3,9,10] The high aggressiveness of systemic lymphomas, immunodeficiency and extranodal involvement predispose to CNS relapse.[7,11] The location of secondary CNSLs in brain parenchyma is mainly similar to that of primary CNSLs. Contrary to primary CNSLs, they may also show exclusively extra-axial location within meninges or spine.[3,9,11]

Since CNSLs may show very variable appearance, a conventional magnetic resonance (MR) examination with contrast injection is not capable of accurately distinguishing them from other intracranial lesions, including tumors, such as gliomas, metastases or even meningiomas. Advanced MR techniques, such as diffusion-weighted imaging (DWI) and perfusion-weighted imaging (PWI), allow for a more detailed analysis of brain tumors and their in vivo differentiation.[12–21]

Diffusion-weighted imaging is a method that evaluates water diffusion in the extracellular space in between the intact cells which constitute a barrier to free movements of water molecules. In tumors, DWI brings information on the tumor cell architecture and the parameter of apparent diffusion coefficient (ADC) is considered as a surrogate marker of tumor cellularity.[3,16,19,20] Lower values of ADC have been reported in malignant tumors, such as high-grade gliomas, due to their high cellularity rate, and in tumors with high nuclear/cytoplasmatic ratios, such as lymphomas and medulloblastomas.[14,17,15,21]

On the other hand, PWI is a method that brings information on cerebral physiology at the capillary level (microvasculature).[12] Among the few PWI techniques, dynamic susceptibility contrast (DSC) magnetic resonance imaging (MRI) is the most often used. Dynamic susceptibility contrast MRI provides maps of cerebral blood volume (CBV) and noninvasive mathematical measurements of relative cerebral blood volume (rCBV).[12,22] In brain tumors, rCBV is defined as the ratio between CBV within the tumor and CBV in the white matter of the contralateral hemisphere. The rCBV parameter correlates with tumor vascularity and is increased in tumors with a high rate of pathologic neoangiogenesis.[7,12] In glial tumors, increased rCBV ratios indicate increased malignancy, but this rule cannot be applied to extra-axial tumors. There are highly vascular extra-axial tumors with high perfusion, e.g., meningiomas, which are benign in terms of biological behavior.[12,15,23] Apart from the CBV maps, PWI also provides perfusion curves, which give insights into the dynamics of the first pass of the contrast material through the microvasculature. An analysis of the perfusion curves has been reported to be very important in the evaluation of brain tumors, in some cases even more useful than an analysis of the CBV maps.[12,13,17,18,24]

Accurate identification of CNSLs is crucial from the clinical point of view. Contrary to other malignant tumors, CNSLs do not undergo a surgical management, but are treated with chemotherapy.[1,6,18,19] At the moment, brain tumors, including CNSLs, still require a biopsy, which is an invasive procedure and can cause unexpected complications.

The aim of our study was a detailed analysis of the conventional MR appearance, as well as diffusion- and perfusion-weighted images of different types of CNSLs in order to establish characteristic imaging patterns, typical for these tumors. To our knowledge, this is the first article presenting diffusion and perfusion results derived from both perfusion maps and curves in various types of CNSLs, both primary and secondary, including immunocompromised and immunodeficient patients. We also discuss the value of different DSC perfusion techniques, with and without pre-bolus, in the accurate diagnosis of CNSLs.[25]

Material and methods

Our material consisted of 16 brain tumors diagnosed in 12 patients (5 men, 7 women) aged 6–84 years with biopsy-proven CNSLs, which were selected from a cohort of 1,060 CNS tumors evaluated with PWI and DWI in our institution in the years 2010–2015. According to the World Health Organization (WHO) system, the evaluated brain tumors were diagnosed either as primary (10 patients) or secondary (2 patients) diffuse large B-cell CNSLs (Table 1). In all patients their clinical history was carefully evaluated. Among primary CNSLs, 8 of 10 patients were found to be immunocompetent, while 2 subjects were immunocompromised (Table 1). Secondary CNSLs were metastases from a systemic nodular lymphoma or extranodular orbital lymphoma (Table 1).

Table 1. Patients' demographics and characteristics of lesions in standard MR examination

Patient	Sex	Age [years]	Immunological status	Comorbidities	Histology	Number of lesions	T1 signal	T2 signal	Edema	Enhancement	Location
primary CNSL											
1	male	78	competence	none	diffuse large B-cell lymphoma	1	hyper	iso	mild	homogenous	corpus callosum
2	female	76	competence	none	diffuse large B-cell lymphoma a	multiple (1 measured)	iso	iso	moderate	homogenous	periventricular white matter
3a, 3b	female	84	competence	none	diffuse large B-cell lymphoma	multiple (2 measured)	iso iso	iso iso	mild moderate	homogenous homogenous	disseminated: periventricular and peripheral, all lobes
4	male	73	competence	none	diffuse large B-cell lymphoma	1	hyper	hypo	mild	homogenous	peripheral, in the right parietal lobe
5	male	65	competence	none	diffuse large B-cell lymphoma	1	hypo	iso	mild	homogenous	peripheral, in the right occipital lobe
6a, 6b	female	61	competence	none	diffuse large B-cell lymphoma a	2	iso iso	hypo hypo	moderate moderate	homogenous with central necrosis homogenous	peripheral, in the left frontal lobe peripheral, in the left parietal lobe
7	female	60	competence	none	diffuse large B-cell lymphoma a	1	hypo	iso	mild	homogenous with central necrosis	peripheral, in the left frontal lobe
8a, 8b	female	73	competence	none	angiocentric diffuse large B-cell lymphoma	multiple (2 measured)	hyper hyper	hyper hyper	mild mild	homogenous homogenous	disseminated: corpus callosum, bilateral white matter along small vessels
9a, 9b	female	46	deficiency due to immunosuppressive treatment	systemic lupus erythematosus	diffuse large B-cell lymphoma	2	hyper hyper	hypo hypo	mild mild	inhomogeneous, peripheral ring inhomogeneous, peripheral ring	peripheral, in the right temporo-parietal region peripheral, in the left occipital lobe
10	male	6	deficiency due to bone marrow transplantation	juvenile xanthogranuloma	B-cell lymphoma associated with EBV	1	hypo	iso	large	homogenous with central necrosis	peripheral, in the frontal lobe
secondary CNSL											
11	male	64	competence	systemic lymphoma	diffuse large B-cell lymphoma	1	hypo	hypo	non	homogenous	pituitary infundibulum
12	female	64	competence	orbital lymphoma	diffuse large B-cell lymphoma	1	hyper	hypo	large	homogenous	in the left basal ganglia

CNSL – central nervous system lymphoma; EBV – Epstein-Barr virus; MR – magnetic resonance; T1 – longitudinal relaxation time; T2 – transverse relaxation time.

After providing written consent, all patients underwent MR examinations of the brain with contrast injection, including diffusion and perfusion sequences. All procedures were performed in accordance with the Helsinki Human Rights consensus, and the study was approved by the Commission of Bioethics at Wroclaw Medical University.

Data acquisition

All examinations were performed on a 1.5 T MR scanner (Signa Hdx; GE Medical Systems, Milwaukee, USA), using a 16-channel head-neck-spine (HNS) coil. Before contrast administration, a standard MR examination was carried out, including axial T1 (longitudinal relaxation time)-weighted images, axial, coronal and sagittal T2 (transverse relaxation time)-weighted images, as well as axial fluid-attenuated inversion recovery (FLAIR) images.

Diffusion-weighted imaging was performed using transverse single-shot echoplanar diffusion-weighted sequence with the following parameters: echo time (TE) – 89.9 ms, repetition time (TR) – 8000 ms, slice thickness – 5 mm, field of view (FOV) – 26 cm, matrix size – 128 × 128, number of excitations (NEX) – 1.0, diffusion sensitive gradient – b = 1000 s/mm^2 in the 3 orthogonal directions, scanning time – 42 s.

Perfusion-weighted imaging was performed with the DSC method using fast echoplanar T2*-weighted gradient echo sequence with the following parameters: TR – 1.900 ms, TE – 80 ms, FOV – 30 cm, matrix size – 192 × 128, slice thickness – 8 mm without spacing, NEX – 1.0. A bolus of a 1.0 mol/L gadobutrol formula (Gadovist; Bayer Health Care, Leverkusen, Germany) in a dose of 0.1 mL/kg of body weight was injected 10 s after the start of image acquisition via a 20-gauge catheter placed in the antecubital vein. Contrast was administered with an automatic injector (Medrad; Bayer Medical Care, Indianola, USA) at a rate of 5 mL/s and was followed by a saline bolus (20 mL at 5 mL/s). The whole perfusion imaging lasted 1 min 26 s, in which sets of images from 13 axial slices were obtained before, during and after contrast injection. After PWI, a postcontrast T1-weighted 3D sequence was performed based on contrast administered earlier in the perfusion examination.

In 2 patients, PWI was performed using the preload leakage correction method. Gadolinium contrast in a dose of 0.05 mmol/kg was administered as a prebolus 3 min before the dynamic phase of DSC T2* perfusion; it was then followed by the standard DSC technique as described above.

In the study, 1 patient (Patient 4) underwent 2 types of perfusion examinations – with (4–1) and without (4–2) a preloading bolus in the interval of 4 weeks.

Data postprocessing

In all cases, the morphological assessment of the lesions was performed on the basis of T1-, T2-weighted and postcontrast T1-weighted images, using visual inspection.

The diffusion- and perfusion-weighted images were postprocessed using Functool software (ADW v. 4.4; GE Medical Systems SCS, Buc, France).

Diffusion-weighted imaging analysis

The measurements of ADC for the whole tumor (ADC_c) and of minimal ADC (ADC_{min}) were assessed. The ADC_c values were obtained by manual outlining of the entire lesion on each slice, and then by calculating the arithmetical means from all measured ADC values. Minimal ADC was measured by placing a small region of interest (ROI) (40–60 mm^2) in the location of the lowest value of this parameter on each slice; the lowest value from all the slices was chosen as the tumoral ADC_{min}. Both ADC_c and ADC_{min} values were normalized to the normal appearing white

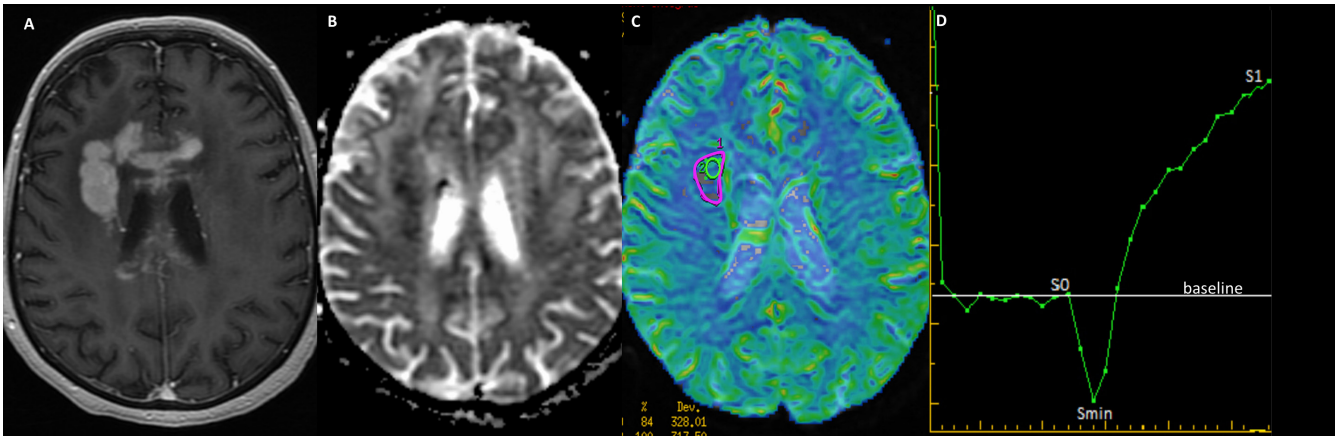

Fig. 1. A typical multifocal primary CNSL located in the basal ganglia and the corpus callosum

A – axial T1-weighted MR image after contrast administration, showing strong enhancement; B – ADC map with restricted diffusion; C – CBV perfusion map with drawn ROIs showing hypoperfusion; D – signal intensity perfusion curve exceeding the baseline level with marked characteristic time points: S0, Smin, S1; ADC – apparent diffusion coefficient; CBV – cerebral blood volume; CNSL – central nervous system lymphoma; MR – magnetic resonance; ROI – region of interest.

matter (NAWM) of the contralateral hemisphere in order to obtain the relative values of these parameters (relative ADC_c – $rADC_c$; relative ADC_{min} – $rADC_{min}$).

Perfusion-weighted imaging analysis

The analysis was based on an evaluation of the CBV parameter on CBV maps, as well as of the values of peak height (PH) and percentage of signal recovery (PSR) derived from perfusion curves. The CBV maps were computed on a pixel-wise basis from the first-pass data as described by Rosen et al.[22] The measurements of CBV were performed by placing ROIs on the CBV maps fused with post-contrast T1-weighted images in order to accurately assess the tumor core (Fig. 1). The values of PSR and PH were calculated from the perfusion curves based on formulas: PSR = (S1 – Smin)/PH, PH = Smin – S0, where: S0 – start of contrast passage, Smin – maximal drop of magnetic susceptibility, S1 – measurement after 24 s from Smin (Fig. 1). All CBV, PH and PSR values were normalized to values from the NAWM of the contralateral hemisphere in order to obtain relative values of all parameters: rCBV, relative PH (rPH) and relative PSR (rPSR).[23]

In each tumor, the measurements of mean values of all perfusion parameters for the whole tumor core ($rCBV_c$, rPH_c, $rPSR_c$) and of maximal values of these parameters ($rCBV_{max}$, rPH_{max}, $rPSR_{max}$) were assessed. The mean values for the whole tumor were obtained by manually outlining the entire lesion on each slice (Fig. 1) and calculating the arithmetical means from all measured values. Maximal values were obtained by placing small ROIs (40–60 mm^2) over several hot spots on each slice (Fig. 1). The highest value from all ROIs was chosen as the tumoral maximal value.

Statistical analysis

Comparisons of diffusion and perfusion values between different subject groups were performed using the t-test with p-values <0.05 set as the significance threshold. Diffusion and perfusion parameters were compared between primary and secondary CNSLs, as well as between primary CNSLs in the immunocompetent and immunodeficient patients. We also compared perfusion parameters acquired with and without a preloading bolus.

Results

Results of standard magnetic resonance examinations

All CNSLs (both primary and secondary) showed variable T1 and T2 appearance ranging from hypo- to hyperintense lesions (Table 1). They were mostly iso- (44%) or hypointense (44%) to the white matter on T2-weighted images, with a different range of surrounding edema (Table 1).

All immunocompetent patients showed lesions with strong homogenous enhancement, while in the immunocompromised patients a heterogenous, also ring-like, enhancement pattern was found (Table 1).

In the group of CNSLs (both primary and secondary) there were subjects with single or multiple lesions (Table 1). The location of foci was variable (Table 1). All primary CNSLs were located intra-axially within the brain parenchyma, while secondary lesions were located either intra-axially (basal ganglia) or extra-axially (pituitary infundibulum).

Diffusion results

All CNSLs showed low mean values of all evaluated diffusion parameters ($ADC_c = 0.70 \times 10^{-3}$, $ADC_{min} = 0.54 \times 10^{-3}$), which were also lower compared to NAWM ($rADC_c = 0.92$ and $rADC_{min} = 0.71$) (Table 2).

Table 2. Results of DWI measurements

Patients	ADC_c [$\times 10^{-3}$]	ADC_{min} [$\times 10^{-3}$]	$rADC_c$	$rADC_{min}$
primary CNSLs				
immunocompetent				
1	0.57	0.42	0.77	0.67
2	0.76	0.47	0.89	0.55
3a	0.81	0.56	1.05	0.72
3b	0.81	0.67	1.05	0.86
4–1	0.69	0.53	0.88	0.73
4–2	0.69	0.62	0.88	0.78
5	0.59	0.52	0.77	0.67
6a	0.65	0.57	0.89	0.78
6b	0.96	0.73	1.33	1.01
7	0.65	0.54	0.93	0.77
8a	0.58	0.47	0.77	0.62
8b	0.65	0.56	0.86	0.74
mean values	0.70	0.55	0.93	0.74
immunodeficient				
9a	0.79	0.51	1.01	0.65
9b	0.65	0.40	0.83	0.57
10	0.67	0.51	0.78	0.59
mean values	0.70	0.47	0.87	0.60
all primary CNSLs				
mean values	0.70	0.54	0.92	0.71
secondary CNSLs				
11	0.59	0.53	0.68	0.62
12	0.80	0.57	1.16	0.83
mean values	0.70	0.55	0.92	0.73
all CNSLs (primary and secondary)				
mean values	0.70	0.54	0.92	0.72

ADC_c – apparent diffusion coefficient for the whole tumor; ADC_{min} – minimal ADC; CNSL – central nervous system lymphoma; DWI – diffusion-weighted imaging; $rADC_c$ – relative ADC_c; $rADC_{min}$ – relative ADC_{min}.

Individual analysis of all subjects showed that 5 out of 16 tumors (31%) revealed ADC_c values similar or slightly higher compared to NAWM (Patients: 3a, 3b, 6b, 9a, 12) while 11 out of 16 tumors (69%) showed lower values, indicating restricted diffusion within the entire tumor core (Table 2). When analyzing ADC_{min}, only 1 subject (Patient 6b) revealed values similar to NAWM. In all other cases, which is 94% of subjects, the values of ADC_{min} were lower than NAWM, which indicated restricted diffusion.

There were no statistically significant differences in all evaluated ADC values between primary and secondary CNSLs, or between immunocompetent and immunodeficient subjects with primary CNSLs (Table 2).

Perfusion results

All CNSLs examined using the DSC perfusion method without a preloading bolus showed low mean values of $rCBV_c$, $rCBV_{max}$, rPH_c, rPH_{max}, as well as high values of $rPSR_c$ and $rPSR_{max}$, indicating hypoperfusion and overshooting of perfusion curve above the baseline level (Table 3).

Primary CNSLs showed significantly lower ($p = 0.02$) values of $rCBV_c$ (mean 0.71; range 0.31–1.41) compared to secondary CNSLs (mean 1.38; range 1.06–1.69). The values of $rCBV_{max}$ in secondary CNSLs were slightly higher compared to primary CNSLs, but the difference did not reach the significant level ($p = 0.08$) (Table 3). The values of $rCBV_{max}$ in primary CNSLs ranged from 0.44 to 2.17, while in secondary CNSLs from 1.66 to 2.22. Only 3 out of 14 tumors (21.4%) showed values of $rCBV_{max}$ higher than 1.75, but not exceeding 2.22. There were no significant differences in the values of perfusion parameters derived from perfusion curves between primary and secondary CNSLs.

When immunocompetent and immunodeficient patients were compared with primary CNCLs, no differences were found in the values of all perfusion parameters between these 2 groups.

Compared to DSC without a preload bolus, primary CNSLs, which were examined using a preload bolus, revealed statistically higher ($p < 0.001$) mean values of $rCBV_c$ (mean 2.10; range 1.95–2.35), $rCBV_{max}$ (mean 2.92; range 2.6–3.34), rPH_c (mean 2.56), and rPH_{max} (mean 3.33), as well as significantly lower rPSR measurements (Table 3). Patient 4 examined with both perfusion techniques also showed significantly different results of all perfusion parameters with higher rCBV and rPH values as well as lower rPSR values in the DSC technique with a use of a preloading bolus (4–1) compared to the follow-up examination without a preload (4–2) (Table 3).

Table 3. Results of PWI measurements

Patients	$rCBV_c$	$rCBV_{max}$	rPH_c	rPH_{max}	$rPSR_c$	$rPSR_{max}$
DSC perfusion without a preload bolus						
primary immunocompetent CNSLs						
1	0.72	1.02	1.20	1.59	1.55	1.80
2	0.40	0.83	0.99	1.30	1.95	2.11
3a	0.45	0.52	0.74	1.10	1.48	1.54
3b	0.91	1.85	0.83	1.14	1.47	2.43
4-2	0.81	1.11	1.22	1.41	1.50	1.85
5	0.53	1.70	0.97	1.76	2.49	3.95
6a	0.31	0.44	1.05	1.29	1.95	2.10
6b	0.53	0.87	0.80	1.85	3.24	3.25
7	1.41	1.65	1.43	1.89	1.31	1.51
mean values	0.67	1.11	1.03	1.48	1.88	2.28
primary immunodeficient CNSLs						
9a	1.12	2.17	1.49	3.01	1.49	1.67
9b	0.93	1.04	1.32	1.70	1.23	1.29
10	0.43	0.79	0.84	0.86	3.78	5.83
mean values	0.82	1.33	1.22	1.86	2.17	2.93
all primary CNSLs						
mean values	0.71	1.17	1.07	1.58	1.95	2.44
secondary CNSLs						
11	1.69	2.22	0.79	1.76	2.28	2.28
12	1.06	1.66	0.98	1.62	2.12	2.12
mean values	1.38	1.94	0.89	1.69	2.20	2.20
all CNSLs (primary and secondary)						
mean values	0.80	1.27	1.05	1.59	1.99	2.41
DSC perfusion with a preload bolus						
8a	2.35	3.34	3.24	4.11	1.54	1.82
8b	1.95	2.60	2.13	2.55	1.46	1.46
4-1	2.01	2.81	2.32	2.97	0.97	1.05
mean values	2.10	2.92	2.56	3.21	1.32	1.44
all DSC examinations (with and without a preload bolus)						
mean values	1.04	1.58	1.31	1.81	1.87	2.24

DSC – dynamic susceptibility contrast; PWI – perfusion-weighted imaging; $rCBV_c$ – relative cerebral blood volume for the whole tumor; $rCBV_{max}$ – relative maximal CBV; rPH_c – relative peak height for the whole tumor; rPH_{max} – relative maximal PH; $rPSR_c$ – relative percentage of signal recovery for the whole tumor; $rPSR_{max}$ – relative maximal PSR.

Discussion

Our study based on the group of 16 CNSLs tumors showed a great variety of radiological appearances on conventional MR sequences, which is typical for these tumors. We observed a wide

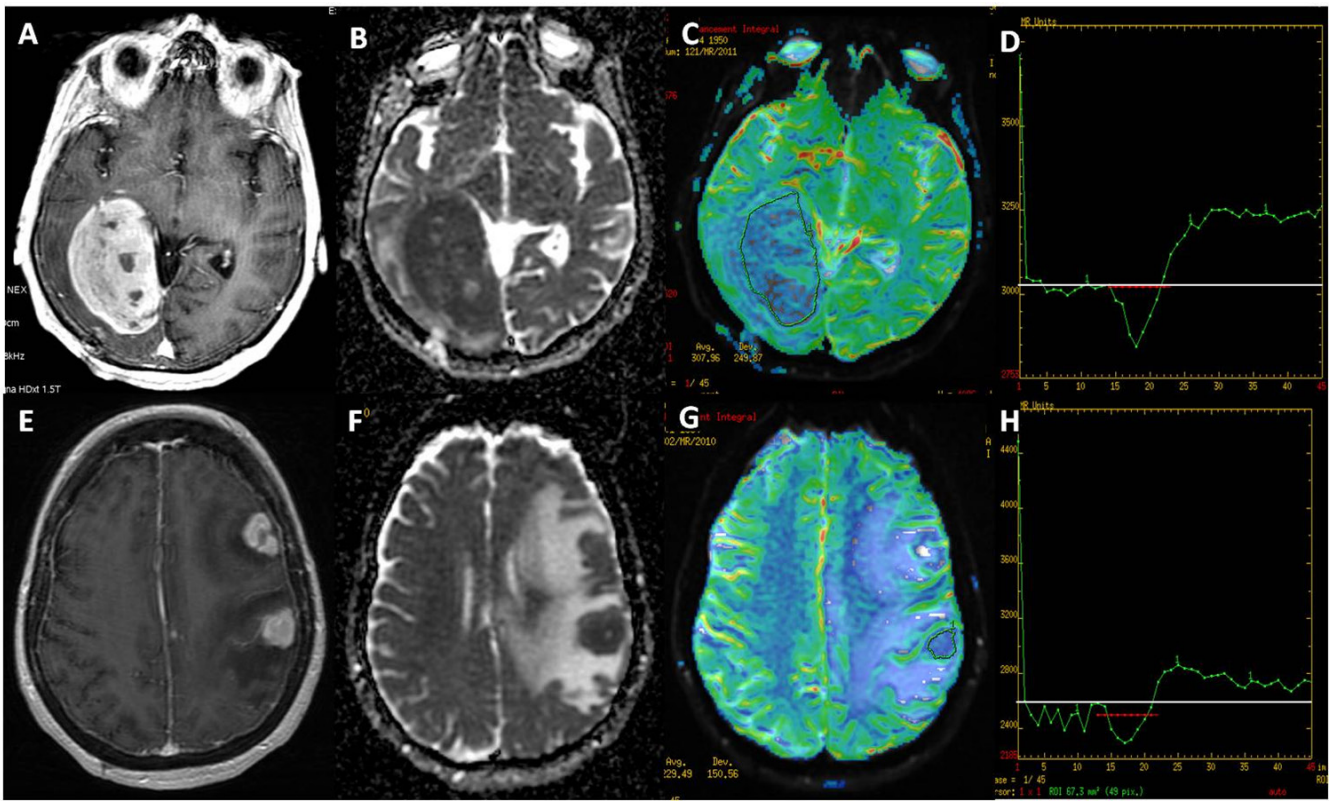

Fig. 2. Primary CNSLs (in immunocompetent patients) mimicking other tumors such as meningioma (A–D) and metastases (E–H)

All CNSLs show strong homogeneous enhancement on postcontrast T1-weighted images (A, E), restricted diffusion on ADC maps (B, F), low perfusion on CBV maps (C, G) and a typical shape of the perfusion curves above the baseline (D, H).
ADC – apparent diffusion coefficient; CBV – cerebral blood volume; CNSL – central nervous system lymphoma.

range of signal changes on T1- and T2-weighted images, different patterns of contrast enhancement, as well as different numbers and locations of tumoral foci.

T2 hypointensity is reported to be one of the very characteristic features of CNSLs, attributed to their high nuclear/cytoplasmatic ratio.[1–3,14] In the group of our subjects, we found low T2 signal in 44% of all CNSLs, T2 isointensity also in 44% of CNSLs, while high T2 signal only in 12% of all subjects. T2 hypointensity was found in all groups of evaluated primary and secondary lymphomas, as well as in immunocompromised and immunocompetent subjects. In our study, all subjects with CNSLs with competent immune system revealed solid and homogenous contrast enhancement (84.6%), which was also reported in the literature.[1–3,14] On the other hand, immunocompromised individuals showed inhomogeneous enhancement, including a peripheral ring-like pattern. This inhomogeneity is found to be typical and is explained by lower focal cellularity, resulting from tumor necrosis in patients with depressed immunity.[1–3,14,16] The number of lesions in each patient varied from a single tumor found in all subject groups to multiple foci characteristic for primary CNSLs in immunocompetent patients. Almost all evaluated tumors showed an intra-axial location, either peripherally, or within deep structures, except for 1 case of secondary lymphoma within pituitary infundibulum, which is also consistent with literature reports.[2,3]

To summarize the findings of standard MR examinations, in our study, primary CNSLs in immunocompetent patients were intra-axial lesions with various T2 signal, as well as strong and solid enhancement, with a tendency to appear in multiple foci. On the other hand, primary CNSLs in immunodeficient patients appeared as T2 hypo- or isointense lesions with inhomogeneous enhancement, including a ring-like pattern with peripheral intra-axial location, while secondary CNSLs were lesions with very similar MR appearance to primary CNSLs in immunocompetent subjects, apart from their tendency to appear in an extra-axial location.

As presented above, CNSLs in our study were a highly variable group of tumors in standard MR imaging, mimicking other focal brain lesions. All cases of single lesions required differentiation from other brain tumors, including gliomas and even meningiomas due to their tendency to contact with meningeal surfaces (Fig. 2 A–D). Multiple homogenous masses with diffuse surrounding edema were highly suggestive of metastases (Fig. 2 E–H), while multiple disseminated lesions strongly mimicked inflammatory changes or angitis in 1 case (Patient 8).

As mentioned by Haldorsen et al. and also confirmed by an analysis of our material, standard MR imaging is not sufficient to unequivocally differentiate CNSLs from other brain lesions, thus newer advanced imaging techniques

should be added to aid the accurate diagnosis of these tumors.[3] Several techniques have been reported to improve the differentiation of CNSLs, including DWI, PWI, MR spectroscopy, and diffusion tensor imaging (DTI).[12,16,19,20] To our knowledge there are still no reports on a detailed analysis of both DWI and PWI in various CNSLs, including primary and secondary disease, as well as various immune status of evaluated patients.

Diffusion-weighted imaging is an imaging technique which may provide information regarding tumor cellularity and biology, based on the fact that cells constitute a barrier to water diffusion. Highly cellular tumors such as lymphomas tend to demonstrate a restriction of water diffusion, and thus decreased values of the ADC parameter.[16,18–20] In our study, an analysis of DWI results showed low mean values of ADC_c and ADC_{min} in the group of all evaluated subjects, which is consistent with previous reports.[16,18–20] We also looked at individual subjects and revealed that in 69% of all evaluated lymphomas, the ADC_c values were lower than in NAWM, indicating homogenously restricted diffusion within the entire tumor load, and when searching for areas of the lowest ADC values (ADC_{min}), 94% of evaluated lesions showed small regions of restricted diffusion.

In our study, we also did not find any significant differences in all evaluated ADC values between primary and secondary, or between immunocompetent and immunodeficient subjects with primary CNSLs, which indicates that restricted diffusion is a consistent DWI finding in all CNSLs. We did not find any other DWI studies comparing primary and secondary lymphomas in the literature. On the other hand, Zacharia et al. evaluated the ADC parameters in immunocompetent and immunodeficient primary CNSLs but without detailed comparisons between these 2 groups of patients.[16] They focused on comparisons between lesions with homogenous, inhomogeneous and ring-like enhancement, reporting restricted diffusion in all tumors except for 2 ring-enhancing lesions, which led to an incorrect diagnosis of the infection. It has to be stressed that in our study of ring-enhancing lymphomas, all DWI parameters were obtained from the periphery of these lesions and in all cases we found large areas of restricted diffusion. It is crucial to identify correctly areas of restricted diffusion in inhomogeneously enhancing lymphomas, since this is a characteristic feature of these tumors, which can be used to differentiate them from others, such as gliomas or metastases, which show higher ADC values or only small areas of restricted diffusion consistent with the most malignant parts of these tumors.[6,14,17,18,21]

In the next part of our study, we also evaluated the results of perfusion examinations. In the majority of cases, we used the DSC perfusion method without a preload, which is the most often performed perfusion technique in the evaluation of focal brain lesions. Relative CBV is the most important perfusion parameter in the evaluation of brain tumors, which correlates with their regional vascularity and is increased in tumors with a high rate of pathologic neoangiogenesis.[12] Since most brain tumors are in some parts inhomogeneous, the parameter of $rCBV_{max}$ is the most important and commonly used in everyday practice as the one reflecting the most malignant areas within a tumor core (the so-called hot spots). In glial tumors, increased rCBV ratios indicate increased malignancy, but this rule cannot be applied to other tumors, for example meningiomas, which are highly perfused lesions, but benign in terms of biological behavior, or lymphomas, which are malignant lesions with relatively low perfusion values. Low values of rCBV in lymphomas can be explained by the histopathological appearance of these tumors – their high cellularity, complete absence of neoangiogenesis and angiocentric growth pattern.[12] In our study, similarly to previous reports, low mean values of rCBV (both $rCBV_c$ and $rCBV_{max}$) ranging from 0.44 to 2.22 were found within all evaluated lymphomas.[3,12–14] Several studies have demonstrated that glioblastomas (GBMs) and metastases may reach very high $rCBV_{max}$ values of 3.0 or even 10.0, mainly due to a high concentration of microvessels,[12,24] and rCBV of 1.75 has been set as the threshold value differentiating low-grade and high-grade gliomas.[26,27] It has to be pointed out that 79% of all CNSLs in our study showed $rCBV_{max}$ values <1.75, similarly to low grade gliomas, and 21% revealed $rCBV_{max}$ values >1.75, but not exceeding 2.22, which is very unusual for high-grade gliomas, metastases or meningiomas. Though lymphomas may strongly mimic high-grade gliomas, metastases or even meningiomas in their conventional MR appearance, they show low perfusion values similarly to low-grade gliomas, which may be a very helpful feature in the correct differential diagnosis of these lesions.

Subsequently, we also evaluated the perfusion curves of CNSLs. Low rPH and high rPSR values were observed in the majority of cases. High $rPSR_{max}$ in lymphomas is consistent with an overshooting of the signal intensity curve above the baseline level, which was observed in 100% of our cases. The rPSR ratio was reported by Mangla et al. to be the most sensitive and specific feature in the differentiation of lymphomas from GBMs and metastases.[12] Furthermore, there are other reports of significantly reduced PSR in metastases and GBMs compared to CNSLs, reflected in the perfusion curve not crossing the baseline.[12,14]

Since hypoperfusion in lymphomas can be explained by hypovascularization and the absence of neoangiogenesis, the exact explanation of the signal intensity curve returning above the baseline level is difficult and not fully understood.[12,14] It is probably due to gadolinium extravasation into the interstitial space and complex T1 and T2 effects, which can alter the shape of the perfusion curve. T2 effects lead to lower signal intensity recovery, while T1 effects cause higher signal intensity recovery.[12,28] In lymphomas, T1 effects, probably due to an extensive accumulation of contrast material in the interstitial space, dominate over T2 effects and cause the characteristic overshooting from the baseline.[12,28,29] However, so far, no definite explanation has been

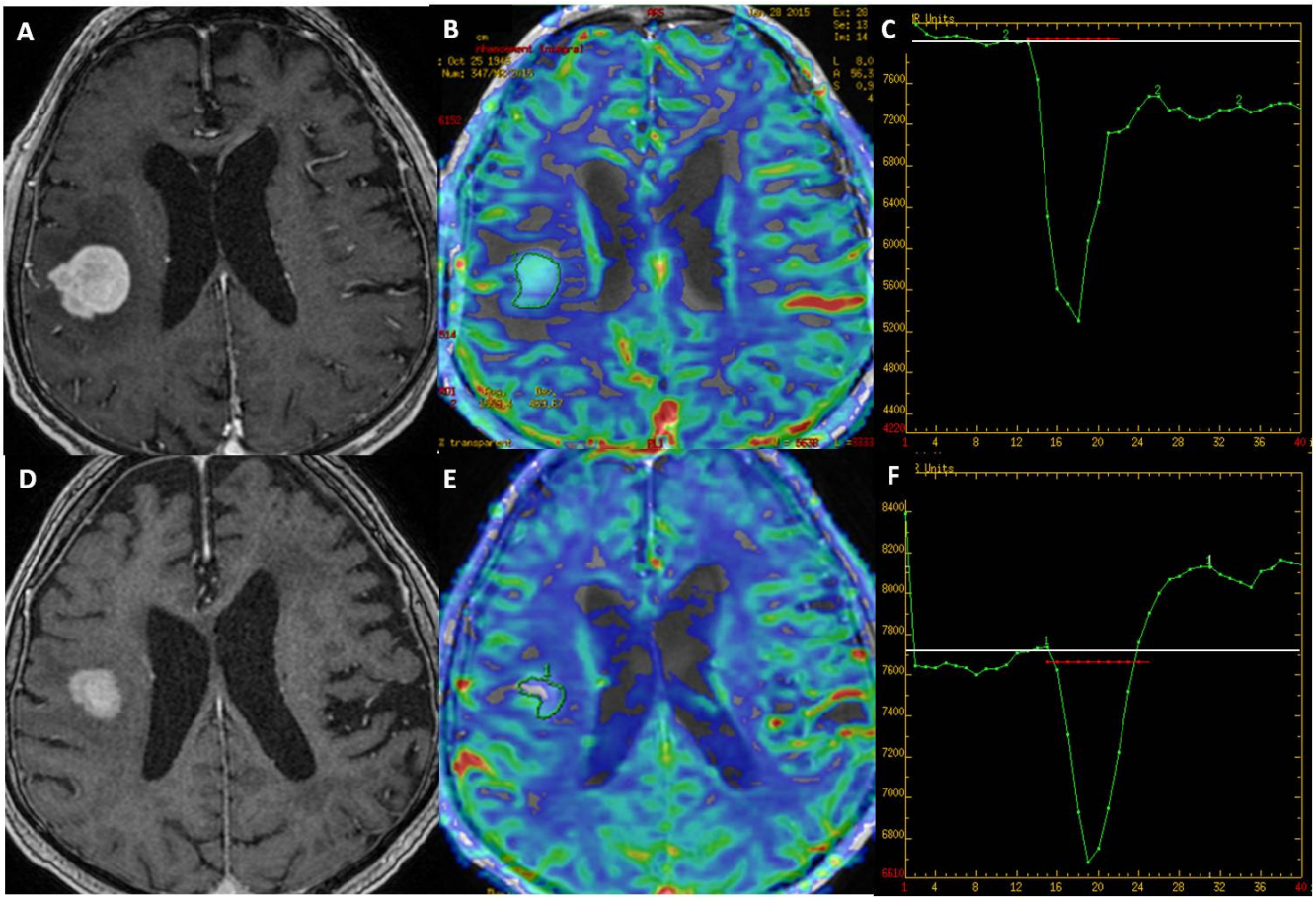

Fig. 3. A patient with a single CNSL lesion in the right parietal lobe examined with 2 DSC perfusion techniques with (A–C) and without (D–F) a preloading bolus

Axial T1-weighted MR images (A, D) after contrast administration, showing strong enhancement. The CBV perfusion map with a preload (B) shows hyperperfusion compared to hypoperfusion seen on the CBV map without a preload (E). The perfusion curve after a preload (C) exceeds the baseline compared to the perfusion curve without a preload, which does not reach the baseline (F).
CBV – cerebral blood volume; CNSL – central nervous system lymphoma; DSC – dynamic susceptibility contrast; MR – magnetic resonance.

given for overshooting in lymphomas in DSC perfusion without a preload. This phenomenon is probably caused by several factors and a complex interplay between them.[12]

Moreover, in our study we also compared all perfusion parameters between primary and secondary CNSLs, as well as between immunocompromised and immunocompetent patients. Secondary CNSLs revealed significantly higher $rCBV_c$ values compared to primary CNSLs, but still lower than 1.75. There were no other significant differences in any other perfusion parameters derived from CBV maps or perfusion curves among all evaluated patients subgroups. To our knowledge there are no reports in the literature that compare perfusion parameters in various lymphoma subgroups.

The last part of our investigation was to compare the results of 2 different perfusion techniques – with and without a preload bolus of contrast. The perfusion results after a preload indicated hyperperfusion of the evaluated lymphomas (high rCBV and rPH values) and showed the perfusion curves with only a partial return to the baseline level (low rPSR values). These results differed significantly from the values obtained in the perfusion technique without a preload.

In a few previous studies their authors have also analyzed CNSLs in PWI with a preload.[15,25,30] Preload dosing techniques have been proposed to minimize and correct for T1-weighted leakage due to blood–brain barrier, as well as T2- and/or T2*-weighted imaging residual effects characteristic for DSC perfusion techniques without a preload. These techniques are useful in differentiating between post-treatment radiation injury and recurrence of high-grade gliomas, where the blood–brain barrier disruption is significant and can lead to an underestimation of rCBV measurements.[7,9,23] On the other hand, a preload in CNSLs elevates their CBV values and effaces the characteristic perfusion curve, making them more similar to perfusion characteristics of high-grade gliomas, metastases or meningiomas. Therefore, in our opinion this technique brings a disadvantage in the case of lymphomas, because it makes their differentiation from other tumors impossible.[15,25,30]

A good practical example illustrating the differences between DSC methods with and without a preload is the case of Patient 4, who was examined with both techniques. The initial examination with a preload resulted in high rCBV values with $rCBV_{max}$ reaching 2.81 and a wrong diagnosis

of a metastasis (Fig. 3 A–C). The follow-up examination without a preload presented typical perfusion characteristics of CNSLs, such as hypoperfusion and the perfusion curve returning above the baseline level, which enabled the correct diagnosis of lymphoma confirmed later in biopsy (Fig. 3 D–F).

Conclusions

Despite their various appearances in conventional MR examinations, CNSLs (both primary or secondary and in patients with different immunological status) show very typical patterns in DWI and PWI without a preload bolus, such as diffusion restriction and hypoperfusion with the signal intensity curves returning above the baseline, respectively. These features enable us to differentiate CNSLs from other brain tumors, such as high-grade gliomas, metastases or meningiomas. In our opinion, advanced MR techniques such as DWI and PWI without a preload, as methods easy to perform and interpret, should be routinely incorporated in the initial workup of all brain tumors.

References

1. Osborn AG, Salzman KL, Barkovich AJ. *Diagnostic imaging: Brain*. 2nd ed. Salt Lake City, UT: Amirsys Publishing; 2010.
2. Haldorsen IS, Krossnes BK, Aarseth JH, et al. Increasing incidence and continued dismal outcome of primary central nervous system lymphoma in Norway 1989–2003: Time trends in a 15-year national survey. *Cancer*. 2007;110(8):1803–1814.
3. Haldorsen IS, Espeland A, Larsson EM. Central nervous system lymphoma: Characteristic findings on traditional and advanced imaging. *Am J Neuroradiol*. 2011;32(6):984–992.
4. Miller DC, Hochberg FH, Harris NL, Gruber ML, Louis DN, Cohen H. Pathology with clinical correlations of primary central nervous system non-Hodgkin's lymphoma. The Massachusetts General Hospital experience 1958–1989. *Cancer*. 1994;74(4):1383–1397.
5. Bhagavathi S, Wilson JD. Primary central nervous system lymphoma. *Arch Pathol Lab Med*. 2008;132(11):1830–1834.
6. Neska-Matuszewska M, Zimny A, Kałwak K, Sąsiadek MJ. Central nervous system lymphoma in a 3-year-old male suffering from a severe juvenile xanthogranuloma – The usefulness of perfusion weighted imaging and diffusion weighted imaging in the diagnostics of pediatric brain tumors. *Pol J Radiol*. 2015;80:31–35.
7. Hill QA, Owen RG. CNS prophylaxis in lymphoma: Who to target and what therapy to use. *Blood Rev*. 2006;20(6):319–332.
8. Krogh-Jensen M, Johansen P, D'Amore F. Primary central nervous system lymphoma in immunocompetent individuals: Histology, Epstein-Barr virus genome, Ki-67 proliferation index, p53 and bcl-2 gene expression. *Leuk Lymphoma*. 1998;30(1–2):131–142.
9. Senocak E, Oguz KK, Ozgen B, et al. Parenchymal lymphoma of the brain on initial MR imaging: A comparative study between primary and secondary brain lymphoma. *Eur J Radiol*. 2011;79(2):288–294.
10. Ferreri AJ, Dolcetti R, Du MQ, et al. Ocular adnexal MALT lymphoma: An intriguing model for antigen-driven lymphomagenesis and microbial-targeted therapy. *Ann Oncol*. 2008;19(5):835–846.
11. Cavaliere R, Petroni G, Lopes MB, Schiff D; International primary central nervous system lymphoma collaborative group. Primary central nervous system posttransplantation lymphoproliferative disorder: An international primary central nervous system lymphoma collaborative group report. *Cancer*. 2010;116(4):863–870.
12. Mangla R, Kolar B, Zhu T, Zhonga J, Almasta J, Ekholma S. Percentage of signal recovery derived from MR dynamic susceptibility contrast imaging is useful to differentiate common enhancing malignant lesions of the brain. *Am J Neuroradiol*. 2011;32(6):1004–1010.
13. Cha S, Lupo JM, Chen MH, et al. Differentiation of glioblastoma multiforme and single brain metastasis by peak height and percentage of signal intensity recovery derived from dynamic susceptibility-weighted contrast-enhanced perfusion MR imaging. *Am J Neuroradiol*. 2007;28(6):1078–1084.
14. Rizzo L, Crasto SG, Moruno PG, et al. Role of diffusion- and perfusion-weighted MR imaging for brain tumour characterisation. *Radiol Med*. 2009;114(4):645–646.
15. Sugahara T, Korogi Y, Tomiguchi S, et al. Posttherapeutic intraaxial brain tumor: The value of perfusion-sensitive contrast-enhanced MR imaging for differentiating tumor recurrence from nonneoplastic contrast-enhancing tissue. *Am J Neuroradiol*. 2000;21(5):901–909.
16. Zacharia TT, Law M, Naidich TP, Leeds NE. Central nervous system lymphoma characterization by diffusion-weighted imaging and MR spectroscopy. *J Neuroimaging*. 2008;18(4):411–417.
17. Calli C, Kitis O, Yunten N, Yurtseven T, Islekel S, Akalin T. Perfusion and diffusion MR imaging in enhancing malignant cerebral tumors. *Eur J Radiol*. 2006;58(3):394–403.
18. Provenzale JM, Mukundan S, Barboriak DP. Diffusion-weighted and perfusion MR imaging for brain tumor characterization and assessment of treatment response. *Radiol*. 2006;239(3):632–649.
19. Barajas RF, Rubenstein JL, Chang JS, Hwang J, Cha S. Diffusion-weighted MR imaging derived apparent diffusion coefficient is predictive of clinical outcome in primary central nervous system lymphomas. *Am J Neuroradiol*. 2012;31(1):60–66.
20. Schroeder PC, Post MJ, Oschatz E, Stadler A, Bruce-Gregorios J, Thurnher MM. Analysis of the utility of diffusion-weighted MRI and apparent diffusion coefficient values in distinguishing central nervous system toxoplasmosis from lymphoma. *Neuroradiol*. 2006;48(10):715–720.
21. Guo AC, Cummings TJ, Dash RC, Provenzale JM. Lymphomas and high-grade astrocytomas: Comparison of water diffusibility and histologic characteristics. *Radiol*. 2002;224(1):177–183.
22. Rosen B, Belliveau J, Vevea J, Brady TJ. Perfusion imaging with NMR contrast agents. *Magn Reson Med*. 1990;14(2):249–265.
23. Zimny A, Sąsiadek M. Contribution of perfusion-weighted magnetic resonance imaging in the differentiation of meningiomas and other extra-axial tumors: Case reports and literature review. *J Neurooncol*. 2011;103(3):777–783.
24. Cha S, Knopp EA, Johnson G, Wetzel SG, Litt AW, Zagzag D. Intracranial mass lesions: Dynamic contrast-enhanced susceptibility-weighted echo-planar perfusion MR imaging. *Radiol*. 2002;223(1):11–29.
25. Hu LS, Baxter LC, Pinnaduwage DS, et al. Optimized preload leakage-correction methods to improve the diagnostic accuracy of dynamic susceptibility-weighted contrast-enhanced perfusion MR imaging in posttreatment gliomas. *Am J Nuroradiol*. 2010;31(1):40–48.
26. Essig M, Anzalone N, Combs SE, et al. MR imaging of neoplastic central nervous system lesions: Review and recommendations for current practice. *Am J Neuroradiol*. 2012;33(5):803–817.
27. Law M, Oh S, Johnson G, et al. Perfusion magnetic resonance imaging predicts patients outcome as an adjunct to histopathology: A second reference standard in the surgical and nonsurgical treatment of low-grade gliomas. *Neurosurgery*. 2006;58(6):1099–1107.
28. Paulson ES, Schmainda KM. Comparison of dynamic susceptibility--weighted contrast-enhanced MR methods: Recommendations for measuring relative cerebral blood volume in brain tumors. *Radiol*. 2008;249(2):601–613.
29. Runge VM, Kirsch JE, Wells JW, Dunworth JN, Hilaire L, Woolfolk CE. Repeat cerebral blood volume assessment with first-pass MR imaging. *J Magn Reson Imaging*. 1994;4(3):457–461.
30. Toh CH, Wei KC, Chang CN, Ng SH, Wong HF. Differentiation of primary central nervous system lymphomas and glioblastomas: Comparisons of diagnostic performance of dynamic susceptibility contrast-enhanced perfusion MR imaging without and with contrast-leakage correction. *Am J Neuroradiol*. 2013;34(6):1145–1149.

Family-based study of association between *MAFB* gene polymorphisms and NSCL/P among Western Han Chinese population

Bihe Zhang[1,B,D], Shijun Duan[1,A–F], Jiayu Shi[2,B,C], Shuyuan Jiang[1,B,C], Fan Feng[3,B,C], Bing Shi[1,A,E], Jia Zhonglin[1,A,C,E,F]

[1] State Key Laboratory of Oral Disease, West China College of Stomatology, Sichuan University, Chengdu, China
[2] Division of Growth and Development and Section of Orthodontics, School of Dentistry, University of California, Los Angeles, USA
[3] Air Force Dujiangyan Aviation Medicine Evaluation and Training Center, Chengdu, China

A – research concept and design; B – collection and/or assembly of data; C – data analysis and interpretation;
D – writing the article; E – critical revision of the article; F – final approval of the article

Advances in Clinical and Experimental Medicine, ISSN 1899-5276 (print), ISSN 2451-2680 (online) *Adv Clin Exp Med*. 2018;27(8):1109–1116

Address for correspondence
Zhonglin Jia
E-mail:zhonglinjia@sina.com

Funding sources
The National Science Funds of China (No. 81600849, No. 81271118) and Scientific Research Funds for Young Teachers of Sichuan University (No. 0040305505088)

Conflict of interest
None declared

Received on March 14, 2017
Reviewed on May 25, 2017
Accepted on June 3, 2017

Abstract

Background. Non-syndromic cleft lip with or without cleft palate (NSCL/P) are the most common human congenital birth defects with a complex etiology. *MAFB* has been reported as a candidate gene involved in the pathogenesis of NSCL/P from genome-wide association study (GWAS) findings, and no replication studies have been performed in Western Han Chinese.

Objectives. The aim of this study was to investigate the associations of *MAFB* among NSCL/P trios in Western Han Chinese.

Material and methods. We selected 6 single nucleotide polymorphisms (SNPs) (rs6072081, rs6065259, rs17820943, rs13041247, rs11698025 and rs6102085) near *MAFB* based on previous GWAS findings and recruited 298 case-parents trios with NSCL/P from Western Han Chinese population, while genotypes were done by SNPscan technology.

Results. Strong evidence of an association was found at rs17820943 ($p = 0.0023$; odds ratio – $OR_{transmission} = 0.7$ and 95% confidence interval [CI]: 0.55–0.88) and rs13041247 ($p = 0.0023$; $OR_{transmission} = 0.7$ and 95% CI: 0.55–0.88) among NSCL/P; genotypic transmission-disequilibrium test (TDT) analysis further confirmed this. C/C homozygote at rs17820943 ($z = 3.44$ and $p = 0.00058$) and T/T homozygote at rs13041247 ($z = 3.14$ and $p = 0.0017$) were over-transmitted among NSCL/P, which indicated they could increase the risk of having an affected baby. Sliding window haplotype analysis showed that haplotypes consisting of C allele at rs17820943 and T allele at rs13041247 were still over-transmitted among NSCL/P (lowest $p = 0.0021$).

Conclusions. This study further confirmed that the targeted SNPs at *MAFB* were associated with NSCL/P trios from Western Han Chinese population, which provides more scientific evidence for the future research and genetic counseling.

Key words: single nucleotide polymorphism, transmission disequilibrium test, *MAFB*, haplotype analysis, non-syndromic cleft lip with or without cleft palate

DOI
10.17219/acem/74388

Introduction

Cleft lip with or without cleft palate (CL/P) are the most common congenital craniofacial birth defects, which can be categorized as an isolated anomaly (identified non-syndromic CL/P – NSCL/P) or as a part of multiple congenital anomalies (identified syndromic CL/P – SCL/P). The cases of NSCL/P are more prevalent (approx. at 70% of all cleft cases), with the worldwide occurrence incidence ranging from 1/500 to 1/2500.[1] Since CL/P influences the structure of the face and oral cavity, the affected children need to confront a wide range of difficulties, including feeding, speech, hearing and dental defects, as well as appearance and psychosocial problems, which can induce long-lasting health and financial burdens.[2] Generally, the prevalence of NSCL/P was 1.42 per 1000 in Chinese newborns, presenting a high frequency among countries worldwide, which is an important public health problem in China.[3] Actually, some epidemiological and biological data suggested NSCL/P might be divided into non-syndromic cleft lip only (NSCLO) and non-syndromic cleft lip with cleft palate (NSCLP) which should be analyzed separately and are considered to have different genetic etiologies and embryo origins.[4,5] The origin of cleft lip was seen as a malformation of the primary palate only, while cleft lip with cleft palate involved both the primary and secondary palates.[4] There were obvious discordances regarding the recurrence risks and transmission patterns between these two subgroups.[5] Therefore, to explore the further possible susceptibility genes, the 2 subgroups should be analyzed separately.

NSCL/P were genetically complex disorders, which included the interaction of multiple genetic and environmental risk factors. The search for susceptibility genes of NSCL/P was undertaken using numerous approaches, including animal experiments, candidate genes, linkage analysis studies, genomic rearrangements; genome-wide association studies (GWAS), and direct sequencing. However, the results were still unsatisfactory.[2,6] As a useful method for unraveling the genetic traits of common human diseases, GWAS quickly became the new standard in genetic analysis at the genome level and it identified multiple strong association susceptibility genes.[7,8] So far, the GWAS of NSCL/P had identified more than 15 susceptible loci, which provided more insights into the genetic etiology of NSCL/P.[9–15] However, the pathogenesis of NSCL/P involving these loci was still unclear. Although the advantages of GWAS were obvious, some potential limitations of this method might influence the results, or miss disease heritability, even leading to a false positive result.[16,17] Population-based association studies were always designed and performed in the majority of GWAS.[7,18] Though the difficulty of sample collection was avoided, the presence of undetected population substructure might be missed or affect the signal of significant association.[7,18] Subsequent family-based association studies (such as case-parents trios study), focusing on limited genetic markers after GWAS findings, were more efficient in correcting the population substructure and more powerful in revealing cryptic relatedness of samples.[7,16]

Up to now, the largest GWAS about non-syndromic orofacial clefts was conducted by Beaty et al., who were the first to report that single nucleotide polymorphisms (SNPs) in or near *MAFB* (v-maf musculoaponeurotic fibrosarcoma oncogene homolog B; located in 20q12) are associated with NSCL/P, with the most significance coming from an analysis of families with Asian ancestry population, including samples from Western Han Chinese collected in our hospital.[12] *MAFB*, encoding a basic leucine zipper (bZIP) transcription factor, had been found to play a significant role in the development of brain, kidney, lens, retina, pancreatic islet cells, and the hematopoietic system.[19] However, according to findings by Beaty et al., the expressions of *MAFB* mRNA and protein had also been demonstrated in both craniofacial neuroectoderm and neural-crest derived from mesoderm between embryonic day 13.5 and 14.5, which suggested that the gene might associate with NSCL/P closely.[12] Then, interactions between *MAFB* and other genes were detected in both European and Asian CL/P populations through gene-gene interaction analysis.[17] Subsequently, several validation studies had been done in the United States, Brazil, Colombia, and China.[20–25] Nonetheless, the results of those studies were inconsistent with each other, as only limited populations were validated in some studies or different research methods were adopted. Then, based on Chinese Han population, Sun et al. conducted a 3-stage case-control GWAS and still found some SNPs (locating in downstream of *MAFB*) at 20q12 involving in orofacial development. The majority of samples in this study also came from the Western Han Chinese population treated in our hospital (West China Hospital of Stomatology, Sichuan University, Chengdu, China).[14]

Although the results of these studies were encouraging, only a part of Chinese population was included in the validation research and associations with certain subgroup of NSCL/P were not fully elucidated by Beaty et al. and Sun et al.[12,14] Meanwhile, the Western Han Chinese ancestry population also contributed to the findings of Beaty et al. and Sun et al.[12,14] To know if the GWAS signals were associated with cleft palate (CP), we previously recruited 144 case-parents trios with CP, and tested the associations with 38 SNPs, which included 6 SNPs at *MAFB* (rs6072081, rs6065259, rs17820943, rs13041247, rs11698025 and rs6102085). A single SNP analysis did not show any significant relevance between *MAFB* and CP; however, interactions between 2 SNPs show that rs6072081 significantly interacted with rs6102085, which indicated that these 2 SNPs may act in the same pathway in the etiology of CP.[26]

Thus, in this study, we used another set of samples with NSCL/P trios different from the ones used in the 2 previous GWASs (Beaty et al. and Sun et al.) and conducted

a validation study with 6 SNPs at MAFB: (rs6072081, rs6065259, rs17820943, rs13041247, rs11698025 and rs6102085) to investigate whether these loci were associated with NSCLO, NSCLP and NSCL/P in Western Han Chinese population.[12,14]

Material and methods

Ethics statement

We obtained a written informed consent from all participants or legal guardians of the affected children younger than 16 years before they were enrolled in the study. The study protocols were reviewed and approved by the Hospital Ethics Committee (HEC) of West China Hospital of Stomatology, Sichuan University, Chengdu, China.

Samples description

Our samples included 298 case-parent trios, who were recruited between 2008 and 2013 from the Cleft Lip and Palate Surgery Department of West China Stomatology College, Sichuan University, Chengdu, China. All probands were checked by professional maxillofacial doctors, with congenital deformities diagnosed as non-syndromic and major developmental delays excluded. All participants were identified as Western Han Chinese according to self-identification. The gender and types of clefts is shown in Table 1.

Table 1. Types of non-syndromic cleft lip with or without cleft palate

Phenotype	Male	Female	Unknown sex	Total
NSCLO	70	57	0	127
NSCLP	111	55	5	171
NSCL/P	181	112	5	298

NSCLO – non-syndromic cleft lip only; NSCLP – non-syndromic cleft lip with cleft palate; NSCL/P – non-syndromic cleft lip with or without cleft palate (NSCLO and NSCLP); NSCPO – non-syndromic cleft palate only.

SNPs selection and genotyping

Based on the findings of Beaty et al., we chose 6 SNPs (rs6072081, rs6065259, rs17820943, rs13041247, rs11698025 and rs6102085) with significant p-values near *MAFB*, with minor allele frequency (MAF) >0.30.[12] Primary information of these SNPs is shown in Table 2.

Venous blood samples were drawn from all participants after being recruited in the study. Genomic DNA was extracted by using the protein precipitation method.[27] All the experiments of genotyping were done by the Genesky Biopharm Technology Company, using SNPscan technology.

Statistical analysis

For each SNP, we checked for deviations by performing the Hardy-Weinberg equilibrium (HWE) test and calculated the MAF among the unaffected parents. Pairwise linkage disequilibrium (LD) was calculated as D' and r^2 for all SNPs to identify LD blocks by the Haploview program (Cambridge, USA). The transmitted target alleles and genotypes from heterozygous parents to the affected child were evaluated by the transmission-disequilibrium test (TDT) analysis, and the Sliding window haplotype transmission disequilibrium analysis was conducted by family-based association test (FBAT) program (Cambridge, USA). We used a Bonferroni correction for the 18 tests to determine a threshold for formal significance of p = 0.0028.

Results

Characteristic information of the study population

Based on clinical manifestations, the selected NSCL/P samples were divided into 2 subgroups, 127 NSCLO cases (42.6%) and 171 NSCLP cases (57.4%), respectively. The observed genotype frequencies of NSCL/P were in agreement with the Hardy-Weinberg equilibrium (p > 0.01) (Table 2), indicating favorable genetic homogeneity within the study population.

Allelic and genotypic TDT analysis

Allelic TDT analysis was assessed on case-parents trios with the transmission of minor alleles from heterozygous informative parents to affected child. The results

Table 2. The minor allele frequency (MAF) and Hardy-Weinberg equilibrium results of single-nucleotide polymorphisms (SNPs)

SNP	BP	SNP function	A1	A2	NSCLO		NSCLP		NSCL/P	
					MAF (%)	HWpval	MAF (%)	HWpval	MAF (%)	HWpval
rs6072081	39261054	intergenic	G	A	40.29	1.00	41.0	0.03	40.59	0.15
rs6065259	39261979	intergenic	A	G	38.17	1.00	37.9	0.23	38.05	0.48
rs17820943	39268516	intergenic	T	C	40.14	1.00	40.4	0.10	40.26	0.24
rs13041247	39269074	intergenic	C	T	40.14	1.00	40.4	0.10	40.26	0.24
rs11698025	39274083	intergenic	A	G	31.20	1.00	33.5	0.58	32.20	0.71
rs6102085	39281629	intergenic	A	G	42.33	1.00	45.2	0.71	43.57	0.80

NSCLO – non-syndromic cleft lip only; NSCLP – non-syndromic cleft lip with cleft palate; NSCL/P –non-syndromic cleft lip with or without cleft palate (NSCLO and NSCLP); HWpval – p-values of the Hardy-Weinberg equilibrium test.

showed that minor allele T rs17820943 (p = 0.0023; odds ratio – $OR_{transmission}$ = 0.7 and 95% confidence interval [CI]: 0.55–0.88) and allele C at rs113041247 (p = 0.0023; $OR_{transmission}$ = 0.7 and 95% CI: 0.55–0.88) was significantly under-transmitted from unaffected parents to probands among NSCL/P, which indicated that these alleles were protective for NSCL/P (Table 3).

Genotypic TDT was used to assess the genotype distribution comparison. The results showed significant over-transmission of C/C homozygote at rs17820943 (z = 3.44 and p = 0.00058), T/T homozygote at rs13041247 (z = 3.14 and p = 0.0017) and G/G homozygote at rs11698025 (z = 3.21 and p = 0.0013) from unaffected parents to probands among NSCL/P. Meanwhile, these 2 SNP markers were over-transmitted from unaffected parents to probands among NSCLP. Then, we observed A/A homozygote at rs6072081 (z = 3.051 and p = 0.0023) and G/G homozygote at rs6065259 (z = 3.38 and p = 0.00073) were also over-transmitted from unaffected parents to probands among NSCL/P (Table 4). However, no significant evidence of association was also identified in both allelic and genotypic TDT analysis for NSCLO.

Table 3. Allelic transmission-disequilibrium test (TDT) results for single nucleotide polymorphisms (SNPs) at *MAFB*

SNP	A1	NSCLO			NSCLP			NSCL/P		
		T/U	OR (95% CI)	p-value	T/U	OR (95% CI)	p-value	T/U	OR (95% CI)	p-value
rs6072081	G	62/75	0.83 (0.59–1.16)	0.27	58/94	0.62 (0.44–0.86)	0.0035	120/169	0.71 (0.56–0.9)	0.0039
rs6065259	A	57/62	0.92 (0.64–1.32)	0.65	53/89	0.6 (0.42–0.84)	0.0025	110/151	0.73 (0.57–0.93)	0.011
rs17820943	T	56/76	0.74 (0.52–1.04)	0.08	63/95	0.66 (0.48–0.91)	0.011	**119/171**	**0.7 (0.55–0.88)**	**0.0023**
rs13041247	C	56/76	0.74 (0.52–1.04)	0.08	63/95	0.66 (0.48–0.91)	0.011	**119/171**	**0.7 (0.55–0.88)**	**0.0023**
rs11698025	A	50/62	0.81 (0.56–1.17)	0.26	51/83	0.61 (0.43–0.87)	0.0057	101/145	0.7 (0.54–0.9)	0.005
rs6102085	A	65/58	1.12 (0.79–1.6)	0.53	62/85	0.73 (0.53–1.01)	0.06	127/143	0.89 (0.7–1.13)	0.33

NSCLO – non-syndromic cleft lip only; NSCLP – non-syndromic cleft lip with cleft palate; NSCL/P – non-syndromic cleft lip with or without cleft palate (NSCLO and NSCLP); A1 – minor allele; OR – odds ratio; 95% CI – 95% confidence interval; bold characters indicate items with p-value less than 0.0028 (Bonferroni correction threshold p-value).

Table 4. Genotypic transmission disequilibrium test (TDT) results for single nucleotide polymorphisms (SNPs) on *MAFB* from family-based association test (FBAT)

SNP	Genotype	NSCLO				NSCLP				NSCL/P			
		afreq	fam#	z	p-value	afreq	fam#	z	p-value	afreq	fam#	z	p-value
rs6072081	G/G	0.13	57	–0.67	0.51	0.15	63	–1.084	0.28	0.14	121	–1.34	0.18
	G/A	0.56	95	–0.72	0.47	0.49	125	–1.7	0.089	0.52	221	–1.68	0.093
	A/A	0.31	83	1.36	0.17	0.36	96	2.89	0.0039	0.34	179	**3.051**	**0.0023**
rs6065259	A/A	0.11	44	–0.17	0.87	0.14	57	–0.43	0.67	0.13	101	–0.44	0.66
	A/G	0.51	88	–0.85	0.39	0.47	118	–2.76	0.0058	0.49	206	–2.65	0.0081
	G/G	0.38	78	1.08	0.28	0.39	93	**3.58**	**0.00034**	0.38	171	**3.38**	**0.00073**
rs17820943	T/T	0.14	54	–1.22	0.22	0.15	69	–0.39	0.7	0.15	124	–1.18	0.24
	T/C	0.53	89	–0.53	0.6	0.49	127	–2.4	0.017	0.51	217	–2.1	0.035
	C/C	0.33	79	1.58	0.11	0.36	98	**3.2**	**0.0014**	0.35	177	**3.44**	**0.00058**
rs13041247	C/C	0.127	53	–1.23	0.22	0.15	68	–0.2	0.84	0.14	122	–1	0.32
	C/T	0.541	88	0	1	0.49	124	–2.51	0.012	0.51	213	–1.99	0.047
	T/T	0.332	77	0.98	0.33	0.36	97	**3.17**	**0.0015**	0.35	175	**3.14**	**0.0017**
rs11698025	G/G	0.43	78	1.5	0.13	0.47	94	**2.98**	**0.0029**	0.45	172	**3.21**	**0.0013**
	G/A	0.47	84	–0.87	0.38	0.44	109	–2.2	0.028	0.45	193	–2.23	0.026
	A/A	0.1	39	–0.81	0.42	0.085	50	–0.7	0.48	0.093	89	–1.061	0.29
rs6102085	A/A	0.2	57	0.071	0.94	0.17	67	–0.93	0.35	0.18	125	–0.72	0.47
	A/G	0.51	94	0.21	0.84	0.49	118	–0.92	0.36	0.5	213	–0.48	0.63
	G/G	0.29	68	–0.32	0.75	0.34	91	1.89	0.059	0.32	159	1.22	0.22

NSCLO – non-syndromic cleft lip only; NSCLP – non-syndromic cleft lip with cleft palate; NSCL/P – non-syndromic cleft lip with or without cleft palate (NSCLO and NSCLP); afreq – allele frequency; fam# – informative family; z – vector of the large sample z statistic; bold characters indicate the items with p-value less than 0.0028 (p-value after Bonferroni correction).

Lactate dehydrogenase and haplotype analysis

Pair-wise lactate dehydrogenase (LD) between these SNPs was calculated by D' and r^2 statistics in Haploview program (Cambridge, USA), and the results showed that rs6072081 and rs6065259 were in high LD (D' > 0.96 and r^2 > 0.80) across the 3 subgroups: NSCLO, NSCLP and NSCL/P (Fig. 1). To test if these 2 SNPs and other adjacent SNPs traveled together with each other from the parents to the affected child, we performed the sliding window haplotype analysis; the results indicated that A-G for rs6072081-rs6065259, A-G-C for rs6072081-rs6065259-rs17820943 and A-G-C-T for rs6072081-rs6065259-rs17820943-rs13041247 were statistically over-transmitted for NSCLP and NSCL/P (lowest z = 3.12 and p = 0.0018) (Table 5).

Discussion

NSCL/P is complex congenital craniofacial defect with serious malformations, including malocclusion, oral and nasal dysfunction. Though there has been great progress made in surgical repair, these malformations still have negative effects on the patients and their families. The past few years saw great advances in the investigation of the pathogenesis of NSCL/P. Since NSCL/P is heterogeneous, screening for the new implications in diverse ethnical populations is critical for providing more evidence in the etiology of NSCL/P. Till now, many putative candidate genes for NSCL/P had been identified successfully by GWAS and other studies. However, because of various genetic backgrounds and limitations of samples, replication studies on those candidate loci/genes among different populations were still inconsistent.[1]

Beaty et al. were the first to report that the *MAFB* gene was associated with NSCL/P and participated in the craniofacial development by performing a GWAS study with the samples originated from Asian and European populations.[12] To check if this gene is causal for NSCL/P in Western Han Chinese population, we selected 6 SNPs (rs6072081, rs6065259, rs17820943, rs13041247, rs11698025 and rs6102085) and replicated them among 298 case-parents trios. Interestingly, we found that rs17820943 (p = 0.0023; $OR_{transmission}$ = 0.7 and 95% CI: 0.55–0.88) and rs13041247 (p = 0.0023, $OR_{transmission}$ = 0.7 and 95% CI: 0.55–0.88) were significantly associated with the NSCL/P (Table 3). Genotypic TDT analysis further confirmed this; C/C homozygote at rs17820943 (z = 3.44 and p = 0.00058) and T/T homozygote at rs13041247 (z = 3.14 and p = 0.0017) were over-transmitted among NSCL/P trios, which indicated they could increase the risk of having an affected baby. Sliding window haplotype analysis showed haplotypes consisting of C allele at rs17820943 and T allele at rs13041247 were still over-transmitted among NSCL/P trios (lowest p = 0.0021).

To test if those 6 SNPs were independent from each other, we performed pair-wise LD analyses. The results showed strong LD between rs6072081 and rs6065259 (D' > 0.96 and r^2 > 0.80) across the 3 subgroups: NSCLO, NSCLP and NSCL/P (Fig. 1); except allelic TDT analysis, genotypic

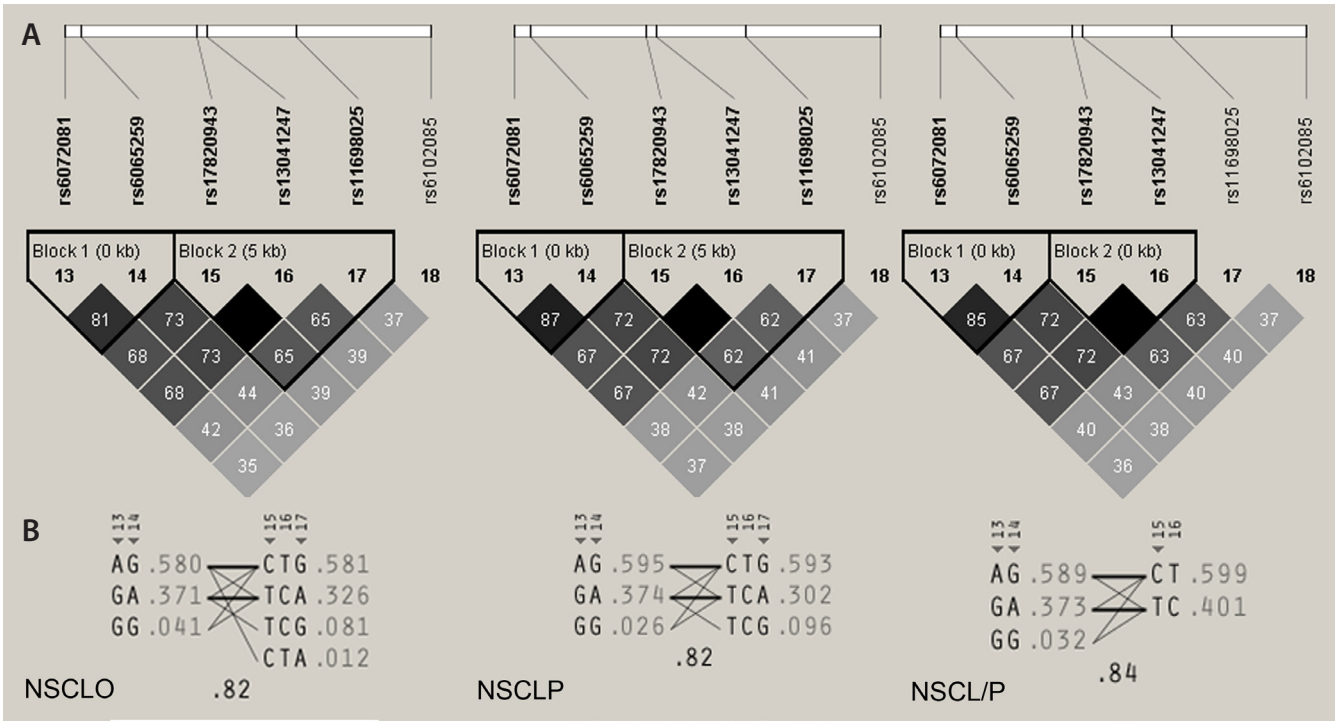

Fig. 1. Linkage disequilibrium blocks for the *MAFB* haplotype analysis

Linkage disequilibrium plot with boxes representing the marker pair relationship plotted between 2 markers.

Table 5. Association between the common *MAFB* haplotypes of single-nucleotide polymorphisms (SNPs) and non-syndromic cleft lip with or without cleft palate (NSCL/P)

SNPs	rs6072081	rs6065259	rs17820943	rs13041247	rs11698025	rs6102085	afreq	fam#	z	p-value
Over-transmitted										
NSCLO	–	–	–	T	G	A	0.11	43.1	2.29	0.022
	–	–	C	T	G	A	0.11	43.1	2.29	0.022
NSCLP	A	G	–	–	–	–	0.59	107	2.83	0.0047
	–	G	C	–	–	–	0.57	109.9	2.36	0.018
	–	–	C	T	–	–	0.60	109	2.27	0.023
	–	–	–	T	G	–	0.59	108.9	2.096	0.036
	A	G	C	–	–	–	0.56	109	2.43	0.015
	–	G	C	T	–	–	0.57	107.9	2.37	0.018
	–	–	C	T	G	–	0.59	108.9	2.072	0.038
	A	G	C	T	–	–	0.56	108	2.43	0.015
NSCL/P	A	G	–	–	–	–	**0.59**	**180**	**3.12**	**0.0018**
	–	G	C	–	–	–	0.58	180	2.66	0.0079
	–	–	C	T	–	–	0.60	175	2.77	0.0056
	–	–	–	T	G	–	0.59	179.9	2.55	0.011
	A	G	C	–	–	–	**0.56**	**179**	**3.07**	**0.0021**
	–	G	C	T	–	–	0.58	178	2.66	0.0079
	–	–	C	T	G	–	0.59	178.9	2.53	0.011
	A	G	C	T		–	**0.56**	**178**	**3.06**	**0.0022**
	–	G	C	T	G	–	0.57	172.9	2.16	0.031
Under-transmitted										
NSCLO	G	G	–	–	–	–	0.04	15	–1.99	0.047
	G	G	C	–	–	–	0.025	10	–2.10	0.036
	G	G	C	T	–	–	0.025	10	–2.10	0.036
NSCLP	G	A	–	–	–	–	0.38	101	–2.48	0.013
	–	A	T	–	–	–	0.36	98	–2.06	0.04
	–	–	T	C	–	–	0.40	109	–2.27	0.023
	–	–	–	C	A	–	0.30	97.9	–2.62	0.0088
	–	–	–	–	A	A	0.27	81.3	–2.27	0.022
	G	A	T	–	–	–	0.35	95	–2.01	0.045
	–	A	T	C	–	–	0.36	98	–2.06	0.04
	–	–	T	C	A	–	0.30	97.9	–2.62	0.0088
	–	–	–	C	A	A	0.26	79.4	–2.33	0.02
	G	A	T	C	–	–	0.35	95	–2.01	0.045
	–	A	T	C	A	–	0.26	82	–2.26	0.024
	–	–	T	C	A	A	0.26	79.4	–2.33	0.020
NSCL/P	G	A	–	–	–	–	0.37	172.9	–2.23	0.026
	G	G	–	–	–	–	0.031	30	–2.11	0.035
	–	A	T	–	–	–	0.35	167.9	–2.08	0.037
	–	–	T	C	–	–	0.4	175	–2.77	0.0056
	–	–	–	C	A	–	0.31	162.7	–2.88	0.004
	–	–	–	–	A	A	0.27	150.8	–2.27	0.023
	–	A	T	C	–	–	0.35	167.9	–2.08	0.037
	–	–	T	C	A	–	0.31	162.7	–2.88	0.004
	–	–	–	C	A	A	0.27	146.9	–2.42	0.015
	–	–	T	C	A	A	0.27	146.9	–2.42	0.015

NSCLO – non-syndromic cleft lip only; NSCLP – non-syndromic cleft lip with cleft palate; afreq – allele frequency; fam# – informative family; z – vector of the large sample z statistic. Listed characters indicate the items with p-value less than 0.05; bold characters indicate the items with p-value less than 0.0028 (p-value after Bonferroni correction).

Table 6. Parent-of-origin effect analysis by cleft types

Cleft groups	SNP	A1	Paternal		Maternal		z	p-value
			T/U	p-value	T/U	p-value		
NSCLO	rs6072081	G	30.5/37.5	0.4	31.5/37.5	0.47	−0.09	0.86
	rs6065259	A	26.5/30.5	0.6	30.5/31.5	0.9	−0.29	0.95
	rs17820943	T	28.5/37.5	0.27	27.5/38.5	0.18	0.18	0.66
	rs13041247	C	28.5/37.5	0.27	27.5/38.5	0.18	0.18	0.86
	rs11698025	A	23.5/29.5	0.41	26.5/32.5	0.43	−0.06	–
	rs6102085	A	31/30	0.9	34/28	0.45	−0.45	0.24
NSCLP	rs6072081	G	32/46	0.11	26/48	0.01	0.75	0.36
	rs6065259	A	29.5/44.5	0.08	23.5/44.5	0.011	0.65	0.63
	rs17820943	T	35.5/46.5	0.22	27.5/48.5	0.016	0.91	0.67
	rs13041247	C	35.5/46.5	0.22	27.5/48.5	0.016	0.91	0.36
	rs11698025	A	23/41	0.024	28/42	0.09	−0.48	0.63
	rs6102085	A	32.5/41.5	0.3	29.5/43.5	0.1	0.43	0.67
NSCL/P	rs6072081	G	62.5/83.5	0.08	57.5/85.5	0.019	0.45	0.65
	rs6065259	A	56/75	0.1	54/76	0.054	0.2	0.84
	rs17820943	T	64/84	0.1	55/87	0.007	0.78	0.44
	rs13041247	C	64/84	0.1	55/87	0.007	0.78	0.44
	rs11698025	A	46.5/70.5	0.027	54.5/74.5	0.08	−0.4	0.69
	rs6102085	A	63.5/71.5	0.49	63.5/71.5	0.49	0	1

NSCLO – non-syndromic cleft lip only; NSCLP – non-syndromic cleft lip with cleft palate; NSCL/P –non-syndromic cleft lip with or without cleft palate (NSCLO and NSCLP); SNP – single nucleotide polymorphism; T/U – transmitted/non-transmitted; z – vector of the large sample z statistic.

TDT and sliding window haplotype analysis both showed that these 2 SNPs were associated with NSCL/P after multiple corrections.

Imprinting effects are increasingly regarded as a foremost source of modifiers in the complex disease. In this study, we performed the parent-of-origin effect analysis with our family-based study design. However, the results showed no significant difference between the maternal and paternal transmission (Table 6).

These 6 SNPs, all located in intergenic regions near *MAFB*, had been observed to be significantly associated with NSCL/P.[12] The intergenic region did not influence the protein structure, but it exerted a potential impact on gene expression; the literature has demonstrated that DNA methylation level was higher in intergenic regions than that in the transcription start site, and it appeared more likely to be inherited. Meanwhile, DNA methylation had been found to be closely related to the alterations in chromatin structure, gene expression and disease.[28]

In summary, this study showed that rs17820943 and rs13041247 at *MAFB* gene were related with NSCL/P from Western Han Chinese, which provides new additional evidence for the pathogenesis of NSCL/P and gives new insights for future research and genetic counseling.

References

1. Mossey PA, Little J, Munger RG, Dixon MJ, Shaw WC. Cleft lip and palate. *Lancet*. 2009;374:1773–1785.
2. Dixon MJ, Marazita ML, Beaty TH, Murray JC. Cleft lip and palate: Understanding genetic and environmental influences. *Nat Rev Genet*. 2011;12:167–178.
3. Dai L, Zhu J, Mao M, et al. Time trends in oral clefts in Chinese newborns: Data from the Chinese National Birth Defects Monitoring Network. *Birth Defects Res A Clin Mol Teratol*. 2010;88:41–47.
4. Harville EW, Wilcox AJ, Lie RT, Vindenes H, Åbyholm F. Cleft lip and palate versus cleft lip only: Are they distinct defects? *Am J Epidemiol*. 2005;162:448–453.
5. Rahimov F, Marazita ML, Visel A, et al. Disruption of an AP-2alpha binding site in an *IRF6* enhancer is associated with cleft lip. *Nat Genet*. 2008;40:1341–1347.
6. Murray JC. Gene/environment causes of cleft lip and/or palate. *Clin Genet*. 2002;61:248–256.
7. Xu H, Mathew G, George V. Family-based genome-wide association study for simulated data of Framingham Heart Study. *BMC Proc*. 2009;3(Suppl 7):S124–S128.
8. Leslie EJ, Taub MA, Liu H, et al. Identification of functional variants for cleft lip with or without cleft palate in or near *PAX7*, *FGFR2* and *NOG* by targeted sequencing of GWAS Loci. *Am J Hum Genet*. 2015;96:397–411.
9. Birnbaum S, Ludwig KU, Reutter H, et al. Key susceptibility locus for nonsyndromic cleft lip with or without cleft palate on chromosome 8q24. *Nat Genet*. 2009;41:473–477.
10. Grant SA, Wang K, Zhang H, et al. A genome-wide association study identifies a locus for nonsyndromic cleft lip with or without cleft palate on 8q24. *J Pediatr*. 2009;155:909–913.
11. Mangold E, Ludwig KU, Birnbaum S, et al. Genome-wide association study identifies two susceptibility loci for nonsyndromic cleft lip with or without cleft palate. *Nat Genet*. 2009;42:24–26.
12. Beaty TH, Murray JC, Marazita ML, et al. A genome-wide association study of cleft lip with and without cleft palate identifies risk variants near *MAFB* and *ABCA4*. *Nat Genet*. 2010;42:525–529.

13. Ludwig KU, Mangold E, Herms S, et al. Genome-wide meta-analyses of nonsyndromic cleft lip with or without cleft palate identify six new risk loci. *Nat Genet*. 2012;44:968–971.
14. Sun Y, Huang Y, Yin A, et al. Genome-wide association study identifies a new susceptibility locus for cleft lip with or without a cleft palate. *Nat Commun*. 2015;6:6414:doi:10.1038/ncomms7414
15. Leslie EJ, Carlson JC, Shaffer JR, et al. A multi-ethnic genome-wide association study identifies novel loci for non-syndromic cleft lip with or without cleft palate on 2p24.2, 17q23 and 19q13. *Hum Mol Genet*. 2016;25(13):2862–2872.
16. Marchini J, Cardon LR, Phillips MS, Donnelly P. The effects of human population structure on large genetic association studies. *Nat Genet*. 2004;36:512–517.
17. Li Q, Kim Y, Suktitipat B, et al. Gene-gene interaction among WNT genes for oral cleft in trios. *Genet Epidemiol*. 2015;39:385–394.
18. Xu H, Shete S. Effects of population structure on genetic association studies. *BMC Genet*. 2005;6(Suppl 1):S109–S113.
19. Yang Y, Cvekl A. Large Maf transcription factors: Cousins of AP-1 proteins and important regulators of cellular differentiation. *Einstein J Biol Med*. 2007;23:2–11.
20. Pan Y, Zhang W, Du Y, et al. Different roles of two novel susceptibility loci for nonsyndromic orofacial clefts in a Chinese Han population. *Am J Med Genet A*. 2011;155A:2180–2185.
21. Yuan QP, Blanton SH, Hecht JT. Association of *ABCA4* and *MAFB* with non-syndromic cleft lip with or without cleft palate. *Am J Med Genet A*. 2011;155A:1469–1471.
22. Lennon CJ, Birkeland AC, Nuňez JA, et al. Association of candidate genes with nonsyndromic clefts in Honduran and Colombian populations. *Laryngoscope*. 2012;122:2082–2087.
23. Fontoura C, Silva RM, Granjeiro JM, Letra A. Further evidence of association of the *ABCA4* gene with cleft lip/palate. *Eur J Oral Sci*. 2012;120:553–557.
24. Mi N, Hao Y, Jiao X, et al. Association study of single nucleotide polymorphisms of *MAFB* with non-syndromic cleft lip with or without cleft palate in a population in Heilongjiang Province, Northern China. *Br J Oral Maxillofac Surg*. 2014;52:746–750.
25. Yin X, Ma L, Li Y, et al. Genetic variants of 20q12 contributed to non-syndromic orofacial clefts susceptibility. *Oral Dis*. 2017;23(1):50–54.
26. Duan SJ, Huang N, Zhang BH, et al. New insights from GWAS for the cleft palate among han Chinese population. *Med Oral Patol Oral Cir Bucal*. 2017;22(2):e219–e227.
27. Yu Q, He S, Zeng N, et al. BMP7 Gene involved in nonsyndromic orofacial clefts in Western Han Chinese. *Med Oral Patol Oral Cir Bucal*. 2015;20:e298–304.
28. Rowlatt A, Hernández-Suárez G, Sanabria-Salas MC, et al. The heritability and patterns of DNA methylation in normal human colorectum. *Hum Mol Gene*t. 2016;25(12):2600–2611.

Nutritional assessment of patients with end-stage renal disease using the MNA scale

Łukasz Rogowski[1,A–D], Mariusz Kusztal[2,C,E], Tomasz Gołębiowski[2,B,C], Katarzyna Bulińska[3,B,C], Agnieszka Zembroń-Łacny[4,E], Joanna Wyka[5,E], Marian Klinger[2,E,F], Marek Woźniewski[3,E,F], Wioletta Dziubek[3,C–F]

[1] Nonpublic Medical College, Wrocław, Poland
[2] Department and Clinic of Nephrology and Transplantation Medicine, Faculty of Medicine, Wroclaw Medical University, Poland
[3] Department of Physiotherapy, University School of Physical Education, Wrocław, Poland
[4] Faculty of Medicine and Health Sciences, University of Zielona Góra, Poland
[5] Department of Human Nutrition, Faculty of Food Science, University of Environmental and Life Sciences, Wrocław, Poland

A – research concept and design; B – collection and/or assembly of data; C – data analysis and interpretation; D – writing the article; E – critical revision of the article; F – final approval of the article

Advances in Clinical and Experimental Medicine, ISSN 1899-5276 (print), ISSN 2451-2680 (online) *Adv Clin Exp Med.* 2018;27(8):1117–1123

Address for correspondence
Mariusz Kusztal
E-mail: mariok@o2.pl

Funding sources
The study was supported by a research grant from the National Science Centre of Poland (No. 2011/03/B/NZ7/01764, grant title: "The effects of exercise training on muscle regeneration activity in hemodialysis patients"; to WD). The funding agency had no role in the study design, collection, analysis, and interpretation of data, or the decision to submit this original work for publication.

Conflict of interest
None declared

Acknowledgements
The authors thank the nursing and medical staff at the Dialysis Center at the University Clinical Hospital in Wrocław for their friendly support.

Received on January 9, 2017
Reviewed on February 15, 2017
Accepted on June 30, 2017

Abstract

Background. Patient malnutrition is a significant problem in the process of rehabilitation and treatment. One of the tools that can reveal the risk of malnutrition is a series of standardized nutritional questionnaires.

Objectives. The aim of the study was to assess the nutritional status of patients with end-stage renal disease (ESRD) by means of the minimal nutritional assessment (MNA) scale.

Material and methods. The study group included respondents suffering from ESRD who were patients of the Dialysis Center at the Clinic of Nephrology and Transplantation Medicine at the University Clinical Hospital in Wrocław. The study was conducted in 47 dialysis patients (22 women and 25 men), mean age 69.68 ±8.95 years. A standardized MNA scale was used to evaluate the nutritional status of the patients.

Results. In the study group, women had a significantly lower score on the MNA scale than men (23.95 vs 25.26 points). Using the MNA scale, the risk of malnutrition was found in 13 patients, while malnutrition was found in 1 patient. Among females, the mean body mass index (BMI) was 27.28, and it was significantly correlated with the MNA score. In males, the mean BMI was 29.61, but it did not correlate with the MNA score. The time spent undergoing renal replacement therapy was 7.63 years for women and 7.24 years for men. This correlated significantly with the MNA score only in the case of men. Significant correlations were established between eating habits and MNA scores in both groups.

Conclusions. The results obtained using the MNA scale showed a significant risk of malnutrition in patients with ESRD. In women only, a low score on the MNA scale significantly correlated with the BMI. The time of renal replacement therapy had a significant impact on the MNA scale only in the case of men. An influence of comorbidities on the MNA scores recorded by men and women was not observed. Major health incidents and other stressful situations significantly affected the nutritional status in men.

Key words: nutritional status, chronic kidney failure, hemodialysis patients, minimal nutritional assessment

DOI
10.17219/acem/75604

Introduction

Kidney failure is an increasingly common disorder, affecting 11% of the world adult population.[1] It was estimated that in 2010 there were about 2 million patients worldwide in the end stage of this disease, i.e., being treated with renal replacement therapy. This number is expected to grow by as much as 7% per year.[2] It is estimated that there are 4 million patients with chronic kidney disease (CKD) in Poland, of whom 17,000 are being treated with renal replacement therapy.[3] For decades, it has been believed that the main cause of kidney disease was glomerulonephritis. However, the rapidly increasing number of cases has compelled the scientific community to re-examine the causes of kidney failure. Several studies have shown a strong correlation between the occurrence of metabolic disorders, such as diabetes and hypertension, and the development of kidney diseases or nephropathy. Knowing the main causes of kidney failure, it is hard not to notice that 2 of the 3 risk factors have a close relationship with the wider phenomenon known as the "diseases of civilization". A very important problem that often occurs and substantially affects the health of patients with CKD is malnutrition.[4–6] Extensive studies of patients with CKD in the Modification of Diet in Renal Disease (MDRD) project recorded weight loss in 21% of patients during the 14 months of observations.[7] Patients treated with long-term renal replacement therapy who have received a diagnosis of malnutrition are at a particularly increased risk of complications, and even death, during dialysis.[8] The problem of poor nutritional status of patients with CKD is even perceived as the main cause of poor clinical prognosis and mortality.[9–12] Numerous studies assessing the nutritional status of patients with CKD, using methods such as anthropometric assessments and biochemical evaluation, have shown a positive correlation with mortality.[4,5,13,14]

The causes of protein-energy malnutrition (PEM) are complex, resulting both from kidney diseases and concomitant diseases. The patients suffer from a general catabolic state, uremia, hormonal imbalance, lipid disorders, general disorders of the metabolism, and increased activity of pro-inflammatory cytokines. The problem of impaired sense of taste and suppression of appetite in patients with CKD is also not without significance and may also be psychological in nature, e.g., cause stress or depression.[5,15,16] The dialysis mechanism itself, in which blood is filtered through a dialyzer, is a heavy burden that could also contribute to malnutrition. The dialysis initiates protein catabolism, impairing the protein synthesis.[17,18] The key inducers of malnutrition are 2 factors: metabolic acidosis (MA) and the insufficient supply of nutrients. Unfortunately, MA is an inherent complication of kidney disease and its extent is dependent on the severity of renal failure.[16] Metabolic acidosis leads to a state of malnutrition, initiating the breakdown of proteins and the oxidation of amino acids, loss of muscle mass, inflammation, and increased mortality.[5,19] Studies have shown that MA leads to a negative nitrogen balance, also reducing the level of albumins.[20,21]

A very important factor that may influence the nutritional status are the dietary restrictions undertaken by the patients. In the course of the diagnosis of kidney disease, as well as diseases that initiate it (diabetes, high blood pressure), patients are shown dietary recommendations that can positively affect the disease process. Patients with CKD are recommended to control the supply of protein and phosphorus. It has been shown that reduced protein intake can prolong the time taken for the disease to evolve into full kidney failure. In addition, a reduced supply of proteins and phosphorus allows for a better control of MA and the electrolyte equilibrium.[10,18,22] Also, in the case of concomitant diseases, such as diabetes, hypertension and cardiovascular diseases, one strategy for supporting treatment is to modify the eating habits, in particular by strictly controlling the quality of energy substrates. Patients with end-stage renal disease (ESRD) no longer have to limit their protein intake (recommendations for healthy subjects); however, their restrictions include limiting the supply of phosphorus.[10] The supply of carbohydrates and fats should be sufficiently high, taking into account physical activity and comorbidities.[10] However, patients without ad hoc supervision by medical personnel or dieticians often cannot balance their diets sufficiently, which can in turn lead to an inadequate supply of nutrients and, eventually, PEM.[5,7,10,11]

A useful tool for the preliminary assessment of the nutritional status of patients is the use of standardized questionnaires evaluating nourishment levels. Such surveys are easy and quick to complete, do not require any special equipment, and can therefore be used by medical personnel and dieticians.[23] If the result is indicative of a "nutritional risk", more accurate (more expensive) methods of assessing nutritional status, e.g., anthropometric, biochemical or image-based assessments, namely, magnetic resonance imaging (MRI) and dual energy X-ray absorptiometry (DXA), can be employed.

In view of the very few reports on the use of minimal nutritional assessment (MNA) scale with stable hemodialysis outpatients, the aim o the study was to assess the nutritional status of patients with ESRD in a chronic hemodialysis therapy program. Secondary research aims were to assess the correlation of MNA scores with body mass index (BMI), the duration of dialysis therapy, and their relationship with the eating habits of ESRD patients, if any.

Materials and methods

The study group included patients over 60 years of age suffering from ESRD, recruited from the dialysis center of the Clinic of Nephrology and Transplantation Medicine at the Wroclaw Medical University and the International Dialysis Centre in Wrocław, Poland.

All patients were informed about the purpose of the questionnaire and signed written informed consent to participate in the study. Inclusion criteria were: a diagnosed CKD, hemodialysis treatment for at least 6 months and age >60 years. Exclusion criteria were: kidney transplant and lack of consent to participate in research.

In order to evaluate the nutritional status of the patients, a standardized full version of MNA scale was used. The MNA scale is a simple nutrition screening and assessment tool, designed to determine the possibility of malnutrition. It was designed mainly for monitoring geriatric patients and, since the majority of CKD patients are chronically ill people over the age of 60 (mean age 69.68 years), the MNA scale was preferred as the most suitable option. An important feature of the MNA scale is that some of the questions are not related to anthropometric characteristics, which (according to present authors) may help in the case of patients with ESRD. These patients usually undergo hemodialysis for 4 h 3 times a week; just before the dialysis they are weighed to determine the increase in the volume of fluid since the last dialysis (the water to be removed during dialysis). With this in mind, the personnel of the dialysis center use the so-called "dry body-weight" – the weight of the body after dialysis with no adverse symptoms (cramps, hypotonia or dizzin ess). This clinically defined dry body-weight may, therefore, change depending on the body's state of catabolism/anabolism and has a close relationship with appetite.

The MNA scale is characterized by high sensitivity and specificity.[24,25] Compared with BMI, it has a higher sensitivity for identifying the states of malnutrition.[26] A great advantage of MNA is its general availability and ease of use (quick diagnosis); therefore, it can be widely used in most healthcare facilities.

The results of the study were statistically analyzed using the STATISTICA v. 12 package (StatSoft, Tulsa, USA). Means and standard deviations (SDs) were determined as basic descriptive statistics. The normality of distributions was ascertained using the Shapiro-Wilk test. When examining differences in the distribution of variables between selected groups of men and women, Student's t-test for independent samples was used when the examined variable had a normal distribution. The exception was the comparison of test results, which did not meet the assumptions of a normal distribution. In this case the Mann-Whitney U test was used. Correlations were evaluated using Spearman's nonparametric rank-order correlation coefficient (p). The statistical significance was determined at a critical level of $\alpha = 0.05$.

Results

In both outpatient dialysis centers, the initial inclusion criteria were met by 80 people. During the study, the group was reduced because of a transplant (2 patients), lack of consent to complete the questionnaire (22 patients) and incorrectly filled questionnaire (9 patients).

Finally, a total of 47 patients remained to the end of the research project; their mean age was 69.68 ±8.95 years, 22 were female and 25 were male. Anthropometric measurements such as body mass and height were obtained, after which BMI values were calculated. Table 1 displays the patients' characteristics.

Table 1. Patient's characteristics

Variable	Females (n = 22)	Males (n = 25)	p-value
Age [years]	67.22 ±8.72	71.84 ±8.75	0.08
Body mass [kg]	67.46 ±18.81	85.22 ±12.45	0.0003
Body height [cm]	156.86 ±6.65	169.68 ±6.41	<0.00001
Waist circumference [cm]	93.11 ±15.34	104.94 ±11.98	0.004
Hip circumference [cm]	100.27 ±13.04	99.12 ±5.39	0.7
Dialysis [years]	7.6 ±4.04	7.24 ±4.49	0.75
Comorbidities [n]	2.63 ±1.36	3.3 ±1.24	0.09

The median MNA score was 25 (interquartile range [IQR] was 24–26,5) for females and 26,5 (IQR 23,5–28) for males. The mean MNA scores for both genders are shown in Fig. 1.

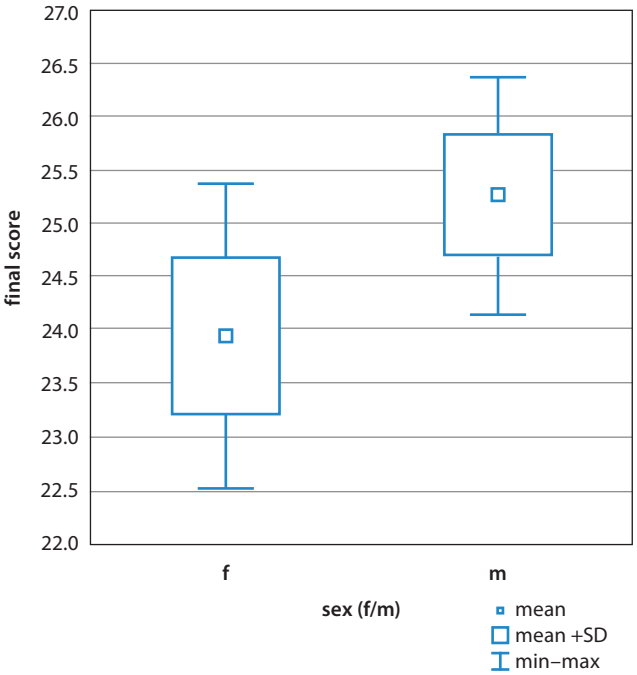

Fig. 1. Mean values of final minimal nutritional assessment (MNA) scores for women and men

Men had a higher mean value of BMI, and a lower SD (4.11). Women showed lower BMI values, while the SD was higher (6.65). It can be concluded that the female group exhibited fewer problems with overweight, while at the same time their body mass was more variable.

Table 2 displays the correlations between MNA scores and anthropometric indices: BMI and number of years of renal replacement therapy. The final scores of the MNA scale demonstrated a significant positive correlation with body mass and BMI scores only in the case of women. An association with the duration of renal replacement therapy and the final MNA scores was demonstrated only in males (Table 2).

Table 2. Spearman's rank correlation coefficients (p) of the final minimal nutritional assessment (MNA) scores with anthropometric indicators, body mass index (BMI) and the number of years of renal replacement therapy

Variable	MNA score for females (n = 22)	MNA score for males (n = 25)
Body mass [kg]	0.64 ($p < 0.05$)	0.007 ($p > 0.05$)
BMI index	0.62 ($p < 0.05$)	0.18 ($p > 0.05$)
Dialysis vintage [years]	−0.32 ($p > 0.05$)	−0.53 ($p < 0.05$)

In men, a clear correlation was observed with the scores for all research questions (Table 3). In women, the correlation was demonstrated only with the scores for the questions about weight loss, food intake amount and subjective assessment of nutritional status; there was no correlation with the scores for the questions about serious health incidents or about the quality of the food intake (dietary restrictions if any).

"A good nutritional status" was achieved by 33 patients, representing 70.2% of the total group. A "risk of malnutrition" was found in 13 patients (27.66% of the total group). The "state of malnutrition" was found in 1 patient (2.13% of the total). Fig. 2 displays nutritional status of men and women with ESRD.

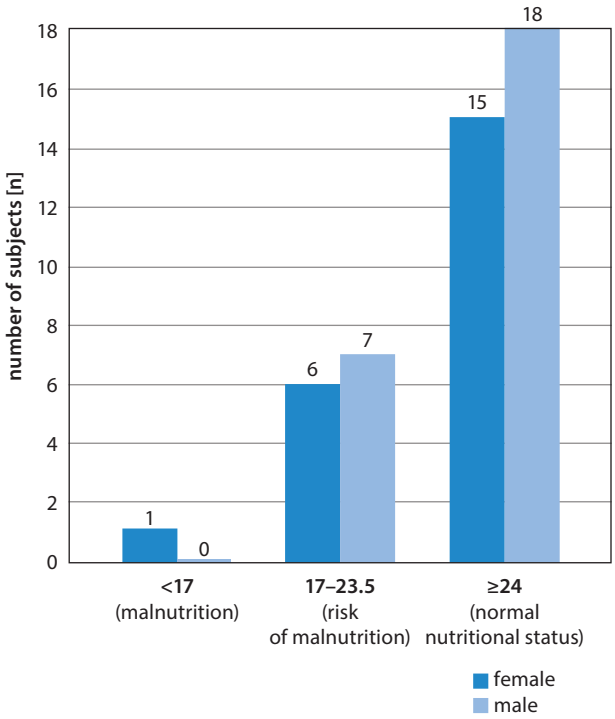

Fig. 2. Nutritional status of men and women with end-stage renal disease (ESRD) (MNA score)

Table 3. Spearman's rank correlation coefficients (p) for the final results with selected questions of the minimal nutritional assessment (MNA) scale

Question	Females (n = 22)	Males (n = 25)
Has there been a reduction in body mass in the past 3 months?	0.59*	0.51*
Has the patient suffered psychological stress or acute disease in the past 3 months?	0.36	0.48*
How many full meals a day does the patient consume?	0.48*	0.48*
Does the patient consume wholesome meals (dairy products, legumes or eggs, meat, fish, poultry)?	0.35	0.51*
Subjective assessment of nutritional status	0.64*	0.58*

* $p < 0.05$.

In the question concerning the reduction in body mass in the previous 3 months, 44% of male subjects and 45.45% of females reported a loss of 1–3 kg. This may be one of the factors explaining the lower MNA results in men, with no significant associations with the BMI (Table 4).

Table 4. Percentage distribution for scores on the question about weight loss

Question b: Weight loss during the last 3 months				
F/M [points]	0	1	2	3
% females*	0.00	4.6	45.4	50.00
% of total**	0.00	2.1	21.3	23.4
% males*	4.0	0.0	44.0	52.0
% of total**	2.1	0.0	23.4	27.7
Total %***	2.1	2.1	44.7	51.0

* in relation to female/male group; ** female/male in relation to whole group; *** female and male in relation to whole group of patients.

In the question about serious, stressogenic situations in the previous 3 months (question d), it was observed that as many as 20% of men reported such an event, while only 4.55% of women. This may also explain the low values of the final MNA score in men, even in the absence of significant correlations with the BMI (Table 5).

Table 5. Percentage ratio of responses to the question about stress/acute diseases

Question d: Has the patient suffered psychological stress or acute disease in the past 3 months?		
F/M [points]	0	2
% females*	4.5	95.5
% of total**	2.1	44.7
% males*	20.0	80.0
% of total**	10.6	42.6
Total %***	12.8	87.2

* in relation to female/male group; ** female/male in relation to whole group; *** female and male in relation to whole group of patients.

Percentage distribution of scores for the question about daily intake of full meals are shown in Table 6.

In the question regarding the number of full meals consumed, the maximum number of points was awarded for eating 3 full meals a day. As many as 40% of men and 31.82% of women reported consuming less than 3 full meals a day. Given the significant correlation of the final score with this question, this may provide an explanation for the lower MNA scores of patients with ESRD (Table 6).

Table 6. Percentage distribution of scores for the question about daily intake of full meals

Question j: How many full meals does the patient eat daily?			
F/M [points]	0	1	2
% females*	4.6	27.3	68.2
% of total**	2.1	12.8	31.9
% males*	0.0	40.0	60.0
% of total**	0.0	21.3	31.9
Total % ***	2.1	34.0	63.8

* in relation to female/male group; ** female/male in relation to whole group; *** female and male in relation to whole group of patients.

In the question regarding the frequency of eating wholesome products, 60% of men and 45.45% of women scored the maximum. This means that 40% of men and 54.54% of women indicated a limitation in terms of providing the body with wholesome products, which could potentially indicate some dietary restrictions (Table 7).

Table 7. Percentage distribution of scores for the question about eating wholesome products

Question k: Does the patient consume at least: 1 dairy product a day; legumes or eggs 2 or more times per week; meat, fish or poultry daily?			
F/M [points]	0	0.5	1
% females*	9.1	45.5	45.5
% of total**	4.3	21.3	21.3
% males*	8.0	32.0	60.0
% of total**	4.3	17.0	31.9
Total % ***	8.5	38.3	63.2

* in relation to female/male group; ** female/male in relation to whole group; *** female and male in relation to whole group of patients.

In the question requesting self-assessment of nutritional status, 92% of men and 77.27% of women did not express any concern about their nutritional status. However, 8% of men and 18.18% of women were not able to give an assessment of their nutritional status, and 4.55% of women reported a state of malnutrition (Table 8).

Table 8. Percentage distribution of scores for the question requesting a subjective assessment of nutritional status

Question o: Self view of nutritional status			
F/M [points]	0	1	2
% females*	4.6	18.2	77.3
% of total**	2.1	8.5	36.8
% males*	0.0	8.0	92.0
% of total**	0.0	4.3	48.9
Total % ***	2.1	12.8	85.1

* in relation to female/male group; ** female/male in relation to whole group; *** female and male in relation to whole group of patients.

Discussion

The medical community, aware of the significance of nutritional status in patient prognosis, has demonstrated that malnutrition is associated with increased mortality.[5,6,9] This fact has even been taken into account in jurisdiction. As of November 8, 2012, an amendment was introduced by the Minister of Health, dated January 1, 2012, introducing an obligation to carry out nutritional status assessment NRS 2002 (Nutritional Risk Screening 2002) or the SGA (Subjective Global Assessment) in each hospital ward, the results of which must accompany the patient disease history. Unfortunately, no such obligation was introduced in outpatient care of clinically stable patients. From the point of view of monitoring patient rehabilitation, a nutritional status assessment should be long-term-oriented and repeated periodically.

Many researchers have tried to evaluate the nutritional status of patients with CKD using dietary questionnaires, anthropometric methods and other techniques. Among dietary questionnaires, the subjective global assessment (SGA) has often been used; its score indicates a positive correlation with the objectively assessed state of nutrition.[27–30]

However, the SGA questionnaire is complex to use, because it requires an extensive physical examination, specifying many anthropometric characteristics.

The MNA scale is used less frequently and takes into account fewer anthropometric factors; however, it has been shown to be just as sensitive in detecting signs of malnutrition as the SGA.[31,32] The MNA scale is recommended in elderly patients, and it is precisely this group of subjects who represent the largest proportion of dialysis patients worldwide. The largest increase among all patients qualified for the dialysis treatment has been recorded in the 70+ age group. For example, in 2012 in Poland, 64% of all qualified persons were over 65 years of age.

In this study, all questions in the MNA scale were completed, even if the result in the 1st part of the MNA did not indicate a risk of malnutrition. This allowed the examination of the influence of factors (questions j and k) related to potential dietary restrictions among patients with ESRD.

Segall et al., in their extensive research using various forms of assessment of nutritional status, showed a strong correlation between malnutrition and risk of mortality in hemodialysis patients (out of 149 patients, 11 patients

who had obtained a low score in the SGA and for biochemical markers of malnutrition died in the follow-up period).[33] They also showed a strong correlation between the presence of diabetes and patient survival.

In this study, using the MNA to test nutritional status, there were 13 cases of malnutrition risk (6 women and 7 men) and 1 case of malnutrition. Significant correlations were demonstrated between the MNA score and body weight and the BMI, but only in women. In studies by other authors, such a correlation appeared in both sexes.[28]

In the studies cited above, no correlation was observed between low BMI in men and an MNA score indicative of malnutrition or the risk thereof. This is not surprising, bearing in mind the phenomenon of reverse epidemiology in the population of dialysis patients, i.e., overweight/obesity predicts lower mortality.[34]

One explanation of this fact could be a negative correlation with the years of renal replacement therapy. On average, women in the examined group were treated with renal replacement therapy for a longer period of time (Table 2), which, considering the changes taking place in the bodies of patients with ESRD, can result in a long-term reduction in body weight and BMI index.[5,19] The examined group of men were treated for a shorter period of time with renal replacement therapy on average (Table 2); therefore, such significant changes in body weight had not yet taken place; however, the variables not associated with body weight (questions about consumed meals, weight loss and dietary restrictions) did have an impact on the negative MNA result.

A random factor should also be taken into account: the examined group of men was characterized by a higher mean BMI (29.61) and a lower SD of this ratio (4.11). In other words, it was more homogenous compared with the group of women. This could also be a cause of the obtained results.

The influence of the length of time in renal replacement therapy on the MNA result can also be observed in the relationship between the median duration of dialysis (6 years) for the entire study group and the score obtained on the MNA questionnaire. Patients who had been undergoing dialysis for less than 6 years had a mean MNA score of 26.04, classifying their nutritional status as good. For the group that had been undergoing dialysis more than 6 years, the mean MNA score was 23.15, classifying them at risk of malnutrition. Similarly, Koor et al. and Brzosko et al. found a correlation between the duration of dialysis therapy and the risk of malnutrition.[28,35] The waist-to-hip ratio (WHR) ratio was not statistically significant in any of the groups.

In the abovementioned tests, the influence of factors related to events that may result in changes in body weight, as well as broader eating habits, were also analyzed. It has been shown that the outcome of MNA correlates with the score for the questions concerning weight loss and stressful events in the 3 months prior to the assessment. According to the authors, the MNA scale shows sensitivity in terms of detecting changes in health, to which patients with ESRD are particularly vulnerable. Patients with ESRD are forced to follow certain dietary restrictions, including the supply of phosphorus.[10,18,22] The question on the number of full meals (question j in the MNA scale) and the type of food products regularly consumed (question k) may reflect the eating habits of respondents and may be particularly important for patients with ESRD. In our study, a significant correlation between the scores for these questions and the result of the MNA scale was found. This may indicate that patients with ESRD, by following dietary recommendations, can counter-intuitively expose themselves to the risk of malnutrition. Similarly, the score on the question requesting a subjective assessment of the nutritional status correlates with the MNA result, indicating that the patients may actually feel a change in their nourishment status, even when their body weight remains normal. It is the opinion of the authors of this study, based on the reports of other authors, that in such circumstances it is necessary to consult with qualified personnel and perform further assessment of the nutritional status using more sensitive methods.[33,35]

The authors concluded that regular screening tests using the MNA scale can be a useful tool in the course of treatment and rehabilitation of patients with ESRD. Patients with ESRD are regularly weighed before commencing hemodialysis, so the sensitivity of the MNA scale can help in the assessment of adverse changes that may lead to the risk of malnutrition, even when normal body weight is maintained. In the case of negative MNA results, the patient should be immediately referred for more detailed tests to assess their nutritional status.

References

1. Zhang QL, Rothenbacher D. Prevalence of chronic kidney disease in population-based studies: Systematic review. *BMC Public Health*. 2008;8:117.
2. Lysaght MJ. Maintenance dialysis population dynamics: Current trends and long-term implications. *J Am Soc Nephrol*. 2002;13 (Suppl 1):37–40.
3. Król E, Rutkowski B. Przewlekła choroba nerek: Klasyfikacja, epidemiologia i diagnostyka. *Forum Nefrologiczne*. 2008;1:1–6.
4. Jadeja YP, Kher V. Protein energy wasting in chronic kidney disease: An update with focus on nutritional interventions to improve outcomes. *Indian J Endocrinol Metab*. 2012;16(2):246–251.
5. Bonanni A, Mannucci I, Verzola D, et al. Protein-energy wasting and mortality in chronic kidney disease. *Int J Environ Res Public Health*. 2011;8(5):1631–1654.
6. Kovesdy CP, Kalantar-Zadeh K. Why is protein-energy wasting associated with mortality in chronic kidney disease? *Semin Nephrol*. 2009;29(1):3–14.
7. Modification of Diet in Renal Disease Study Group. The modification of diet in renal disease study: Design, methods and results from the feasibility study. *Am J Kidney Dis*. 1992;20(1):18–33.
8. Lowrie EG, Lew NL. Death risk in hemodialysis patients: The predictive value of commonly measured variables and an evaluation of death rate differences between facilities. *Am J Kidney Dis*. 1990;15(5):458–482.
9. Peev V, Nayer A, Contreras G. Dyslipidemia, malnutrition, inflammation, cardiovascular disease and mortality in chronic kidney disease. *Curr Opin Lipidol*. 2014;25(1):54–60.
10. Toigo G, Aparicio M, Attman P, et al. Expert Working Group report on nutrition in adult patients with renal insufficiency (part 1 of 2). *Clin Nutr*. 2000;19(3):197–207.

11. Ikizler TA, Hakim RM. Nutrition in end-stage renal disease. *Kidney Int*. 1996;50(2):343–357.
12. Leavey SF, Strawderman RL, Jones CA, Port FK, Held PJ. Simple nutritional indicators as independent predictors of mortality in hemodialysis patients. *Am J Kidney Dis*. 1998;31(6):997–1006.
13. Jiang MY, Hwang JC, Lu YH, Wang CT. Clinical implications and outcome prediction in chronic hemodialysis patients with lower serum potassium×uric acid product. *Eur J Intern Med*. 2015;26(8):646–651.
14. Qureshi AR, Alvestrand A, Danielsson A, et al. Factors predicting malnutrition in hemodialysis patients: A cross-sectional study. *Kidney Int*. 1998;53(3):773–782.
15. Lynch KE, Lynch R, Curhan GC, Brunelli SM. Altered taste perception and nutritional status among hemodialysis patients. *J Ren Nutr*. 2013;23(4):288–295.
16. Kraut JA, Kurtz I. Metabolic acidosis of CKD: Diagnosis, clinical characteristics, and treatment. *Am J Kidney Dis*. 2005;45(6):978–993.
17. Ikizler TA, Pupim LB, Brouillette JR, et al. Hemodialysis stimulates muscle and whole body protein loss and alters substrate oxidation. *Am J Physiol Endocrinol Metab*. 2002;282(1):E107–116.
18. Stenvinkel P, Heimbürger O, Lindholm B, Kaysen GA, Bergström J. Are there two types of malnutrition in chronic renal failure? Evidence for relationships between malnutrition, infla mmation and atherosclerosis (MIA syndrome). *Nephrol Dial Transplant*. 2000;15(7):953–960.
19. Kraut JA, Madias NE. Metabolic acidosis of CKD: An update. *Am J Kidney Dis*. 2016;67(2):307–317.
20. Movilli E, Bossini N, Viola BF, et al. Evidence for an independent role of metabolic acidosis on nutritional status in hemodialysis patients. *Nephrol Dial Transplant*. 1998;13:674–678.
21. Ballmer PE, McNurlan MA, Hulter HN, Anderson SE, Garlick PJ, Krapf R. Chronic metabolic acidosis decreases albumin synthesis and induces negative nitrogen balance in humans. *J Clin Invest*. 1995;95(1):39–45.
22. Fouque D, Laville M. Low protein diets for chronic kidney disease in non-diabetic adults. *Cochrane Database Syst Rev*. 2009;8(3):6–8.
23. Green SM, Watson R. Nutritional screening and assessment tools for older adults: Literature review. *J Adv Nurs*. 2006;54(4):477–490.
24. Guigoz Y. The Mini Nutritional Assessment (MNA) review of the literature: What does it tell us? *J Nutr Health Aging*. 2006;10(6):466–485.
25. Vellas B, Guigoz Y, Garry PJ, et al. The Mini Nutritional Assessment (MNA) and its use in grading the nutritional state of elderly patients. *Nutrition*. 1999;15(2):116–122.
26. Burman M, Säätelä S, Carlsson M, Olofsson B, Gustafson Y, Hörnsten C. Body mass index, mini nutritional assessment, and their association with five-year mortality in very old people. *J Nutr Health Aging*. 2015;19:461–467.
27. Kondrup J, Allison SP, Elia M, Vellas B, Plauth M. ESPEN guidelines for nutrition screening 2002. *Clin Nutr*. 2003;22:415–421.
28. Koor BE, Nakhaie MR, Babaie S. Nutritional assessment and its correlation with anthropometric measurements in hemodialysis patients. *Saudi J Kidney Dis Transpl*. 2015;26(4):697–701.
29. Steiber A, Leon JB, Secker D, et al. Multicenter study of the validity and reliability of subjective global assessment in the hemodialysis population. *J Ren Nutr*. 2007;17(5):336–342.
30. Tan SK, Loh YH, Choong LH, Suhail SM. Subjective global assessment for nutritional assessment of hospitalized patients requiring hemodialysis: A prospective cohort study. *Nephrology (Carlton)*. 2016;21(11):944–949.
31. Santin FG, Bigogno FG, Dias Rodrigues JC, Cuppari L, Avesani CM. Concurrent and predictive validity of composite methods to assess nutritional status in older adults on hemodialysis. *J Ren Nutr*. 2016;26(1):18–25.
32. Tsai AC, Wang JY, Chang TL, Li TY. A comparison of the full Mini Nutritional Assessment, short-form Mini Nutritional Assessment, and Subjective Global Assessment to predict the risk of protein-energy malnutrition in patients on peritoneal dialysis: A cross-sectional study. *Int J Nurs Stud*. 2013;50(1):83–89.
33. Segall L, Mardare NG, Ungureanu S, et al. Nutritional status evaluation and survival in hemodialysis patients in one center from Romania. *Nephrol Dial Transplant*. 2009;24(8):2536–2540.
34. Ladhani M, Craig JC, Irving M, Clayton PA, Wong G. Obesity and the risk of cardiovascular and all-cause mortality in chronic kidney disease: A systematic review and meta-analysis. *Nephrol Dial Transplant*. 2017;32(3):439–449.
35. Brzosko S, Hryszko T, Kłopotowski M, Myśliwiec M. Validation of Mini Nutritional Assessment scale in peritoneal dialysis patients. *Arch Med Sci*. 2013;9(4):669–676.

Correlation analysis for school-age children's height and refractive errors

Jiawei Chen[A–F], Zhenguo Chen[A,B,F], Sisi Lin[A,B,D,F], Jiayu Zhang[B–D], Qiang Wang[B,D], Hongliang Zhong[B,E,F], Daqiu Cai[C,E,F]

Department of Ophthalmology, 3rd Affiliated Hospital of Wenzhou Medical University, China

A – research concept and design; B – collection and/or assembly of data; C – data analysis and interpretation; D – writing the article; E – critical revision of the article; F – final approval of the article

Advances in Clinical and Experimental Medicine, ISSN 1899-5276 (print), ISSN 2451-2680 (online) *Adv Clin Exp Med*. 2018;27(8):1125–1130

Address for correspondence
Zhenguo Chen
E-mail: chenzhenguo016@163.com

Funding sources
The study was supported by research grants from the project of Science and Technology Bureau in Ruian, China (20130211).

Conflict of interest
None declared

Received on March 20, 2017
Reviewed on April 11, 2017
Accepted on October 20, 2017

Abstract

Background. During the rapid physical and mental development, school-age children, who are beginning the learning phase, have an increasingly heavy burden on their eyes.

Objectives. The aim of this study was to analyze the association of refractive errors with body height in children aged 7–14 years.

Material and methods. A total of 1,696 children aged 7–14 years were consecutively enrolled. Children's age, sex, height, uncorrected and corrected visual acuity were collected. Children's refractive errors were tested using static retinoscopy, and converted to the spherical equivalent refraction. The prevalence of refractive errors in different height groups were measured.

Results. The children were divided into an ultra-low-height group, a low-height group, a high-height group and an ultra-high-height group as per the height standard of children aged 3–16 years generally used in China. With the increase of body height, the prevalence of myopia was also increased, which was 39.2% in the ultra-low-height group, 46.3% in the low-height group, 49.1% in the high-height group, and 58.0% in the ultra-high-height group. Most of the myopic children suffered from low myopia. Results from the regression analysis showed that there was no difference in the prevalence of myopia between the high--height group and ultra-high-height group ($p = 0.145$), but it was increased significantly proportionately to the increase of body height ($p < 0.001$).

Conclusions. The prevalence of myopia exhibits an increased tendency with height development in children aged 7–14 years. Additionally, school-age children often develop low or moderate myopia rather than high myopia.

Key words: height, refractive error, school-age children

DOI
10.17219/acem/78773

Introduction

During rapid physical and mental development, school-age children, who are beginning the learning phase, have an increasingly heavy burden put on their eyes. Myopia is the most common form of refractive error.[1] China is one of those countries with the highest prevalence of myopia in the world, and, moreover, with the economic and scientific development, the prevalence of juvenile myopia is increasing every year.[2]

It is noticed that a child's body height increases quickly during the refractive development and involves multiple factors.[3] However, the correlation between the body height and refractive development of school-age children has rarely been reported.

A study in China involving 553 twin pairs showed that the axial length (AL) and height were concomitant in children between the ages of 7 and 15 years.[4] This study found that boys experienced more pronounced changes in stature, whereas girls had greater changes in AL. This suggested that the growth of the eye and the changes in height may be governed by different mechanisms. Still, previous experience has suggested that children with relatively high-height are more likely to develop myopia, but there is no relevant data to confirm this. Therefore, to explore the correlation between the body height and refractive errors in school-age children, we collected and analyzed the clinical data from 1,696 school-age children in this study.

Material and methods

Participants

From June 2012 to June 2014, 1,696 school-age children (3,392 eyes) seeking medical advice at the Department of Ophthalmology, 3rd Affiliated Hospital of Wenzhou Medical University, China, were enrolled in this study, including 1,000 boys (2,000 eyes) and 696 girls (1,392 eyes). The spherical equivalent ranged from +6.5 D to –11.5 D. These children never had any ocular surgery and intraocular disease, which was confirmed by a slit lamp and ophthalmoscope, and those with orthokeratology lens or rigid contact lens were excluded.

Informed consent

The study protocol was approved by the Ethics Committee of the hospital. The benefits and risks of participating in the trial were explained to the children's guardians, and written informed consent was obtained before the trial.

Data measurement and collection

Children's sex, age, height [cm], uncorrected and corrected visual acuity were measured and recorded. A cycloplegic agent, 10 g/L cyclopentolate, was dropped into the eyes 3 times with an interval of 5 min. After 20 min, children with the absence of the pupillary light reflex and the pupil size of >6 mm were confirmed to have cycloplegia. After 30 min, static retinoscopy was used to determine refractive errors in children with cycloplegia by an experienced optometrist, and the data was converted to the spherical equivalent refraction that was equal to the spherical power plus 1/2 cylinder power. After that, all the children were assigned into hyperopia (≥0.50 D), emmetropia (from –0.75 D to 0.50 D), myopia (≤–0.75 D) groups. Furthermore, the myopia group was subdivided into low myopia (from –3.0 D to –0.75 D), moderate myopia (from –6.0 D to –3.0 D) and high myopia (≤–6.0 D) groups.

According to the height standard of children aged 3–16 years generally used in China, these children were divided into different groups according to their age, respectively.[5] Subjects of the same age were divided into ultra-low-height group (≤3 percentile height), low-height group (3–50 percentile height), high-height group (50–97 percentile height), and ultra-high-height group (>97 percentile height).

Statistical analysis

Measurement data is expressed as the mean ± standard deviation (SD) and statistically analyzed by SPSS 11.5 (SPSS Inc., Chicago, USA). Multivariate non-conditional logistic regression analysis was used to establish a regression analysis model based on refractive errors and body height. A value of $p < 0.05$ was considered statistically significant.

Results

General information

A total of 1,696 school-age children (3,392 eyes), 7–14 years of age, were recruited in this study. Their spherical equivalent ranged from +6.5 D to –11.5 D and the mean height was 140.53 ±12.89 cm. There were 1,000 boys (2,000 eyes) with the spherical equivalent ranging from +6.25 D to –8.00 D and the mean height of 140.39 ±12.42 cm; 696 girls (1,392 eyes) with the spherical equivalent ranging from +5.00 D to –7.00 D and the mean height of 140.80 ±13.51 cm.

Refractive development in children

All the age groups of school-age children (7–14 years) were summed up as follows: 148 children (88 boys, 60 girls) in the ultra-low-height group, 808 (500 boys, 308 girls) in the low-height group, 640 (372 boys, 268 girls) in the high-height group, 100 (40 boys, 60 girls) in the ultra-high-height group.

As shown in Fig. 1, the prevalence of myopia was 39.2% in the ultra-low-height group, 46.3% in the low-height group, 49.1% in the high-height group, and 58.0% in the

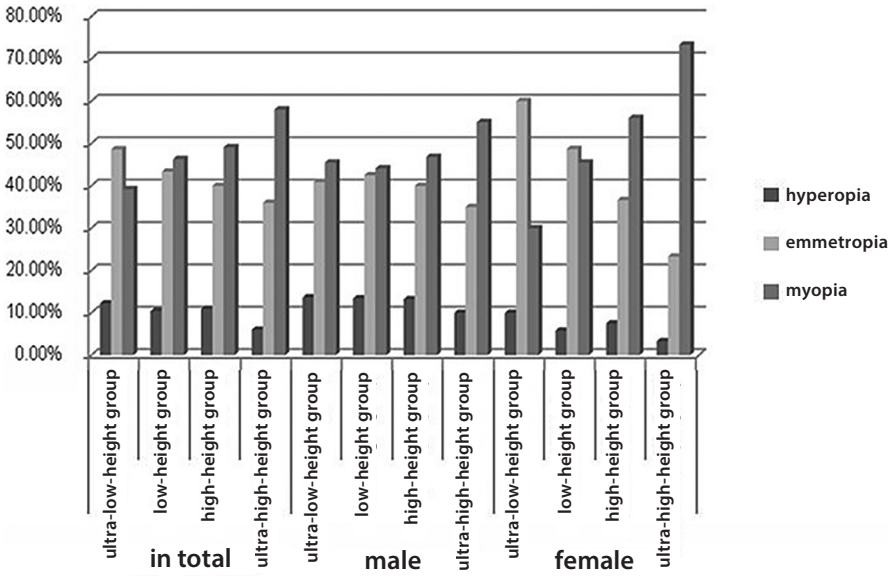

Fig. 1. Prevalence of myopia, emmetropia and hyperopia in school-age children from different height groups

ultra-high-height group, indicating the prevalence of myopia had increased along with the increase of the body height. Conversely, the prevalence of emmetropia was decreased with the increasing body height, which was 48.6%, 43.3%, 40.0%, and 36.0% in the 4 height groups, respectively. Additionally, no significant correlation was found between body height and the prevalence of hyperopia, which was 12.2%, 10.4%, 10.9% and 6.0% in the 4 height groups, respectively.

For the boys, the prevalence of myopia was 45.5%, 44.1%, 46.8%, and 55.0% in the ultra-low-height group, low-height group, high-height group, and ultra-high-height group, respectively; the prevalence of emmetropia was 40.9%, 42.5%, 40.0%, and 35.0%, respectively; the prevalence of hyperopia was 13.60%, 13.4%, 13.2%, and 10.0%, respectively. The prevalence rates of both emmetropia and hyperopia were lower in the ultra-high-height group than in the other 3 groups.

For the girls, the prevalence of myopia in the 4 groups was ordered from low to high: the ultra-low-height group (30.0%) < low-height group (45.5%) < high-height group (56.0%) < ultra-high-height group (73.3%); the prevalence of emmetropia was ordered from high to low as follows: the ultra-low-height group (60.0%) > low-height group (48.7%) > high-height group (36.5%) > ultra-high-height group (23.4%). The prevalence of hyperopia was 10.0% in the ultra-low-height group, which was the highest compared with 5.8% in the low-height group, 7.5% in the high-height group and 3.3% in the ultra-high-height group, i.e., the prevalence of hyperopia was the highest in the ultra-low-height group, but had no association with the height growth.

The degree of myopia in these school-age children who mainly suffered from low-to-moderate myopia is provided in Fig. 2. The prevalence of high myopia was the lowest, sequentially followed by that of moderate myopia and low myopia. Moreover, there was no significant difference in the degree of myopia among the 4 height groups.

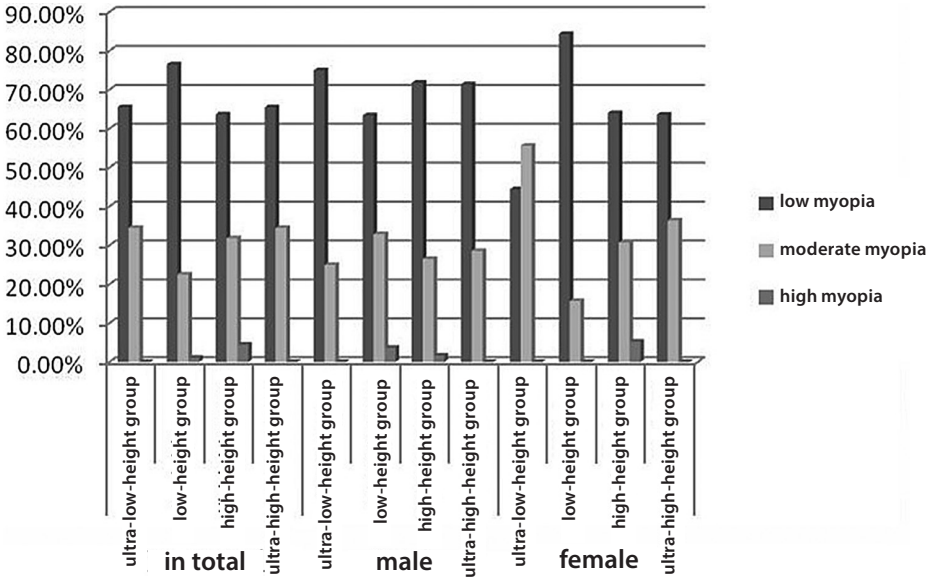

Fig. 2. Prevalence of low, moderate or high myopia in school-age children from different height groups

Refractive errors in different height groups

In the ultra-low-height group, the mean spherical equivalent was –1.01 ±1.46 D (range: from 0.75 to –4.50 D) for the boys and –0.76 ±1.55 D (range: from 1.25 to –3.75 D) for the girls. The overall mean spherical equivalent of the ultra-low-height group was –0.92 ±1.49 D (range: from 1.25 to –4.50 D).

In the low-height group, the mean spherical equivalent was –0.98 ±1.71 D (range: from 6.25 to –6.50 D) for the boys and –0.86 ±1.19 D (range: from 1.25 to –5.50 D) for the girls. The overall mean spherical equivalent of the low-height group was –0.94 ±1.53 D (range: from 6.25 to –6.50 D).

In the high-height group, the mean spherical equivalent was –1.08 ±1.90 D (range: from 5.25 to –8.00 D) for the boys and –1.36 ±2.02 D (range: from 5.25 to –7.00 D) for the girls. The overall mean spherical equivalent of the high-height group was –1.20 ±1.95 D (range: from 5.25 to –8.00 D).

In the ultra-high-height group, the mean spherical equivalent was –0.75 ±1.42 D (range: from 0.75 to –4.25) for the boys and –1.91 ±1.63 D (range: from 0.75 to –5.25 D) for the girls. The overall mean spherical equivalent of the ultra-high-height group was –1.45 ±1.64 D (range: from 0.75 to –5.25 D).

Body height in school-age children

These school-age children mostly had normal body height. Of the 1,000 boys, 8.8% were in the ultra-low-height group, 50% in the low-height group, 37.2% in the high-height group, and 4.0% in the ultra-high-height group; of the 696 girls, 5.8% were in the ultra-low-height group, 44.3% in the low-height group, 38.5% in the high-height group, and 8.6% in the ultra-high-height group. Overall, there were 8.7% of the children in the ultra-low-height group, 47.6% in the low-height group, 37.7% in the high-height group, and 5.9% in the ultra-high-height group.

Regression analysis of refractive errors

The collinearity analysis revealed that age was highly collinear with eyes, gender and body height. Results from the likelihood ratio test showed that left, right or bilateral eyes had no significant differences in the regression model, where not age ($p = 0.601$; >0.05), but gender and height exhibited significant differences ($p < 0.05$). Results from the regression analysis of refractive errors with gender and height are shown in Table 1.

With the height growth, the number of children with hyperopia was decreased. Moreover, the prevalence rate of hyperopia was higher in the boys than in the girls. But no significant difference in the prevalence of hyperopia was found among the 4 height groups ($p > 0.05$). In contrast, the increasing prevalence of myopia was driven by the increase in the body height. But there were no significant differences between the high-height and ultra-high-height groups ($p = 0.145$) as well as between boys and girls ($p = 0.880$).

Regression analysis of degree of myopia

The colinearity analysis showed that age was highly collinear with eyes, gender and body height. Results from the likelihood ratio test showed gender ($p = 0.369$; >0.05) and eyes ($p = 0.602$; >0.05) had no significant differences in the regression model, where not age, but the body height exhibited a significant difference ($p < 0.05$). Results from the regression analysis of refractive errors with the body height are shown in Table 2.

Table 1. Multivariate non-conditional logistic regression analysis of the refractive status with gender and height in school-age children

Refractive status[a]		Correlation coefficient	df	Sig.	p-value
Hyperopia	intercept	–2.349	1	0.000	–
	ultra-low-height group	0.370	1	0.161	1.448
	low-height group	0.347	1	0.149	1.414
	high-height group	0.540	1	0.026	1.715
	ultra-high-height group	0[b]	0	–	–
	boys	0.666	1	0.000	1.946
	girls	0[b]	0	–	–
Myopia	intercept	0.631	1	0.000	–
	ultra-low-height group	–0.618	1	0.000	0.539
	low-height group	–0.422	1	0.000	0.656
	high-height group	–0.224	1	0.034	0.800
	ultra-high-height group	0[b]	0	–	–
	boys	–0.105	1	0.023	0.900
	girls	0[b]	0	–	–

Sig. – significance level; [a] emmetropia serves as reference; [b] ultra-high-height group serves as reference.

Table 2. Multivariate non-conditional logistic regression analysis of the degree of myopia with age and height in school-age children

Degree of myopia[a]		Correlation coefficient	df	Sig.	p-value
Low myopia	intercept	18.399	1	0.000	–
	ultra-low-height group	0.000	1	1.000	1.000
	low-height group	–14.129	1	0.000	7.306×10^{-7}
	high-height group	–15.740	1	0.000	1.460×10^{-7}
	ultra-high-height group	0[b]	0	–	–
Moderate myopia	intercept	17.757	1	0.000	–
	ultra-low-height group	0.000	1	1.000	1.000
	low-height group	–14.713	1	0.000	4.077×10^{-7}
	high-height group	–15.791	1	–	1.387×10^{-7}
	ultra-high-height group	0[b]	0	–	–

Sig. – significance level; [a] high myopia serves as reference; [b] ultra-high-height group serves as reference.

The prevalence of low myopia showed no significant difference between the ultra-low-height and ultra-high-height group ($p = 1.000$), but it was significantly higher in the ultra-high-height group than in the low- and high-height groups ($p < 0.001$). The prevalence of moderate myopia was significantly lower in the low-height group than in the high-height group ($p < 0.001$), but there was no significant difference between the ultra-low-height and ultra-high-height groups ($p = 1.000$).

Discussion

The refractive development of children is related to many factors, such as close work, especially in reading, writing, watching TV, etc. Such major environmental factors, especially the wide application of electronic equipment, can result in an increase in children's myopia; secondly, there is a certain relationship between the education levels and the refractive development.[6–8] Myopia is in a close relationship with genetic factors; if the parents or siblings have high myopia, the incidence of myopia will be increased.[9,10] But the main factor in the refractive development is the growth of the eye axis. Research shows that the axial growth 0.3–0.5 mm rose has risen by an average of 1 diopter.[11,12] A large number of studies suggest the correlation between the eye axis and height. The study by Saw et al. showed that in Singaporean children, the AL was +0.29 mm longer in boys and +0.32 mm longer in girls for every 0.10 m difference in height.[13] The data from Wong et al. showed that among Singaporean Chinese adults, taller persons were more likely to have longer AL.[14] In the study by Wang et al., longitudinal changes of AL and height were concluded to occur concomitantly in children.[4] In a study by Ojaimi et al., of 1,765 Sydney year-1 school students, children in the 1st quintile for height had an average AL of 22.39 ±0.04 mm, compared with 22.76 ±0.04 mm in children in the 5th quintile.[15] Our study aimed to explore the correlation between the types of refractive errors and the same-age children height.

In our study, school-age children aged 7–14 mainly developed hyperopia and emmetropia, but nearly half of these children suffered from myopia with an incidence of 47.5%. The prevalence rates of low, moderate and high myopia were 69.9%, 27.9%, and 2.2%, respectively. Compared with the boys, the prevalence of myopia was slightly higher, but the prevalence of moderate myopia was slightly lower in the girls.

Among the children of the same age, the overall prevalence of myopia was increased in proportion to the increased body height in both boys and girls. That is, the higher the body height, the higher the incidence of myopia. For the boys, the prevalence rate of hyperopia was similar among the ultra-low-height, low-height and high-height groups, but it was a little lower in the ultra-high-height group compared with the former 3 groups. For the girls, the prevalence rate of hyperopia was similar among the low-height, high-height and ultra-high-height groups, but it was slightly lower in the ultra-low-height group compared with the former 3 groups. The overall prevalence of hyperopia showed a decreasing trend along the increase of the body height, with a dramatical decrease in the ultra-high-height group. For the boys, the prevalence of emmetropia was higher in the high-height and ultra-high-height groups than in the ultra-low-height and low-height groups; the contrary was the case for the girls, where the prevalence of emmetropia was lower in the high-height and ultra-high-height groups than in the ultra-low-height and low-height groups.

Low myopia was the main type of myopia in the 4 height groups. In the ultra-low-height and ultra-high-height groups, the prevalence of moderate myopia was lower in the boys than in the girls; but in the low- and high-height groups, i.e., within the normal range of height, the prevalence of moderate myopia was higher in the boys than in the girls. Compared with low and moderate myopia, high myopia was less reported in the 4 height groups, and what is more, there was no high myopia case in the ultra-low-height and ultra-high-height groups. In the low-height group, only few boys suffered from high myopia; however,

high myopia was found both in the boys and in the girls from the high-height group. However, the occurrence and development of high myopia were close associated with a genetic factor, and further studies are needed to confirm the direct connection between high myopia and the body height.

School-age children mostly have normal height. In this study, only 8.7% of children were assigned to the ultra-low-height group and 5.9% were in the ultra-high-height group. In the ultra-low-height group, the boys and girls were in equal proportions; in the ultra-high-height group, the proportion of girls was higher than that of boys.

Findings from the multivariate non-conditional logistic regression analysis showed that at the same age, an increase in the prevalence of myopia was proportional to the increase of the body height, but there was no difference between the high-height and ultra-high-height group. Myopic children mostly suffered from low myopia, followed by moderate myopia. Additionally, there were many children developing moderate myopia in the high-height group with a higher prevalence of moderate myopia. These results indicate that the intraocular structure develops relatively fast in children who are taller than their peers. There is a consensus that the extension of the optic axis plays an important role in myopia occurrence and development.[16–19] Some studies suggest that the height development is associated with the optic axis, i.e., the optic axis increases proportionally in the children with a rapid development in the body height, thereby resulting in an quickened increase in refractive errors.[15]

Whether there are corresponding endocrine changes related to the increase of body height that accelerate the development of myopia need to be further studied. Here, the refractive monitoring is preferred for school-age children who are taller than their peers. Considering the relatively high incidence of high myopia in the ultra-low-height and ultra-high-height groups, a large-sample study will be carried out in the future.

References

1. Saw S, Katz J, Schein OD, Chew S, Chan T. Epidemiology of myopia. *Epidemiol Rev.* 1996;18(2):175–187.
2. Fredrick DR. Myopia. *BMJ.* 2002;324:1195–1199.
3. Hua M, Mo XF. Factors influencing axial length and the predictive value of axial length for myopia. *Zhonghua Yanshiguangxue yu Shijuekexue Zazhi.* 2013;25:441–444.
4. Wang D, Ding X, Liu B, Zhang J, He M. Longitudinal changes of axial length and height are associated and concomitant in children. *Invest Ophthalmol Vis Sci.* 2011;52(11):7949–7953.
5. Li H, Ji CY. Height and weight standardized growth charts for Chinese children and adolescents aged 0 to 18 years. *Zhonghua Erke Zazhi.* 2009;47:487–492.
6. Saw SM, Hong R, Zhang M, et al. Near-work activity and myopia in rural and urban schoolchildren in China. *J Pediatr Ophthalmol Strabismus.* 2001;38(3):149–155.
7. Saw S, Chua W, Hong C, et al. Nearwork in early-onset myopia. *Invest Ophthalmol Vis Sci.* 2002;43(2):332–339.
8. Ip JM, Saw SM, Rose KA, et al. Role of near work in myopia: Findings in a sample of Australian school children. *Invest Ophthalmol Vis Sci.* 2008;49(7):2903–2910.
9. Teikari JM, Donnell JAO, Kaprio J, Koskenvuo M. Impact of heredity in myopia. *Hum Hered.* 1991;41(3):151–156.
10. Fotouhi A, Etemadi A, Hashemi H, Zeraati H, Baileywilson JE, Mohammad K. Familial aggregation of myopia in the Tehran Eye Study: Estimation of the sibling and parent-offspring recurrence risk ratios. *Br J Ophthalmol.* 2007;91(11):1440–1444.
11. Grosvenor T, Scott R. Role of the axial length/corneal radius ratio in determining the refractive state of the eye. *Optom Vis Sci.* 1994; 71(9):573–579.
12. Mallen EAH, Gammoh Y, Albdour MD, Sayegh FN. Refractive error and ocular biometry in Jordanian adults. *Ophthalmic Physiol Opt.* 2005;25(4):302–309.
13. Saw SM, Chua WH, Hong CY, et al. Height and its relationship to refraction and biometry parameters in Singapore Chinese children. *Invest Ophthalmol Vis Sci.* 2002;43(5):1408–1413.
14. Wong TY, Foster P, Johnson GJ, Klein BEK, Seah SKL. The relationship between ocular dimensions and refraction with adult stature: The Tanjong Pagar survey. *Invest Ophthalmol Vis Sci.* 2001;42(6):1237–1242.
15. Ojaimi E, Morgan IG, Robaei D, et al. Effect of stature and other anthropometric parameters on eye size and refraction in a population-based study of Australian children. *Invest Ophthalmol Vis Sci.* 2005;46(12):4424–4429.
16. Hepsen IF, Evereklioglu C, Bayramlar H. The effect of reading and near-work on the development of myopia in emmetropic boys: A prospective, controlled, three-year follow-up study. *Vision Res.* 2001;41(19):2511–2520.
17. Long PZ, Yang GJ, Liao ZH. Optic axial length and myopia. *Zhonghua Yanke Zazhi.* 1998;75:132–145.
18. Grosvenor T, Goss DA. Role of the cornea in emmetropia and myopia. *Optom Vis Sci.* 1998;75(2):132–145.
19. Flitcroft DI. Emmetropisation and the aetiology of refractive errors. *Eye.* 2014;28(2):169–179.

Quantitative anatomy of the liver visceral surface in the human fetus

Monika Paruszewska-Achtel[A–D], Małgorzata Dombek[A–C], Mateusz Badura[B,C], Gabriela M. Elminowska-Wenda[B,C], Marcin Wiśniewski[B], Michał Szpinda[A,D–F]

Department of Normal Anatomy, Collegium Medicum in Bydgoszcz, Nicolaus Copernicus University in Toruń, Poland

A – research concept and design; B – collection and/or assembly of data; C – data analysis and interpretation; D – writing the article; E – critical revision of the article; F – final approval of the article

Advances in Clinical and Experimental Medicine, ISSN 1899-5276 (print), ISSN 2451-2680 (online) *Adv Clin Exp Med*. 2018;27(8):1131–1139

Address for correspondence
Michał Szpinda
E-mail: michal.szpinda@cm.umk.pl

Funding sources
None declared

Conflict of interest
None declared

Received on March 4, 2016
Reviewed on March 26, 2017
Accepted on June 2, 2017

Abstract

Background. Understanding liver growth is relevant in both determining the status of normative fetal development and prenatal detection of its disorders.

Objectives. This study attempted to examine age-specific reference intervals and the best-fit growth dynamics of the liver visceral surface for hepatic height, length, isthmic diameter, oblique diameters, circumferences of individual lobes, and total liver circumference.

Material and methods. Using anatomical, digital and statistical methods, the liver visceral surface was measured in 69 human fetuses of both sexes (32 males and 37 females) aged 18–30 weeks, derived from spontaneous abortions and stillbirths.

Results. The statistical analysis showed no sex differences. The best growth models mostly followed natural logarithmic functions, except for the length of the fissure for ligamentum teres hepatis and the length of fossa for gallbladder, which increased commensurately. Neither the length of fissure for ductus venosus nor the length of sulcus for inferior vena cava modeled the best-fit curves. The vertical-to-transverse diameter ratio of the liver was constant and averaged 0.75 ±0.12, while the isthmus ratio significantly altered from 0.78 ±0.07 at 18–19 weeks through 0.68 ±0.05 at 26–27 weeks to 0.72 ±0.07 at 28–30 weeks of gestation.

Conclusions. With no sexual differences, the liver morphometric parameters increased either logarithmically (lengths of: transverse diameter, vertical diameter, right oblique diameter, left oblique diameter, isthmic diameter and porta hepatis, circumferences of: right lobe, left lobe, quadrate lobe, caudate lobe, and total liver circumference) or proportionately (length of fissure for ligamentum teres hepatis, length of fossa for gallbladder). The quantitative data of the growing liver may be relevant in both the ultrasound monitoring of fetuses and early detection of congenital liver anomalies.

Key words: liver, human fetus, size, visceral surface, growth dynamics

DOI
10.17219/acem/74375

Introduction

Liver size is a beneficial parameter in the diagnosis and monitoring of intrauterine growth retardation (IUGR), as well as in determining the status of fetal growth.[1–4] Its abnormal size may result from maternal gestational diabetes, isoimmunization, intrauterine infections, heart malformations, tumors, some metabolic diseases, and either microsomia or macrosomia.[5–9] The fetal liver is the very first organ to reveal an abnormal pregnancy.[10] Reduction in liver size may be caused by IUGR, fetal erythroblastosis, anemia, thalassemia, and disturbances in the transport of oxygen with Bart's hemoglobin.[11–14] According to Fleischer et al., liver size is a good indicator of clinical pregnancies complicated by serological conflicts.[5] As a useful reference parameter for ultrasound examination, liver size provides us with quantitative and qualitative information concerning both liver structure and function.[15] Both autopsy examinations and modern in utero imaging techniques provide suitable quantitative evidence about fetal growth and organ development.[16] Knowledge on the normative liver growth is relevant in monitoring normal development and plays an essential role in prenatal detection of its malformations.[17]

To date, however, apart from anatomical research on the quantitative analysis of the fetal liver performed by Albay et al., no nomograms concerning its visceral surface have been computed.[12] Thus, in the present study we aimed to examine the liver visceral surface, as follows:

- age-specific reference intervals with respect to gestational age of the 15 linear hepatic dimensions (height, length, right and left oblique diameters, isthmic diameter, length of fissure for ligamentum teres hepatis, length of fissure for ductus venosus, length of fossa for gallbladder, length of sulcus for inferior vena cava, and length of porta hepatis, as well as circumferences of 4 individual lobes and total circumference);
- possible sex differences in the parameters studied;
- the best-fit growth curves for each morphometric parameter studied;
- the relative growth dynamics of the fetal liver (transverse-to-vertical diameter ratio, isthmus ratio).

Material and methods

The research material consisted of 69 human fetuses of both sexes (32 males and 37 females) aged from 18 to 30 weeks, of Caucasian ethnic origin (Table 1), collected at the Department of Normal Anatomy of our university (Collegium Medicum in Bydgoszcz, Nicolaus Copernicus University in Toruń, Poland). All samples had been gathered between the years 1989 and 1999 from spontaneous abortions or stillbirths, and then preserved in neutral formalin solution. Legal and ethical issues were approved by the University Research Ethics Committee (reference: KB 161/2013). Fetal age determination was based on the crown-rump length (CRL), known date of the 1st day of the maternal menstrual period, and the 5 fetal anthropometric measurements (head circumference, bi-parietal diameter, occipitofrontal diameter, abdominal circumference, and femur length) assessed by early 2nd trimester ultrasound scans.[18–26] As a prerequisite, we excluded fetuses with chromosomal abnormalities or intrauterine growth restriction, as well as from multiple pregnancies, from diabetic mothers and those with severe infections.

Table 1. Distribution of the fetuses examined

Fetal age [weeks]	Crown-rump length [mm]			n	Sex	
	median	min	max		males	females
18	139.5	131.0	143.0	4	3	1
19	152.5	145.0	155.0	6	4	2
20	161.0	159.0	167.0	7	3	4
21	175.0	170.0	180.0	7	5	2
22	185.5	181.0	190.0	6	1	5
23	199.5	195.0	204.0	6	4	2
24	212.0	205.0	214.0	10	2	8
25	215.0	215.0	220.0	5	2	3
26	233.0	225.0	233.0	3	1	2
27	240.5	235.0	242.0	4	2	2
28	253.0	247.0	253.0	7	1	6
30	264.0	263.0	265.0	4	4	0

For anatomists dealing with fetuses, the most objective information for establishing fetal ages is the crown-rump length, when compared to the known data of the beginning of the last maternal menstrual period or to ultrasonic measurements of head circumference, bi-parietal diameter, occipitofrontal diameter, abdominal circumference, and femur length.

Anatomical method

After having been fixed in 10% formalin solution for 12–24 months, fetuses were anatomically dissected through median and transverse laparotomy with the removal of the liver. Since no liver malformations were macroscopically perceived in the individuals studied, the examined sample could rightly be considered normal.

Digital image analysis

The visceral surface of each isolated liver with a millimeter scale was placed vertically to the optical lens axis, recorded with the use of a Canon 550D camera (Canon, Inc., Tokyo, Japan) and digitalized to TIFF images (Fig. 1). Next the morphometric measurements were performed using the digital image analysis system of NIS-Elements AR 3.0 (Nikon Corporation, Tokyo, Japan), with the greatest accuracy to the nearest 0.01 mm. In each specimen, the following 15 measurements in mm (Fig. 2 A–F) and 2 calculations on the visceral surface of the liver were performed:

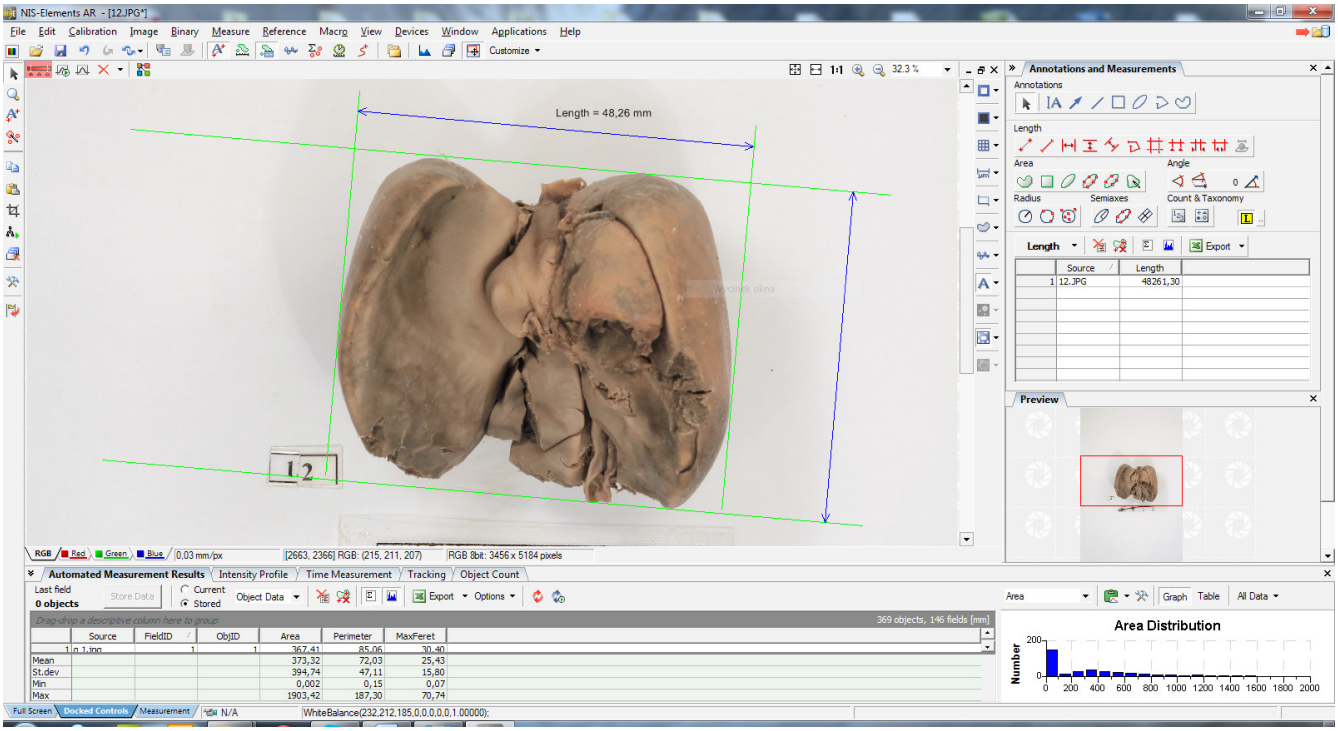

Fig. 1. A screen of digital image analysis of NIS Elements AR 3.0 (Nikon Corporation, Tokyo, Japan) while assessing the transverse and vertical diameters

– transverse diameter of the liver, corresponding to the greatest horizontal distance of the liver between its right and left borderlines (Fig. 2 B);
– vertical diameter of the liver, corresponding to the greatest vertical distance of the liver between its superior and inferior borderlines (Fig. 2 B);
– isthmic diameter of the liver, corresponding to the shortest horizontal distance of the liver between its right and left borderlines (Fig 2 B);
– right oblique diameter, corresponding to the longest oblique distance of the liver between its uppermost point of the right borderline to the lowermost point of the left borderline (Fig. 2 C);
– left oblique diameter, corresponding to the longest oblique distance of the liver between its uppermost point of the left borderline to the lowermost point of the right borderline (Fig. 2 C);
– length of fissure for ligamentum teres hepatis (Fig. 2 D);
– length of fissure for ductus venosus (Fig. 2 D);
– length of fossa for gallbladder (Fig. 2 D);
– length of sulcus for inferior vena cava (Fig. 2 D);
– length of porta hepatis (Fig. 2 D);
– circumference of right lobe (Fig. 2 E);
– circumference of left lobe (Fig. 2 E);
– circumference of quadrate lobe (Fig. 2 E);
– circumference of caudate lobe (Fig. 2 E);
– total liver circumference (Fig. 2 F);
– transverse-to-vertical ratio, corresponding to a quotient of the transverse diameter to the vertical diameter;
– isthmus ratio, corresponding to a quotient of the isthmus diameter to the vertical diameter.

Statistical analysis

All measurements were done by 2 independent researchers (M.P.A., M.B.). Each measurement was performed 3 times under the same conditions, but at different times, and then averaged. The differences between repeated measurements, as the intra-observer variation, were assessed by the one-way analysis of variance (ANOVA) test for paired data and post hoc Tukey's honest significant difference (HSD) test.[17] Thus, in order to examine the inter-observer reproducibility, the intra-class correlation coefficients (ICC) were calculated. In the present study, we used the STATISTICA v. 10 (StatSoft Inc., Tulsa, USA) and PQStat v. 1.6.2. (PQStat Software, Poznań, Poland) programs to analyze all the numerical data. The studied fetuses were separated into 12 1-week intervals, not equally distributed with respect to the fetal age. Obviously, some 1-week intervals did not represent adequate samples, including either 4 (fetuses aged 18, 27 and 30 weeks) or 3 (fetuses aged 26 weeks) specimens only. As the initial step, the first 4 intervals (18–21 weeks), the successive 4 intervals (22–25 weeks) and the last consecutive 4 intervals (26–30 weeks) were aggregated. To examine possible sex differences, we used the Student's t-test for the following 3 age groups: 18–21 (n = 24), 22–25 (n = 27) and 26–30 (n = 18) weeks. The one-way ANOVA test for unpaired data and post hoc Tukey's honest significant difference (HSD) test were used for the 3 aforementioned age groups to check whether or not significant differences existed with age. Furthermore, to choose the best-fit curve for each parameter vs gestational age, the highest coefficient of determination (R^2) was selected, and then the linear or nonlinear regression

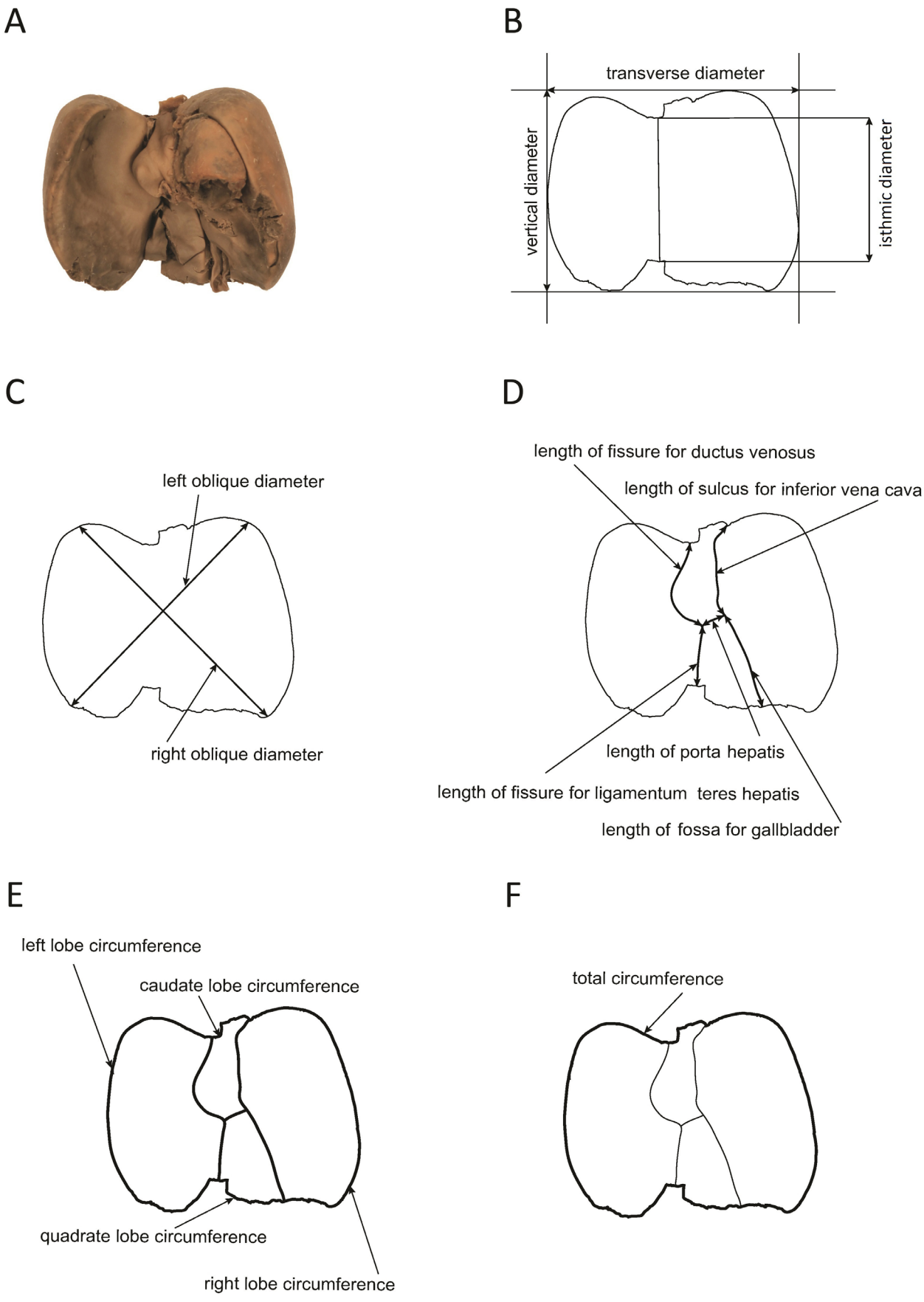

Fig. 2. Measurements of the fetal liver on its visceral surface in a female fetus aged 23 weeks (A)

B – transverse, vertical and isthmic diameters; C – right and left oblique diameters; D – lengths of fissure for ligamentum teres hepatis, fissure for ductus venosus, fossa for gallbladder, sulcus for inferior vena cava, and porta hepatis; E – circumferences of the liver lobes; F – total liver circumference.

analysis was computed. The relative liver growth was estimated as the transverse-to-vertical ratio and the isthmus ratio. A p-value <0.05 was considered statistically significant.

Results

No statistically significant differences were found in assessing both the intra-observer and inter-observer reproducibility of liver measurements ($p > 0.05$). As displayed in Table 2, the ICC calculated with respect to 2 independent observers were statistically significant ($p < 0.0001$) and of excellent reproducibility. The individual morphometric values obtained were characterized by the normality of distribution and homogeneity of variance. Due to this, quantitative variables were expressed as mean ± standard deviation (SD). The statistical analysis of numerical data showed no significant differences between male and female fetuses (Table 3). As a result, all individual parameters have been displayed aggregately for the entire sample (Tables 4–6).

The best growth models for the parameters studied along with their R^2 values were displayed in Table 7.

In order to objectify the obtained measurements in fetuses of different age, we calculated the relative growth of the liver as both the transverse-to-vertical diameter ratio and isthmus ratio. The transverse-to-vertical diameter ratio reached the value of 0.75 ±0.12, while the isthmus ratio significantly altered from 0.78 ±0.07 at 18–19 weeks through 0.68 ±0.05 at 26–27 weeks to 0.72 ±0.07 at 28–30 weeks of gestation.

Table 2. Intra-class correlation coefficient (ICC) values for inter-observer reproducibility

Parameter	ICC (2,1)
Transverse diameter	0.999*
Vertical diameter	0.998*
Right oblique diameter	0.998*
Left oblique diameter	0.999*
Isthmic diameter	0.997*
Length of fissure for ligamentum teres hepatis	0.994*
Length of fissure for ductus venosus	0.986*
Length of fossa for gallbladder	0.995*
Length of sulcus for inferior vena cava	0.990*
Porta hepatis	0.979*
Right lobe circumference	1.000*
Left lobe circumference	1.000*
Quadrate lobe circumference	0.999*
Caudate lobe circumference	0.998*
Total liver circumference	1.000*

* statistically significant ($p < 0.0001$).

Table 3. Statistical analysis of fetal dimorphism

Parameter	18–21 weeks					22–25 weeks					26–30 weeks				
	male, n = 15		female, n = 9		p-value	male, n = 9		female, n = 16		p-value	male, n = 8		female, n = 10		p-value
	mean	SD	mean	SD		mean	SD	mean	SD		mean	SD	mean	SD	
Transverse diameter	33.5	5.8	35.6	4.7	0.372	45.8	5.0	44.7	5.0	0.587	53.1	5.0	53.0	8.4	0.988
Vertical diameter	25.0	4.2	27.4	4.9	0.210	32.5	5.7	33.4	6.2	0.737	40.7	3.8	40.0	4.5	0.714
Right oblique diameter	32.6	4.7	36.2	4.9	0.110	43.9	5.8	43.8	4.2	0.958	52.1	4.6	49.2	4.1	0.175
Left oblique diameter	33.4	5.7	35.7	5.6	0.358	44.6	5.4	45.2	6.3	0.800	52.4	5.7	51.4	7.0	0.753
Isthmic diameter	19.5	3.8	20.6	3.5	0.466	23.7	4.6	24.2	4.5	0.791	29.2	5.5	27.8	3.2	0.501
Length of fissure for ligamentum teres hepatis	11.0	2.1	11.5	2.5	0.569	13.8	2.4	14.9	3.5	0.383	19.7	3.7	18.2	3.2	0.375
Length of fissure for ductus venosus	10.4	2.2	11.5	2.1	0.257	14.2	2.4	13.6	3.6	0.617	14.2	3.1	14.5	3.1	0.809
Length of fossa for gallbladder	12.3	2.4	13.0	2.2	0.500	16.6	4.0	15.7	2.9	0.501	22.7	1.2	21.6	4.0	0.460
Length of sulcus for inferior vena cava	10.2	2.6	10.8	2.4	0.566	14.1	2.5	13.8	3.2	0.835	14.4	3.0	14.6	2.8	0.883
Length of porta hepatic	5.1	1.0	5.3	1.0	0.631	8.3	1.2	7.5	1.6	0.156	9.2	1.1	9.4	1.7	0.703
Right lobe circumference	70.0	12.5	75.2	12.3	0.329	92.8	14.8	95.6	12.0	0.608	116.0	12.2	110.5	10.9	0.330
Left lobe circumference	68.1	15.2	73.7	13.3	0.366	89.0	12.5	93.7	20.7	0.538	114.7	19.1	111.1	11.6	0.635
Quadrate lobe circumference	38.4	6.2	38.7	7.7	0.920	52.8	10.1	46.6	9.0	0.115	61.2	6.7	61.6	9.6	0.906
Caudate lobe circumference	32.5	6.4	34.5	4.6	0.438	42.4	4.7	42.0	7.0	0.868	48.5	10.6	47.8	7.7	0.876
Total liver circumference	107.7	20.5	115.4	18.9	0.368	145.2	17.1	150.9	23.5	0.523	184.5	25.7	181.8	22.4	0.812

SD – standard deviation.

Table 4. Diameters of the growing liver in the human fetus

Age [weeks]	n	Diameter [mm]									
		transverse		vertical		isthmic		right oblique		left oblique	
		mean	SD	mean	SD	mean	SD	mean	SD	mean	SD
18	4	29.64	6.21	21.51	3.84	15.82	2.63	29.02	5.10	29.56	4.92
19	6	32.04	2.32	23.48	4.14	18.64	3.11	31.82	2.33	30.72	3.43
20	7	35.22	4.25	27.69	3.83	21.37	3.36	35.64	5.66	36.50	4.68
21	7	37.87	5.93	28.79	3.14	21.84	3.04	36.63	3.66	37.78	5.40
18–21	**24**	**34.27[(a)]**	**5.42**	**25.93[(a)]**	**4.52**	**19.90[(a)]**	**3.67**	**33.87[(a)]**	**4.99**	**34.27[(a)]**	**5.61**
22	6	40.02	2.99	29.16	5.14	21.94	4.67	39.19	3.56	40.02	2.99
23	6	44.45	3.71	33.70	4.25	23.60	3.83	43.59	4.83	44.45	3.71
24	10	45.05	3.51	33.67	6.38	24.50	3.15	44.15	3.31	45.05	3.51
25	5	51.89	2.47	35.86	6.98	26.34	6.75	49.21	2.03	51.89	2.47
22–25	**27**	**45.07[(b)]**	**4.95**	**33.08[(b)]**	**5.95**	**24.07[(b)]**	**4.43**	**43.86[(b)]**	**4.68**	**45.07[(b)]**	**4.95**
26	3	48.99	0.21	36.92	2.56	27.07	0.17	49.37	3.48	45.07	2.69
27	4	52.77	6.92	39.36	3.61	25.39	2.23	47.44	6.55	47.05	6.58
28	7	54.00	9.22	41.18	4.79	29.03	3.40	50.38	2.79	52.13	7.30
30	4	54.73	5.68	42.17	3.50	31.42	7.07	54.64	2.95	55.84	4.76
26–30	**18**	**53.05[(c)]**	**6.93**	**40.29[(c)]**	**4.09**	**28.43[(c)]**	**4.30**	**50.50[(c)]**	**4.44**	**51.82[(c)]**	**6.26**
(a) vs (b)		$p < 0.001$		$p < 0.001$		$p < 0.01$		$p < 0.001$		$p < 0.001$	
(a) vs (c)		$p < 0.001$		$p < 0.001$		$p < 0.001$		$p < 0.001$		$p < 0.001$	
(b) vs (c)		$p < 0.001$		$p < 0.001$		$p < 0.01$		$p < 0.001$		$p < 0.01$	

Means between the 3 age groups of 18–21, 22–25 and 26–30 weeks, marked by letters [(a)], [(b)] and [(c)] differ significantly (in bold). SD – standard deviation.

Discussion

Understanding the normative liver growth is crucial in both monitoring normal fetal development and prenatal detection of inherited faults. The present study intended to examine age-specific reference intervals and growth dynamics which are best-fit for the gestational age with respect to the linear dimensions of the liver measured on its visceral surface. Apart from that, we attempted to present their relative growth by introducing 2 liver ratios, namely the transverse-to-vertical diameter ratio and the isthmus ratio.

We considered the data obtained in the current examination to be both normative and factual. This statement results from the following 3 reasons. Firstly, the fetal sample presented neither explicit, extrinsic, nor intrinsic malformations. Secondly, the material under examination was comparable, because the fetuses had been immersed in formalin solution for 15–20 years. According to the professional literature, shrinkage in formalin did not exceed 1% with reference to any linear dimension of the liver.[18–27] Furthermore, the size of the liver in situ was virtually unfettered by formalin solution, since some liver linear dimensions, i.e., height, as well as transverse and sagittal diameters, achieved in the present series, accurately corresponded with those obtained by Chang et al., when measuring in utero fetuses of the same age with the use of 3D–ultrasound.[3] Thirdly, in order to measure the liver parameters, an optimized digital image system (NIS-Elements AR 3.0.; Nikon) was used. It is noteworthy that digital image analysis is an objective method to quantitatively assess the growing liver. Notably, all the studied parameters were clearly defined, outlined by a cursor and so gauged.

The present study is the first to provide objective numerical information about the visceral surface of the growing liver in human fetuses at 18–30 weeks. Since the statistical analysis did not show any sexual differences in terms of the parameters studied, our findings have been displayed aggregately without regard to sex.

To date, however, only Albay et al., on the basis of autopsied human fetuses aged 9–40 weeks, provided algebraic data concerning the linear parameters on the hepatic visceral surface, volume and weight of the liver.[12] These authors found the liver width to increase from 39 ±12 mm to 67 ±11 mm in the period of 13–37 weeks. Their findings coincide with our results in the material under examination, at which the length of transverse diameter on the hepatic visceral surface increased from 29.64 ±6.21 in a 18-week fetus to 54.73 ±5.68 mm in a 30-week fetus. Also, in the fetuses aged 13–37 weeks, Albay et al. revealed an increase in liver height from 25 ±8 mm to 41 ±7 mm.[12] This parameter turned out to be equal to our liver vertical diameter, which increased from 21.51 ±3.84 mm to 42.17 ±3.50 mm. Of note, we found both the liver

Table 5. Lengths of the growing liver in the human fetus

Length [mm]											
Age [weeks]	n	fissure for ligamentum teres hepatis		fissure for ductus venosus		fossa for gallbladder		sulcus for inferior vena cava		porta hepatis	
		mean	SD	mean	SD	mean	SD	mean	SD	mean	SD
18	4	9.42	1.48	8.89	2.15	11.25	1.89	7.42	1.05	4.60	0.96
19	6	10.50	2.03	9.69	1.49	11.19	2.41	9.34	1.97	4.98	1.07
20	7	11.72	2.67	12.18	1.53	13.29	2.22	12.07	1.52	5.13	0.60
21	7	12.25	1.73	11.51	2.17	13.82	1.73	11.52	2.50	5.65	1.20
18–21	**24**	**11.19[(a)]**	**2.22**	**10.81[(a)]**	**2.15**	**12.58[(a)]**	**2.29**	**10.45[(a)]**	**2.50**	**5.15[(a)]**	**0.99**
22	6	12.96	2.43	12.11	1.87	12.70	1.99	11.86	2.87	7.53	1.56
23	6	12.97	2.14	14.71	2.58	16.71	2.73	15.26	2.26	7.98	1.14
24	10	15.32	2.94	14.37	3.28	16.05	2.25	14.52	2.34	7.82	1.82
25	5	16.76	4.07	13.58	4.83	19.08	3.57	13.60	4.05	7.64	1.34
22–25	**27**	**14.54[(b)]**	**3.15**	**13.80[(b)]**	**3.30**	**16.01[(b)]**	**3.22**	**13.92[(b)]**	**2.92**	**7.76[(b)]**	**1.47**
26	3	18.03	0.50	14.23	3.18	20.84	0.65	12.10	2.10	8.29	0.90
27	4	15.73	3.12	14.00	2.87	20.13	2.63	15.50	4.09	9.78	2.33
28	7	19.66	2.28	14.51	3.26	22.96	4.15	14.11	1.96	9.16	1.21
30	4	21.36	4.77	14.59	3.86	23.38	1.22	15.93	2.77	9.86	0.70
26–30	**18**	**18.89[(c)]**	**3.43**	**14.37[(b)]**	**3.01**	**22.07[(c)]**	**3.08**	**14.49[(b)]**	**2.82**	**9.31[(c)]**	**1.40**
(a) vs (b)		$p < 0.001$		$p < 0.01$		$p < 0.001$		$p < 0.001$		$p < 0.001$	
(a) vs (c)		$p < 0.001$		$p < 0.01$		$p < 0.001$		$p < 0.001$		$p < 0.001$	
(b) vs (c)		$p < 0.001$		$p > 0.05$		$p < 0.001$		$p > 0.05$		$p < 0.01$	

Means between the 3 age groups of 18–21, 22–25 and 26–30 weeks marked by letters [(a)], [(b)] and [(c)] differ significantly (in bold). SD – standard deviation.

transverse and vertical diameters to grow in accordance with logarithmic functions. Apart from the aforementioned parameters on the hepatic visceral surface, Albay et al. examined the width of the right, left, quadrate, and caudate lobes, as well as the height of the quadrate and caudate lobes at 4 age ranges: 9–12, 13–25, 26–37, and 38–40 weeks of gestation.[12] However, we do not comment on these results, as we did not examine them at all.

According to Albay et al., porta hepatis did not alter its position with relation to the right and left hepatic borders.[12] Instead, with relation to the superior and inferior liver borders, porta hepatis shifted cephalad. In other words, the quadrate lobe lengthened more rapidly than the caudate one. To some extent, these results remain in line with our findings in the present study, because we have corroborated a greater increase in both the length of fissure for ligamentum teres hepatis and the length of fossa for gallbladder when compared to the lengths of fissures for both ductus venosus and inferior vena cava. As ascertained in the present study, an increase in length of both the fissure for ligamentum teres hepatis and fossa for gallbladder succeeded linearly. On the contrary, the lengthening of fissures for both ductus venosus and inferior vena cava proved to be unpredictable.

The lack of numerical information concerning the oblique diameters, isthmus and circumferences of the liver given in this paper limits our debate on this subject.

In order to match the best-fit model for a particular parameter of the growing liver, we initially computed different statistically significant regressions from logarithmic and square root functions through linear and quadrate functions to different polynomial functions. After that, we compared their R^2 values and finally selected the highest one. Eventually, in our study we discerned 2 disparate types of growth, presented by natural logarithmic and linear functions. A logarithmic increase indicates a gradual deceleration with age, while a linear increase is strictly commensurate. Natural logarithmic growths referred to: transverse diameter, vertical diameter, isthmus of the liver, right oblique diameter, left oblique diameter, length of fissure for ductus venosus, length of sulcus for inferior vena cava, length of porta hepatis, circumference of the right lobe, circumference of the left lobe, circumference of the quadrate lobe, circumference of the caudate lobe, and total liver circumference. On the other hand, only 2 liver parameters, i.e., length of fissure for ligamentum teres hepatis and length of fossa for gallbladder, grew linearly. The greatest R^2 values were typical of the following parameters: total liver circumference ($R^2 = 0.83$), transverse diameter ($R^2 = 0.77$), right oblique diameter ($R^2 = 0.77$), right lobe circumference ($R^2 = 0.76$), left lobe circumference ($R^2 = 0.74$), isthmic diameter ($R^2 = 0.74$), length of fossa for gallbladder ($R^2 = 0.74$), left oblique diameter ($R^2 = 0.72$),

and vertical diameter (R^2 = 0.71). The intermediate values of R^2 were typical of the length of porta hepatis (R^2 = 0.68), and the length of fissure for ligamentum teres hepatis (R^2 = 0.64) and quadrate lobe circumference (R^2 = 0.64). The lowest R^2 values were characterized by caudate lobe circumference (R^2 = 0.58). Because of a great inter-individual variability we did not manage to match any growth curves for the lengths of fissure for ductus venosus and of sulcus for inferior vena cava.

In the current study, we found no shape variation of the liver. In this aspect, our research does not correspond with the observations made by Albay et al., who perceived the 4 different shapes of the fetal liver: squared, trapezoid, rectangular, and triangular.[12] Furthermore, we observed no liver malformations, similarly to Haffajee et al. and Wang et al.[28,29] These authors reported relevant cases of the fetal liver beyond week 17 with the gallbladder completely covered with hepatic parenchyma.

Table 6. Circumferences of the growing liver in the human fetus

Age [weeks]	n	Circumference [mm]									
		right lobe		left lobe		quadrate lobe		caudate lobe		total	
		mean	SD	mean	SD	mean	SD	mean	SD	mean	SD
18	4	60.45	11.52	55.67	12.58	35.43	2.26	27.04	7.00	91.15	16.17
19	6	65.92	10.73	61.03	6.22	37.93	6.36	31.89	4.21	98.86	9.24
20	7	77.40	10.32	76.17	11.25	37.05	8.89	36.37	3.79	117.65	16.09
21	7	78.15	11.02	80.31	13.32	42.34	5.16	34.85	5.67	124.66	19.39
18–21	**24**	**71.92$^{(a)}$**	**12.45**	**70.18$^{(a)}$**	**14.45**	**38.54$^{(a)}$**	**6.62**	**33.25$^{(a)}$**	**5.77**	**110.58$^{(a)}$**	**19.88**
22	6	83.24	9.08	78.37	9.99	40.68	5.76	38.62	5.86	128.23	7.35
23	6	95.88	11.12	89.03	16.34	51.45	10.87	41.61	6.29	145.45	13.96
24	10	94.51	10.56	95.79	18.12	47.93	8.50	42.36	3.00	151.03	20.39
25	5	107.24	12.80	105.04	20.77	56.23	8.51	46.42	9.81	174.01	16.68
22–25	**27**	**94.66$^{(b)}$**	**12.82**	**92.13$^{(b)}$**	**18.27**	**48.64$^{(b)}$**	**9.64**	**42.11$^{(b)}$**	**6.21**	**148.98$^{(b)}$**	**21.42**
26	3	103.55	6.23	98.28	11.23	61.24	3.56	41.69	4.32	159.16	6.23
27	4	109.03	16.27	106.28	11.12	55.71	9.81	46.66	7.72	173.25	24.51
28	7	114.41	6.64	115.21	10.16	63.53	9.16	48.46	7.97	188.07	18.58
30	4	121.29	12.76	125.59	19.11	63.61	7.21	53.60	12.52	201.89	22.70
26–30	**18**	**112.93$^{(c)}$**	**11.49**	**112.71$^{(c)}$**	**15.02**	**61.43$^{(c)}$**	**8.24**	**48.07$^{(c)}$**	**8.81**	**183.03$^{(c)}$**	**23.25**
(a) vs (b)		p < 0.001		p < 0.001		p < 0.001		p < 0.001		p < 0.001	
(a) vs (c)		p < 0.001		p < 0.001		p < 0.001		p < 0.001		p < 0.001	
(b) vs (c)		p < 0.001		p < 0.001		p < 0.001		p < 0.05		p < 0.001	

Means between the 3 age groups of 18–21, 22–25 and 26–30 weeks marked by letters $^{(a)}$, $^{(b)}$ and $^{(c)}$ differ significantly (in bold). SD – standard deviation.

Table 7. The best-fit regression formulas for the fetal liver

Parameter	Regression formula	R^2 value	F	p-value
Transverse diameter	y = –125.518 + 53.754 × ln (Age) ±4.198	0.77	219.31	<0.001
Vertical diameter	y = –98.969 + 41.840 × ln (Age) ±3.911	0.71	161.85	<0.001
Right oblique diameter	y = –110.111 + 48.557 × ln (Age) ±3.721	0.77	227.02	<0.001
Left oblique diameter	y = –117.329 + 50.964 × ln (Age) ±4.597	0.72	169.75	<0.001
Isthmic diameter	y = –53.900 + 24.693 × ln (Age) ±3.205	0.74	80.01	<0.001
Length of fissure for ligamentum teres hepatis	y = –8.733 + 0.996 × Age ±2.513	0.64	115.67	<0.001
Length of fossa for gallbladder	y = –9.387 + 1.095 × Age ±2.220	0.74	184.09	<0.001
Porta hepatis	y = –26.986 + 10.870 × ln (Age) ±1.115	0.68	131.28	<0.001
Right lobe circumference	y = –287.401 + 120.550 × ln (Age) ±10.003	0.76	206.38	<0.001
Left lobe circumference	y = –295.715 + 122.097 × ln (Age) ±10.450	0.74	181.63	<0.001
Quadrate lobe circumference	y = –144.413 + 61.299 × ln (Age) ±6.670	0.64	116.44	<0.001
Caudate lobe circumference	y = –100.827 + 45.013 × ln (Age) ±5.415	0.58	86.16	<0.001
Total liver circumference	y = –517.502 + 210.340 × ln (Age) ±13.714	0.83	317.38	<0.001

F – critical value; R^2 – coefficient of determination.

Conclusions

The visceral liver surface reveals no sexual dimorphism in terms of its morphometric parameters.

The majority of the liver linear dimensions follow natural logarithmic functions, whereas the 2 linear dimensions (length of fissure for ligamentum teres hepatis, length of fossa for gallbladder) follow proportionately.

The transverse-to-vertical diameter ratio of the liver is relatively constant, while the isthmic ratio is unstable throughout the examined period.

The numerical data concerning the growing liver may be considered normative for particular fetal ages and relevant in both the ultrasound monitoring of in utero fetuses and early detection of inherited liver anomalies.

References

1. Murao F, Senoh D, Takamiya O, Yamamoto K, Hasegawa K, Kitao M. Ultrasonic evaluation of liver development in the fetus in utero. *Gynecol Obstet Invest*. 1989;28(4):198–201.
2. Murao F, Takamiya O, Yamamoto K, Iwanari O. Detection of intrauterine growth retardation based on measurement of size of the liver. *Gynecol Obstet Invest*. 1990;29(1):26–31.
3. Chang CH, Yu CH, Chang FM, Ko HC, Chen HY. The assessment of normal fetal liver volume by three-dimensional ultrasound. *Ultrasound Med Biol*. 2003;26(6):1123–1129.
4. Pardi G, Cetin I. Human fetal growth and organ development: 50 years of discoveries. *Am J Obstet Gynecol*. 2006;194(4):1088–1099.
5. Fleischer AC, Manning FA, Jeanty P, Romero R. *Sonography in Obstetrics and Gynecology. Principles and Practice*. 6th ed. New York, NY: McGraw-Hill Professional; 2001:109–130,411–432.
6. Ghidini A, Sirtori M, Romero R, Yarkoni S, Solomon L, Hobbins JC. Hepatosplenomegaly as the only prenatal finding in fetus with pyruvate kinase deficiency anemia. *Am J Perinatol*. 1991;8(1):44–46.
7. Murao E, Takamori H, Hata K, Hata T, Kitao M. Fetal liver measurement by ultrasonography. *Int J Gynecol Obstet*. 1987;25(5):381–385.
8. Murao F, Takamori H, Aoki S, Hata K, Hata T, Yamamoto K. Ultrasonographic measurement of the human fetal liver in utero. *Gynecol Obstet Invest*. 1987;24(3):145–150.
9. Naeye RL. Infants of diabetic mothers: A quantitative, morphologic study. *Pediatrics*. 1965;35:980–988.
10. Vintzileos AM, Campbell WA, Storlazzi E, Mirochnick MH, Escoto DT, Nochimson DJ. Fetal liver ultrasound measurement in isoimmunized pregnancies. *Obstet Gynecol*. 1986;68(2):162–167.
11. Weiner S. *The Isoimmunized Pregnancy. Perinatal Medicine Management of the High Risk Fetus and Neonate*. 2nd ed. Baltimore, MD: Williams and Wilkins; 1978:267–289.
12. Albay S, Mehmet A, Malas MA, Cetin E, Cankara N, Karahan N. Development of the liver during the fetal period. *Saudi Med J*. 2005;26(11):1710–1715.
13. Hedrick HL, Danzer E, Merchant A, et al. Liver position and lung-to-head ratio for prediction of extracorporeal membrane oxygenation and survival in isolated left congenital diaphragmatic hernia. *Am J Obstet Gynecol*. 2007;197(4):422.e1–4.
14. Silver RM. Fetal death. *Obstet Gynecol*. 2007;109(1):153–167.
15. Aviram R, Shpan DK, Markovitch O, Fishman A, Tepper R. Three-dimensional first trimester fetal volumetry comparison with crown rump length. *Early Hum Dev*. 2004;80(1):1–5.
16. Breeze ACG, Gallagher FA, Lomas DJ, Smith GCS, Lees CC. Postmortem fetal organ volumetry using magnetic resonance imaging and comparison to organ weights at conventional autopsy. *Ultrasound Obstet Gynecol*. 2008;31(2):187–193.
17. Paruszewska-Achtel M. *Morphometric study of the liver in human fetuses* [doctoral thesis, in Polish]. Bydgoszcz, Poland: Nicolaus Copernicus University; 2014.
18. Szpinda M, Baumgart M, Szpinda A, et al. Cross-sectional study of the ossification center of the C1–S5 vertebral bodies. *Surg Radiol Anat*. 2013;35(5):395–402.
19. Szpinda M, Baumgart M, Szpinda A, Woźniak A, Mila-Kierzenkowska C. Cross-sectional study of the neural ossification centers of vertebrae C1–S5 in the human fetus. *Surg Radiol Anat*. 2013;35(8):701–711.
20. Szpinda M, Baumgart M, Szpinda A, et al. Morphometric study of the T6 vertebra and its three ossification centers in the human fetus. *Surg Radiol Anat*. 2013;35(10):901–916.
21. Szpinda M, Daroszewski M, Woźniak A, et al. Novel patterns for the growing main bronchi in the human fetus: An anatomical, digital and statistical study. *Surg Radiol Anat*. 2013;36(1):55–65.
22. Szpinda M, Daroszewski M, Woźniak A, Szpinda A, Mila-Kierzenkowska C. Tracheal dimensions in human fetuses: An anatomical, digital and statistical study. *Surg Radiol Anat*. 2012;34:317–323.
23. Szpinda M, Paruszewska-Achtel M, Woźniak A, Badura M, Mila-Kierzenkowska C, Wiśniewski M. Three-dimensional growth dynamics of the liver in the human fetus. *Surg Radiol Anat*. 2015;37:439–448.
24. Szpinda M, Paruszewska-Achtel M, Woźniak A, et al. Volumetric growth of the liver in the human fetus: An anatomical, hydrostatic, and statistical study. *Biomed Res Int*. 2015;2015:858162. doi: 10.1155/2015/858162
25. Szpinda M, Siedlaczek W, Szpinda A, Woźniak A, Mila-Kierzenkowska C, Wiśniewski M. Volumetric growth of the lungs in human fetuses: An anatomical, hydrostatic and statistical study. *Surg Radiol Anat*. 2014;36(8):813–820.
26. Bożiłow W, Sawicki K. *Metody badań zmienności cech anatomicznych człowieka podczas rozwoju prenatalnego i okołoporodowego*. Wrocław, Poland: Akademia Medyczna; 1980.
27. Gworys B. *Problem oceny wieku u płodów i noworodków ludzkich* [rozprawa habilitacyjna]. Wrocław, Poland: Akademia Medyczna; 1999.
28. Haffajee MR. The fetal gallbladder: Morphology and morphometry by microdissection. *Surg Radiol Anat*. 2000;22(5–6):261–270.
29. Wang BJ, Kim JH, Yu HC, Rodriguez-Vazquez JF, Murakami G, Cho BH. Fetal intrahepatic gallbladder and topographical anatomy of the liver hilar region and hepatocystic triangle. *Clin Anat*. 2012;25(5):619–627.

Correlation between malnutrition, body mass index and complications in patients with urinary bladder cancer who underwent radical cystectomy

Marta Swalarz[1,A–D], Grzegorz Swalarz[2,B,D], Kajetan Juszczak[3,B,C,E,F], Piotr Maciukiewicz[3,B], Krzysztof Czurak[4,B], Marcin Matuszewski[4,B], Dominika Gajewska[5,B], Marcin Słojewski[5,B], Rafał Bogacki[6,B], Piotr Bryniarski[6,A–C,E,F], Andrzej Paradysz[6,A,B], Mateusz Kadłubowski[7,B], Tomasz Drewa[7,A,B], Ewa Genge[8,C,E,F]

[1] Silesian Center of UROVITA, Chorzów, Poland
[2] Department of Surgery and Urology, Upper Silesian Child Health Center, Katowice, Poland
[3] Department of Urology, Memorial Rydygier Hospital, Kraków, Poland
[4] Department of Urology, University Clinical Centre, Gdańsk, Poland
[5] Department of Urology and Urological Oncology, Pomeranian Medical University, Szczecin, Poland
[6] Department of Urology, Medical University of Silesia, Zabrze, Poland
[7] Division of General and Oncological Urology, Specialized Municipal Hospital, Toruń, Poland
[8] Department of Economic and Financial Analysis, University of Economics, Katowice, Poland

A – research concept and design; B – collection and/or assembly of data; C – data analysis and interpretation; D – writing the article; E – critical revision of the article; F – final approval of the article

Advances in Clinical and Experimental Medicine, ISSN 1899-5276 (print), ISSN 2451-2680 (online) *Adv Clin Exp Med*. 2018;27(8):1141–1147

Address for correspondence
Marta Swalarz
E-mail: martusiaswalarz@gmail.com

Funding sources
None declared

Conflict of interest
None declared

Acknowledgements
Special thanks to PhD Andrzej Szurkowski for the opportunity to conduct the research and to all professors and doctors involved in this project.

Received on August 23, 2016
Reviewed on March 5, 2017
Accepted on March 14, 2018

DOI
10.17219/acem/89863

Abstract

Background. Nutrition is the 3rd most important factor in surgery, following anesthesia and asepsis. Until now, it has been a poorly explored field of urology. The relationship between malnutrition and postoperative complications has been proven beyond doubt in general surgery, where 30% of patients are operated in a malnutrition state.

Objectives. The aim of our work was to assess the influence of malnutrition, defined by nutritional risk screening (NRS) scale and body mass index (BMI), on postoperative results in patients with bladder cancer after radical cystectomy.

Material and methods. The research was carried out at 8 urological centers between 2012 and 2014, and included patients with bladder cancer at stage from T2 to T4, who underwent radical cystectomy. The degree of malnutrition was assessed with the aid of the NRS 2002 questionnaire. Other examined parameters were BMI, age, type of operation, and the number of complications, the latter of which were measured by applying the Clavien-Dindo scale.

Results. A total of 125 patients were enrolled in our study, out of whom 64 (51.2%) were undernourished. According to the BMI, most of the patients were overweight – 50 (40%) or had normal body weight – 49 (39.2%); 24 (19.2%) were obese, and 2 (1.6%) were underweight.

Conclusions. There was no relationship between malnutrition, defined by the NRS scale, and postoperative complications, and we did not find a significant relationship between the other tested variables. We observed only 1 significant relationship between the nutrition state, measured by BMI scale, and the degree in Clavien-Dindo scale. Body mass index under 18.5 and over 30 increased postoperative complications. Nowadays, the recommended scale is NRS 2002, which is based mostly on loss of weight. In our patients, qualitative malnutrition is more probable than quantitative malnutrition.

Key words: malnutrition, bladder cancer, postoperative complications, radical cystectomy, Clavien-Dindo scale

Introduction

Nutrition is the 3rd most important factor in surgery, following anesthesia and asepsis. The World Health Organization (WHO) defines malnutrition as "occurring at the cellular imbalance between the demand for nutrients and energy supply and demand, which can satisfy the growth with, vital functions and perform certain functions". Basically, incorrect nutrition occurs when the body does not receive enough energy (quantitative malnutrition – weight loss) or essential nutrients, such as protein, vitamins, minerals and other nutrients needed to maintain healthy tissues and organs (quantitative malnutrition – e.g., vitamin deficiency). Both kinds of malnutrition can naturally coexist in the same patient. Such a condition is not limited only to patients who are obviously malnourished; it can also affect overweight and obese people. Malnutrition results from little consumption or not digesting or absorbing essential nutrients with regard to the needs of the body, or from the excretion of these nutrients faster than they can be completed. Loss of nutrients may be accelerated by a wide variety of factors, including surgery, diarrhea, severe intestinal dysfunctions, burns, sweating, severe bleeding, or as in our case, hematuria, renal failure or cancer. Malnutrition in hospitalized patients is a common phenomenon and its consequences are underestimated. According to reports, about 35–55% of patients admitted to hospital are malnourished and this situation has not changed since the early 1970s.[1,2]

Undernutrition affects the structure and function of certain cells, tissues and organs. We used to define malnutrition by dysfunctions of organs, when undernutrition already changes particular biochemical parameters (serum albumin level, lymphocytes level, etc.). But dysfunction of organs is not the best indicator of malnutrition, because it's malnutrition occurs much earlier. Research was undertaken to establish classification systems that can recognize disturbances in nutritional state faster, so that the improper trend of nutrition could be quickly reversed, thus preventing the dysfunction of cells.

In our paper we used the Nutritional Risk Screening 2002 (NRS 2002) scale, recommended by the European Society for Clinical Nutrition and Metabolism (ESPEN), Polish Society of Parenteral Nutrition, Enteral Nutrition and Metabolism (POLSPEN), and National Insurance Organization (NFZ), to detect and define undernutrition. This scale was also chosen to describe malnutrition due to its international popularity and usefulness. In Poland, each adult patient admitted to hospital should undergo a nutritional assessment test using NRS or SGA (Subjective Global Assessment) scale. The purpose was to detect the presence of undernutrition and also to detect patients at risk of developing undernutrition in hospital conditions. Chosen parameters show the moment when prevention steps should be taken to avoid function deteriorations, worsening of postoperative complications and prolonged recovery time, which result in increased hospitalization costs. The latest research, describes the impairment of function as a result of various extents of weight loss, with various rates of weight loss from various initial nutritional statures, on the basis of these studies, the NRS scale was created and is widespread. Controlled trials again found that such an approach has excellent inter-rater reliability, concurrent validity with other tools, and predictive validity (length of hospital stay, mortality in elderly wards and discharge destination in orthopedic patients). These optimistic scores have convinced us to check if by assessing the nutritional state we can really predict the probability of postoperative complication severity in urological patients undergoing radical cystectomy (RC). These patients suffer from many complications. That is why we are still looking for factors which could decrease the number of complications. One of these factors could be poor preoperative nutritional status, which is a proven risk factor for adverse outcomes after major surgery.

Malnutrition does not affect only people who are underweight. Increasingly more often it concerns overweight or obese people, whose diet consists of consuming high amounts of calories, mostly from carbohydrates, which are low in vitamins and minerals. The number of people worldwide who are overweight or obese is still growing and nowadays amounts to 2.1 billion. In Poland it constitutes 53% of the population; moreover, if we consider people over 45 years of age, it amounts to 77% of the population. The average body mass index (BMI) in Poland is 25.9. The relationship between BMI and cancer has been proven, which also applies to bladder cancer (BCa).[3]

Obesity is a risk factor responsible for an increased number of postoperative complications in surgery and orthopedics.[4,5] Bladder cancer ranks 4th in men and 8th in women, as far as incidence of all malignant tumors in Poland is considered. Annually, there are 5,700 new cases, out of which 25% are in T2–T4 stage. RC remains a gold standard treatment for muscle-invasive BCa and plays a role in non-muscle-invasive disease. About 2/3 of patients suffer from 1 or more complications, such as excessive loss of blood, urinary leakage, venous thromboembolic disease, digestive tract symptoms, ureteral reflux, acute renal failure, etc.[6,7]

The relationship between malnutrition and postoperative complications has been proven beyond doubt in general surgery. Until now, it has been a poorly explored area in the field of urology. Therefore, we decided to evaluate the correlation between malnutrition, BMI and complications in patients with urinary bladder cancer who underwent RC.

Material and methods

A multicenter study aimed at examining the state of malnutrition in patients who had undergone RC, was carried out at 8 urological centers (21 patients from hospitals in Toruń, 20 from a hospital in Gdańsk, 20 from

Szczecin, 3 from Kraków, and 61 from 4 Silesian hospitals – Chorzów, Zabrze, Bielsko-Biała, and Katowice) between 2012 and 2014. The study was not a medical experiment, which explains why approval from the bioethics committee was not necessary. A total of 125 patients (mean age 65.2; median 64) were examined and our study group consisted of 14% women and 86% men. All patients who were prepared to RC were screened by NRS 2002 to estimate nutritional status. According to that scale, patients were asked to give their weight from 3 months before, and we measured their body mass prior to surgery. The percentage of body mass loss was calculated, and also other variables given in the NRS 2002 questionnaire were taken into consideration, such as the following: BMI, food intake, age, and severity of disease. According to ESPEN guidelines, all patients who received a score ≥3 were considered patients nutritionally at risk who should have a nutritional care plan prepared. Patients with a score over 2 in the NRS scale were considered nutritionally deficient (ND) patients. Only patients who had undergone RC because of muscle-invasive BC (in T2–T4 stage) were admitted to this research, while RC due to other reasons was an exclusion criterion. Due to the fact that it was the same disease and the same stage of the disease (T2–T4), all patients got 2 points in NRS scale for the severity of disease.

The variable in our study was nutritional state (NS), which is a binary variable: NND – not nutritionally deficient (patients with score under 3), and ND – nutritionally deficient (patients with score over 2). The other variable was the degree of malnutrition (DM), depending on the number of points, which had 4 categories: NN – normal nutrition; DM1 – 1st degree of malnutrition, which constituted patients who got 3 (1 + 2) points in the NRS scale, i.e., those whose loss of weight amounted to 5–10% of body mass within last 3 months, whose food intake was between 50–75% of normal requirement in preceding week, or who were over 70 years of age; DM2 – constituted patients who got 4 (2 + 2) points in NRS scale, i.e., those who were in the 2nd degree of malnutrition, whose loss of weight was more than 10% of body mass within last 3 months, whose food intake, was between 25–60% of normal requirement in the preceding week or their BMI indicates undernutrition, so was between 18.5–20.5 or was in the 1st degree of malnutrition because of weight loss or food intake and who were over 70 years of age; DM3 – patients in the 3rd degree of malnutrition, who got 5 (3 + 2) points in NRS scale, i.e., those whose loss of weight was over 15% of body mass within last 3 months, whose food intake was below 25% of normal requirement in the preceding week, whose BMI was under 18.5 or was in the 2nd degree of malnutrition because of weight loss or food intake, and who were over 70 years of age. All patients from the ND group were asked to give causes for their loss of body mass.

Aside from our patients being classified according to the NRS scale, their BMI was also calculated, and the patients were divided into categories according to the BMI scale: BMI1 – underweight patients with a BMI under 18.5; BMI2 patients with normal body weight and BMI from 18.5 up to 25; BMI3 overweight patients with a BMI from 25 up to 30; and BMI4 – obese patients with a BMI over 30. Moreover, out of ND variables, we selected patients with a BMI over 25 and we created an additional group, which consisted of obese or overweight patients who were at the same time undernourished, due to big body mass loss within last 3 months. Other examined parameters were the type of operation and postoperative complications measured in the Clavien-Dindo scale. If the patient had above 2 points in the Clavien-Dindo scale, we considered it as clinically important. The total duration of the study was approx. 2 years. We must admit that in some hospitals parenteral nutrition and blood infusion (when hemoglobin level is <8) after RC were the standard procedure of postoperative care.

Statistical analysis

The χ^2 test and the Fisher's exact test (for contingency tables with small counts) for independence were used to assess the relationships between categorical variables and the eta correlation coefficient was used as a correlation indicator for variables measured on mixed scales. Correspondence analysis was applied as a statistical visualization method for picturing the associations between the levels of a 2-way contingency table. SPPS and R statistical software packages (SPSS Inc., Chicago, USA) were used in our computations.

Results

Out of 125 patients (mean age 65.2: median 64), 61 (48.8%) were not nutritionally deficient (NND) and 64 (51.2%) were nutritionally deficient (ND) (Table 1). Regarding the degree of malnutrition, most patients were in the DM1 category – 29 (23.2%), DM2 constituted 20 (16%) patients and DM3 constituted 15 (12%) (Table 2). The main cause of malnutrition was mostly the disease itself (chronic hematuria and pain, which resulted in the loss of appetite); other causes was stress before the surgery, deliberately going on a diet, or undergoing neoadjuvant chemotherapy, which lowered patients' appetite and resulted in weight loss. According to the BMI scale, BMI3 and BMI2 constituted almost the same number of patients: BMI3 – 50 (40%), BMI2 – 49 (39.2%) and BMI4 – 24 (19.2%). This suggested that 54.4% of our patients were overweight or obese, which is much lower than in the Polish population, where the percentage of people over 45 years of age with a BMI over 25 amounts to 77%, BMI1–2 (1.6%). The group of obese and overweight patients, who had become malnourished before surgery due to big body mass loss, constituted 36 (28.8%) patients.

Table 1. Contingency table for "nutritional status" and complications in Clavien-Dindo scale variables

Score in Clavien-Dindo scale/ nutritional status	NND	ND
1	19 (15.2%)	15 (12%)
2	36 (28.8%)	37 (29.6%)
3	2 (1.6%)	4 (3.2%)
4	3 (2.4%)	4 (3.2%)
5	1 (0.8%)	4 (3.2%)

NND – not nutritionally deficient; ND – nutritionally deficient.

The number of clinically important complications over 2 in the Clavien-Dindo scale in NS variables was 18 (14.4%) of patients (Table 1) and was slightly higher in categories of ND patients – 12 (9.6%) (4 [3.2%] + 4 [3.2%] + 4 [3.2%]) to 6 (4.8%) (2 [1.6%] + 3 [3.2%] + 1 [0.8%]) in NND patients. The degree in the Clavien-Dindo scale compared to the degree of malnutrition variable showed that the group of patients, in which serious complications were most likely to occur, was DM2, where 25% (5 out of 20) of patients had complications above 2, while in the DM1 group it was 17.2% (5 out of 29) and in DM3 – 13% (2 out of 15); in the NN group serious complications could be observed only in 9.8% (6 out of 61) of patients (Table 2). The rate of complications according to the BMI scale is presented in Table 3. The most popular urinary diversion was the Bricker method, performed in 87 (69.6%) patients, while ureterocutaneostomy was performed in 31 (24.8%) patients and ileal neobladder reconstruction by the Student's t-test was performed in 7 (5.6%) patients (Table 4).

Results of statistical analysis

Pearson's χ^2 test of independence was used to check whether a statistically significant relationship between variables existed. Due to the small sample sizes (cell size below 5 expected occurrences), the Fisher's exact test for contingency tables with small samples was used. The frequency distribution of the variables was analyzed on the basis of cross tabulations, which provided a basic picture of the interrelation between variables. Most patients who had clinical, but not serious complications, were nutritionally normal. The results of the Pearson's χ^2 and the Fisher's exact tests between different pairs of variables, as well as eta correlation coefficient, are given in Table 5. In the conducted tests, only 1 significant relationship between nutrition state, measured by BMI, and the degree in Clavien-Dindo scale ($p = 0.0274$) was observed. Therefore, the null hypothesis could not be rejected and a significant relationship between those variables was observed.

Correspondence analysis was applied as an exploratory data analytic technique to present relationships among the categories of those variables (BMI and complications). In Fig. 1, the proximity of the 4th degree of complication

Table 2. Contingency table for degree of malnutrition (DM) and complications in Clavien-Dindo scale variables

Score in Clavien-Dindo scale	NN	DM1	DM2	DM3
1	19 (15.2%)	7 (5.6%)	3 (2.4%)	5 (4%)
2	36 (28.8%)	17 (13.6%)	12 (9.6%)	8 (6.4%)
3	2 (1.6%)	2 (1.6%)	1 (0.8%)	1 (0.8%)
4	3 (2.4%)	0	3 (2.4%)	1 (0.8%)
5	1 (0.8%)	3 (2.4%)	1 (0.8%)	0

NN – nutritionally normal; DM1 – 1st degree of malnutrition; DM2 – 2nd degree of malnutrition; DM3 – 3rd degree of malnutrition.

Table 3. Number of complications in Clavien-Dindo scale in nutritional groups according to the body mass index (BMI) scale

Score in Clavien-Dindo scale	BMI1	BMI2	BMI3	BMI4
1	0	16 (12.8%)	15 (12%)	3 (2.4%)
2	1 (0.8%)	22 (17.6%)	30 (24%)	20 (16%)
3	1 (0.8%)	5 (4%)	0	0
4	0	4 (3.2%)	2 (1.6%)	1 (0.8%)
5	0	2 (1.6%)	3 (2.4%)	0

BMI1 – under 18.5; BMI2 – 18.5–24.9; BMI3 – 25–29.9; BMI4 – above 30.

Table 4. Number of complications in Clavien-Dindo scale in patients with different urinary diversions

Score in Clavien-Dindo scale	Bricker	Studer	Ureterocutaneostomy
1	21 (16.8%)	4 (3.2%)	9 (7.2%)
2	53 (42.4%)	2 (1.6%)	18 (14.4%)
3	4 (3.2%)	0	2 (1.6%)
4	7 (5.6%)	0	0
5	2 (1.6%)	1 (0.8%)	2 (1.6%)

Table 5. Measures of relationships and significance levels

Relationship	Statistic	p-value	
		χ^2	Fisher's exact test
NS–complications	$\chi^2 = 3.6743$	0.4519	0.4740
DM–complications	$\chi^2 = 11.7798$	0.4635	0.3952
BMI–complications	$\chi^2 = 24.8512$	0.0155	0.0274
Bricker–complications	$\chi^2 = 6.4500$	0.1680	0.1406
Studer–complications	$\chi^2 = 6.3064$	0.1774	0.1473
Ureterocutaneostomy–complications	$\chi^2 = 2.6720$	0.6141	0.6389
Bricker–DM	$\chi^2 = 2.3417$	0.5046	0.5266
Studer–DM	$\chi^2 = 2.9466$	0.3999	0.5782
Ureterocutaneostomy–DM	$\chi^2 = 5.4272$	0.1431	0.1557
Age–complications	$\eta = 0.423$	0.1830	–

DM – degree of malnutrition; χ^2 – Pearson's χ^2 test.

to the circle representing the 1st category of BMI indicates that the 4th degree in Clavien-Dindo scale is associated with the underweight patients. The association between patients with normal body weight (BMI2) and overweight patients (BMI3) with the 2nd degree of complications can be noticed as well.

It might seem difficult to find associations between categories of the variables, which is why Ward's method was used; it is one of the best classification methods to interpret the perception map of the correspondence analysis. The categories were clustered on the basis of calculated coordinates. As a result of clustering analysis, a dendrogram was created using the R statistical package (Fig. 2). On the basis of Silhoutte index (the measure of cluster separation), 3 clusters, which describe the relationship between examined categories, were selected. The 1st cluster consisted of obese patients associated with 3rd degree in Clavien-Dindo scale. In the 2nd cluster, the association between patients with normal body weight and overweight with the 2nd degree of complications can be observed. In the 3rd cluster, the underweight patients are strongly associated with the 4th degree in the Clavien-Dindo scale and weakly associated with the 1st and 5th category of complications.

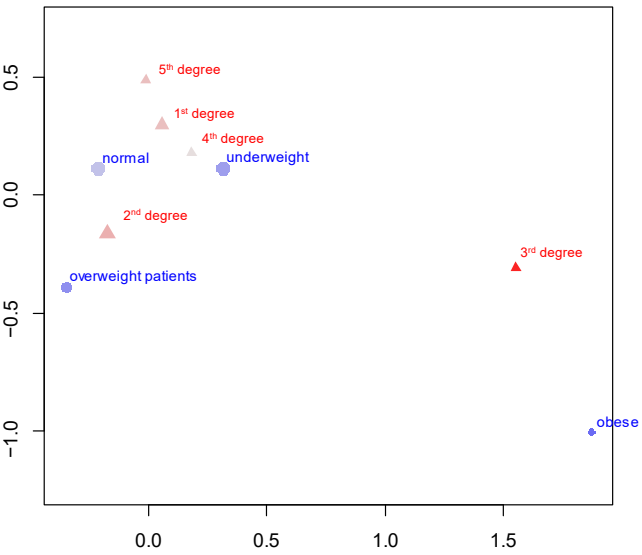

Fig. 1. Correspondence analysis plot

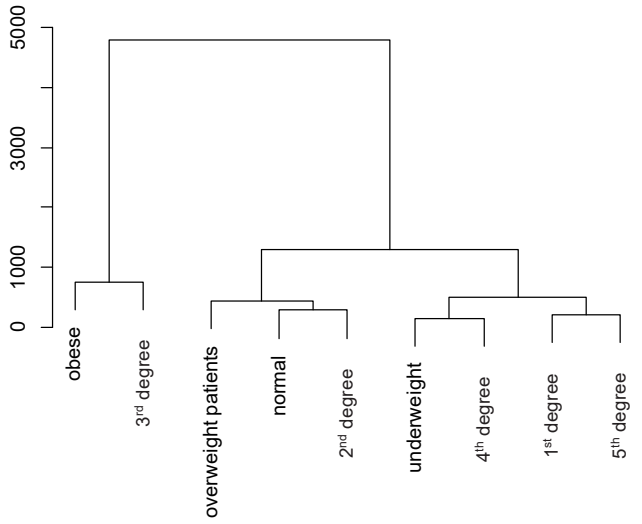

Fig. 2. Dendrogram for different categories of variables: complications in Clavien-Dindo scale and body mass index (BMI)

Discussion

In our study, more complications were found in the ND group, but no statistical relationship between those variables was noticed.[5,8–12] It is possible that increasing the number of patients in the study group could lead us to different conclusions. We should remember that malnutrition, defined by the NRS scale, constitutes patients not only in an undernutrition state, but also patients at risk of malnutrition, i.e., the status in which patients are in an imbalance between the amount of absorbed and used substances. This creates disturbances in the structure and function of cells and organs. The main problem in urological patients is chronic hematuria causing a loss of a lot of nutritional substances, which may induce malnutrition without a decrease in weight.

Therefore, further prospective studies are needed to more precisely determine the usefulness of measuring nutritional status by the NRS scale. Age and the selected type of urinary diversion also did not increase the amount of complications in a significant way.[9,12] A relationship between complications and BMI was the only significant relationship that we could notice also in other studies.[3,7,13,14] In the group of ND overweight or obesity, no increased number of complications was noticed either. Based on those facts, it should be further examined if losing mass in the case of patients with BMI over 25 is a protective factor. Of course, losing mass will never be a goal for patients with cancer. However, it requires further studies to make sure if putting our patients on a healthy norm-caloric diet will help them to limit the number of complications.

Many reports show which vitamins and minerals are in deficiency in our population; it is also well known which microelements are necessary for wounds to heal properly. However, this knowledge is not utilized well enough before important and cost-generating procedures like RC. The patients who undergo RC, besides cancer, suffer from a lot of other diseases; therefore, their condition should be optimized before the operation. Seriously ill patients should be provided with a nutritional, physical and mental health program as a standard procedure. An American survey conducted in 2014, entitled "Optimizing a frail elderly patient for radical cystectomy with a prehabilitation program", proposes and shows a holistic preparation program, including nutritional counseling, protein supplementation, anxiety reduction, and a moderate exercise program.[15] This prehabilitation program was also checked

in patients after colorectal surgery.[16] An individualized approach and precise preparation of patients proved to increase recovery in walking capacity, as well as emotional and cognitive functions, and also decreased the number of postoperative complications.

In order to improve the nutritional status in an optimized way, we should have reliable information which patients are in need of special nutritional support. Good nutritional markers or scales, which show the real nutritional problems of patients, are of primary importance.

According to the classification of NRS 2002 scale, in our study, 51.2% of patients were undernutritioned, which is a high number. In contrast to general surgery, undernutrition classified in such a way does not influence postoperative complications. The most frequent cause of losing weight was the disease itself. The possible explanation of this fact is that due to chronic hematuria, the urological patient is more likely to suffer from qualitative rather than from quantitative malnutrition. Consequently, a patient without weight loss may be malnourished. Therefore, the scale NRS 2002 does not seem to be adequate, as it does not reflect the real condition of the nutritional state of our patients, who, despite no weight loss, may have serious element deficits, e.g., iron and other minerals, which are absolutely necessary for proper healing of wounds after operation. It is possible that measuring other biochemical indices, e.g., erythrocyte count, hemoglobin concentration, American Society of Anesthesiologists (ASA) classification score over 3, ferritin serum concentration, C-reactive protein (CRP) neutrophil-to-lymphocyte ratio, as well as the level of antioxidant vitamins (A, C, E, D), vitamin B_{12} and folic acid, will be useful for more reliable diagnosing of underfed patients who need nutritional support.[6,17–24] Serum albumin is omitted in the new nutritional scales, which is why during planning this survey we did not take this parameter into consideration. Some research works say that "albumin and other visceral protein should no longer be considered as nutritional markers, but as inflammatory response markers", while others claim that "serum levels of albumin, prealbumin, transferrin and IGF-1, and delayed hypersensitivity and total lymphocyte count may be valid to help stratify risk. However, it is not appropriate to consider these as markers of adequacy of nourishment in the sick patient."[13,14] A number of composite measures of nutritional status were proposed, although no standardized method of nutrition evaluation exists, especially for urological patients.[12] Nutritional Risk Screening 2002 is nowadays a validated index, but it is based on subjective information, which could limit its applicability. It consists mainly of BMI, weight loss, amount of food intake, age and disease severity that determine the risk of postoperative complications. The usefulness of this scale is well proven in surgery. Nonetheless, in urology, a good correlation between those variables could not be found. Only 1 research work from US confirmed the relationship between NRS 2002 and complications in patients after RC.[6] In other research, malnutrition did not influence the duration of patients' stay in the urological ward.[9] In a retrospective study of 905 patients, consisting of measuring BMI, weight loss and preoperative albumin level, "only preoperative albumin level was significantly associated with all-cause mortality (…) within 90 days".[8] In our study, the BMI indicator itself was much more reliable. As we can see from the correspondence analysis and dendrogram, undernutrition and obesity are associated with higher rate in Clavien-Dindo scale. There is no doubt that the "best patient" to be operated is the patient with normal body weight or little overweight, and in good nutritional condition. However, we have to face the problem of an increasing number of malnutrition and obesity patients in our society and find ways how to decrease the complication rates in those patients. Body mass index was also a better parameter than weight loss in a multicenter prospective cohort study of 2,258 patients who underwent major intra-abdominal cancer surgery; patients with a preoperative BMI <18.5 had greater than a 5-fold increased risk of perioperative mortality.[21] Even if in urology the correlation is not so strong, we should try to identify the nutritional status more precisely. It seems desirable to apply nutritional intervention, especially in well-identified malnourished patients, and, as a result, decrease the number of postoperative complications. Nevertheless, today there are no studies evaluating the role of nutrition supplementation in patients with urinary bladder cancer. Therefore, larger-scale prospective studies are needed to determine what are the best markers for nutritional status and whether nutritional intervention helps to decrease the number of complications in nutritionally deficient patients undergoing RC.[22] For the patients with BMI above 30, who have a higher occurrence of bladder cancer and also, what was observed in our study, higher postoperative complications rate after RC, probably the best way to decrease postoperative complications will be motivating them to lose weight when their cancer is at the early stage (T1) and a radical cystectomy is a distant prospective.[3] Decreasing the amount of inflammatory and angiogenic factors, which are produced in fat tissue, could help stop the development of cancer. As the latest research shows, obesity is a 3 times more frequent cause of death as compared to undernutrition. A dramatic increase of BMI in the population is terrifying, as almost 30% of cancers could be avoided if we managed to keep the BMI under 25.[23] Therefore, the best solution is, in our case, keeping BMI between 18.5 and 30 to avoid potential problems. We have to be aware that both extremes in BMI will increase postoperative complications and we should try to apply more preventive treatment to decrease our patients' postoperative suffering.

The conducted study shows some limitations – complications were measured during hospitalization, which, in turn, does not exclude the general influence on higher mortality rate in longer time after operation; and some patients underwent neoadjuvant chemotherapy, which could be an interfering factor. Nevertheless, the study was multicenter.

Conclusions

There is no relationship between malnutrition, measured in the NRS scale, and postoperative complications in cases of patients with urinary bladder cancer after radical cystectomy. Only 1 significant relationship between the nutrition states was observed, measured by BMI scale and the degree in Clavien-Dindo scale. BMI under 18.5 and over 30 increases postoperative complications.

Nutritional Risk Screening 2002 is based mostly on loss of weight and identifies patients who are in undernutrition state and at risk of undernutrition and who may improve their condition by nutritional intervention. Such defined malnutrition does not show any correlation with postoperative complications in patients undergoing RC. In this case, qualitative malnutrition is more probable than the quantitative one. An evaluation tool should be sought to determine malnutrition status in patients with bladder cancer more precisely and more attention should be paid to qualitative malnutrition, since quantity is important when it involves a quality change. Greater precision in identifying patients in need of nutritional support would certainly help in achieving better long-term results. Multimodal pre-rehabilitation program before surgery appears to be a promising perspective for the future.

References

1. Jarosz M, Dzieniszewski J, Szczygieł B, et al. Nutritional status of patients in hospitals in Poland. II. More thorough assessment of nutritional status of adult patients. *Pol Merkur Lekarski.* 2003;15:151–154.
2. Dzieniszewski J, Jarosz M, Szczygieł B, et al. Nutritional status of patients in hospitals in Poland. I. Screening of adult patients. *Pol Merkur Lekarski.* 2003;15:144–150.
3. Qin Q, Xu X, Wang X, Zheng XY. Obesity and risk of bladder cancer: A meta-analysis of cohort studies. *Asian Pac J Cancer Prev.* 2013;14(5):3117–3121.
4. Burrus MT, Werner BC, Yarboro SR. Obesity is associated with increased postoperative complications after operative management of tibial shaft fractures. *Injury.* 2016;47(2):465–470.
5. Stevens SM, O'Connell BP, Meyer TA. Obesity related complications in surgery. *Curr Opin Otolaryngol Head Neck Surg.* 2015;23(5):341–347.
6. Cerantola Y, Valerio M, Hubner M, Iglesias K, Vaucher L, Jichlinski P. Are patients at nutritional risk more prone to complications after major urological surgery? Prevention and management of complications following radical cystectomy for bladder cancer. *J Urol.* 2013;190(6):2126–2132.
7. Roghmann F, Gockel M, Schmidt J, et al. Complications after ileal conduit: Urinary diversion-associated complications after radical cystectomy [in German]. *Urologe A.* 2015;54(4):533–541.
8. Munbauhal G, Drouin SJ, Mozer P, et al. Malnourishment in bladder cancer and the role of immunonutrition at the time of cystectomy: An overview for urologists. *BJU Int.* 2014;114(2):177–184.
9. Jensen BT, Laustsen S, Petersen AK, et al. Preoperative risk factors related to bladder cancer rehabilitation: A registry study. *Eur J Clin Nutr.* 2013;67(9):917–921.
10. Herranz Amo F, Garcia Peris P, Jara Rascon J, et. al. Usefulness of total parenteral nutrition in radical surgery for bladder cancer [in Spanish]. *Actas Urol Esp.* 1991;15(5):429–436.
11. Cantiello F, Cicione A, Autorino R, et al. Metabolic syndrome, obesity, and radical cystectomy complications: A clavien classification system-based analysis. *Clin Genitourin Cancer.* 2014;12(5):384–393.
12. Shpata V, Prendushi X, Kreka M, Kola I, Kurti F, Ohri I. Malnutrition at the time of surgery affects negatively the clinical outcome of critically ill patients with gastrointestinal cancer. *Med Arch.* 2014;68(4):263–267.
13. Xu T, Zhu Z, Wang X, et al. Impact of body mass on recurrence and progression in Chinese patients with Ta, T1 urothelial bladder cancer. *Int Urol Nephrol.* 2015;47(7):1135–1141.
14. Comploj E, West J, Mian M, et al. Comparison of complications from radical cystectomy between old-old versus oldest-old patients. *Urol Int.* 2015;94(1):25–30.
15. Carli F, Awasthi R, Gillis C, Kassouf W. Optimizing a frail elderly patient for radical cystectomy with a prehabilitation program. *Can Urol Assoc J.* 2014;(11–12):E884–E887.
16. Li C, Carli F, Lee L, et al. Impact of trimodal prehabilitation program on functional recovery after colorectal cancer surgery: A pilot study. *Surg Endosc.* 2013;27(4):1072–1082.
17. Chang SS, Cookson MS, Baumgartner RG, Wells N, Smith JA. Analysis of early complications after radical cystectomy: Results of a collaborative care pathway. *J Urol.* 2002;167(5):2012–2016.
18. Barbosa-Silva MC. Subjective and objective nutritional assessment methods: What do they really assess? *Curr Opin Clin Nutr Metab Care.* 2008;11(3):248–254.
19. Seres DS. Surrogate nutrition markers, malnutrition, and adequacy of nutrition support. *Nutr Clin Pract.* 2005;20(3):308–313.
20. Schiesser M, Kirchhoff P, Muller MK, Schäfer M, Clavien PA. The correlation of nutrition risk index, nutrition risk score, and bioimpedance analysis withpostoperative complications in patients under going gastrointestinal surgery. *Surgery.* 2009;145(5):519–526.
21. Kinn AC, Lantz B. Vitamin B_{12} deficiency after irradiation for bladder carcinoma. *J Urol.* 1984;131(5):888–890.
22. Mullen JT, Davenport DL, Hutter MM, et al. Impact of body mass index on perioperative outcomes in patients undergoing major intraabdominal cancer surgery. *Ann Surg Oncol.* 2008;15(8):2164–2172.
23. Kiyama T, Witte MB, Thornton FJ, Barbul A. The route of nutrition support affects the early phase of wound healing. *JPEN J Parenter Enteral Nutr.* 1998;22(8):276–279.
24. Bhaskaran K, Douglas I, Forbes H, dos-Santos-Silva I, Leon DA, Smeeth L. Body-mass index and risk of 22 specific cancers: A population-based cohort study of 5.24 million UK adults. *Lancet.* 2014;384(9945):755–765.

Genetic aspects of primary hyperaldosteronism

Weronika Korzyńska[1,A–D], Anna Jodkowska[1,A,C–E], Katarzyna Gosławska[1,B], Katarzyna Bogunia-Kubik[1,2,A,E,F], Grzegorz Mazur[1,F]

[1] Department and Clinic of Internal and Occupational Diseases and Hypertension, Wroclaw Medical University, Poland
[2] Laboratory of Clinical Immunogenetics and Pharmacogenetics, Institute of Immunology and Experimental Therapy, Polish Academy of Sciences, Wrocław, Poland

A – research concept and design; B – collection and/or assembly of data; C – data analysis and interpretation; D – writing the article; E – critical revision of the article; F – final approval of the article

Advances in Clinical and Experimental Medicine, ISSN 1899–5276 (print), ISSN 2451–2680 (online) *Adv Clin Exp Med*. 2018;27(8):1149–1158

Address for correspondence
Anna Jodkowska
E-mail: anna.jodkowska@umed.wroc.pl

Funding sources
None declared

Conflict of interest
None declared

Received on November 6, 2016
Reviewed on December 28, 2016
Accepted on March 8, 2017

Abstract

Primary hyperaldosteronism (PHA) is the most common form of secondary hypertension of hormonal origin. It affects about 10% of all hypertensive patients. It is connected with increased morbidity and mortality from cardiovascular diseases (CVD) compared to patients with essential hypertension, at a similar age. Usually, it is an effect of bilateral adrenal hyperplasia (BAH) or aldosterone-producing adenoma (APA), rarer causes of PHA are: unilateral adrenal hyperplasia, aldosterone-producing adrenocortical carcinoma, ectopic aldosterone-producing tumors, and familial hyperaldosteronism (FH). Recent genetic studies have thrown a new light on the pathogenesis of PHA, classifying it as a channelopathy. Several mutations within the ion channels encoding genes have been identified. A possible link between PHA and polymorphism of aldosterone synthase gene and ion channel genes is still being investigated. In this manuscript, we focus on the genetic aspects of PHA, and present an up-to-date compilation of available data with a widened pathogenetic approach.

Key words: gene polymorphism, aldosterone, primary hyperaldosteronism, ion channels, angiotensine II

DOI
10.17219/acem/69390

Introduction

Primary hyperaldosteronism (PHA) is the most common cause of secondary hypertension of hormonal origin. It can possibly concern over 10% of hypertensive patients.[1] Its occurrence ranges from 8 to 30% in different reports, depending on the diagnostic criteria and the sample. In the large prospective PAPY study, primary hyperaldosteronism occurred in 11.2% of newly diagnosed hypertensive patients.[2,3] The prevalence of PHA augments with an increase of blood pressure value and among patients with resistant hypertension it reaches up to 20%. Primary hyperaldosteronism was first described by Conn in the 1950s.[4] The cause of the syndrome is excessive autonomous secretion of aldosterone, which appears to be relatively independent on the renin–angiotensin–aldosterone system (RAAS), adrenocorticotropic hormone (ACTH), and the extracellular concentration of potassium ions.[1]

Primary hyperaldosteronism is not a homogenous pathogenetic syndrome. It frequently occurs as the effect of bilateral adrenal hyperplasia (BAH) known also as idiopathic hyperaldosteronism (IHA) and aldosterone-producing adenoma (APA). Bilateral adrenal hyperplasia and APAs both represent about 95% cases of PHA (35% APA and 60% IHA).[2] Less often PHA is a result of unilateral adrenal hyperplasia, and in very rare cases it is caused by aldosterone-producing adrenocortical carcinoma, ectopic aldosterone-producing tumors, and familial aldosteronism (FA).[2]

Primary hyperaldosteronism is connected with increased morbidity and mortality from cardiovascular diseases (CVD) compared to patients with essential hypertension of a similar age.[5] Patients with PHA are at a higher risk of suffering a heart attack, stroke, and atrial fibrillation.[5] They are affected more frequently by metabolic syndrome as well.[6]

An excess of aldosterone exerts a number of adverse effects on a variety of organs and tissues. It has been reported to increase collagen synthesis, leading to heart muscle fibrosis, concentric remodeling and thickening of the left ventricular wall, as well as to predispose to the deterioration of left ventricular diastolic function.[7,8] In addition, excess of aldosterone contributes to the damage of the small vessels and to the progress of nephropathy.[9] Patients with PHA, compared to essential hypertensives, have a higher initial concentration of the C-reactive protein and interleukin 6.[10,11] Moreover, they are characterized by the increased thickness of the carotid intima-media, increased arterial stiffness, and more advanced vascular endothelial dysfunction than those with essential hypertension.[12]

There is now a growing interest in genetic determination of PHA. Recently, new forms of familial hereditary aldosteronism have been described. A number of somatic mutations connected with the APAs' appearance have been shown as well. In this manuscript we focus on the genetic aspects of primary hyperaldosteronism. We present an up-to-date compilation of available data broadened by the pathogenetic approach.

Aldosterone: regulative physiology

Aldosterone is a steroid hormone synthetized from cholesterol exclusively in the adrenal glomerulosa layer by the aldosterone synthase (CYP11B2). However, there is also some data of its possible synthesis in other human tissues such as the heart, aorta, pulmonary arteries, and brain.[13] Cholesterol used in aldosterone production may be of various origins, including de novo synthesis from cholesterol esters or the uptake of low-density lipoproteins (LDL). The schematic diagram of aldosterone synthesis is presented in Fig. 1.

Aldosterone synthase (CYP11B2), located exclusively in the adrenal zona glomerulosa, is highly homologous to 11β-hydroxylase (CYP11B1), which catalyzes the final step of cortisol synthesis and is located in the zona fasciculata of the adrenal gland. Genes encoding CYP11B1 and CYP11B2 are placed on chromosome 8q21-22 in close proximity to each other. This proximity plays an important role in the pathogenesis of familial aldosteronism type 1.[14]

There are many factors known to regulate aldosterone secretion. The most important are considered: angiotensin II, changes of extracellular potassium ion concentration, and adrenocorticotropic hormone (ACTH).[15]

Adrenal glomerulosa layer cells maintain negative resting membrane potential (hyperpolarization), which is primarily retained by activity of ion channels: TASK 1 and 3 channels (TASK; twike-related acid sensitive K^+ channels) and Kir channels (K^+ inwardly rectifying potassium channels).[16] Another channels contributing to the maintenance of a negative resting potential are ATPases. Na^+/K^+ ATPase transports $2K^+$ ions into the cell and removes $3Na^+$ ions outside the cell and the Ca^{2+} ATPase removes calcium ions outside the cell, both using the energy from ATP hydrolysis. An important role in the homeostasis of the zona glomerulosa cells is also played by voltage dependent calcium channels: low-voltage activated calcium channels (type T, $Ca_v3.x$) and high-voltage activated calcium channels (type L, $Ca_v1.x$). Both are closed during the rest cell membrane hyperpolarization and opened during its depolarization, resulting in calcium ion entrance into the cell.[16]

The increase of intracellular calcium concentration plays a crucial role in the majority of signaling pathways of aldosterone production. It enhances the activity of cholesterol ester hydrolase, thereby increasing the bioavailability of cholesterol (a substrate for further aldosterone production), and augments "cytoskeletal" delivery of cholesterol in the vicinity of the outer mitochondrial membrane. Increased concentration of intracellular calcium also enhances mitochondrial oxidative metabolism and the formation of cofactors required for aldosterone synthase (CYP11B2) and cortisol synthase CYP11B1. Calcium ions also enhance the transcription and translation of StAR protein which in turn increases the transport of cholesterol into the internal mitochondrium membrane.[16]

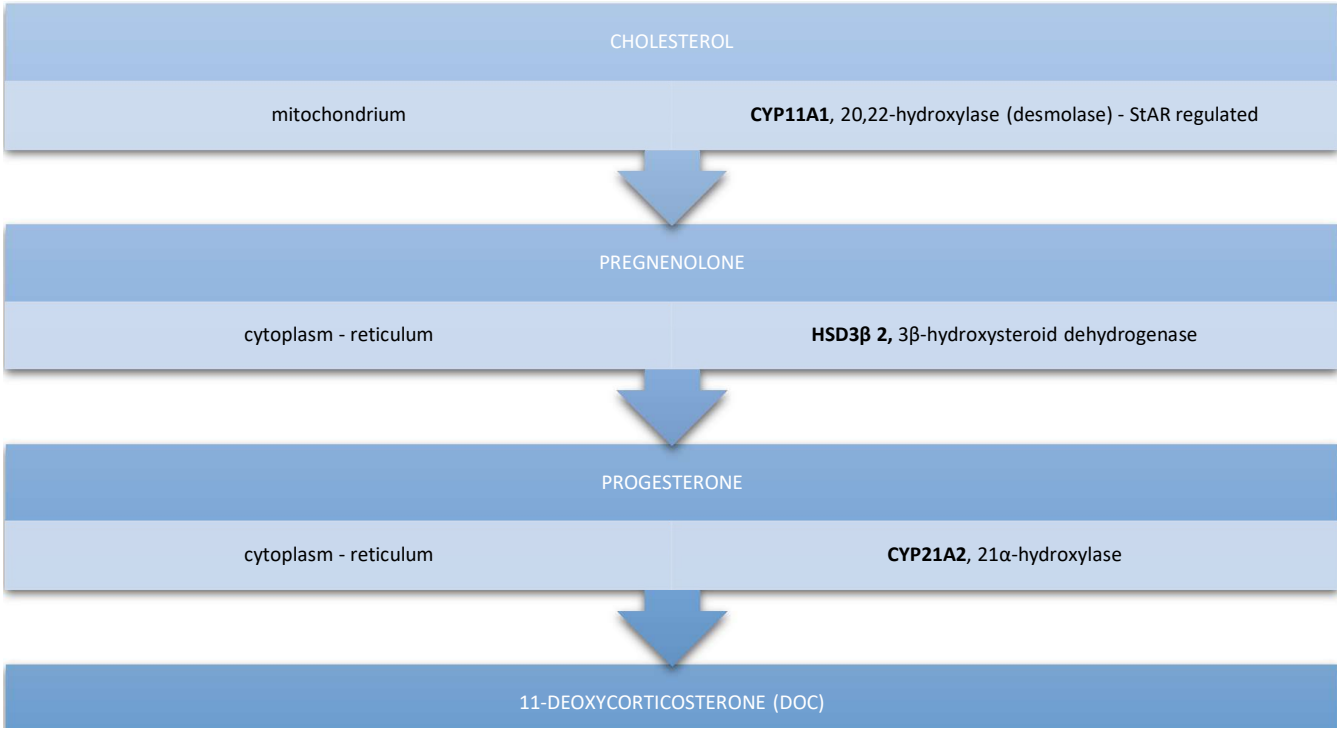

Fig. 1. A schematic diagram of aldosterone synthesis. Cholesterol is transported into the mitochondrium, where it is converted to pregnenolone by enzyme CYP11A1 (desmolase). This step is strictly controlled by the steroidogenic acute regulatory protein (protein StAR). Pregnenolone is then released into the cytoplasm, where it is converted to progesterone by the HSD3B2 dehydrogenase. In a further step progesterone undergoes 21-hydroxylation mediated by CYP21A2, synthetizing 11-deoxycorticosterone (DOC). The last step of the conversion of DOC to aldosterone takes place in the mitochondria of the adrenal zona glomerulosa cells exclusively and it is catalyzed by aldosterone synthase – CYP11B2. It consists of 3 reactions: 11β-hydroxylation, 18-hydroxylation and 18-methyloxidation

The most important regulator of the aldosterone synthesis is angiotensin II (ATII). It has been shown that chronic stimulation of angiotensin II leads to hyperplasia of the adrenal cells and increased expression of CYP11B2 and then to excessive secretion of aldosterone.[13] The direct mechanism is shown in Fig. 2. Binding of angiotensin II to angiotensin II type 1 receptor (AT1R) on the adrenal zona glomerulosa cells surface leads to TASK channels, Kir 3.4 channels, and the sodium-potassium pump closure. This results in cell membrane depolarization.[15] The consequence of a membrane depolarization is the opening of the voltage dependent L- and T-type calcium channels allowing calcium influx into the cell. Calcium mobilization activates a cascade of calcium dependent protein kinases (calcium-calmodulin protein kinases – CaMK), which enhances the expression of aldosterone synthase.

Joining ATII to its AT1R receptor triggers also other mechanisms of aldosterone secretion. It is known to activate phospholipase C, which hydrolyzes phosphatidylinositol 4,5-bisphosphate (PIP2) into inositol 1,4,5-trisphosphate (IP3) and 1,2-diacylglycerol (DAG). These act as follows:

– IP3 stimulates the release of calcium from the endoplasmic reticulum, leading to an increase of intracellular calcium concentration and contributing to the calcium dependent protein kinases activation;

– DAG activates protein kinase C (PKC), which slows the cortisol synthesis pathway by inhibiting transcription of 17-alpha-hydroxylase (CYP17), which competitively promotes aldosterone synthesis, increasing the amount of substrate for it;

– both DAG and its metabolite 12-hydroxyeicosatetraenoic acid (12-HETE) via the protein kinase D (PKD) activate CREB proteins, which further phosphorylate and modulate the expression of StAR protein and lead to increased transcription of aldosterone synthase (CYP11B2).[15]

Another important factor stimulating aldosterone secretion is a change in extracellular potassium ions concentration. The increase in extracellular potassium ion concentration induces the depolarization of the adrenal glomerulosa zone cells. It leads to voltage-dependent calcium channels opening and calcium influx. Calcium mobilization results in the activation of the calcium dependent protein kinases – CaMK, which in turn phosphorylate transcription factors stimulating CYP11B2 transcription.[15]

Among other factors affecting the secretion of aldosterone, adrenocorticotropic hormone should be mentioned. ACTH binds to MC2R (mineralocorticoid type 2 receptor), which activates adenylate cyclase (AC). Adenylate cyclase converts ATP to cAMP, which stimulates the activity of cAMP-dependent kinases including protein kinase

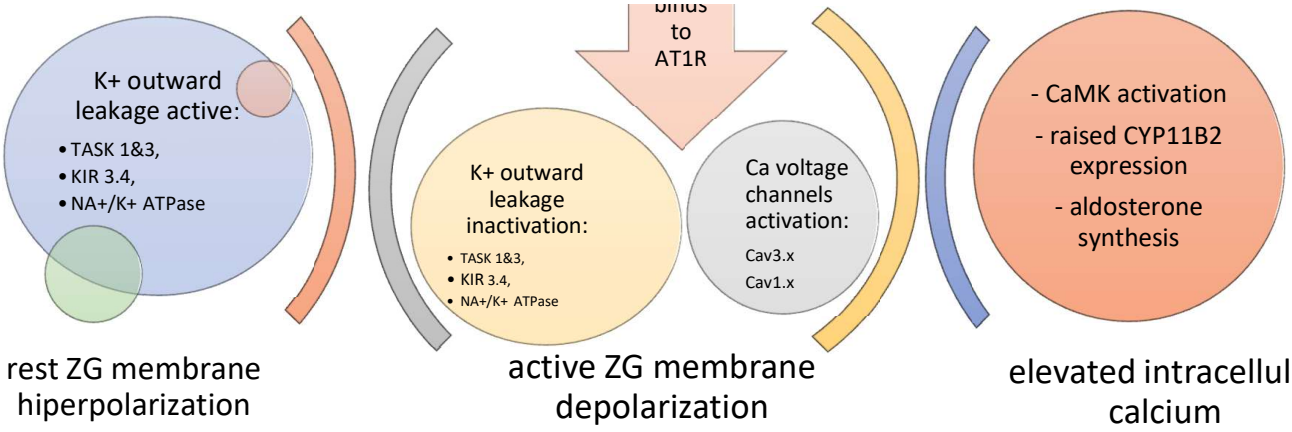

Fig. 2. A schematic diagram of rest and active ion equilibrium in the adrenal zona glomerulosa (ZG) cells. Binding of angiotensin II (AT II) to the AT1R receptor (angiotensin II type 1 receptor) on the adrenal zona glomerulosa cells surface leads to TASK channels, Kir 3.4 channels and the sodium-potassium pump closure. This results in cell membrane depolarization. The consequence of a membrane depolarization is opening of the voltage dependent L and T-type calcium channels (Cav3.x and Cav1.x) allowing calcium influx into the cell. Calcium mobilization activates a cascade of calcium dependent protein kinases (CaMK, calcium-calmodulin protein kinases), which enhances the expression of aldosterone synthase (CYP11B2) and enlarges synthesis of aldosterone

A (PKA). Protein kinase A induces a slow influx of calcium into zona glomerulosa cells by L-type calcium channels; it also regulates the transcriptional activity of CREB proteins, phosphorylates, and activates the StAR protein. The StAR protein increases the transcription of CYP11B2 and aldosterone production.[15] It has also been shown that, apart from cAMP pathway, ACTH stimulates the aldosterone production through macrophage-derived factor, steroidogenesis-inducing protein and calmidazolium.[13]

Somatic mutations in ion channels and hyperaldosteronism

Widely conducted genetic studies in the recent few years help to clarify the pathogenesis of PHA and classify the disease as a channelopathy. Pathological, excessive production of aldosterone in PHA is considered to be the result of somatic mutations appearing at different levels of aldosterone synthesis: concerning not only key enzymes but the dysfunction of ion channels as well. The selected mutations in ion channel encoding genes are presented in Table 1.

KCNJ5

In 2011 Choi et al., sequenced an exome from aldosterone-producing adenomas and identified few somatic *KCNJ5* gene mutations, which made a breakthrough in the understanding of the genetics of PHA.[17] The *KCNJ5* gene is located on chromosome 11q24.3 and encodes ion potassium channel Kir3.4. Under physiological conditions, Kir3.4 channel is responsible for the removal of potassium ions out of the cell and the maintenance of the membrane hyperpolarization. Together with ion-channel Kir3.1, it may form a high-active heterotetramer or less-active homotetramer. Choi et al. investigated the material from 22 APA patients and identified 2 types of somatic point mutations: G151R p.Gly151Arg, and L168R p.Leu168Arg (Table 1). Glycine – G151 is the first glycine belonging to the GYG motif (glycine–tyrosine–glycine) in the coding region of the potassium channel selectivity filter.[17] The side chain of leucine – L168 closely adheres to the side chain of tyrosine in mentioned GYG motif.[17] The described mutations cause a loss of Kir3.4 filter selectivity, which results in intracellular sodium current and the depolarization of the cell membrane independently on AT receptor binding. Depolarization triggers an opening of the voltage-gated calcium channels and the appearance of the intracellular calcium influx. The increase in the intracellular calcium concentration initializes a cascade of mechanisms, leading to increased aldosterone production and adrenal zona glomerulosa cells proliferation as described previously. Another somatic point mutation in *KCNJ5* gene – p.Thy158Ala (T158A), which was identified by Mulatero et al. in 2012.[18] This mutation was earlier investigated by Choi et al. as a germline mutation in familial hyperaldosteronism type 3.[17] It similarly leads to a loss of selectivity filter, sodium current influx, and cell membrane depolarization. So far, several somatic mutations in *KCNJ5* have been described – p.Ile157del, p.Glu145Gln (E145Q), and p.Trp126Arg (W126R); however, they occur extremely rarely.[19–21] Recent research allowed us to identify some further mutations of *KCNJ5*.[22–24] Scholl et al. described the presence of point mutations: I157K, F154C, and insertions I150_G151insM and I144_E145insAI, located within the coding region of the ion channel selectivity filter as well.[22] Zheng et al. described different mutation c.445-446insGAA, p.T148-T149insR, while Wang et al. identified 3 new mutations – a point mutation E147Q, an insertion mutation c.448–449insCAACAACCA and duplication G153_G164dup.[23–24] Current data allows us to estimate the prevalence of somatic *KCNJ5* gene mutations among

Table 1. Mutations detected in patients with primary aldosteronism

Gene	Description and protein	Chromosome	Mutation
KCNJ5	potassium voltage-gated channel subfamily J member 5 known as: KIR3.4, GIRK4, CIR, KATP1, LQT13	11q24.3.	somatic: G151R p.Gly151Arg L168R p.Leu168Arg T158A p.Thy158Ala p.Ile157del E145Q p.Glu145Gln W126R p.Trp126Arg I157K p.Ile157Lys F154C p.Phe154Cys I150_G151insM I144_E145insAI E147Q p.Glu147Gln p.G153_G164dup, c.457–492dupG-G, c.448–449insCAACAACCA germline: T158A p.Thy158Ala G151R p.Gly151Arg G151E p.Gly151Glu I157S p.Ile157Ser
ATP1A1	ATPase Na^+/K^+ transporting subunit alpha 1	1p21	somatic: L104R p.Leu104Arg V332G p.Val332Gly p.Phe100_Leu104del G99R p.Gly99Arg p.GluGluThrAla963Ser
ATP2B3	ATPase plasma membrane Ca^{2+} transporting 3 known as: CLA2, OPCA, PMCA3, SCAX1, CFAP39, PMCA3a	Xq28	somatic: p.Leu425_Val426del p.Val426_pVal427del p.Arg428-Val429del c.1281_1286delGGCTGT V426G_V427Q_A428_L433del p.Val424_Leu425del
CACNA1D	calcium voltage-gated channel subunit alpha 1 D known as: Ca_v1.3, CACH3, CACN4, PASNA, CCHL1A2, CACNL1A2	3p14.3	somatic: G403R p.Gly403Arg I770M p.Ile770Met I750M p.Ile750Met F747L p.Phe747Leu R990H p.Arg990His P1336R p.Pro1336Arg V259D p.Val259Asp V748I p.Val748Ile germline: G403R p.Gly403Asp I770M p.Ile770Met
CACNA1H	calcium voltage-gated channel subunit alpha 1 H known as: Ca_v3.2, ECA6, EIG6, HALD4, CACNA1HB	16p13.3	germline: M1549V p.Met1549Val
CTNNB1	catenin beta 1 known as: CTNNB, MRD19, armadillo	3p22.1	somatic: S45F p.Ser45Phe S45P p.Ser45Pro S33C p.Ser33Cys
ARMC5	armadillo repeat containing 5 known as: AIMAH2	16p11.2	germline: R898W p.Arg989Trp P826H p.Pro826His F14Y p.Phe14Tyr L156F p.Leu156Phe I170V p.Ile170Val G323A p.Gly323Ala P507L p.Pro507Leu T643M p.Thr643Met G798A p.Gly798Ala

patients with APAs to about 40%.[19–21] Female patients are more often carriers of these mutations than male, which is estimated up to 56–68% of females in different reports.[20,23,25,26] Aldosterone producing adenomas (APAs) carrying *KCNJ5* gene mutation were usually larger than APAs without mutation.[20,23] Furthermore, carriers of these mutations had higher excretion of aldosterone and lower serum potassium level than non-carriers.[23]

ATP1A1 and *ATP2B3*

Beuschlein et al. in 2013 performed an exome sequencing of material derived from 9 patients with APA and wild type of Kir3.4 channel, and identified the presence of somatic mutations in other genes – *ATP1A1* and *ATP2B3*.[27] In larger material, derived from 308 patients with APA, they confirmed the presence of the *ATP1A1* and *ATP2B3* mutations in 6.8% of cases.[27] There was no simultaneous presence of both mutations in any case.

The *ATP1A1* gene is located on chromosome 1p21 and encodes the alpha-1 subunit Na^+/K^+ ATPase. The pump is composed of 10 transmembrane segments labeled from M1 to M10. As previously mentioned, it is involved in maintaining a negative membrane resting potential (Fig. 2). Mutated ATPase has a lower affinity to potassium ions. It passively transports sodium and potassium ions into the cell, which results in the depolarization of the membrane, opening of the voltage-gated calcium channels and an increase in the intracellular calcium concentration all without angiotensin II action.[27] The 1st mutation described by Beuschlein et al. was related to the segment M1 of ATPase – p.Leu104Arg (L104R), the 2nd to the segment M4 – p.Val332Gly (V332G), and then deletion in p.Phe100_Leu104del was identified. These genetic changes lead to a rupture of glutamic acid at position 334, a key area for the proper binding of the sodium and potassium ions.[27] Williams et al. identified another point mutation in *ATP1A1* – p.Gly99Arg (G99R), and estimated the prevalence of the *ATP1A1* mutant in about 6.3% of patients.[21] Another confirmed *ATP1A1* mutation was a substitution p.GluGluThrAla963Ser in the segment M9.[28] Moreover, Åkerström et al. reported 6 novel *ATP1A1* mutations and determined the frequency of their occurrence at a similar level – 6.1%.[26]

The *ATP2B3* gene is located on chromosome X and encodes Ca^{2+} ATPase, a member of the same type ATPases family as the Na^+/K^+ ATPase. It is similarly composed of 10 transmembrane segments. The Ca^{2+} ATPase plays an important role in the maintenance of intracellular calcium homeostasis being responsible for the removal of calcium ions from the cell's cytoplasm. Two mutations of Ca^{2+} ATPase in the key area for calcium ion binding have been described: p.Leu425_Val426del, p.Val426_pVal427del.[27] Their presence concerns the M4 transmembrane segment of the pump and results in the improper binding of calcium ions, which impairs the function of the pump.

Further studies by Scholl et al., Åkerström et al., Dutta et al. and Murakami et al. led to the identification of further *ATP2B3* mutations including: c.1281_1286delGGCTGT, p.Arg428-Val429del, V426G_V427Q_A428_L433del, p.Val424_Leu425del.[22,26,29,30]

It has been observed that (*ATP1A1* and *ATP2B3*) mutants had a higher membrane level of depolarization than the cells without mutation. Both Na^+/K^+ ATPase and Ca^{2+} ATPase mutations occurred more frequently in male than female patients.[27] The general prevalence of these mutations in patients with APAs was estimated to about 3.0%.[22,26]

CACNA1D

The point mutation in the *CACNA1D* gene may lead to the development of hyperaldosteronism as well.[24,26,28,31] *CACNA1D* gene is located on chromosome 3p14.3 and encodes the calcium ion channel $Ca_v1.3$ belonging to the L-type voltage-dependent calcium channel family. It is composed of 4 homologous elements, each consisting of 6 membrane-spanning segments (referred to as S1 to S6). Subsequent mutations of the *CACNA1D*: p.Gly403Arg, p.Ile770Met, p.Ile750Met, p.Phe747Leu, p.Arg990His, p.Pro1336Arg, p.Val259Asp, V748I were identified by Wang et al., Åkerström et al., Azizan et al. and Scholl et al.[24,26,28,31] The mutations lead to the opening of the calcium channels with the lower membrane potential, which results in earlier calcium current influx, an increase in the intracellular calcium concentration and aldosterone production. The incidence of these mutations in different studies range from 3.0–7.8%. They occur more often in male than in female patients.[26,31] It has been shown that dihydropyridine calcium channel blockers are weak inhibitors of $Ca_v1.3$ so that they are considered to be effective therapy in APA patients carrying *CACNA1D* mutations.[31]

There is also data of somatic mutations in *CTNNB1* gene in PHA patients, primarily found in some solid cancers.[28,31] *CTNNB1* encodes for beta catenin 1 involved in signal transduction pathways of cell growth regulation, stem cells and embryonic development. It is located on chromosome 3p22.1.[32] Mutations in *CTNNB1* seem to be rare in APAs.[28,31,32] Some authors hypothesize they are gender specific.[33]

Germline mutations and familial hyperaldosteronism

The basis of familial hyperaldosteronism (FH) are germline mutations in genes encoding ion channels and enzymes involved in aldosterone synthesis. Mutations responsible for the excessive production of aldosterone in the familial hyperaldosteronism type I, III and IV have been identified, while the gene responsible for the FH type II still remains undetected.[34]

Familial hyperaldosteronism type I (FH1), known as glucocorticoid-remediable aldosteronism (GRA) affects about 1% of patients with PHA.[1] It is characterized by severe hypertension of early-onset, often developing before the age of 20. Its molecular basis was described by Lifton et al. in 1992.[14] The essence of FH1 is the phenomenon of a crossing over between 5' promoter region of the 11 beta-hydroxylase and 3' region of the aldosterone synthase, which are situated very closely to chromosome 8. As a result of a chimeric gene creation, aldosterone secretion occurs in the zona fasciculata of the adrenal cortex, becomes the subject of ACTH action and shows a characteristic circadian rhythm similarly to cortisol. In the FH1 treatment, small doses of dexamethasone are effective, reducing blood aldosterone level reduction, and normalizing blood pressure.[1]

Familial hyperaldosteronism type II (FH2), first described by Gordon et al. in 1991, is considered to affect up to 6% of patients with PHA.[34,35] Phenotypically, patients with FH2 do not differ significantly from patients with sporadic PHA.[34] Familial hyperaldosteronism type II is mainly characterized by a positive family history of primary aldosteronism in at least 2 first-degree relatives.[1] So far, no gene responsible for the development of the disease has been determined. The linkage to the region 7p22 is also considered, but the data is controversial and requires further confirmation.[36,37] There are opinions that it could be a result of familial accumulation of sporadic PHA as well.[34]

The first mention of another possible familial hyperaldosteronism, type III (FH3), came in 2008 from Geller et al., who described the case of a father and 2 daughters suffering from severe hypertension of early onset. It was accompanied by deep hypokalemia, massive hypertrophy of both adrenal glands, and high urine concentrations of steroid hybrids 18-oxocortisol and 18-hydroxycortisol, but with no response to dexamethasone treatment, which distinguished them completely from FH1.[38] The direct pathogenesis of the syndrome was unknown until Choi et al. described a similar case of a family. They performed sequencing of the *KCNJ5* gene and identified a germline heterozygous point mutation – T158, which allowed to distinguish a new familial hyperaldosteronism type III (FH3).[17] The mutation involves threonine – T158 lying in the area of potassium ion filter selectivity and results in the loss of its selectivity. This leads to an increased sodium inward current, cell membrane depolarization and the opening of the voltage-gated calcium channels. Calcium mobilization activates a cascade of calcium signaling pathways resulting in constantly increased aldosterone production and autonomous proliferation of glomerulosa cells.[17] Scholl et al. identified the germline *KCNJ5* mutations of: G151R and G151E, while another one – I157S – was described by Charmandari et al.[39,40] It was observed that the G151R and T158A mutation carriers are characterized by severe aldosteronism escalating with age, a significant adrenal hyperplasia, and poor response to treatment with spironolactone. On the other hand, patients carrying the G151E mutation do not have adrenal hyperplasia, the disease has early onset, but a mild course; they also better respond to treatment with spironolactone. According to Scholl et al., this may be a result of increased apoptosis of cells with this type of mutation.[39]

Very recently, Scholl et al. performed an exome sequencing in 40 unrelated patients with early onset of hypertension by the age of 10 and hyperaldosteronism.[41] They revealed the same heterozygous mutation in the *CACNA1H* gene – M1549V in 5 (12.5%) subjects. It allowed us to identify a new type IV of familial aldosteronism (FH4). The *CACNA1H* gene is located on chromosome 16p13.3 and encodes the α1 subunit of the T-type voltage dependent calcium channel $Ca_v3.2$. The *CACNA1H* mutation results in impaired channel activation and slower inactivation, which consequently leads to increased intracellular Ca^{2+} concentration and aldosterone production.[41]

Consecutive studies among patients with primary aldosteronism phenotype revealed germline mutations in *CACNA1D* gene. CACNA1D encodes for L-type voltage dependent calcium channel $Ca_v1.3$. Two point germline mutations: p.Gly403Asp and p.Ile770Met in the *CACNA1D* gene were present in 2 of 100 tested patients with early onset of PH.[31] Because the representation (2%) of this germline mutation was too small, new familial phenotype of primary aldosteronism has not been determined. Interestingly, patients who carried these mutations presented numerous additional symptoms besides hypertension, such as cerebral palsy, cortical blindness, seizures, spastic quadriplegia, neuromuscular disorders or mental retardation. It may suggest a much broader impact of these mutations on other cells and tissues, especially since it is known that beside adrenal glomerulosa cells the *CACNA1D* expression was detected in other tissues like heart, neurons, cochlear hair cells, muscle cells, and others.[31,42]

In patients with PHA the ARMC5 genetic alterations were also identified.[43] This tumor-suppressor gene was originally found in cortisol-producing macronodular adrenal hyperplasia. ARMC5 gene is located on chromosome 16p11.2 and is a member of the ARM (armadillo/beta-catenin-like repeat) superfamily. The ARM-repeat is a 42 amino acids motif repeated tandemly.[44] It is implicated in protein-protein interactions. In 56 PHA patients Zilbermint et al. identified 12 germline ARMC5 mutations in 20 unrelated and 2 related patients (39.3%), especially African Americans.[43] Recently, Mulatero et al. described 18 successive ARMC5 mutations in Caucasian patients.[45] There is little available data; however, germline ARMC5 variants might be associated with PHA.

Polymorphisms of genes encoding ion channels

Given the association between the *KCNJ5* gene mutations and primary aldosteronism, establishing the relationship between genetic polymorphisms in *KCNJ5* and susceptibility to PHA in hypertensive population seems to be important. Murthy et al. suggested a possible link of PHA with the E282Q polymorphism, which was found in 12 out of 251 patients with PHA (it is about 5%).[46] Li et al. evaluated some associations of the rs3740835 (C/A) and rs2604204 (A/C) *KCNJ5* polymorphisms with unilateral and bilateral aldosteronism. The study included 1,043 hypertensive patients (83 with unilateral aldosteronism, 142 with bilateral aldosteronism, and 818 with essential hypertension). Researchers showed a possible link between rs3740835 (C/A) polymorphism and unilateral hyperaldosteronism, but did not find the relationship with respect to bilateral hyperaldosteronism. The association between the rs2604204 (A/C) polymorphism and

either unilateral or bilateral hyperaldosteronism has not been confirmed.[47]

So far, a small number of studies does not allow us to establish a unique link between polymorphisms of the *KCNJ5* gene and primary aldosteronism. Analysis of the *KCNJ5* polymorphisms, and possibly of the other above-mentioned genes, e.g. *CACNA1D*, requires further research.

Mutations and polymorphisms in aldosterone synthase gene

Aldosterone synthase, the key enzyme involved in the last step of aldosterone synthesis, is encoded by the *CYP11B2* gene. The association between *CYP11B2* polymorphisms and excessive production of aldosterone and hypertension have been investigated. However, the data is divergent about the relationship between aldosterone synthase gene polymorphisms and hyperaldosteronism.

There are 2 common polymorphisms of the *CYP11B2* gene: C to T substitution in position – 344 and a variant of intron 2. The first polymorphism C-344T is located in the promoter area of aldosterone synthase and is related to steroidogenic factor binding protein (SF-1) involved in the regulation of CYP11B2 transcription. The second polymorphism, a variant of intron 2, is also known as a conversion allele because of the transference of the part of intron 2 of CYP11B1 to CYP11B2.[48]

A possible association between C-344T polymorphism and serum aldosterone level in normotensive patients was described by Paillard in 1999. It was suggested that the presence of the allele T is associated with a higher level of serum aldosterone.[49]

In 2007 Sokooian et al. performed a meta-analysis concerning the linkage of the C-344T polymorphism with primary hypertension. They analyzed the data from 19 studies (mainly case-control and cohort studies) involving 5,343 patients with primary hypertension and 5,882 individuals from the control group. This analysis showed a relationship between -344C allele (CC genotype) with a 17% reduction of the risk of hypertension compared to homozygous genotype TT.[50] A further meta-analysis performed by Li et al., based on 29 studies (8,482 case and 8,560 controls) of the Chinese population, also suggested a significant association of C-344T polymorphism with hypertension.[51] On the contrary, the study of Chen et al. did not confirm the association of this polymorphism with increased susceptibility to hypertension.[52] The latter meta-analysis consisted of 18 studies (4,739 case and 3,793 controls).

Inglis et al. evaluated the relationship between the *CYP11B2* polymorphisms and increased secretion of aldosterone in patients with hormonally active adrenal adenoma. The frequency of the 344T allele and conversion allele differed significantly in APA patients when compared to the healthy control group. However, these researchers did not find statistical significance in the frequency of these alleles in the material from APAs in relation to the control genomic DNA. It is assumed that these genotypes may rather predispose people to an increased aldosterone production than to tumor growth.[53] Jia et al. performed a meta-analysis of available case-control studies to assess the relationship between *CYP11B2* polymorphisms and primary hyperaldosteronism. They analyzed 7 studies concerning T-344C substitution (which were attended by 621 case and 1,027 controls) and 3 studies of the A2718G polymorphism (327 case and 336 controls). The study group consisted of patients with idiopathic aldosteronism (IHA) or aldosterone producing adenoma (APA), while patients with essential hypertension or without hypertension were included in the control group. The researchers found a relationship between T-344C polymorphism (recessive model) with idiopathic aldosteronism, but did not observe a similar relationship between patients with adrenal adenomas. There was no sufficient evidence and data to establish the relationship with the A2718G polymorphism and increased risk of PHA. Their study suggests that the -344C allele may be associated with a lower risk of developing idiopathic primary aldosteronism.[54]

The association between transcription rate of *CYP11B2* gene and its own polymorphism T-1651C was studied. McManus et al. found that the transcriptional repressor – APEX1 binds the -1651T allele stronger than the -1651C allele, which results in reduced *CYP11B2* expression and consequently lower aldosterone production. The authors also reported a correlation between the variant -1651T and lower excretion rates of aldosterone metabolites.[55]

Summary

Primary hyperaldosteronism is an important clinical problem, considering its high prevalence among hypertensive subjects and unequivocally increased cardiovascular risk. Elucidating the pathophysiology and improving diagnostics of the disease is of great concern. Widely conducted genetic studies have shed new light on the pathogenesis of PHA, classifying primary hyperaldosteronism as a channelopathy. There is a significant frequency of somatic and germline mutations in ion channel encoding genes in PHA patients. The data is still inconsistent. In fact, there is numerous evidence of a predicted significance available in the literature; however, there is still a lack of a so-called "game changer" bringing the final conclusion for therapeutic and, hopefully, preventive strategies for the whole population. The possible link between gene polymorphism of aldosterone synthase or ion channels and both primary hypertensive disease and primary aldosteronism requires further research. The genetic investigation hopes to find new solutions for the future. Identifying carriers of potentially prognostic genetic variants would not only contribute to a more precise diagnosis, but to the development of a specific, new treatment as well.

References

1. Funder JW, Carey RM, Mantero F, et al. Case detection, diagnosis, and treatment: An endocrine society clinical practice guideline. *J Clin Endocrinol Metab*. 2016;101:1889–1916.
2. Fagugli RM, Taglioni C. Changes in the perceived epidemiology of primary hyperaldosteronism. *Int J Hypertens*. 2011;2011:162804.
3. Rossi GP, Bernini G, Caliumi C, et al. A prospective study of the prevalence of primary aldosteronism in 1,125 hypertensive patients. *J Am Coll Cardiol*. 2006;48:2293–2300.
4. Conn JW. Primary aldosteronism, a new clinical syndrome. *J Lab Clin Med*. 1955;45:3–17.
5. Milliez P, Girerd X, Plouin PF, Blacher J, Safar ME, Mourad JJ. Evidence for an increased rate of cardiovascular events in patients with primary aldosteronism. *J Am Coll Cardiol*. 2005;45:1243–1248.
6. Fallo F, Veglio F, Bertello C, et al. Prevalence and characteristics of the metabolic syndrome in primary aldosteronism. *J Clin Endocrinol Metab*. 2006;91:454–459.
7. Weber KT, Brilla CG. Pathological hypertrophy and cardiac interstitium. Fibrosis and renin–angiotensin–aldosterone system. *Circulation*. 1991;83:1849–1865.
8. Stowasser M, Sharman J, Leano R, et al. Evidence for abnormal left ventricular structure and function in normotensive individuals with familial hyperaldosteronism type I. *J Clin Endocrinol Metab*. 2005;90: 5070–5076.
9. Sechi LA, Fabio A, Bazzocchi M, Uzzau A, Catena C. Intrarenal hemodynamics in primary aldosteronism before and after treatment. *J Clin Endocrinol Metab*. 2009;94:1191–1197.
10. Freel EM, Mark PB, Weir RAP, et al. Demonstration of blood pressure-independent noninfarct myocardial fibrosis in primary aldosteronism: A cardiac magnetic resonance imaging study. *Circ Cardiovasc Imaging*. 2012;5:740–747.
11. Staermose S, Marwick TH, Gordon RD, Cowley D, Dowling A, Stowasser M. Elevated serum interleukin 6 levels in normotensive individuals with familial hyperaldosteronism type 1. *Hypertension*. 2009;53:31–33.
12. Bernini G, Galetta F, Franzoni F, et al. Arterial stiffness, intima-media thickness and carotid artery fibrosis in patients with primary aldosteronism. *J Hypertens*. 2008;26:2399–2405.
13. Connell JMC, Davies E. The new biology of aldosterone. *J Endocrinol*. 2005;186:1–20.
14. Lifton RP, Dluhy RG, Powers M, et al. A chimaeric 11 beta-hydroxylase/aldosterone synthase gene causes glucocorticoid-remediable aldosteronism and human hypertension. *Nature*. 1992;355:262–265.
15. Hattangady NG, Olala LO, Bollag WB, Rainey WE. Acute and chronic regulation of aldosterone production. *Mol Cell Endocrinol*. 2012;350:151–162.
16. Guagliardo NA, Yao J, Hu C, Barrett PQ: Minireview: Aldosterone biosynthesis: Electrically gated for our protection. *Endocrinology*. 2012;153:3579–3586.
17. Choi M, Scholl UI, Yue P, et al. K^+ channel mutations in adrenal aldosterone-producing adenomas and hereditary hypertension. *Science*. 2011;331:768–772.
18. Mulatero P, Tauber P, Zennaro MC, et al. KCNJ5 mutations in European families with nonglucocorticoid remediable familial hyperaldosteronism. *Hypertension*. 2012;59:235–240.
19. Azizan EAB, Murthy M, Stowasser M, et al. Somatic mutations affecting the selectivity filter of KCNJ5 are frequent in 2 large unselected collections of adrenal aldosteronomas. *Hypertension*. 2012;59:587–591.
20. Åkerström T, Crona J, Delgado Verdugo A, et al. Comprehensive re-sequencing of adrenal aldosterone producing lesions reveal three somatic mutations near the KCNJ5 potassium channel selectivity filter. *PLoS One*. 2012;7:1–7.
21. Williams TA, Monticone S, Schack VR, et al. Somatic ATP1A1, ATP2B3, and KCNJ5 mutations in aldosterone-producing adenomas. *Hypertension*. 2014;63:188–195.
22. Scholl UI, Healy JM, Thiel A, et al. Novel somatic mutations in primary hyperaldosteronism are related to the clinical, radiological and pathological phenotype. *Clin Endocrinol* (*Oxf*). 2015;83:779–789.
23. Zheng FF, Zhu LM, Nie AF, et al. Clinical characteristics of somatic mutations in Chinese patients with aldosterone-producing adenoma. *Hypertension*. 2015;65:622–628.
24. Wang B, Li X, Zhang X, et al. Prevalence and characterization of somatic mutations in Chinese aldosterone-producing adenoma patients. *Medicine* (*Baltimore*). 2015;94:e708.
25. Zennaro MC, Jeunemaitre X, Boulkroun S. Integrating genetics and genomics in primary aldosteronism. *Hypertension*. 2012;60:580–588.
26. Åkerström T, Willenberg HS, Cupisti K, et al. Novel somatic mutations and distinct molecular signature in aldosterone-producing adenomas. *Endocr Relat Cancer*. 2015;22:735–744.
27. Beuschlein F, Boulkroun S, Osswald A, et al. Somatic mutations in ATP1A1 and ATP2B3 lead to aldosterone-producing adenomas and secondary hypertension. *Nat Genet*. 2013;45:440–442.
28. Azizan EA, Poulsen H, Tuluc P, et al. Somatic mutations in ATP1A1 and CACNA1D underlie a common subtype of adrenal hypertension. *Nat Genet*. 2013;45:1055–1060.
29. Dutta RK, Welander J, Brauckhoff M, et al. Complementary somatic mutations of KCNJ5, ATP1A1, and ATP2B3 in sporadic aldosterone producing adrenal adenomas. *Endocr Relat Cancer*. 2014;21:3–6.
30. Murakami M, Yoshimoto T, Minami I, et al. A novel somatic deletion mutation of ATP2B3 in aldosterone-producing adenoma. *Endocr Pathol*. 2015;26:328–333.
31. Scholl UI, Goh G, Stölting G, et al. Somatic and germline CACNA1D calcium channel mutations in aldosterone-producing adenomas and primary aldosteronism. *Nat Genet*. 2013;45:1050–1054.
32. CTNNB1 catenin beta 1. ncbi.nlm.nih.gov https://www.ncbi.nlm.nih.gov/gene/1499. Updated June 10, 2018. Accessed June 13, 2018.
33. Dutta RK, Soderkvist P, Grimm O. Genetics of primary hyperaldosteronism. *Endocr Relat Cancer*. 2016;23:R437–R454.
34. Mulatero P, Tizzani D, Viola A, et al. Prevalence and characteristics of familial hyperaldosteronism: The PATOGEN study (Primary aldosteronism in TOrino-GENetic forms). *Hypertension*. 2011;58:797–803.
35. Gordon RD, Stowasser M, Tunny TJ, Klemm SA, Finn WL, Krek AL. Clinical and pathological diversity of primary aldosteronism, including a new familial variety. *Clin Exp Pharmacol Physiol*. 1991;18:283–286.
36. So A, Duffy DL, Gordon RD, et al. Familial hyperaldosteronism type II is linked to the chromosome 7p22 region but also shows predicted heterogeneity. *J Hypertens*. 2005;23:1477–1484.
37. Carss KJ, Stowasser M, Gordon RD, O'Shaughnessy KM. Further study of chromosome 7p22 to identify the molecular basis of familial hyperaldosteronism type II. *J Hum Hypertens*. 2011;25:560–564.
38. Geller DS, Zhang J, Wisgerhof MV, Shackleton C, Kashgarian M, Lifton RP. A novel form of human mendelian hypertension featuring nonglucocorticoid – remediable aldosteronism. *J Clin Endocrinol Metab*. 2008;93:3117–3123.
39. Scholl UI, Nelson-Williams C, Yue P, et al. Hypertension with or without adrenal hyperplasia due to different inherited mutations in the potassium channel KCNJ5. *Proc Natl Acad Sci USA*. 2012;109:2533–2538.
40. Charmandari E, Sertedaki A, Kino T, et al. A novel point mutation in the KCNJ5 gene causing primary hyperaldosteronism and early-onset autosomal dominant hypertension. *J Clin Endocrinol Metab*. 2012;97:1532–1539.
41. Scholl UI, Stolting G, Nelson-Williams C. Recurrent gain of function mutation in calcium channel CACNA1H causes early-onset hypertension with primary aldosteronism. *Elife*. 2015;4:e06315. doi: 10.7554/eLife.06315
42. CACNA1D Gene. genecards.org. https://www.genecards.org/cgi-bin/carddisp.pl?gene=CACNA1D. Accessed July 27, 2016.
43. Zilbermint M, Xekouki P, Faucz FR, et al. Primary aldosteronism and ARMC5 variants. *J Clin Endocrinol Metab*. 2015;100:E900–909.
44. ARMC5 armadillo repeat containing 5. ncbi.nlm.nih.gov. https://www.ncbi.nlm.nih.gov/gene/79798. Updated June 3, 2018. Accessed June 13, 2018.
45. Mulatero P, Schiavi F, Williams TA, et al. ARMC5 mutation analysis in patients with primary aldosteronism and bilateral adrenal lesions. *J Hum Hypertens*. 2016;30:374–378.
46. Murthy M, Xu S, Massimo G, et al. Role for germline mutations and a rare coding single nucleotide polymorphism within the KCNJ5 potassium channel in a large cohort of sporadic cases of primary aldosteronism. *Hypertension*. 2014;63:783–789.
47. Li N, Shi C, Li H, et al. Association of KCNJ5 gene rs3740835(C/A) and rs2604204(A/C) polymorphism with unilateral and bilateral primary aldosteronism. *Chinese J Med Genet*. 2014;31:233–237.
48. White PC, Slutsker L. Haplotype analysis of CYP11B2. *Endocr Res*. 1995; 21:437–442.
49. Paillard F, Chansel D, Brand E, et al. Genotype-phenotype relationships for the renin–angiotensin–aldosterone system in a normal population. *Hypertension*. 1999;34:423–429.

50. Sookoian S, Gianotti TF, González CD, Pirola CJ. Association of the C-344T aldosterone synthase gene variant with essential hypertension: A meta-analysis. *J Hypertens*. 2007;25:5–13.
51. Li W, Liu C. The -344C/T polymorphism in the CYP11B2 gene is associated with essential hypertension in the Chinese. *JRAAS*. 2014;15:150–155.
52. Chen J, Jing J, Tan H, Song M, Yu S, Huang L. Lack of association of CYP11B2-344C/T polymorphism with essential hypertension: A meta-analysis. *Int J Clin Exp Med*. 2015;8:9162–9167.
53. Inglis GC, Plouin PF, Friel EC, Davies E, Fraser R, Connell JMC. Polymorphic differences from normal in the aldosterone synthase gene (CYP11B2) in patients with primary hyperaldosteronism and adrenal tumour (Conn's syndrome). *Clin Endocrinol* (*Oxf*). 2001;54:725–730.
54. Jia M, Zhang H, Song X, et al. Association of CYP11B2 polymorphisms with susceptibility to primary aldosteronism: A meta-analysis. *Endocr J*. 2013;60:861–870.
55. McManus F, Sands W, Diver L, et al. APEX1 regulation of aldosterone synthase gene transcription is disrupted by a common polymorphism in humans. *Circ Res*. 2012;111:212–219.

Mandibular ridge reconstruction: A review of contemporary methods

Natalia Dorosz[A,C], Marzena Dominiak[E,F]

Department of Oral Surgery, Wroclaw Medical University, Poland

A – research concept and design; B – collection and/or assembly of data; C – data analysis and interpretation;
D – writing the article; E – critical revision of the article; F – final approval of the article

Advances in Clinical and Experimental Medicine, ISSN 1899-5276 (print), ISSN 2451-2680 (online) *Adv Clin Exp Med*. 2018;27(8):1159–1168

Address for correspondence
Natalia Dorosz
E-mail: nataliadorosz1@gmail.com

Funding sources
None declared

Conflict of interest
None declared

Received on December 7, 2016
Reviewed on December 29, 2016
Accepted on May 24, 2017

Abstract

Reconstruction can be very problematic in the case of mandibular alveolar bone loss, which can also hinder the implant restorative treatment. The aim of the study was to present current views on reconstructing the alveolar part of mandibular bone, which allows the insertion of implants and then the placement of denture. Based on the available literature, the efficacy of various techniques of filling of mandibular bone losses was described and compared. Reconstruction with autogenous bone block graft had been used as a gold standard. Recently, other techniques have appeared that offer better functional and esthetics results. They include reconstruction with allogeneic bone block graft, osteotomy allowing immediate insertion of implants, bone distraction, guided bone regeneration using titanium mesh (Ti-mesh), new techniques using scaffolds (biphasic calcium phosphate, poly-lactide-co-glycolide/tricalcium phosphate, bioresorbable polycaprolactone), Sonic Weld Technique® (Tuttlingen, Germany) using resorbable membrane and pins with polymer lactide acid (PLA), and the tent technique. These abovementioned techniques allow solving the problem of insufficient amount of bone for prosthetic treatment.

Key words: allogeneic bone, titanium mesh, scaffold, resorbable pins, tent technique

DOI
10.17219/acem/74054

Introduction

Mandibular ridge atrophy often results in difficulties and compromises in prosthodontic treatment. It manifests itself in insufficient retention of the lower restorations or prosthetic base overload pain. The lack of restoration causes eating and speaking difficulties, but also adversely affects the appearance and mood of the patient.[1] The use of dental implants as prosthetic pillars for fixed dentures could be the solution to this problem. It is one of the most common, predictable, fully functional and esthetic methods to replace missing teeth.[2,3] A sufficient amount of bone is necessary to ensure the long-term success of dental implants. According to the research, it is believed that minimum amount of bone required for implantation is 4 mm in width and 7 mm in the vertical dimension.[4] When the mandibular ridge is decreased, especially because of periodontitis, inserting short implants is often insufficient. Shallow vestibule and small amount of the keratinized gingiva significantly reduces effective application of dental restorations. Another consequence of using short implants with a small vertical dimension of mandibular ridge is the increased distance between the implant and the occlusal plane that induces unfavorable biomechanical forces. Increasing the vertical and horizontal dimension of alveolar ridge enables us to achieve optimal conditions for teeth reconstruction, including function and esthetics.[1]

The aim of the study was to present a review of the literature concerning the possibility of mandibular ridge defects reconstruction.

Methods used in mandibular ridge reconstructions include: bone blocks taken from extra- or intraoral site,[5,6] allogenic material blocks,[7–9] bone distraction,[10] osteotomy,[11–13] controlled bone regeneration using resorbable or non-resorbable membrane[14,15] or titanium mesh (Ti-mesh) and modern methods using biphasic calcium phosphate (BCP),[16] polylactide glycolic tricalcium phosphate[17] and polylactide media gelatin scaffolds (PLC),[18,19] bioresorbable pins,[20] and "tent technique."[21] To increase the amount of space for long implants, transposition of the inferior alveolar nerve can also be performed.[22–24]

Autologous bone

Autologous bone was considered the golden standard of jaw atrophy treatment because of its osteogenic, osteoinductive and osteoconductive properties. However, to get the bone material, it is necessary to conduct an additional procedure that could lead to numerous complications, including infection, bleeding, pain, edema, destruction of blood vessels or nerves, and high degree of resorption. The availability of autogenic bone is limited. Vascularized bone grafts may be used to reduce the risk of bone graft resorption, particularly in extensive reconstructions.

Vascularized grafts in comparison to nonvascularized ones have uninterrupted blood flow through microvascular anastomosis. As a result, the bone is nourished, healing time can be reduced and complications such as infection or resorption occur less frequently than in nonvascularized grafts. This method can be particularly useful after a mandible resection. While harvesting the graft in one area and placing it in another, there are 2 places where intra- and post-operative complications may occur. The important properties that affect the post-performance effect is the presence of living osteocytes in the graft, which develop their functions by providing immediate circulation, allowing the graft to be stabilized regardless of bone block vascularization. Survival of the graft is not determined by its size or the extent of contact between the graft and the bone.[25] Vascularized graft survival rate equals 96%, whereas nonvascularized grafts have a survival rate of 69%. A particularly important advantage they have over nonvascularized grafts is with deficiencies bigger than 6 cm and when tissue recipient region has earlier been inflamed.

Places to harvest bone for mandible reconstruction are the fibula, iliac crest, scapula, and forearm radial bone. In the past, allografts were used from ribs and the metatarsus, but due to the numerous disadvantages, such as thinness and difficulty in matching shape, they have fallen into disuse.[26]

Vascularized fibula flap

A vascularized fibula flap provides a good base for implants. The efficacy of this treatment was described by Kramer et al., who examined 51 implants in 16 patients.[61] In this study, the authors reported that out of 51 implants inserted in 16 patients only one was rejected. Because of soft tissue inflammation, 2 implants remained undiscovered. Therefore, the effectiveness of treatment reached 96%.

Fibula graft involves the smallest risk of complications of all vascularized grafts.[27] The discrepancy between the amount of fibula material and the bone loss can be a great impediment in prosthetic reconstruction. The average height of mandible (including dentition) is 2–3 cm and the height of the fibula flap is 1–1.2 cm. Thus, dividing fibula for several parts by osteotomy may be the solution, allowing for esthetic and functional reconstruction. A 25 cm long transplant can be taken from the fibula without compromising its blood supply. The fibula is supplied with blood by the sagittal artery and vein common peroneal, both 15 cm long. Usually, the newly created jaw contour depends on the curvature of the plate formed preoperatively.[28] A stereolithography model allows for planning a preoperative treatment, designing suitable shape and cuts, shortening surgery and significantly increasing the accuracy and functionality of the transplant.[29]

The possibility to conduct 2 operations (fibula resection and mandible reconstruction) at the same time is an important advantage.[30] The results of 10-year-long Hidalgo observations show that a fully functional and esthetic

effect was achieved in 70% of the patients, and the appropriate amount of bone was maintained in 92–93% of cases.[27] Postoperative complications in the donor site were minor; they included walking pain (24–28%) and small instability within the ankle. The problem of ankle instability and pain can be solved by leaving the distal part of fibula. As in any surgery, the donor and recipient may suffer from complications such as bleeding, hematoma, pleural, infection, and dehiscence. One possible complication in the recipient site may be an unsuccessful transplantation (5% patients). Among the predisposing factors to such complications are previously mentioned technical difficulties during the procedure (related to designing, collecting or matching graft and making vascular connections), external compression (too tight wound closure, hematoma, twisted artery), problems associated with recipient site (prior radiotherapy, postoperative sepsis), and other general diseases.[25]

Attachment of neurosensory component increased reconstruction possibility. Lateral peroneal skin nerve was incorporated to the graft.[31]

Other vascularized grafts

Another place to harvest vascularized graft may be the iliac crest. This method allows collecting long (6–16 cm) and wide graft of appropriate thickness containing compact and spongy bone. The flap has a natural curvature, which can be used in jaw oval reconstruction. Peripheral iliac arteries are 5–7 cm long. Thus, significant amount of bone may be collected, contrary to that obtained from the fibula.[30]

In the study by Maiorana et al., the collected and properly fitted graft was attached to the jaw bone using titanium plates and screws. Next, surgical anastomoses were built. The treatment required hospitalization for 14 days.[32] Approximately 5 months after alveolar ridge reconstruction, patients were provided with implants. In 1 out of 4 patients, fracture of the hip bone graft after implantation happened. After proper dental implants osteointegration and healing of the wounds, the missing teeth were supplemented. After a half-year and a 3-year control, there were no complications or pathological changes – it proves new formed bone creates very good conditions for implants. Treatment was successful in 95.2%.[33]

The bone curvature often makes it difficult to create anterior mandible shape, and grafts collected with surrounding mucosa and skin leads to difficulties in obtaining good esthetic results. Extensive preparation and a section of oblique and transverse muscles are required when collecting a graft, as this might create the risk of postoperative hernia (this complication can be prevented by a thorough closing of the abdominal wall). Another complication that may occur when collecting a large flap is cutting the skin thigh nerve and following numbness in this area. In older patients, treatment in this area often causes pain and impaired walking in the early postoperative period. Because of these drawbacks, iliac crest graft is usually used as a second choice to collect bone flap when it is not possible to collect it from the fibula.[30]

Another place to collect bone graft is the forearm, where the bone is nourished by the radial artery and the accompanying veins or superficial veins. The graft may be approx. 10–14 cm long. Its advantages include the presence of vascular pedicle, and appropriate length and diameter that enables creating graft. There is a risk of radius fracture, so the graft thickness should not exceed 30% diameter of the radial bone.[34] In addition, some difficulties may occur with restoring the proper shape of the bone; moreover, the height obtained after the surgery may appear as insufficient for implants.

Since 1982, scapular grafts, which included skin and bone, were used for jaw bone reconstruction. A graft from this area can be up to 14 cm long. Peripheral artery and vein are capable of nourishing large bone graft and mucous membrane. Also, there is an elastic connection between the bone and the mucous membrane. A significant disadvantage of a graft is its location that does not allow simultaneous resection of the mandible and collecting graft. When, after resection, extensive cavity and lack of soft tissue exist, an additional graft with fragment of latissimus dorsi musculus can be collected. Because of good blood supply, graft can be properly shaped. Vessels are 6–9 cm long. The quality of the scapular bone in the context of implantological and prosthetic treatment is usually worse than when the material is taken from fibula or iliac crest. After the procedure, mild pain may occur, but it does not restrict normal life activity.[26]

Allogenic bone from tissue bank

Allogenic bone taken from tissue bank can be an alternative bone block to the autogenous one. All complications connected with the donor can be avoided.[7] During the process of removing immunogenic properties, its biomechanical properties do not change.[8] Stabilization of allogenic bone block is necessary for vascularization and bone remodeling.[9]

Allogenic transplants are taken from individuals of the same species. They exhibit osteoconductive and slight osteoinductive properties, which are often sufficient to initiate osteogenesis. An additional source of these factors can be platelet rich plasma (PRP). Platelet rich plasma accelerates the process of graft remodeling and increases the density of newly formed bone.[8] In addition, this method enables the construction of a 3-dimensional bone model designed by computed tomography (CT). In the next step, allogenic material is shaped to exactly fill the bone defect. The block is sterilized and transferred to the patient's mouth. In one of the studies, a 5-month observation confirmed the quality of newly formed cortical and cancellous bone.[7]

In another study, fresh-frozen blocks of allogenic cortical-cancellous bone were used.[9] Augmentation was performed using the onlay technique. After cutting and detaching the full-thickness vestibular graft, holes were drilled into the bone in order to improve grafts blood supply. Lingual graft was not detached. Allogenic material had been processed and matched ex tempore, and then fixed in the recipient site using titanium microscrews. Collagen membranes were used to seal xenogenic materials. Screws were removed after 16 weeks, and implantation procedure was performed. In a study group of 10 patients, the procedure was successful in 8 of them. Failure of treatment in 2 patients had occurred due to premature resorption of allogenic material and the development of local inflammatory process.[9]

Using a technique that utilizes freshly frozen allogenic bone requires a device for its storing and conditioning. When autogenous bone harvesting surgery is inadvisable, the allogenic bone allows for the reconstruction of defects. Grafts made preoperatively on a 3D model significantly shorten the procedure time and allow the precise shape of jaw bone defect to be obtained.

Bone distraction

This method is used in the treatment of numerous bone deformities; it was described by Ilizarov, who studied and systematized its biological basis.[35] According to the first principle, continuous distraction of the bone causes stress reaction upon stretching, rapid growth and regeneration. According to the second principle, the mechanical load and the need for blood affect the rate of growth and shape of the new-formed bone.[36] Bone blood supply during osteodistraction comes from the lingual periosteum, where the mucosa and periosteum remain attached at all times.[37] Distraction of alveolar ridge can be divided into vertical and horizontal. Increasing the vertical dimension of the decreased mandibular ridge enables subsequent implant or prosthetic treatment. Along with the reconstruction of the bone, soft tissues are reconstructed using the same mechanism.[35] The effect of extending bone length uses a mechanism of healing process by progressive stretching of 2 split bone segments.

After the proper osteotomy, process of bone lengthening is divided into 3 phases. First phase – inertia – lasts 24–72 h; it is a period between osteotomy, fixing osteodistractive device and onset of distraction. At this time, clot formation occurs between bone fragments, then it is transformed into granulation tissue and soft callus. Granulation tissue is replaced by fibrous tissue. After inertia, the distraction phase follows, when the daily extending span of distractive device that connects segments of bone progressively moves bone fragments. Increased stretching of soft callus induce enhancement of metabolic activity and bone formation. Bone growth equals 1–2 mm a day. Once the desired amount of bone is obtained, the final stage follows – stabilization phase. At this point, mineralization and remodeling of newly formed bone occurs, which takes about 6–12 weeks.[36]

In comparison to autogenous bone graft or alloplastic materials, bone created in the osteodistraction process shows the absence of postoperative resorption and fewer complications. Simultaneous reconstruction of soft tissues eliminates its deficiency. Another big advantage of this method is the short time needed to achieve the correct amount of alveolar bone.[10,38]

The average increase of bone to be obtained is between 8.2 mm and 13 mm. In the study by Kumar et al. and Gerber-Leszczyszyn et al., high quality bone for dental implants was obtained and restoration was introduced.[35,36]

Complications that may occur during osteodistraction include the bad position of bone segment or its fracture, errors in new tissue formation and bone infections. During the entire osteodistraction process, the occurring complications may be related to the distractor device, distraction phase and phase of consolidation: early fracture (2%), late fracture (17%), bleeding or hematoma (4%), infection (6%), skin perforations (2%), mucosal dehiscence (8%), sensory disturbances (28%), hanging chin (13%), and failures associated with inserting dental implants (13%). The sensory disturbances may be caused by mental nerve irritation while establishing or removing the distractor.[37]

Transposition of the inferior alveolar nerve

Carrying out the procedure of implanting suitable length implants may not be possible in case of significant mandibular ridge resorption or reduction of the distance between ridge and vault of inferior alveolar nerve canal.[22,23] Transposition of the inferior alveolar nerve may allow inserting longer implants into the bone, which would provide better stabilization.[23] There are 2 methods of inferior alveolar nerve transposition. The first one incudes mental foramen to bone fragment during osteotomy cuts, whereas the second method leaves it intact, when cuts are made distally from it. The size of the bone block depends on the number of implants to be inserted.[22] Vertical cuts should be distanced about 3–4 mm from mental foramen. This distance reduces the risk of neurosensory disorders after surgery.[24] After detaching the bone fragment and gently removing it from the proximity of the nerve with a special rounded and polished hook, a bundle of vascular and nervous bunch was moved away and held down with a wide, elastic band for the time of implant placing.

Pulling nervous vascular bundle or using force on the nerve must be reduced to avoid the risk of damage, a wide contact, instead of single point pressure, should be used. During the procedure, the nerve should be humidified by saliva. After completing the treatment, the vascular

nervous bundle has to be placed in the initial position. Direct contact between the nerve and implant is inadvisable. A membrane, a bone block or newly formed bone may be used to separate them.[24]

Not using a mental foramen violation causes less risk of nerve damage (33.3%) in comparison with the method including a mental foramen (77.8%)[23], and fewer post-operative complications.[22] One of the major complications after surgery is lack of feeling in the lower lip, which, according to the study of Kan et al. concerned 7 out of 21 operated areas.[23] This neurosensory disturbance did not affect the patients' daily life. In a study by Nocini et al., numbness occurred postoperatively in patients, especially in mental nerve area, but anesthesia or paresthesia did not appear.[22] Intraoperative complications that may occur include mandibular fracture, postoperative infection, and hemorrhage. When the blood supply to nerves is impaired – usually when the nerve is damaged – nerve necrosis in its distal part may occur. Another method is to create a channel in outer layer of mandibular compact bone, where the nerve can be transferred. In the study by Kan et al., implementation preceded by inferior alveolar nerve transposition ended osteointegration at 93.8%.[23] However, the increased distance between the alveolar part of the mandible and the occlusal plane causes many difficulties in esthetic supplementation. Horizontal forces of chewing, which impact dental implants, have a destructive influence on the surrounding bone.[21]

Osteotomy

The osteotomic technique is a one-step expansion of the alveolar ridge in buccal-lingual dimension and dental implants insertion. A huge advantage of this method is a significant reduction in the time of treatment from the beginning of the procedure to the final prosthetic supply (no bone augmentation is performed).[11]

In a 5-year study by Engelke et al., the efficacy of this method amounted to 86.2%. The average marginal bone loss was 1.7 mm.[12] Researchers observed a lower level of infection than with guided tissue regeneration (GTR) techniques using membranes. According to this research, the minimum ridge width for the procedure with a reduced risk of complications such as perforation is 3.12 mm.[13]

After the muco-periosteal flap was detached, a segmented separation of vestibular cortical lamina was performed in order to move it to the position it had occupied before the extraction.[13] Using a diamond disk or Piezosurgery® (Mectron, Genova, Italy), a vertical cut was made to mobilize the vestibular bone fragment.[13] Vertical cuts were made 5 mm mesially and distally from the planned implantation. Using osteotomes, the base of the lamina was broken and placed buccally. During mobilization, the periosteum should not be interrupted. Implants were placed in the space between bone fragments without further preparation. Microscrews provided bone and implant stability. It is possible to use a granulate form material to provide additional protection or polytetrafluoroethylene membrane (e-PTFE) or polylactide membranes. After 4–6 months, the microscrews were removed, the implants were revealed and healing abutments fixed. Prosthetic treatment begins around 3 weeks after the implants are revealed.[13]

The use of new technologies

Rapid prototyping

Immediate prototyping (rapid prototyping – RP) allows for the creation of structures and models by the use of a computer and computed tomography. Rapid prototyping can be divided into 2 groups: addition (build-up of material) and the material cutting from the block.

Two commonly used technologies of immediate production of individual models (prototypes) are 3D printing (3DP) and stereolithography. 3D printing is characterized by high precision, faster printing and lower production cost than stereolithography. This technology is applied to the virtual treatment planning, production of models used as a template to carry out cuts, or drilling the matrix for the retaining screw (if proper material or mesh scaffold is too fragile). It also makes it possible to prepare the mesh and scaffold for the reconstruction.[26,39,40] Preoperative preparation of the appropriate model shortens the operating time, and thus the exposure of tissues to infection, long-term lack of nutrition and stretching.

The use of computer-aided design/computer-aided manufacturing (CAD/CAM) also allows us to obtain the desired shape of the scaffold or mesh, which is perfectly fitted to the bone loss. The shape is created using mirror algorithm of the opposite site, or by using hole-filling technology. In some cases, both algorithms are used to obtain the desired shape of the final product.[41]

Stereolithography is a very popular RP technology based on the conversion of monomer from a resin in a hard polymer after UV radiation. This technique is more precise and enables – as opposed to the alternative of cutting – the production of complex internal structures. The process is not widely used because of its high cost, long preparation time and limited size of the final object.

New technologies are also used to design bioresorbable scaffolds and titanium, polyglicolactyde and tricalcium phosphate meshes to reconstruct a decreased mandibular ridge.

Titanium mesh reconstruction

Functional bone reconstruction is also allowed by guided bone regeneration (GBR) with mixed autogenous and xenogeneic bone and titanium mesh generated with the aid of CAD/CAM technology. Titanium mesh (Ti-mesh) with

a thickness of 0.2 mm is used for the reconstruction. This thickness creates enough space for the material, making it possible to obtain the desired, durable shape of the alveolar ridge, prevent soft tissue collapse, following the compression and displacement of the material.[42] Some authors define the thickness of 0.2 mm as optimal – it has inherent rigidity to maintain graft and protect new forming bone, but is flexible enough to minimize the risk of mucosa dehiscence.[43] Due to the presence of pores, Ti-mesh does not block the blood flow from the bone and the mucous membrane.[42] The most common post-surgery complication is soft tissue dehiscence, but the risk is much smaller in comparison to the use of a membrane. There is no inflammation at the exposed site due to the biocompatibility of titanium.[44,32] On the surface of titanium, titanium oxide layer is formed passively, causing cell adhesion and colonization, as well as osteocytes differentiation on the surgical side. According to the research of Lizio et al., each 1 cm^2 of uncovered mesh reduces 16.3% of the planned bone growth. There is also a relationship between early exposure and planned volume of newly formed bone.[45] Proussaefs et al. noted that Ti-mesh exposure causes horizontal and vertical bone loss of 8–10%.[46] Before dental implants insertion, the mesh has to be removed. The shape of the mesh was designed and constructed prior to surgery (using RP).[46] Manual forming did not allow obtaining a perfect shape or smooth edges, and it also heightens the risk of soft tissue dehiscence. The mesh is stiff, so manual forming is difficult and time-consuming. The risk of dehiscence is increased by superficial muscles position and insufficient mucosa amount.[47]

Different materials may be used to fill the bone loss. Autogenic material can be sourced extra- or intraorally. The most common extraoral sources for harvesting material are hip bone, fibula and scapula, and the most common intraoral sources are the angle of the mandible, mentum, and mandible branch.[48]

The material obtained extraorally undergoes resorption to a significant extent, whereas the amount of material harvested intraorally is often insufficient. This limitation can be avoided by using xenogeneic materials, e.g., deproteinized inorganic bovine bone matrix (DBBM), which has osteoconductive properties. Mixture of powdered autologous material with DBBM has osteoconductive properties of the DBBM material and osteogenic and osteoconductive properties of the autogenous material.[49] In a study by Lizio et al., autologous bone powder and inorganic bovine bone was used in the proportion of 70:30. Simion et al. used this material in the proportion of 1:1.[14,45]

Surgical technique

Autogenous bone material may be collected extra- and intraorally, both have advantages and disadvantages. If autogenous bone material is collected extraorally, there is another procedure to be conducted under general anesthesia; however, if the bone material is collected intraorally, local anesthesia is sufficient. In the study conducted by Zaffe and D'Avenia, bone was pulverized and mixed with inorganic DBBM in the ratio of 70:30.[48] At the top of toothless mandibular ridge, a horizontal and then a vertical cut was made, releasing the full-thickness buccal-lingual flap. Then, the fibrous tissue was removed and perforations in the bone to a marrow space with a small surgical drill were made to increase bleeding and adaptation of bone material.

Titanium 3-dimensional mesh, which had been made before the procedure, was completely filled with augmentative material, placed in a prepared location and stabilized with titanium miniscrews.[48] Then, the periosteum of the buccal flap was cut to allow its coronal shift, and the wound was tightly stitched.[50]

Postoperative antibiotics and pain therapy should be introduced. Patients should avoid harming postoperative area by adhering to a soft diet for 3 weeks and maintaining proper oral hygiene, rinsing the mouth with 0.2% chlorhexidine solution and applying a 0.2% chlorhexidine gel on the wound 2 times a day. Patients should not wear removable dentures for 4 weeks after the surgery.[50]

Postoperative histological analysis

Just before implantation, a punch biopsy with an inner diameter of 2.6 mm was performed in the postoperative site.[47] The biopsies were placed in 10% formalin solution for a period longer than 48 h. After proper preparation, all specimens' mixture bone (36.47%), connective tissue (49.18%) and the material particles DBBM (14.35%) were observed. There was no indication of inflammation or resorption. In the case of early titanium mesh exposure, the proportion of the newly formed bone in the specimen was smaller.[47]

Measurements of newly formed bone were also taken from pre- and postoperative CT.[47] One month after inserting dental implants, the level of newly formed bone was 8.6 mm, 6 months after it was 7.1 mm. According to this study, 6 months after augmentation, bone resorption equaled 15.11% and did not rise after the implant treatment.[47]

Bioresorbable hydroxyapatite and poly-L-lactide mesh

The mesh formed from hydroxyapatite (HA)/poly-L--lactide (PLLA) is stronger than the pure PLLA mesh and influences faster bone formation; it is also bioresorbable and, therefore, does not require reoperation in order for it to be removed from the mucous membrane. The process of total resorption takes 3–5 years.[51] The composite in 40% of its weight is composed of the sintered HA. The scaffold is designed on the basis of CT and is created in the process of stereolithography. In Matsuo et al.'s study

on the mandibular ridge reconstruction, a particulate cancellous bone and marrow (PCBM) of the iliac crest were used and then placed in the mesh with an addition of PRP.[52] The filled mesh was placed in a prepared place with screws. A 0.8 mm thick HA/PLLA mesh (standard Ti-mesh thickness is 0.2 mm) provides rigid attachment comparable to titanium mesh. Important advantage in comparison with titanium mesh is no need to remove the mesh prior to the dental implants insertion. No X-ray contrast makes it difficult to track the effects of the procedure.[52] According to Louis et al., the average size of new manufactured bone was 10–12 mm.[53] Histologically, bone formation and remodeling were observed within the macropores. Mineralized bone in macropores was combined with fragments of scaffold and BCP, where rows of osteoblasts were visible. In macropores, arteries and veins of various size can also be observed, which prove that the bone was alive.[54]

Sonic Weld Technique® – resorbable membrane and pins with polymer lactide acid

The use of thermoplastic membranes and resorbable prefabricated pins made of polymer lactide acid (PLA) is a modern technique that increases the vertical and transverse dimension of the mandibular ridge. It can also be used to stabilize the membrane during sinus lifts surgery, GBR, bone defects reconstruction in proximity to dental implants (shell technique) or to stabilize the bone transplant.

Pins are inserted into the bone (using ultrasound) and placed in Havers channels, which provides them with a stable fixing. They act like a scaffold and support the biomaterial and membrane covering it. The full time of pin resorption is more than 9 months.

Because the pins and the membrane are resorbable, there is no need for second surgery to remove them. The membrane can be shaped in 70°C water, allowing long and complicated 3DP or stereolithography procedures to be avoided. When the desired shape is obtained and the membrane is cooled below 70°C, it becomes rigid. Stiffness provides the space beneath it and ensures there is no pressure on new forming bone. The membrane is attached to pins that ensure its stability. The technique also allows changing the shape of pins and rounding the sharp edges using special ultrasonic tips, even after a diaphragm placement. If additional stabilization is needed, it is possible to use longer pins at the site of the reconstructed defect.

The advantages of the method are: short operation time, low invasiveness and no need for second surgery, low risk of xenogeneic material displacement. Perforation of the membrane allows good circulation from the periosteum. The limitations are the small possibility of the alveolar ridge width restoration and a limited amount of soft tissue to cover reconstruction.[20]

Tent technique using titanium screws, allogenic bone and bioresorbable membrane

Tent technique allows the reconstruction of a large loss of the mandibular ridge. It is predictable and allows to achieve esthetic results without the use of autogenous bone. Additional studies are necessary to evaluate the long-term effects of this procedure.

The tent technique enables the alveolar ridge to be augmented in patients who have loss of vertical dimension exceeding 7 mm. To rebuild the ridge height, titanium screws with a 1.5 mm diameter were used.[55] They were inserted partially into the alveolar ridge, protruding 5–7 mm above the alveolar ridge to keep the soft tissue above the bone defect filled with allogeneic material mixed with the patient's blood. Allogenic material completely covered the titanium screws. Resorbable membrane was used in order to prevent allogenic material resorption and the expansion of soft tissue. Newly formed bone was examined and dental implants were inserted 4–5 months after augmentation. In cases where the edge of mandibular ridge shape required corrections, allogenic bone was applied during implant insertion.

In the study of Simion et al., an average increase of alveolar ridge increase reached 9.7 mm.[14] The condition qualifying a patient for surgery was a vertical alveolar bone loss of more than 7 mm, and the width of the ridge bigger than 4 mm. In 2 patients, dehiscence occurred that resulted in the loss of allogenic bone. Osteointegration had occurred in all implants. An histological examination showed an average quantity of bone (around 43%) in the collected material. In all specimens, a correct pattern of cancellous bone was observed, as well as a good connection with bone trabeculles.

Biphasic calcium phosphate scaffold

The structure of BCP is similar to the mineralized bone. It has suitable mechanical properties. Biphasic calcium phosphate has good porosity for vascularization and diffusion of nutrients, whereas chemical properties of its surface allow the adhesion of osteogenic cells and proliferation. Moreover, it is biocompatible and has osteoconductive and osteoinductive properties.

In the study of Mangano et al., scaffold was planned individually on the basis of CT and produced using CAD/CAM block containing 70% beta-tricalcium phosphate and 30% HA. Scaffold in shape of bone defect was obtained.[16,56] In its center there is a hole for the stabilizing screw. Replica of the scaffold – made from polytetrafluoroethylene (PTFE) – is used as a template for drilling the bed needed to stabilize the screws (BCP scaffold is fragile and could be broken if not handled properly). Both the scaffold and its replica require sterilization prior to surgery. One of the main limitations to the use of BCP scaffold is the maximum size for the deficit – 12 mm high and 10 mm wide. It is dictated by the need for adequate

diffusion of oxygen and nutrients through the entire structure.[56] Osteoblasts require a high concentration of oxygen for the bone matrix production; the higher the permeability of the vascular scaffold, the higher the efficiency of a new bone formation.[16]

During the procedure, the muco-periosteal flap was detached under local anesthesia, a replica of PTFE was positioned, a precise bed for the stabilizing screw was drilled, and then the replica was removed.[56] Prior to the application of the appropriate BCP scaffold, a few small holes in the atrophic mandible bone to the medullary canal were drilled to provoke bleeding the presence of blood assure growth factors, platelet rich and poor plasma and fibrin – they induce healing process and tissue regeneration. After preparing the recipient site, the BCP scaffold was imposed in the correct position, fixed with screw and covered with a fibrin membrane.

The scaffold acts as a sponge absorbing the blood from the bone. The recombinant bone morphogenetic protein (RBMP) is used to increase scaffolds osteoinductive properties. BMP-2 belongs to the family of TGF-β that is present during the bone development and healing; it can be used for the new bone formation within the scaffold.[57] Lan Levengood et al. researched BCP scaffold and observed that the density of bone cells per mm^2 in the micropores (not related to macropores) of BCP scaffolds was significantly higher after 3, 12 and 24 weeks than in the control group, where the scaffold BCP did not contain additional BMPs.[54]

The aim of the histological evaluation was to rate the quality bone that was formed by augmentation. Two biopsies were performed (in the place prepared for the implant) with a trephine 2 × 10 mm. The histological examination revealed the presence of dense, mature bone, leukemia, newly generated spaces, and trabecular bone surrounded by residual BCP molecules. The presence of new blood vessels in the bone marrow was observed.[17]

An important advantage of this method is a significant reduction in treatment time. The time required for accurate design and construction of the scaffold is certainly a disadvantage.

Poly-lactide-co-glycolide/tricalcium phosphate scaffold

Modern method, but still in the area of research in mandibular ridge reconstruction is poly-lactide-co-glycolide (PLGA) and tricalcium phosphate (TCP) scaffold. The mechanical properties of the scaffold are similar to the human cancellous bone.[58] The average diameter of macropore is 380 μm (sufficient macropore volume to enable vascularization and regeneration of mature Haversian systems of bone), micropores 3–5 μm and porosity of the scaffold 87.4%. If the porosity is too low, there may be too few quality connections between pores; also low susceptibility to tissue growth and increased degradation time may occur because insufficient amount of surface is in contact with body fluids. The scaffold designed for a patient has a smooth outer surface and a porous inner surface. On the outer, smooth surface, the gingiva is circumferentially rested, also preventing its ingrowth, promoting bone growth within the scaffold.[58]

In the study conducted by Ruhe et al., holes were drilled into the bone marrow before the insertion of dental implants.[60] This way the scaffold tightly adheres to the bone, and osteoblasts and progenitor cells are involved in bone formation. The progenitor cells of the matrix of human bone marrow mesenchymal stem (HBMSCs) are capable of adhesion and proliferation on the stage, which is why biocompatibility was confirmed. The disadvantages of the PLGA/TCP material are PLGA hydrophobicity, thereby inhibiting cell adhesion and regeneration of tissues after the implantation of the scaffold. The degree of degradation of the PLGA does not correspond to the degree of tissue regeneration. Poly-lactide-co-glycolide metabolic products have acidic character and toxic effect on tissue. They accumulate during scaffold degradation and cause aseptic inflammation. Compared to PLGA, TCP has a higher degree of degradation and its surface has hydrophilic properties. TCP degradation products are alkaline and they can neutralize and alleviate the toxic effects of metabolites PLGA. Tricalcium phosphate has poor mechanical properties, but in TCP particles, the deposition of PLGA improves the strength of the material, reduces hydrophobicity and enhances the ability of cells to adhere to the surface of the material.[59] Tricalcium phosphate increases the biocompatibility of the material and the total degradation time of PLGA/TCP material is similar to the natural bone formation.[60]

Bioresorbable polycaprolactone scaffold in the 3D technology

The initial phase of research uses 3D selective laser melting polycaprolactone (PCL) scaffold containing 4% HA.[18] Polycaprolactone is a biocompatible and biodegradable synthetic polymer that has a high mechanical strength and low production cost. The process of PCL degradation in a living body is slow and involves hydrolysis. The decomposition products do not cause acidification.[19] Polycaprolactone scaffold can be sterilized with ethylene oxide.

Rasperini et al. used a scaffold made in 3D technology using patients CBCT to cover the recession of lower canines' root that occurred as a result of the loss of connective tissue attachment.[18] After full-thickness flap detachment, mechanical instrumentation of the root was done and EDTA agent was applied. Then, a solution of human recombinant platelet-derived growth factor-BB (rhPDGF BB) was applied on its surface. The PCL scaffold was immersed in the solution for 15 min and then filled with blood derived from the recipient region. The scaffold was fixed with resorbable poly-D and L-lactide pins. The operation area was covered with a flap and sutured using non-resorbable sutures.[18]

No inflammatory process or dehiscence was detected during the control visit after 12 months. In the abovementioned study, 3 mm tissues attachment and partial coverage of the tooth root was obtained. During 13 months, exposure of the scaffold has been observed. Despite the use of professional oral hygiene tools, amelogenins gel and systemic administration of antibiotics, it was necessary to remove the scaffold – partially at first, and then completely. After 14 months, there was initial healing of the connective tissue and minimal bone reparation.[18]

According to the authors, the scaffold should have a greater porosity to allow vascularization and less dense structure to undergo faster resorption, and thus prevent dehiscence, exposure, and bacterial infection.[18]

Summary

Reconstructing the vertical dimension of the mandibular ridge requires great competence from the surgeon performing the surgery. The emergence of new reconstruction techniques allows the functional and esthetic reconstruction even when there is extensive bone loss. The aim of this treatment is to produce a fully functional bone to enable proper stability and retention for dental implants and prosthetic devices. The choice of method depends on the bone and soft tissue loss extension, availability of autogenous bone to be harvested and access to modern technology – stereolithography, CAD/CAM, or osteodystractors.

References

1. Perdijk FBT, Meijer GJ, van Strijen PJ, Koole R. Complications in alveolar distraction osteogenesis of the atrophic mandible. *Int J Oral Maxillofac Surg*. 2007;36(10):916–921.
2. Mangano F, Macchi A, Caprioglio A, Sammons L, Piattelli A, Mangano C. Survival and complication rates of fixed restorations supported by locking-taper implants: A prospective study with 1 to 10 years of follow-up. *J Prosthodont*. 2014;23(6):434–444.
3. Mangano F, Shibli JA, Sammons RL, Veronesi G, Piattelli A, Mangano C. Clinical outcome of narrow-diameter (3.3-mm) locking-taper implants: A prospective study with 1 to 10 years of follow-up. *Int J Oral Maxillofac Implants*. 2014;29(2):448–455.
4. Poli PP, Beretta M, Ciccu M, Maiorana C. Alveolar ridge augmentation with titanium mesh. A retrospective clinical study. *Open Dent J*. 2014;8:148–158.
5. Misch CM. Comparison of intraoral donor sites for onlay grafting prior to implant placement. *Int J Oral Maxillofac Implants*. 1997;12(6):767–776.
6. Mehta RKP, Deschler DG. Mandibular reconstruction in 2004: An analysis of different techniques. *Curr Opin Otolaryngol Head Neck Surg*. 2004;12(4):288–293.
7. Keith JD, Salama MA. Ochrona i augmentacja wyrostka zębodołowego zwiększa przewidywalność i poprawia efekt estetyczny leczenia implantologicznego. *Implants*. 2010;5(2):20–26.
8. Szadowski M, Popowski W, Frank S, Nieckula P, Kamiński A, Wojtowicz A. Odbudowa ubytku kostnego w przednim odcinku szczęki allogennym blokiem kostnym wzbogaconym PRP. *Implants*. 2015;10(2):18–24.
9. Dudek D, Żaba M, Barć-Czarnecka M, et al. Augmentacja kości szczękowych z zastosowaniem kości ludzkiej świeżo mrożonej – kliniczne doświadczenia własne. *Implants*. 2015;10(2):30–37.
10. Yun KI, Choi H, Wright RF, Ahn HS, Chang BM, Kim HJ. Efficacy of alveolar vertical distraction osteogenesis and autogenous bone grafting for dental implants: Systematic review and meta-analysis. *Int J Oral Maxillofac Implants*. 2016;31(1):26–36.
11. Teng F, Zhang Q, Wu M, Rachana S, Ou G. Clinical use of ridge-splitting combined with ridge expansion osteotomy, sandwich bone augmentation, and simultaneous implantation. *Br J Oral Maxillofac Surg*. 2014;52(8):703–708.
12. Engelke WG, Diederichs CG, Jacobs HG, Deckwer I. Alveolar reconstruction with splitting osteotomy and microfixation of implants. *Int J Oral Maxillofac Implants*. 1997;12(3):310–318.
13. Kao DW, Fiorellini JP. Comparison of ridge expansion and ridge splitting techniques for narrow alveolar ridge in a Swine cadaver model. *Int J Periodontics Restorative Dent*. 2015;35(3):e44–49.
14. Simion M, Fontana F, Rasperini G, Maiorana C. Vertical ridge augmentation by expanded-polytetrafluoroethylene membrane and a combination of intraoral autogenous bone graft and deproteinized anorganic bovine bone (Bio Oss). *Clin Oral Implants Res*. 2007;18(5):620–629.
15. Cordaro L, Amadé DS, Cordaro M. Clinical results of alveolar ridge augmentation with mandibular block bone grafts in partially edentulous patients prior to implant placement. *Clin Oral Implants Res*. 2002;13(1):103–111.
16. Mangano FG, Zecca PA, van Noort R, et al. Custom-made computer-aided-design/computer-aided-manufacturing biphasic calcium-phosphate. *Case Rep Dent*. 2015;2015:941265.
17. Moldovan I, Juncar M, Dinu C, et al. Mandibular reconstruction using free vascularized iliac crest grafts and dental implants. *Clujul Med*. 2015;88(3):391–394.
18. Rasperini G, Pilipchuk SP, Flanagan CL, et al. 3D printed bioresorbable scaffold for periodontal repair. *J Dent Res*. 2015;94(Suppl 9):153S–157S.
19. Rong D, Chen P, Yang Y, et al. Fabrication of gelatin/PCL electrospun fiber mat with bone powder and the study of its biocompatibility. *J Funct Biomater*. 2016;7(1):6.
20. Pilling E, Mai R, Theissig F, Stadlinger B, Loukota R, Eckelt U. An experimental in vivo analysis of the resorption to ultrasound activated pins (Sonic weld) and standard biodegradable screws (ResorbX) in sheep. *Br J Oral Maxillofac Surg*. 2007;45(6):447–450.
21. Le B, Rohrer MD, Prasad HS. Screw "tent-pole" grafting technique for reconstruction of large vertical alveolar ridge defects using human mineralized allograft for implant site preparation. *J Oral Maxillofac Surg*. 2010;68(2):428–435.
22. Nocini PF, De Santis D, Fracasso E, Zanette G. Clinical and electrophysiological assessment of inferior alveolar nerve function after lateral nerve transposition. *Clin Oral Implants Res*. 1999;10(2):120–130.
23. Kan JY, Lozada JL, Goodacre CJ, Davis WH, Hanisch O. Endosseous implant placement in conjunction with inferior alveolar nerve transposition: An evaluation of neurosensory disturbance. *Int J Oral Maxillofac Implants*. 1997;12(4):463–471.
24. Sharma R. Trigeminal Nerve Injuries. Medical Journal, Armed Forces India. 2015;71(1):42.
25. Hoffman GR, Islam S, Eisenberg RL. Microvascular reconstruction of the mouth, face and jaws. Oromandibular reconstruction – free fibula flap. *Aust Dent J*. 2012;57(3):379–387.
26. Goh BT, Lee S, Tideman H, Stoelinga PJ. Mandibular reconstruction in adults: A review. *Int J Oral Maxillofac Surg*. 2008;37(7):597–605.
27. Hidalgo DA. Fibula free flap: A new method of mandible reconstruction. *Plast Reconstr Surg*. 1989;84(1):71–79.
28. Marchetti C, Bianchi A, Mazzoni S, Cipriani R, Campobassi A. Oromandibular reconstruction using a fibula osteocutaneous free flap: Four different "preplating" techniques. *Plast Reconstr Surg*. 2006;118(3):643–651.
29. Kokosis G, Schmitz R, Powers DB, Erdmann D. Mandibular reconstruction using the free vascularized fibula graft: An overview of different modifications. *Arch Plast Surg*. 2016;43(1):3–9.
30. Chim H, Salgado CJ, Mardini S, Chen HC. Reconstruction of mandibular defects. *Semin Plast Surg*. 2010;24(2):188–197.
31. Boyd JB, Caton AM, Mulholland RS, Tong L, Granzow JW. The sensate fibula osteocutaneous flap: Neurosomal anatomy. *J Plast Reconstr Aesthet Surg*. 2013;66(12):1688–1694.
32. Maiorana C, Santoro F, Rabagliati M, Salina S. Evaluation of the use of iliac cancellous bone and anorganic bovine bone in the reconstruction of the atrophic maxilla with titanium mesh: A clinical and histologic investigation. *Int J Oral Maxillofac Implants*. 2001;16(3):427–432.
33. Navarro Cuellar C, Caicoya SJ, Acero Sanz JJ, Navarro Cuellar I, Muela CM, Navarro Vila C. Mandibular reconstruction with iliac crest free flap, nasolabial flap, and osseointegrated implants. *J Oral Maxillofac Surg*. 2014;72(6):1226.e1-15.

34. Thoma A, Khadaroo R, Grigenas O, et al. Oromandibular reconstruction with the radial-forearm osteocutaneous flap: Experience with 60 consecutive cases. *Plast Reconstr Surg*. 1999;104(2):368–378.
35. Kumar KAJ, Masrom AK, Patil K, Kunusoth R, Begum F, Venkatesh V. Evaluation of vertical bone gain following alveolar distraction osteogenesis in the anterior edentulous mandible: A clinical study. *J Maxillofac Oral Surg*. 2014;13(4):539–545.
36. Gerber-Leszczyszyn H, Pawlak W, Łuczak K. Wykorzystanie wewnątrzustnych dystraktorów kostnych w leczeniu ubytków pourazowych wyrostka zębodołowego żuchwy – opis przypadku. *Dent Med Probl*. 2003;40(1):155–157.
37. Perdijk FB, Meijer GJ, Strijen PJ, Koole R. Complications in alveolar distraction osteogenesis of the atrophic mandible. *Int J Oral Maxillofac Surg*. 2007;36(10):916–921.
38. Mampilly MO, Rao LP, Sequiera J, Sripathi Rao BH, Chandra J, Rai G. Rehabilitation of edentulous atrophic anterior mandible – The role of vertical alveolar distraction osteogenesis. *J Clin Diagn Res*. 2014;8(11):ZR01–ZR03.
39. Li J, Zhang L, Lv S, Li S, Wang N, Zhang Z. Fabrication of individual scaffolds based on a patient-specific alveolar bone defect model. *J Biotechnol*. 2011;151(1):87–93.
40. Ciocca L, De Crescenzio F, Fantini M, Scotti R. CAD/CAM and rapid prototyped scaffold construction for bone regenerative medicine and surgical transfer of virtual planning: A pilot study. *Comput Med Imaging Graph*. 2009;33(1):58–62.
41. Liu YF, Zhu FD, Dong XT, Peng W. Digital design of scaffold for mandibular defect repair based on tissue engineering. *J Zhejiang Univ Sci B*. 2011;12(9):769–779.
42. Yamada H, Nakaoka K, Horiuchi T, et al. Mandibular reconstruction using custom-made titanium mesh tray and particulate cancellous bone and marrow harvested from bilateral posterior ilia. *J Plast Surg Hand Surg*. 2014;48(3):183–190.
43. Roccuzzo M, Ramieri G, Spada MC, Bianchi SD, Berrone S. Vertical alveolar ridge augmentation by means of a titanium mesh and autogenous bone grafts. *Clin Oral Implants Res*. 2004;15(1):73–81.
44. Roccuzzo M, Ramieri G, Bunino M, Berrone S. Autogenous bone graft alone or associated with titanium mesh for vertical alveolar ridge augmentation: A controlled clinical trial. *Clin Oral Implants Res*. 2007;18(3):286–294.
45. Lizio G, Corinaldesi G, Marchetti C. Alveolar ridge reconstruction with titanium mesh: A three-dimensional evaluation of factors affecting bone augmentation. *Int J Oral Maxillofac Implants*. 2014;29(6): 1354–1363.
46. Miyamoto I, Funaki K, Yamauchi K, Kodama T, Takahashi T. Alveolar ridge reconstruction with titanium mesh and autogenous particulate bone graft: Computed tomography-based evaluations of augmented bone quality and quantity. *Clin Implant Dent Relat Res*. 2012;14(2):304–311.
47. Proussaefs P, Lozada J. Use of titanium mesh for staged localized alveolar ridge augmentation: Clinical and histologic-histomorphometric evaluation. *J Oral Implantol*. 2006;32(5):237–247.
48. Zaffe D, D'Avenia F. A novel bone scraper for intraoral harvesting: A device for filling small bone defects. *Clin Oral Implants Res*. 2007;18(4):525–533.
49. Yildirim M, Spiekermann H, Handt S, Edelhoff D. Maxillary sinus augmentation with the xenograft Bio-Oss and autogenous intraoral bone for qualitative improvement of the implant site: A histologic and histomorphometric clinical study in humans. *Int J Oral Maxillofac Implants*. 2001;16(1):23–33.
50. Poli PP, Beretta M, Cicciù M, Maiorana C. Alveolar ridge augmentation with titanium mesh. A retrospective clinical study. *Open Dent J*. 2014;8:148–158.
51. Shikinami Y, Matsusue Y, Nakamura T. The complete process of bioresorption and bone replacement using devices made of forged composites of raw hydroxyapatite particles/poly l-lactide (F-u-HA/PLLA). *Biomaterials*. 2005;26(27):5542–5551.
52. Matsuo A, Chiba H, Takahashi H, Toyoda J, Abukawa H. Clinical application of a custom-made bioresorbable raw particulate hydroxyapatite/poly-L-lactide mesh tray for mandibular reconstruction. *Odontology*. 2010;98(1):85–88.
53. Louis P, Holmes J, Fernandes R. Resorbable mesh as a containment system in reconstruction of the atrophic mandible fracture. *J Oral Maxillofac Surg*. 2004;62(6):719–723.
54. Lan Levengood SK, Polak SJ, Poellmann MJ, et al. The effect of BMP-2 on micro- and macroscale osteointegration of biphasic calcium phosphate scaffolds with multiscale porosity. *Acta Biomater*. 2010;6(8):3283–3291.
55. Dominiak M, Gedrange T. New ways of reconstructing complex bone defects in the alveolar ridge. In: Dominiak M, Gedrange T, eds. Esthetics in Implantology. Wrocław: BF Remigiusz Dyńka; 2013;193–214.
56. Mangano F, Macchi A, Shibli JA, et al. Maxillary ridge augmentation with custom-made CAD/CAM scaffolds. A 1-year prospective study on 10 patients. *J Oral Implantol*. 2014;40(5):561–569.
57. Chen D, Zhao M, Mundy GR. Bone morphogenetic proteins. *Growth Factors*. 2004;22(4):233–241.
58. Spath S, Drescher P, Seitz H. Impact of particle size of ceramic granule blends on mechanical strength and porosity of 3D printed scaffolds. *Materials (Basel)*. 2015;8(8):4720–4732.
59. Jansen JA, Vehof JW, Ruhe PQ, et al. Growth factor-loaded scaffolds for bone engineering. *J Control Release*. 2005;101(1–3):127–136.
60. Ruhe PQ, Hedberg EL, Padron NT, Spauwen PH, Jansen JA, Mikos AG. rhBMP-2 release from injectable poly(DL-lactic-co-glycolic acid)/calcium-phosphate cement composites. *J Bone Joint Surg Am*. 2003;85-A(Suppl 3):75–81.
61. Kramer FJ, Dempf R, Bremer B. *Clin Oral Implants Res*. 2005;16(1):80–88.

Advances
in Clinical and Experimental
Medicine